

Ultracold Atoms in Resonator-Generated Optical Lattices

DISSERTATION

zur Erlangung des akademischen Grades

Doktor der Naturwissenschaften

an der

Fakultät für Mathematik, Informatik und Physik

der

Leopold-Franzens-Universität Innsbruck

vorgelegt von

MMag. rer. nat. Christoph Maschler

Oktober 2007

To Bettina and my mother.

ABSTRACT

The field of atomic, molecular and optical physics (AMO) has experienced tremendous progress the last 20 years. Two prominent examples in this context are (i) systems of cold atoms in optical lattices, for instance, allowing for investigations of fundamental questions of traditional condensed matter physics, and (ii) systems of atoms in optical resonators, enabling single-atom manipulations and leading to a variety of new phenomena. Moreover, both of these systems offer a plethora of applications for quantum information processing.

This thesis presents my work based on a generalization of models for cold atoms in optical lattices by including a high- Q optical cavity to the dynamics. This provides new perspectives to investigate collective effects of atoms in optical resonators and to study fundamental issues of strongly correlated systems. The thesis is divided into three parts corresponding to conceptually different topics. The work was performed at the Institute for Theoretical Physics at the University of Innsbruck under the supervision of Prof. Helmut Ritsch.

The first part of this thesis is devoted to investigations concerning the dynamics of systems of cold atoms in resonator-generated optical lattices. Here we derive a generalized Bose-Hubbard Hamiltonian, describing the dynamical evolution of the atom-cavity system and discuss the influence of the cavity degree of freedom on various properties of strongly correlated systems in optical lattices. Moreover, we identify a regime, where the cavity field can be eliminated, which provides a significant simplification of the model.

In the second part, we present two proposals for non-destructive probing of the atomic phase of an ensemble of cold atoms in an optical lattice by means of cavity QED. The first method consists of angle-resolved measurements of photon number and variance via off-resonant collective light scattering into a cavity. This provides information about atom-number fluctuations, pair correlations and quantum fluctuations without single-site access. The second method, fundamentally different from the first, shows how to map atomic quantum statistics on transmission spectra of high- Q cavities. The predicted effects of both proposals are accessible in experiments that recently became possible.

Collective interactions of atoms enclosed in a cavity and coherently excited by a laser field, impinging perpendicularly on the cavity axis, lead to self-organization of the atoms within the optical lattice. In the last part of this thesis, we accomplish a quantum mechanical analysis of the onset of this self-ordering process. We show that atom-field entanglement plays a crucial role in the spatial reordering of the atoms from a homogeneous towards one of two possible ordered states.

ZUSAMMENFASSUNG

Auf dem Gebiet der atomaren, molekularen und optischen Physik (AMO) konnten während der letzten 20 Jahre enorme Fortschritte erzielt werden. Zwei herausragende Beispiele in diesem Zusammenhang sind (i) Systeme kalter Atome in optischen Gittern, die unter anderem die Untersuchung fundamentaler Fragestellungen aus dem Gebiet der Physik der kondensierten Materie erlauben, und (ii) Systeme von Atomen in optischen Hohlraumresonatoren, die es erlauben einzelne Atome zu manipulieren und zu einer Vielzahl an neuartigen Phänomenen führen. Überdies bieten beide Systeme ein breites Spektrum an Anwendungsmöglichkeiten im Bereich der Quanteninformationsverarbeitung an.

In der vorliegenden Dissertation sind meine Forschungsergebnisse über eine Verallgemeinerung von Modellen, die kalte Atome in optischen Gittern - unter Hinzunahme eines Hohlraumresonators mit hohem Gütefaktor - beschreiben, zusammengefasst. Es lassen sich daraus neue Perspektiven zur Untersuchung kollektiver Effekte von Atomen in optischen Resonatoren und zum Studium von fundamentalen Fragestellungen stark korrelierter Systeme ableiten. Die vorliegende Dissertation ist in drei Abschnitte unterteilt, entsprechend den dreie konzeptionell unterschiedlichen Themengebieten. Diese Arbeit wurde am Institut für theoretische Physik der Universität Innsbruck durchgeführt und von Prof. Helmut Ritsch betreut.

Die Dynamik von Systemen von kalten Atomen in optischen Gittern, die von Hohlraumresonatoren erzeugt werden, wird im ersten Abschnitt dieser Dissertation eingehend untersucht. Hier leiten wir einen verallgemeinerten Bose-Hubbard Hamilton-Operator her, der die dynamische Entwicklung des Atom-Hohlraum Systems beschreibt und, diskutieren den Einfluss des Hohlraums auf verschiedene Eigenschaften von stark korrelierten Systemen in optischen Gittern. Außerdem weisen wir einen Bereich aus, in dem das Hohlraumfeld aus der Dynamik adiabatisch eliminiert werden kann, was zu einer erheblichen Vereinfachung dieses Modells führt.

Im zweiten Abschnitt schlagen wir zwei Methoden zur zerstörungsfreien Messung der atomaren Phase eines Ensembles kalter Atome in optischen Gittern mittels Hohlraum-Quantenelektrodynamik vor. Die erste dieser Methoden besteht aus winkel-auflösenden Messungen der Anzahl an Photonen und ihrer Varianz durch nicht-resonante, kollektive Lichtstreuung in den Hohlraum. Dies liefert Informationen über Fluktuationen der Atomzahl, Paarkorrelationen und Quantenfluktuationen, ohne Zugang zu einzelnen Gitterplätzen haben zu müssen. Die zweite Methode, die sich von der ersten fundamental unterscheidet, zeigt, wie man atomare Quantenstatistik auf Transmissionsspektren eines Hohlraumresonators mit

hohem Gütefaktor abbilden kann. Die vorhergesagten Effekte beider Vorschläge können in heute möglichen Experimenten beobachtet werden.

Kollektive Wechselwirkungen zwischen Atomen in einem Hohlraumresonator, die von einem senkrecht auf die longitudinale Achse des Hohlraums einfallenden Laser angeregt werden, führen zur Selbstorganisation der Atome innerhalb des Gitters. Im letzten Abschnitt dieser Dissertation führen wir eine quantenmechanische Analyse der Entstehung dieses Selbstorganisationsprozesses durch. Wir zeigen, dass die Verschränkung zwischen Atom und Hohlraumfeld ein wesentliches Element in der räumlichen Umordnung von einem homogenen Zustand, hin zu einem der zwei möglichen geordneten Zustände, ist.

DANKSAGUNG

Nach den vielen Jahren meiner akademischen Ausbildung, deren Abschluss diese Dissertation darstellt, ist es nun an der Zeit all jenen zu danken, die wesentlich zum Gelingen dieses Vorhabens beigetragen haben.

Als Erstes möchte ich mich von ganzem Herzen bei meiner Mutter bedanken, die mir meine gesamte Ausbildung überhaupt erst ermöglicht hat. Sie hat mich stets mit ganzer Kraft unterstützt und ist auch bei Rückschlägen immer hinter mir gestanden. Meinem Vater danke ich für die finanzielle Unterstützung.

In akademischer Hinsicht möchte ich mich natürlich zuerst bei meinem Betreuer Prof. Helmut Ritsch bedanken, der mir trotz etwas schwieriger Begleitumstände die Möglichkeit bot, in seiner Gruppe mitzuarbeiten. Er hatte für alle Fragen stets ein offenes Ohr und auf kollegiale Art und Weise lenkte er, mit großer physikalischer Intuition und einem reichhaltigen Reservoir an Ideen, meine Arbeit in die richtige Bahn. Dabei übersah er verständnisvoll, dass einige Nebenbeschäftigungen, wie das Erstellen meiner Mathematik Diplomarbeit, das Unterrichtspraktikum oder das nicht zu vermeidende Übel des Präsenzdienstes, es mir nicht immer erlaubten mich mit letzter Konsequenz meiner Forschungsarbeit zu widmen. Bei Prof. Peter Zoller und Prof. Wolfgang Förg-Rob möchte ich mich für die Betreuung meiner Diplomarbeiten in Physik und Mathematik, ohne die ein Doktoratsstudium gar nicht erst möglich wäre, bedanken. Ich möchte hier auch alle momentanen und ehemaligen Mitglieder des Arbeitsbereiches Quantenoptik und Quanteninformation erwähnen, die es mir mit ihrem Einsatz ermöglichten, in einem inspirierenden Umfeld zu arbeiten, das wissenschaftlich weltweit keinen Vergleich zu scheuen braucht. Allen Vortragenden der Mathematik- und Physik Institute, insbesondere Prof. Ignácio Cirac, nunmehriger Direktor des Max Planck Instituts für Quantenoptik in Garching, danke ich für ihre Versuche, mir in zahlreichen interessanten und lehrreichen Vorlesungen etwas beizubringen. Den Mitgliedern unserer Forschungsgruppe Thomas Salzburger, Andras Vukics, Igor Mekhov, Janos Asbóth, Hashem Zoubi und den zwei "Diplomis" Wolfgang Niedenzu und Tobias Griesser sowie Peter Domokos, Giovanna Morigi und Prof. Maciej Lewenstein bin ich für viele stimulierende Diskussionen und Unterstützung bei physikalischen Fragestellungen dankbar. Für rasche und unkomplizierte Unterstützung in bürokratischer und computertechnischer Hinsicht danke ich unseren Sekretärinnen Marion Grünbacher, Nicole Jorda und Elke Wölflmaier sowie den Systemadministratoren Hans Embacher und Julio Lamas-Knapp.

Das Studium und die Forschungsarbeit in Innsbruck bot mir die Gelegenheit zahlreiche interessante Menschen kennen zu lernen, mit ihnen über Physik, aber auch Gott und die

Welt zu diskutieren, und lustige und gesellige Abende zu verleben. Erwähnen möchte ich hier meine Physikerkollegen Walter Rantner (der vergeblich versuchte uns den Rudersport und die englische Küche schmackhaft zu machen), Patrick Jussel, Andi Griessner, Uwe Dorner (der uns erst viel zu spät das köstliche *Tannenzäpfle* vorstellte), Viktor Steixner, Stefano Cerrito (der uns in die Kunst des Espresso-Kochens einführte), Nikola Lalic und ganz besonders Andrea Micheli (der Dank seines Fachwissens auch eine niemals versiegende Quelle bei vielen Physik- und Computerproblemen war). Dasselbe gilt für meine Mathematik-Kollegen Lukas Neumann, Markus Haltmeier und Thomas Niederklapfer. Viel Spaß bereitete mir auch die jährliche Teilnahme am Innsbrucker Stadtlauf im Team der *Running Waves* mit Andrew Daley, Peter Rabl und Konstanze Jähne. Anerkennung gebührt dabei unseren Kontrahenten vom Institut für Experimentalphysik, die ihre alljährlichen Triumphe über uns nicht über Gebühr auskosteten.

Mit meinen Freunden vom Naturwissenschaftlichen Panoptikum Innsbruck (NPI) Christofer Tautermann, Robert Morandell, Hannes Perschinka, Stefan Steidl, Peter Lampacher, Wolfgang Stöggel und ganz besonders Bernd und Markus Wellenzohn durfte ich viele lustige und glückliche, aber auch kuriose Momente erleben. Leider mussten wir letztes Jahr gemeinsam auch die schmerzhaften Schattenseiten des Lebens erfahren, als unser treuer Freund Markus Loferer, der für mich in vielerlei Hinsicht ein Vorbild war, viel zu früh aus dem Leben scheiden musste.

Bedanken möchte ich mich auch bei meinen Freunden Thomas “Fuzzi” Wachtler, der mein Interesse für finanzwirtschaftliche Fragestellungen geweckt hat, und Thomas Walser, dessen Wohnung zu Beginn meiner Studienzeit beinahe täglicher Treffpunkt war, was unter Umständen mit der Existenz eines Fernsehers und dem prall gefüllten Kühlschrank zusammenhängen könnte. Martin Ladner, Arno Mautner, Benedikt Tremel und Robert Millinger danke ich für schweißtreibende Einheiten am Rad sowie mit den Langlauf- und Tourenski. Dasselbe gilt für die “USI Schwimmgruppe” mit unserem Trainer Gunnar Innerhofer. Schlussendlich möchte ich mich noch bei Prof. Christoph Leubner und bei Dr. Markus Gangl von der Patentanwaltskanzlei Torggler & Hofinger für die Unterstützung bei der Jobsuche bedanken.

Bei all jenen, die sich dieser Auflistung zugehörig fühlen, die ich aber (natürlich nur unabsichtlich) vergessen habe, möchte ich mich entschuldigen. Außerdem habe ich sämtliche akademischen Titel geflissentlich vernachlässigt. Wer will, kann beinahe vor jeden Namen hier ein *Dr.* setzen.

Der größte Dank überhaupt gebührt aber meiner Lebensgefährtin Bettina, die mich während all dieser Jahre uneigennützig unterstützt und mich aus so manchem Motivationssloch wieder herausgeholt hat. Dabei hat sie - vor allem während der letzten, sehr stressigen Phase des Erstellens dieser Arbeit - vieles in Kauf nehmen müssen. Danke für alles!

Christoph Maschler, 27. September 2007.

CONTENTS

Abstract	v
Zusammenfassung	viii
Danksagung	ix
Contents	xiv
Chapter 1. General Introduction	1
I Ultracold Atoms in Optical Lattices Enclosed in an Optical Cavity	25
Chapter 2. Background: Cold Atoms in Optical Lattices	27
2.1 Optical Lattices	27
2.1.1 Optical Potentials - The AC-Stark Shift	27
2.1.2 Spontaneous Emission	29
2.1.3 Lattice Geometry	30
2.2 A Single Particle in an Optical Lattice	30
2.2.1 Harmonic Oscillator Approximation	31
2.2.2 Bloch Functions	31
2.2.3 Wannier Functions	32
2.3 The Bose-Hubbard Model	34
2.3.1 Microscopic Derivation of the Bose-Hubbard Hamiltonian	35
2.3.2 The Superfluid State and the Mott Insulator State	41

Chapter 3. Background: Basics of Cavity Quantum Electrodynamics (CQED)	45
3.1 Atoms in Optical Cavities	45
3.1.1 Optical Cavities	45
3.1.2 The Jaynes-Cummings Hamiltonian	48
3.1.3 Open Systems - Dissipation	51
3.2 Resonator-Generated Optical Lattices	55
3.2.1 Adiabatic Elimination of the Excited States	55
3.2.2 Intracavity trapping potential	57
3.3 Transverse Motion	59
Chapter 4. Publication: Quantum Motion of Laser-Driven Atoms in a Cavity Field	63
4.1 Introduction	63
4.2 Model	65
4.3 System Dynamics	67
4.3.1 Mapping to an oscillator with time dependent frequency	67
4.3.2 Coupled equations for atomic expectation values and the field	69
4.3.3 Steady state properties	70
4.4 Cavity cooling in the quantum regime	72
4.5 Conclusions	78
Chapter 5. Publication: Cold Atom Dynamics in a Quantum Optical Lattice Potential	81
Chapter 6. Publication: Ultracold Atoms in Optical Lattices Generated by Quantized Light Fields	91
6.1 Introduction	91
6.2 Model	93
6.3 Cavity pump	99
6.3.1 Field-eliminated Hamiltonian	100
6.3.2 Field-eliminated density operator	102
6.3.3 Quantum phase transitions in an optical lattice	105
6.3.4 Comparison with the full dynamics of the master equation	110
6.4 Atom pumping	114

6.4.1	Field-eliminated Hamiltonian	115
6.4.2	Self-organization of atoms in an optical lattice	117
6.5	Conclusions	118
II	Probing Atomic Phases in Optical Lattices	125
Chapter 7. Publication: Cavity Enhanced Light Scattering in Optical Lattices to Probe Atomic Quantum Statistics		127
Chapter 8. Publication: Light Scattering from Ultracold Atoms in Optical Lattices as an Optical Probe of Quantum Statistics		137
8.1	Introduction	137
8.2	General model	139
8.3	Scattering from a deep lattice and classical analogy	143
8.4	Relation between quantum statistics of atoms and characteristics of scattered light	144
8.4.1	Probing quantum statistics by intensity and amplitude measurements	144
8.4.2	Quadrature measurements	146
8.4.3	Photon number fluctuations	147
8.4.4	Phase-sensitive and spectral measurements	148
8.5	Quantum statistical properties of typical atomic distributions	149
8.6	Example: 1D optical lattice in a transversally pumped cavity	152
8.7	Results and Discussion	153
8.7.1	Two traveling waves and discussion of essential physics	154
8.7.2	Standing waves	156
8.7.3	Quadratures and photon statistics	159
8.8	Conclusions	161
Chapter 9. Publication: Probing Quantum Phases of Ultracold Atoms in Optical Lattices by Transmission Spectra in Cavity QED		167
III	Self-Organization of Atoms in Optical Lattices	179

Chapter 10. Background: Self-Organization of Atoms in a Cavity	181
10.1 Collective Cooling and Spatial Self-Organization of Atoms	181
10.2 The Bose-Hubbard Hamiltonian for Transverse Motion	184
 Chapter 11. Publication: Entanglement Assisted Fast Reordering of Atoms in an Optical Lattice within a Cavity at $T = 0$	 189
 Chapter 12. Publication: Microscopic Physics of Quantum Self- Organisation of Optical Lattices in Cavities	 199
12.1 Introduction	199
12.2 System, Models	200
12.3 Discussion	203
12.4 Single-particle dynamics	204
12.5 Two-particle dynamics	207
12.6 Conclusions	212
 Curriculum Vitae	 215

CHAPTER 1

GENERAL INTRODUCTION

In science one tries to tell people, in such a way as to be understood by everyone, something that no one ever knew before. But in poetry, it's the exact opposite.
Paul Dirac

The work presented in this thesis is based in the field of atomic, molecular and optical (AMO) physics and focuses on the theory of cold atoms in optical lattices and cavity quantum electrodynamics, both topics with impressive progress in the last century. Atoms in optical cavities show a multifarious nonlinear behavior, due to the complex mutual interference of the atomic positions and the intracavity field. The main objective of this work is to utilize these nonlinear effects and provide new perspectives in the field of cold atoms in optical lattices.

Introduction

As already indicated by its name, AMO physics incorporates a wide variety of research areas, each marking its own subject with important achievements with broad impact. Nevertheless, there are strong interactions between the various research areas, establishing a fruitful interdisciplinary symbiosis. Atomic physics addresses questions concerning the properties of atoms and their structure as well as collisions between atoms and interactions with solids and external fields. Molecular physics investigates the structure and properties of molecules and their clusters. Finally, modern optical sciences covers a broad spectrum of topics, e.g. nonlinear and ultrafast optics, coherent sources of light and quantum optics.

Besides the aforementioned variety of addressed issues, AMO research provides the means for answering fundamental physical questions by facilitating the most accurate techniques of measurement, available in physics. As a matter of fact, highly accurate measurements of time (and equivalently frequency), feasible with amazing precision, are allocated by atomic physics.

Moreover, AMO physics develops new concepts and technologies with broad impact, whose recipients are branches as diverse as astronomy, biology, chemistry, computational and material science, engineering, medicine and telecommunication. As a valuable side-effect, the necessary experimental and computational tools in the development of AMO sciences are applied in other areas too.

A common feature in the biggest part of AMO physics is that the progress of theory accompanies the progress in experimental research, leading to testable theoretical predictions,

while other branches of physics suffer from a divergence of theoretical results and experimental verification. Hence, the role of theoretical work in AMO research is twofold: It proposes new experiments as well as it formulates new concepts and develops new theoretical tools to allow for a further understanding of open questions in AMO physics as well as in other areas of physics.

The mutual actuation of theoretical and experimental progress, and the applicability of AMO physics to give insight to problems, originating from other branches of physics, ensure that AMO physics keeps being a growing, highly active field with broad impact. As an indicator of this may serve the fact that the Nobel committee of Sweden has awarded several Nobel prizes to the AMO community in recent years.

General Historical Development of Atom-Optics

The 14th of December 1900 marked the beginning of a new physical era. At that time, Max Planck presented his visionary idea of discretized energy levels to derive the formula for blackbody radiation [1]. Although Planck himself attached no deeper relevance to this ad hoc considerations, a revolution of the physical view of the world was irrevocably initiated.

Quantum Theory, which arose from that origin, was then developed during the 1920s by people like Bohr, Born, Schrödinger and Heisenberg, and was initially purely fundamental research. It accounted for the stability and the emission spectra of atoms and molecules and furthermore could explain phenomena, in contrast to classical physics, like the photoelectric [2] and the Compton effect [3].

Spectacular observations soon demonstrated the counter-intuitive nature of quantum mechanics, for instance the wave nature of matter [4]. However, an experimental investigation of other phenomena, located in the heart of quantum theory, like entanglement and the corresponding Schrödinger-cat paradox, seemed beyond an ever possible realization. At that time, experimental techniques were much too less sophisticated, to allow for a manipulation and observation of single atoms.

The most important step towards manipulation at an ultimate quantum level was the invention of the laser 50 years ago [5], certainly the invention of AMO physics with the broadest influence on other physical branches. Primarily considered as a fancy laboratory toy, the facility of creating coherent, nearly monochromatic light pulses became the very tool in experimental physics. Evidently, not one of the modern experiments mentioned in this thesis is thinkable without the existence of lasers. Besides the wide applications in metrology, completely new branches like laser spectroscopy [6], laser chemistry [7], or in principle even quantum optics [8–10] were established or essentially promoted; not to forget the applications of laser technology in our everyday life.

Let us glance at the development of the laser and its applications towards the realization of the state-of-the-art techniques, providing the necessary equipment for today's fascinating experiments. For a long time, manipulation of single atoms or molecules seemed an unimaginable task. Nevertheless, AMO physics was able to overcome all technological and theoretical hurdles. First, trapping of single ions, pioneered by Paul and Dehmelt [11, 12],

was realized in groundbreaking [13, 14]. As a second step, laser cooling enabled efficient cooling of neutral atoms to very low temperatures. In its simplest form, Doppler cooling, atoms absorb photons, red detuned from the atomic resonance frequency, from counter-propagating laser beams. Spontaneous re-emitting of photons in random directions leads to a net cooling force [15–18]. More elaborate schemes, allowing for cooling atoms below the Doppler limit, followed. Schemes like polarization-gradient cooling [19] or velocity-selective coherent population trapping (VSCPT) [20] were able to cool certain species of atoms to temperatures in the nano-Kelvin regime. For reviews of the fascinating subject of cooling and trapping of atoms and ions with light, awarded with the Nobel prize in 1997 for Claude Cohen-Tannoudji, Steven Chu and William Phillips, see [21–25].

With this high level of control and manipulation, the next step was the realization of a phenomenon, known already since the 1920s. Bose and Einstein [26, 27] realized that a macroscopic fraction of bosons, cooled to extremely low temperatures, occupy the same single-particle quantum state. Finally in 1995, the first experimental realizations of a so-called Bose-Einstein condensate (BEC) [28–31] were accomplished with dilute atomic vapors [32–34]. In addition to the above mentioned laser-based cooling methods, a new method, evaporative cooling [35–38], had to be invented, to provide for the extremely low temperatures of few micro-Kelvin to nano-Kelvin and the necessary phase-space densities of $10^{13} - 10^{15} \text{ cm}^{-3}$ to observe the phase transition. Since BEC is the matter counterpart of laser light, it envisioned similar intriguing perspectives. In the first years after these pioneering experiments, the research focused upon studies concerning the wave nature of matter. Among others, this included investigations and observations of interference fringes of matter waves, superfluid properties and collective excitations in BEC, nonlinear wave mixing, as well as the realization of an atom laser [39–42]. Additionally, it was possible to create BEC for a variety of atomic species. The current list of established BECs contains all stable bosonic isotopes of alkali atoms [36], i.e. Hydrogen, Lithium, Sodium, Potassium, two isotopes of Rubidium and Cesium [43], as well as Chromium [44], Ytterbium [45], and metastable Helium [46, 47].

Even though an impressive level of control over single atomic systems was already reached, to obtain the above mentioned BEC of Cesium, more had to be done. With the help of magnetic [48–51] and optical Feshbach resonances [52–54] it was possible to tune the on-site interactions, by ramping an external magnetic field, from repulsive to attractive or vice versa. This was a key ingredient for the production of the Cesium BEC. Moreover, it allowed for exploring new physical effects and spellbinding applications in the context of many-particle physics. For instance, new quantum phases were realized, like degenerate Fermi gases [55–58] and Bose-Fermi mixtures [59–62]. By ramping across the resonance, ultracold molecules can be formed from pairs of atoms, condensing to a molecular BECs [63–70], as well as to diatomic heteronuclear molecular BECs [71–73]. Furthermore, it was possible to observe several theoretically predicted phenomena, like the BEC-BCS crossover, in quantum degenerate Fermi gases [74–80] or the incidence of trimer states, the so-called Efimov states [81].

Obviously, the tendency of AMO research was towards the study of fundamental questions in many-body physics. To allow for an investigation of strongly correlated systems, cold atoms had to be implemented in optical lattices. The development of this novel research field within the last 10 years will be presented in the subsequent section.

Beforehand, we want to mention that AMO physics plays an important role in another highly active branch of physics. After Feynman had noticed the fundamental significance of

entanglement of quantum states when it comes to numerically simulate physics [82], the field of *quantum information processing and quantum computation* arose, with impressive progress in a relatively short time [83–86]. In the meantime a number of applications were provided by this theory, like quantum cryptography, which makes it possible that two parties can communicate completely secure via quantum channels [87–90]. There are already systems using these techniques commercially available.

To realize the ultimate goal of this field, a universal quantum computer, several models have been invented. For instance, the quantum circuit model [83], the one-way quantum computer [91–94], adiabatic quantum computing [95–99] and topological quantum computation [100–104]. All of these schemes have in common that initialization and read-out procedures, for the storage and processing of the basic unit of quantum information (q-byte), realized by a quantum two-level system, have to be realized. Further conditions are scalability and long coherence times [105]. As a matter of fact, several AMO systems, fulfill more or less all of these requirements, and are promising candidates for the implementation of quantum information processing and quantum computing [106–119].

Cold Atoms in Optical Lattices

After studying weakly interacting dilute gases, tuning collisional properties via Feshbach resonances, opened up the the possibility of investigation of strongly correlated phases.

Hubbard-type lattice models typically emerge from questions, concerning strongly correlated systems in traditional condensed matter physics. In a seminal work Dieter Jaksch and coworkers showed [120], that cold atoms, loaded and trapped in optical lattices allow for engineering such strongly correlated systems within the field of AMO physics. The periodic arrays of (optical) potential wells are provided by so-called optical lattices (see chapter 2), which are created by counter-propagating laser fields.

A major advantage of AMO physics, compared to solid state physics, is the impressive level of control over many of the relevant parameters of their systems. This opened up a plethora of promising applications in the theory of condensed matter physics, where experimental verifications of theoretical predictions are a much harder task. By means of AMO physics, several phenomena of condensed matter physics could be observed for the first time. Firstly, it was possible to experimentally observe the predicted phase transition from the Mott insulator phase to the superfluid phase [121–123], as demonstrated by beautiful experiments of Greiner et al. [124, 125].

Adjusting the parameters of the optical lattice and external fields, allow for a serious toolbox of techniques to control the dynamic of the atoms in the lattice [126]. Easily the lattice depth can be varied, by changing the power of the intersecting lasers. This results in a reduced tunneling rate of the atoms. Furthermore, even on-site interactions inside lattice wells can be tailored using Feshbach resonances [127]. A modification of the configuration of the lattice lasers, a plurality of lattice geometries are possible, e.g. rectangular, triangular and Kagomé lattices [126, 128–130]. If the intensities of the lasers differ from direction to direction, non-homogeneous lattices are generated. Hence, effectively two-dimensional or one-dimensional lattices can be generated, when the optical potentials in one or two directions

are very deep. Hence, the atoms are very tightly trapped in these directions. For this reason, it was possible to realize systems of hard-core bosons in 1D [131, 132], observe the Mott insulator to superfluid transition in 1D [133–135] and 2D [136]. Moreover, cold atoms in optical lattices allowed for an experimental observation of fascinating predictions from low-dimensional physics, like the equivalence of a system of strongly interacting, hard-core 1D Bosons (Tonks-Girardeau gas) and non-interacting 1D Fermions [137, 138]. This equivalence is known as *fermionization*. Very recently, the group of Jean Dalibard demonstrated the existence of the Berezinskii-Kosterlitz-Thouless phase transition in 2D [139].

Several theoretical proposals exist for the applications of these techniques to investigate extended systems, including spin models with interesting new phases [130, 140–143], the Kondo effect and other issues concerning impurities [144, 145], spin glass systems [146], lattice gauge theories [147], properties of Luttinger liquids [148], and investigations concerning the superfluidity of Fermions [149, 150].

In general, optical lattices are very uniform and only few impurities are present, which assists the engineering of the condensed matter lattice models. Besides, superimposing lattices with commensurate frequencies allows to create superlattices with complex structure [151]. Disordered systems can be studied by applying non-commensurate frequencies, leading to pseudo-random disorder, whereas adding a laser speckle pattern generates random disorder [130, 146].

Cold atoms in optical lattices are well isolated and relatively insensitive to perturbations from the environment. This leads to coherent dynamics on long timescales [152], compared to systems in condensed matter physics. A consequence of this good isolation is the possibility of the creation of repulsively bound atom pairs, by means of Feshbach resonances, as recently observed [153]. Finally, these systems are accessible for several types of spectroscopic measurements, like interference experiments from atoms released from the traps [124, 125] and detection of coincidences and density-density correlations [154–156].

AMO physics provides perspectives for the implementation of quantum information and engineering entanglement using cold atoms in optical lattices. Besides the long coherence times, implied by the exceptionally well isolation of these systems, another advantage is their inherent scalability. Several proposals to perform gate operations exist, including operations via collisional or dipole interactions [157–160], operations based on atomic tunneling between adjacent wells [161, 162] or based on the motional state of atoms [163], as well as operations based on strong dipole-dipole interactions between Rydberg atoms [164]. Cluster states are required to perform one-way quantum computing. A one-dimensional version of these states have been created, by entangling a large array of atoms via controlled collisions [165]. A subtle task is the individual addressing of atoms in the particular sites optical lattices. One possible way to resolve these difficulties is to use marker atoms [166].

However, at the present time, the primary function of systems of cold atoms in optical lattices, is to simulate models from traditional condensed matter physics, which are intractable there [167]. This agrees with the visionary idea of Feynman, established already 30 years ago [82].

The present thesis provides a first step to merge systems of cold atoms in optical lattices with another versatile element of quantum optics, namely optical cavity resonators. Along the lines of cold atoms, the investigations - both in experiment and theory - of this system

have experienced tremendous progress within the last decade. A brief introduction to basic theoretical results of cavity quantum electrodynamics (CQED), required for the rest of this thesis, is presented in chapter 3. The next section is devoted to a sketch of the historical development of the field.

Cavity Quantum Electrodynamics (CQED)

As a matter of principle, the theory of cavity quantum electrodynamics was inherently included immediately from the first appearance of quantum theory, since Planck considered quantized modes of the electromagnetic field inside a cavity [1]. However, modern CQED deals with the interaction of atoms, enclosed in a resonator, with (few) modes of the intra-cavity field.

The interaction between atoms and the electromagnetic field, in particular the light field, in free space is straightforward. Matter influences light via a refractive index, to be inserted in Maxwell's equation. On the other hand, light exerts forces on particles, entering Newton's equations. Is the atom enclosed by a resonator, which implies specific boundary conditions for the field, the situation drastically changes. The dynamics of light and matter is no longer independent, since they mutually influence each other. Especially in the strong coupling regime, where the atom is strongly coupled to a single cavity mode (see chapter 3), the cavity and the atom have to be considered as a single entity, the atom-cavity system.

The origin of modern CQED lies in the 1940s, where Purcell recognized that the modified boundary conditions for the electromagnetic field have a grave influence on the spontaneous emission rate of atoms enclosed in the cavity [168]. This is known as the Purcell effect. However, the cavity here merely plays a passive role, by modifying the density of the mode, which interacts with the atom. The dynamical influence of the cavity field plays only a minor role here. As we pointed out in the sections before, single-atom experiments require a high level of experimental tools. Hence, the observation of the modified atomic lifetimes due to the presence of a cavity, succeeded almost 40 years after Purcell's prediction [169–171]. The interaction strength with (quantized) field modes is determined by the electric dipole moment of the atom (the interaction of atoms with quantized resonator modes was first described by Jaynes [172]). Hence, these experiments were performed using the large dipole moment of Rydberg atoms, as proposed by Kleppner [173].

To explore the ultimate quantum level, where the cavity light field dynamics is no longer irrelevant, the system has to reside in the so-called *strong coupling regime*. There, the coupling strength, given by the single-photon Rabi-frequency (see chapter 3), has to exceed all possible dissipative processes (mainly, spontaneous emission rate of the atoms and the loss rate loss of cavity photons) and the inverse of the interaction time.

Primarily, the strong coupling regime, was reached for microwave cavities in the 1980s [174, 175]. Since then, a rich variety of theoretically predicted effects have been observed, including Rabi oscillations in a small quantum field [176], sub-Poissonian [177] and trapping field states [178], bistable behavior [179], as well as a direct proof of field quantization [180], decoherence of quantum superpositions [181] and Fock state generation [182, 183].

In the optical domain, reaching the strong coupling regime is a much more demanding task. Due to the short wavelength, tiny cavities, with a length in the micro-meter regime, are needed. Hence, the photons have to undertake many round-trips in the cavity, which has to be provided by extremely good mirrors. In the seminal experiment of Thompson et al. [184], the so-called vacuum Rabi-splitting (see chapter 3) of the transmission spectrum of a probe laser was observed. During the aforementioned round-trips, the atom is constantly absorbing a photon followed by a re-emission into the cavity mode. This oscillatory exchange of excitation could be observed [185], using a homodyne measurement of a transmitted field.

The efforts for reaching the optical strong coupling regime are worthwhile. The photons carry a larger momentum, which amounts to larger forces exerted on the atoms at an absorption event. This leads to astonishing effects and prospective applications. For instance, laser-cooled atoms, traversing the cavity, can be individually detected [186–188]. The laser-cooling scheme slows down the atoms, yielding a long interaction time. This allows to observe the effects of the light field on the atom, which itself alters the light field. Hence, the combined dynamics of the atom-cavity field is visible [189, 190]. To carry this mechanism to the extremes, Hood et al. [191] and Pinkse et al. [192] demonstrated the trapping of a single atom in the light field of only a single photon.

Extended manipulations require enhanced extra trapping time of the atom. Trapping of atoms in free space by means of optical dipole force traps, consisting of an optical beam, far red-detuned from the atomic resonance, was already accomplished. Hence, it was evident to implement such a far off-resonant trap (FORT) in an optical resonator and decouple the trapping from the interaction with the (quantized) cavity mode. For red detuning, the dipole force trap induces an attractive force towards the field antinodes of the optical beam. For a proper choice of the beam’s frequency, strongly enhanced trapping times are achieved for atoms near the center of the cavity [193, 194]. Recently, the group of Rempe established a blue-detuned dipole trap, where the atoms are attracted towards the nodes of the potential. Due to the absence of large Stark shifts for all atomic states in such a trap, the free-space properties of the atoms are hardly influenced. This has several advantages concerning fluctuation and heating issues [195].

An major drawback of laser-cooling is the requirement of closed optical cycles, to constantly repeat scattering events, which provides for the dissipation of energy. Unfortunately, several particles do not meet this requirement. This especially holds for molecules with their continuum-like spectra of rotational and vibrational states. Here, the atom-cavity system provides a different possibility for dissipation. In the strong-coupling limit, where the atom and the cavity form one entity, the reaction of the light field on atomic motion does not occur immediately. This delay leads to a dissipative force and energy, which is stored in the cavity field, can leak out of the cavity via loss of photons. This dynamical cavity cooling was proposed first by our group [196], and has been thoroughly studied since then [197–199]. The experimental realization of this cooling scheme was first done by Maunz et al. [200]. The achievable limit of the cooling temperature scales with the cavity loss rate, which can be significantly lower than the Doppler limit. Moreover, since no closed optical cycle is needed, dynamical cavity cooling provides promising perspectives to efficiently cool molecules, as suggested by Vuletić and Chu [201], or even atomic qubits [202].

In the aforementioned experiments, a probe laser was driving the cavity via one of its mirrors. Variations of this configuration, including the application of a laser field, transversally

to the cavity axis, which directly excites the atom, allowed for cooling in the directions of this driving laser field [203–205]. In combination with laser-cooling and an additional dipole trap in radial directions, cavity cooling in all spatial directions was realized [206].

Another configuration consists of several mirrors, assembling a ring cavity, where the enclosed atom is interacting with two counterpropagating modes [207–209].

Cavity QED also provides interesting features for many-body physics. If many atoms are present, collective effects in standard cavities [210] or in ring cavities [211–215] were observed. One prominent example of these collective effects is the spatial self-organization of atoms in transversally pumped cavities, as predicted in our group [216, 217] and firstly observed by Black et al. [218].

Let us finally regard the relevance of CQED for quantum information processing. There its role is twofold: On the one hand, it serves as a tool. Several quantum information applications, based on AMO proposals, require a deterministic source of single photons [109], a so-called photon pistol. Single photons “on demand” were provided by means of optical cavities [219–222]. Furthermore, the vacuum Rabi splitting in a cavity (see chapter 3) allows for state-sensitive detection of atoms [189, 190, 193]. On the other hand, various proposals for an active role of cavities for quantum information processing exist [223]. Atoms, strongly coupled to a cavity mode, constitute a matter-light interface, with which the implementation of a quantum gate between single photon qubits [224] or the mapping of quantum states between atoms and photons [225], is possible.

Overview

Besides the present general introduction, this thesis contains seven articles and one preprint, together with three extra chapters, clarifying the theoretical background of the publications. Each chapter contains its own bibliography. At the beginning of each article, a short note indicates the primary contribution of the author of the present thesis to that article.

The thesis is divided into three parts. Part I, *Ultracold Atoms in Optical Lattices Enclosed in an Optical Cavity*, provides in two chapters a brief theoretical introduction to the two main topics, discussed in this thesis. Chapter 2 introduces the field of *Cold Atoms in Optical Lattices* and chapter 3 gives an introduction to *Cavity Quantum Electrodynamics*. Two articles and one preprint follow in the subsequent chapters. In chapter 4 we elaborate on the issue of *Quantized Motion of Laser-Driven Atoms in a Cavity Field*, where we consider a single potential well of the optical potential inside the resonator. Chapter 5, *Cold Atom Dynamics in a Quantum Optical Lattice Potential* outlines the basic features of strongly-correlated ultracold atoms in an optical lattice, which itself is generated by the resonator. Here, a generalization of the Bose-Hubbard model is presented. Finally, chapter 6 discusses in depth this model and its restrictions, considers further properties and provides possible applications.

Part II of this thesis, *Probing Atomic Phases in Optical Lattices*, contains three articles, where we propose new methods for non-destructively probing the atomic phase of an ensemble of cold atoms in an optical lattice, by means of cavity QED. The first, in chapter 7, *Cavity Enhanced Light Scattering in Optical Lattices to Probe Atomic Quantum Statistics*, gives

an outline of the general mechanism, how angle resolved measurements of photon number and variance are capable of supplying information about atom-number fluctuations and pair correlations. An in-depth analysis of this method is provided in chapter 8, *Light Scattering from Ultracold Atoms in Optical Lattices as an Optical Probe of Quantum Statistics*. Here, off-resonant collective light scattering from ultracold atoms trapped in an optical lattice is generally studied. All the calculations of the various statistical quantities, necessary for the proposal of chapter 7 are provided here. Chapter 9, *Probing Quantum Phases of Ultracold Atoms in Optical Lattices by Transmission Spectra in Cavity QED*, points out a fundamentally different, but also nondestructive method of probing atomic phases. Here, we show how to map atomic quantum statistics on transmission spectra of high- Q cavities. The predicted effects in this part are accessible in experiments that have recently become possible and allow, for instance, for a detailed observation of the Mott insulator to superfluid phase transition.

The third part of this thesis, *Self-Organization of Atoms in Optical Lattices*, is devoted to a microscopic analysis of the collective self-ordering process. After an introduction, provided in chapter 10, two articles are presented. Chapter 11, *Entanglement Assisted Fast Reordering of Atoms in an Optical Lattice within a Cavity at $T = 0$* , elaborates on the relevance of atom-field entanglement in a spatial atomic reordering process towards an ordered state in a transversally pumped cavity. We discuss several possible approaches to this issue, showing that entanglement, absent in a semiclassical treatment, is a generic feature for quantum phase transitions in optical potentials. This discussion is extended in chapter 12, *Microscopic Physics of Quantum Self-Organization of Optical Lattices in Cavities*, where a detailed discussion of the results of the foregoing article is presented and extended calculations are accomplished.

The thesis is concluded with a curriculum vitae.

Bibliography

- [1] M. Planck, *Zur Theorie des Gesetzes der Energieverteilung im Normalspektrum*, Verh. Deut. Phys. Ges. **2**, 202 (1900).
- [2] A. Einstein, *Über einen die Erzeugung und Verwandlung des Lichtes betreffenden heuristischen Gesichtspunkt*, Ann. Phys. **322**, 132 (1905).
- [3] A. H. Compton, *A Quantum Theory of the Scattering of X-Rays by Light Elements*, Phys. Rev. **21**, 483 (1923).
- [4] C. Davisson and L. H. Germer, *Diffraction of Electrons by a Crystal of Nickel*, Phys. Rev. **30**, 705 (1927).
- [5] A. L. Schawlow and C. H. Townes, *Infrared and Optical Masers*, Phys. Rev. **112**, 1940 (1958).
- [6] See, for example, W. Demtröder, *Laser Spectroscopy*, 3rd Ed. (Springer, Berlin, 2003).
- [7] See, for example, H. H. Telle, A. G. Ureña, and R. J. Donovan, *Laser Chemistry: Spectroscopy, Dynamics and Applications*, (John Wiley and Sons, New York, 2007).

-
- [8] C. Cohen-Tannoudji, J. Dupont-Roc, and G. Grynberg, *Atom-Photon Interactions: Basic Processes and Applications*, (John Wiley and Sons, New York, 1992).
 - [9] D. F. Walls and G. J. Milburn, *Quantum Optics*, (Springer, Heidelberg, 1994).
 - [10] M. O. Scully and M. S. Zubairy, *Quantum Optics*, (Cambridge University Press, Cambridge, 1997).
 - [11] H. G. Dehmelt, *Radiofrequency Spectroscopy of Stored Ions I: Storage*, Adv. At. Mol. Phys. **3**, 53 (1967); H. G. Dehmelt, *Radiofrequency Spectroscopy of Stored Ions II: Spectroscopy*, Adv. At. Mol. Phys. **5**, 109 (1969).
 - [12] W. Paul, *Electromagnetic Traps for Charged and Neutral Particles*, Rev. Mod. Phys. **62**, 531 (1990).
 - [13] W. Neuhauser, M. Hohenstatt, P. E. Toschek, and H. Dehmelt, *Localized Visible Ba^+ Mono-Ion Oscillator*, Phys. Rev. A **22**, 1137 (1980).
 - [14] D. J. Wineland and W. M. Itano, *Spectroscopy of a Single Mg^+ Ion*, Phys. Lett. **82A**, 75 (1981).
 - [15] T. W. Hänsch and A. L. Schawlow, *Cooling of Gases by Laser Radiation*, Opt. Comm. **13**, 68 (1975).
 - [16] D. J. Wineland, R. E. Drullinger, and F. L. Walls, *Radiation-Pressure Cooling of Bound Resonant Absorbers*, Phys. Rev. Lett. **40**, 1639 (1978).
 - [17] V. S. Letokhov and V. G. Minogin, *Laser Radiation Pressure Force on Free Atoms*, Phys. Rep. **73**, 1 (1981).
 - [18] J. Prodan, A. Migdall, W. D. Phillips, I. So, and H. Metcalf, *Stopping Atoms with Laser Light*, Phys. Rev. Lett. **54**, 992 (1985); A. L. Migdall, J. V. Prodan, W. D. Phillips, T. H. Bergeman, and H. J. Metcalf, *First Observation of Magnetically Trapped Neutral Atoms*, Phys. Rev. Lett. **54**, 2596 (1985).
 - [19] J. Dalibard and C. Cohen-Tannoudji, *Laser Cooling Below the Doppler Limit by Polarization Gradients: Simple Theoretical Models*, J. Opt. Soc. Am. B **6**, 2023 (1989).
 - [20] A. Aspect, E. Arimondo, R. Kaiser, N. Vansteenkiste, and C. Cohen-Tannoudji, *Laser Cooling Below the One-Photon Recoil Energy by Velocity-Selective Coherent Population Trapping*, Phys. Rev. Lett. **61**, 826 (1988).
 - [21] S. Chu, *Nobel Lecture: The Manipulation of Neutral Particles*, Rev. Mod. Phys. **70**, 685 (1998).
 - [22] C. Cohen-Tannoudji, *Nobel Lecture: Manipulating Atoms with Photons*, Rev. Mod. Phys. **70**, 707 (1998).
 - [23] W. D. Phillips, *Nobel Lecture: Laser Cooling and Trapping of Neutral Atoms*, Rev. Mod. Phys. **70**, 721 (1998).

- [24] H. J. Metcalf and P. van der Straten, *Laser Cooling and Trapping*, (Springer, New York, 1999).
- [25] C. E. Wieman, D. E. Pritchard, and D. J. Wineland, *Atom Cooling, Trapping, and Quantum Manipulation*, Rev. Mod. Phys. **71**, S253 (1999).
- [26] S. N. Bose, *Plancks Gesetz und Lichtquantenhypothese*, Z. Phys. **26**, 178 (1924).
- [27] A. Einstein, *Quantentheorie des einatomigen idealen Gases*, Sitzungsberichte der Preussischen Akademie der Wissenschaften, Physikalisch-mathematische Klasse, p. 261 (1924).
- [28] F. Dalfovo, S. Giorgini, L. Pitaevskii, and S. Stringari, *Theory of Bose-Einstein Condensation in Trapped Gases*, Rev. Mod. Phys. **71**, 463 (1999).
- [29] A. Leggett, *Bose-Einstein Condensation in the Alkali Gases: Some Fundamental Concepts*, Rev. Mod. Phys. **73**, 307 (2001).
- [30] C. Pethick and H. Smith, *Bose-Einstein Condensation in Dilute Gases*, (Cambridge University Press, Cambridge, 2001).
- [31] L. Pitaevskii and S. Stringari, *Bose-Einstein Condensation*, (Oxford University Press, Oxford, 2003).
- [32] M. H. Anderson, J. R. Ensher, M. R. Matthews, C. E. Wieman, and E. A. Cornell, *Observation of Bose-Einstein Condensation in a Dilute Atomic Vapor*, Science **269**, 198 (1995).
- [33] C. C. Bradley, C. A. Sackett, J. J. Tollett, and R. G. Hulet, *Evidence of Bose-Einstein Condensation in an Atomic Gas with Attractive Interactions*, Phys. Rev. Lett. **75**, 1687 (1995).
- [34] K. B. Davis, M. -O. Mewes, M. R. Andrews, N. J. van Druten, D. S. Durfee, D. M. Kurn, and W. Ketterle, *Bose-Einstein Condensation in a Gas of Sodium Atoms*, Phys. Rev. Lett. **75**, 3969 (1995).
- [35] See for example, W. Ketterle and N. J. van Druten, *Evaporative Cooling of Trapped Atoms*, Adv. At. Mol. Opt. Phys. **37**, 181 (1996).
- [36] For an overview, see *Ultracold Matter*, Nature Insight, Nature (London) **416**, 205-246 (2002).
- [37] C. C. Bradley, C. A. Sackett, and R. G. Hulet, *Bose-Einstein Condensation of Lithium: Observation of Limited Condensate Number*, Phys. Rev. Lett. **78**, 985 (1997).
- [38] M. D. Barrett, J. A. Sauer, and M. S. Chapman, *All-Optical Formation of an Atomic Bose-Einstein Condensate*, Phys. Rev. Lett. **87**, 010404 (2001).
- [39] D. S. Jin, J. R. Ensher, M. R. Matthews, C. E. Wieman, and E. A. Cornell, *Collective Excitations of a Bose-Einstein Condensate in a Dilute Gas*, Phys. Rev. Lett. **77**, 420 (1996).

-
- [40] M. O. Mewes, M. R. Andrews, N. J. van Druten, D. M. Kurn, D. S. Durfee, C. G. Townsend, and W. Ketterle, *Collective Excitations of a Bose-Einstein Condensate in a Magnetic Trap*, Phys. Rev. Lett. **77**, 988 (1996).
 - [41] M. R. Andrews, C. G. Townsend, H. J. Miesner, D. S. Durfee, D. M. Kurn, and W. Ketterle, *Observation of Interference Between Two Bose Condensates*, Science **275**, 637 (1997).
 - [42] M. O. Mewes, M. R. Andrews, D. M. Kurn, D. S. Durfee, C. G. Townsend, and W. Ketterle, *Output Coupler for Bose-Einstein Condensed Atoms*, Phys. Rev. Lett. **78**, 582-585 (1997).
 - [43] T. Weber, J. Herbig, M. Mark, H. -C. Nägerl, and R. Grimm, *Bose-Einstein Condensation of Cesium*, Science **299**, 232 (2003).
 - [44] A. Griesmaier, J. Werner, S. Hensler, J. Stuhler, and T. Pfau, *Bose-Einstein Condensation of Chromium*, Phys. Rev. Lett. **94**, 160401 (2005).
 - [45] Y. Takasu, K. Maki, K. Komori, T. Takano, K. Honda, M. Kumakura, T. Yabuzaki, and Y. Takahashi, *Spin-Singlet Bose-Einstein Condensation of Two-Electron Atoms*, Phys. Rev. Lett. **91**, 040404 (2003).
 - [46] A. Robert, O. Sirjean, A. Browaeys, J. Poupard, S. Nowak, D. Boiron, C. I. Westbrook, and A. Aspect, *A Bose-Einstein Condensate of Metastable Atoms*, Science **292**, 461 (2001).
 - [47] F. Pereira Dos Santos, J. Leonard, J. Wang, C. J. Barrelet, F. Perales, E. Rasel, C. S. Unnikrishnan, M. Leduc, and C. Cohen-Tannoudji, *Bose-Einstein Condensation of Metastable Helium*, Phys. Rev. Lett. **86**, 3459 (2001).
 - [48] S. Inouye, M. R. Andrews, J. Stenger, H. -J. Miesner, D. M. Stamper-Kurn, and W. Ketterle, *Observation of Feshbach resonances in a Bose-Einstein condensate*, Nature (London) **392**, 151 (1998).
 - [49] J. L. Roberts, N. R. Claussen, J. P. Burke, Jr. , C. H. Greene, E. A. Cornell, and C. E. Wieman, *Resonant Magnetic Field Control of Elastic Scattering in Cold ^{85}Rb* , Phys. Rev. Lett. **81**, 5109 (1998).
 - [50] Ph. W. Courteille, R. S. Freeland, D. J. Heinzen, F. A. van Abeelen, and B. J. Verhaar, *Observation of a Feshbach Resonance in Cold Atom Scattering*, Phys. Rev. Lett. **81**, 69 (1998).
 - [51] S. L. Cornish, N. R. Claussen, J. L. Roberts, E. A. Cornell, and C. E. Wieman, *Stable ^{85}Rb Bose-Einstein Condensates with Widely Tunable Interactions*, Phys. Rev. Lett. **85**, 1795 (2000).
 - [52] P. O. Fedichev, Yu. Kagan, G. V. Shlyapnikov, and J. T. M. Walraven, *Influence of Nearly Resonant Light on the Scattering Length in Low-Temperature Atomic Gases* Phys. Rev. Lett. **77**, 2913 (1996).

- [53] J. Bohn and P. Julienne, *Prospects for Influencing Scattering Lengths with Far-Off-Resonant Light*, Phys. Rev. A **56**, 1486 (1997).
- [54] M. Theis, G. Thalhammer, K. Winkler, M. Hellwig, G. Ruff, R. Grimm, and J. Hecker Denschlag, *Tuning the Scattering Length with an Optically Induced Feshbach Resonance*, Phys. Rev. Lett. **93**, 123001 (2004).
- [55] B. DeMarco and D. S. Jin, *Onset of Fermi Degeneracy in a Trapped Atomic*, Science **285**, 1703 (1999).
- [56] A. G. Truscott, K. E. Strecker, W. I. McAlexander, G. B. Partridge, and R. G. Hulet, *Observation of Fermi Pressure in a Gas of Trapped Atoms*, Science **291**, 2570 (2001).
- [57] T. Loftus, C. A. Regal, C. Ticknor, J. L. Bohn, and D. S. Jin, *Resonant Control of Elastic Collisions in an Optically Trapped Fermi Gas of Atoms*, Phys. Rev. Lett. **88**, 173201 (2002).
- [58] L. Pezzé, L. Pitaevskii, A. Smerzi, S. Stringari, G. Modugno, E. de Mirandes, F. Ferlaino, H. Ott, G. Roati, and M. Inguscio, *Insulating Behavior of a Trapped Ideal Fermi Gas*, Phys. Rev. Lett. **93**, 120401 (2004).
- [59] G. Roati, F. Riboli, G. Modugno, and M. Inguscio, *Fermi-Bose Quantum Degenerate ^{40}K - ^{87}Rb Mixture with Attractive Interaction*, Phys. Rev. Lett. **89**, 150403 (2002).
- [60] A. Simoni, F. Ferlaino, G. Roati, G. Modugno, and M. Inguscio, *Magnetic Control of the Interaction in Ultracold K-Rb Mixtures*, Phys. Rev. Lett. **90**, 163202 (2003).
- [61] F. Ferlaino, C. D’Errico, G. Roati, M. Zaccanti, M. Inguscio, G. Modugno, and A. Simoni, *Feshbach Spectroscopy of a K-Rb Atomic Mixture*, Phys. Rev. A **73**, 040702(R) (2006).
- [62] M. Zaccanti, C. D’Errico, F. Ferlaino, G. Roati, M. Inguscio, and G. Modugno, *Control of the Interaction in a Fermi-Bose Mixture*, Phys. Rev. A **74**, 041605(R) (2006).
- [63] R. Wynar, R. S. Freeland, D. J. Han, C. Ryu, and D. J. Heinzen, *Molecules in a Bose-Einstein Condensate*, Science **287**, 1016 (2000).
- [64] E. A. Donley, N. R. Claussen, S. T. Thompson, and C. E. Wieman, *Atom-Molecule Coherence in a Bose-Einstein Condensate*, Nature (London) **417**, 529 (2002).
- [65] M. Greiner, C. A. Regal, and D. S. Jin, *Emergence of a Molecular Bose-Einstein Condensate from a Fermi Gas*, Nature (London) **426**, 537 (2003).
- [66] M. W. Zwierlein, C. A. Stan, C. H. Schunck, S. M. F. Raupach, S. Gupta, Z. Hadzibabic, and W. Ketterle, *Observation of Bose-Einstein Condensation of Molecules*, Phys. Rev. Lett. **91**, 250401 (2003).
- [67] S. Jochim, M. Bartenstein, A. Altmeyer, G. Hendl, S. Riedl, C. Chin, J. Hecker Denschlag, and R. Grimm, *Bose-Einstein Condensation of Molecules*, Science **302**, 2101 (2003).

-
- [68] J. Herbig, T. Kraemer, M. Mark, T. Weber, C. Chin, H. -C. Nägerl, and R. Grimm, *Preparation of a Pure Molecular Quantum Gas*, Science **301**, 1510 (2003).
- [69] K. E. Strecker, G. B. Partridge, and R. G. Hulet, *Conversion of an Atomic Fermi Gas to a Long-Lived Molecular Bose Gas*, Phys. Rev. Lett. **91**, 080406 (2003).
- [70] J. Cubizolles, T. Bourdel, S. J. J. M. F. Kokkelmans, G. V. Shlyapnikov, and C. Salomon, *Production of Long-Lived Ultracold Li_2 Molecules from a Fermi Gas*, Phys. Rev. Lett. **91**, 240401 (2003).
- [71] S. Inouye, J. Goldwin, M. L. Olsen, C. Ticknor, J. L. Bohn, and D. S. Jin, *Observation of Heteronuclear Feshbach Resonances in a Mixture of Bosons and Fermions*, Phys. Rev. Lett. **93**, 183201 (2004).
- [72] C. A. Stan, M. W. Zwierlein, C. H. Schunck, S. M. F. Raupach, and W. Ketterle, *Observation of Feshbach Resonances between Two Different Atomic Species*, Phys. Rev. Lett. **93**, 143001 (2004).
- [73] S. Ospelkaus, C. Ospelkaus, L. Humbert, K. Sengstock, and K. Bongs, *Tuning of Heteronuclear Interactions in a Degenerate Fermi-Bose Mixture*, Phys. Rev. Lett. **97**, 120403 (2006).
- [74] C. A. Regal, M. Greiner, and D. S. Jin, *Observation of Resonance Condensation of Fermionic Atom Pairs*, Phys. Rev. Lett. **92**, 040403 (2004).
- [75] M. Bartenstein, A. Altmeyer, S. Riedl, S. Jochim, C. Chin, J. Hecker Denschlag, and R. Grimm, *Crossover from a Molecular Bose-Einstein Condensate to a Degenerate Fermi Gas*, Phys. Rev. Lett. **92**, 120401 (2004).
- [76] T. Bourdel, L. Khaykovich, J. Cubizolles, J. Zhang, F. Chevy, M. Teichmann, L. Tarruell, S. J. J. M. F. Kokkelmans, and C. Salomon, *Experimental Study of the BEC-BCS Crossover Region in Lithium 6*, Phys. Rev. Lett. **93**, 050401 (2004).
- [77] C. Chin, M. Bartenstein, A. Altmeyer, S. Riedl, S. Jochim, J. Hecker Denschlag, and R. Grimm, *Observation of the Pairing Gap in a Strongly Interacting Fermi Gas*, Science **305**, 1128 (2004).
- [78] J. Kinast, S. L. Hemmer, M. E. Gehm, A. Turlapov, and J. E. Thomas, *Evidence for Superfluidity in a Resonantly Interacting Fermi Gas*, Phys. Rev. Lett. **92**, 150402 (2004).
- [79] G. B. Partridge, K. E. Strecker, R. I. Kamar, M. W. Jack, and R. G. Hulet, *Molecular Probe of Pairing in the BEC-BCS Crossover*, Phys. Rev. Lett. **95**, 020404 (2005).
- [80] M. W. Zwierlein, J. R. Abo-Shaeer, A. Schirotzek, C. H. Schunck, and W. Ketterle, *Vortices and Superfluidity in a Strongly Interacting Fermi Gas*, Nature (London) **435**, 1047 (2005).
- [81] T. Kraemer, M. Mark, P. Waldburger, J. G. Danzl, C. Chin, B. Engeser, A. D. Lange, K. Pilch, A. Jaakkola, H. -C. Nägerl, and R. Grimm, *Evidence for Efimov Quantum States in an Ultracold Gas of Caesium Atoms*, Nature (London) **440**, 315 (2006).

- [82] R. Feynman, *Simulating Physics with Computers*, Int. J. Theor. Phys. **21**, 467 (1982).
- [83] M. A. Nielsen and I. L. Chuang, *Quantum Information and Quantum Computation* (Cambridge University Press, Cambridge, 2000).
- [84] C. H. Bennett and D. P. DiVincenzo, *Quantum Information and Computation*, Nature (London) **404**, 247 (2000).
- [85] P. W. Shor, *Algorithms for Quantum Computation: Discrete Logarithms and Factoring*, in Proc. 35th Annual Symp. Foundations of Computer Science (Ed. Goldwasser), p. 124 (IEEE Computer Society Press, Los Alamitos, California, 1994).
- [86] J. I. Cirac and P. Zoller, *New Frontiers in Quantum Information with Atoms and Ions*, Phys. Today **57**, 38 (2004).
- [87] C. H. Bennett and G. Brassard, *Quantum Cryptography: Public Key Distribution and Coin Tossing*, in Proc. of the IEEE International Conference on Computers, Systems and Signal Processing, **175** (IEEE, New York, 1984).
- [88] A. K. Ekert, *Quantum Cryptography Based on Bell's Theorem*, Phys. Rev. Lett. **67**, 661 (1991).
- [89] N. Gisin, G. Ribordy, W. Tittel, and H. Zbinden, *Quantum Cryptography*, Rev. Mod. Phys. **74**, 145 (2002).
- [90] C. Monroe, *Quantum Information Processing with Atoms and Photons*, Nature (London) **416**, 238 (2002).
- [91] R. Raussendorf and H. -J. Briegel, *A One-Way Quantum Computer*, Phys. Rev. Lett. **86**, 5188 (2001).
- [92] R. Raussendorf, D. E. Browne, and H. -J. Briegel, *Measurement-Based Quantum Computation on Cluster States*, Phys. Rev. A **68**, 022312 (2003).
- [93] L. -M. Duan and R. Raussendorf, *Efficient Quantum Computation with Probabilistic Quantum Gates*, Phys. Rev. Lett. **95**, 080503 (2005).
- [94] M. A. Nielsen and C. M. Dawson, *Fault-Tolerant Quantum Computation with Cluster States*, Phys. Rev. A **71**, 042323 (2005).
- [95] E. Farhi, J. Goldstone, S. Gutmann, J. Lapan, A. Lundgren, and D. Preda, *A Quantum Adiabatic Evolution Algorithm Applied to Random Instances of an NP-Complete Problem*, Science **292**, 472 (2001).
- [96] A. M. Childs, E. Farhi, and J. Preskill, *Robustness of Adiabatic Quantum Computation*, Phys. Rev. A **65**, 012322 (2002).
- [97] D. Aharonov, W. van Dam, J. Kempe, Z. Landau, S. Lloyd, and O. Regev, *Adiabatic Quantum Computation is Equivalent to Standard Quantum Computation*, in Proc. of the 45th Annual Symposium on the Foundations of Computer Science (FOCS'04), 42 (IEEE Computer Society Press, Los Alamitos, California, 2004).

-
- [98] M. S. Sarandy and D. A. Lidar, *Adiabatic Quantum Computation in Open Systems*, Phys. Rev. Lett. **95**, 250503 (2005).
 - [99] S. P. Jordan, E. Farhi, and P. W. Shor, *Error-Correcting Codes for Adiabatic Quantum Computation*, Phys. Rev. A **74**, 052322 (2006).
 - [100] L. B. Ioffe, M. V. Feigel'Man, A. Ioselevich, D. Ivanov, M. Troyer, and G. Blatter, *Topologically Protected Quantum Bits Using Josephson Junction Arrays*, Nature (London) **415**, 503 (2002).
 - [101] M. H. Freedman, A. Kitaev, and Z. Wang, *Simulation of Topological Field Theories by Quantum Computers*, Commun. Math. Phys. **227**, 587 (2002).
 - [102] E. Dennis, A. Kitaev, A. Landahl, and J. Preskill, *Topological Quantum Memory*, J. Math. Phys. **43**, 4452 (2002).
 - [103] A. Yu. Kitaev, *Fault-Tolerant Quantum Computation by Anyons*, Annals of Physics **303**, 2 (2003).
 - [104] P. Zanardi and S. Lloyd, *Topological Protection and Quantum Noiseless Subsystems*, Phys. Rev. Lett. **90**, 067902 (2003).
 - [105] D. P. DiVincenzo, *The Physical Implementation of Quantum Computation*, Fortschr. Phys. **48**, 771 (2000).
 - [106] J. I. Cirac and P. Zoller, *Quantum Computations with Cold Trapped Ions*, Phys. Rev. Lett. **74**, 4091 (1995).
 - [107] J. I. Cirac and P. Zoller, *A Scalable Quantum Computer with Ions in an Array of Microtraps*, Nature (London) **404**, 579 (2000).
 - [108] G. J. Milburn, S. Schneider, and D. F. V. James, *Ion Trap Quantum Computing with Warm Ions*, Fortschr. Phys. **48**, 801 (2000).
 - [109] E. Knill, R. Laflamme, and G. J. Milburn, *A Scheme for Efficient Quantum Computation with Linear Optics*, Nature (London) **409**, 46 (2001).
 - [110] G. K. Brennen, I. H. Deutsch, and C. J. Williams, *Quantum Logic for Trapped Atoms via Molecular Hyperfine Interactions*, Phys. Rev. A **65**, 022313 (2002).
 - [111] D. Kielpinski, C. Monroe, and D. J. Wineland, *Architecture for a Large-Scale Ion-Trap Quantum Computer*, Nature (London) **417**, 709 (2002).
 - [112] F. De Martini, V. Buzèk, F. Sciarrino, and C. Sias, *Experimental Realization of the Quantum Universal NOT Gate*, Nature (London) **419**, 815 (2002).
 - [113] F. Schmidt-Kaler, H. Häffner, M. Riebe, S. Gulde, G. P. T. Lancaster, T. Deuschle, C. Becher, C. F. Roos, J. Eschner, and R. Blatt, *Realization of the Cirac-Zoller Controlled-NOT Quantum Gate*, Nature (London) **422**, 408 (2003).

- [114] D. Leibfried, B. DeMarco, V. Meyer, D. Lucas, M. Barrett, J. Britton, W. M. Itano, B. Jelenkovic, C. Langer, T. Rosenband, and D. J. Wineland, *Experimental Demonstration of a Robust, High-Fidelity Geometric Two Ion-Qubit Phase Gate*, Nature (London) **422**, 412 (2003).
- [115] J. L. O'Brien, G. J. Pryde, A. G. White, T. C. Ralph, and D. Branning, *Demonstration of an All-Optical Quantum Controlled-NOT Gate*, Nature (London) **426**, 264 (2003).
- [116] M. D. Barrett, J. Chiaverini, T. Schaetz, J. Britton, W. M. Itano, J. D. Jost, E. Knill, C. Langer, D. Leibfried, R. Ozeri, and D. J. Wineland, *Deterministic Quantum Teleportation of Atomic Qubits*, Nature (London) **429**, 737 (2004).
- [117] J. Chiaverini, D. Leibfried, T. Schaetz, M. D. Barrett, R. B. Blakestad, J. Britton, W. M. Itano, J. D. Jost, E. Knill, C. Langer, R. Ozeri, and D. J. Wineland, *Realization of Quantum Error Correction*, Nature (London) **432**, 602 (2004).
- [118] T. Schaetz, M. D. Barrett, D. Leibfried, J. Chiaverini, J. Britton, W. M. Itano, J. D. Jost, C. Langer, and D. J. Wineland, *Quantum Dense Coding with Atomic Qubits*, Phys. Rev. Lett. **93**, 040505 (2004).
- [119] P. Walther, K. J. Resch, T. Rudolph, E. Schenck, H. Weinfurter, V. Vedral, M. Aspelmeyer, and A. Zeilinger, *Experimental One-Way Quantum Computing*, Nature (London) **434**, 169 (2005).
- [120] D. Jaksch, C. Bruder, J. I. Cirac, C. W. Gardiner, and P. Zoller, *Cold Bosonic Atoms in Optical Lattices*, Phys. Rev. Lett. **81**, 3108 (1998).
- [121] M. P. A. Fisher, P. B. Weichman, G. Grinstein, and D. S. Fisher, *Boson localization and the Superfluid-Insulator Transition*, Phys. Rev. B **40**, 546 (1989).
- [122] S. Sachdev, *Quantum Phase Transitions*, (Cambridge University Press, Cambridge, 1999).
- [123] W. Zwerger, *Mott-Hubbard transition of Cold Atoms in Optical Lattices*, J. Opt. B **5**, 9 (2003).
- [124] M. Greiner, O. Mandel, T. Esslinger, T. W. Hänsch, and I. Bloch, *Quantum Phase Transition from a Superfluid to a Mott Insulator in a Gas of Ultracold Atoms*, Nature (London) **415**, 39 (2002).
- [125] M. Greiner, O. Mandel, Th. W. Hänsch, and I. Bloch, *Collapse and Revival of the Matter Wave Field of a Bose-Einstein Condensate*, Nature (London) **419**, 51 (2002).
- [126] D. Jaksch and P. Zoller, *The Cold Atom Hubbard Toolbox*, Annals of Physics **315**, 52 (2005).
- [127] E. L. Bolda, E. Tiesinga, and P. S. Julienne, *Effective-Scattering-Length Model of Ultracold Atomic Collisions and Feshbach Resonances in Tight Harmonic Traps*, Phys. Rev. A **66**, 013403 (2002).
- [128] P. S. Jessen and I. H. Deutsch, *Optical Lattices*, Adv. At. Mol. Opt. Phys. **37**, 95 (1996).

- [129] L. Santos, M. A. Baranov, J. I. Cirac, H. U. Everts, H. Fehrmann, and M. Lewenstein, *Atomic Quantum Gases in Kagomé Lattices*, Phys. Rev. Lett. **93**, 030601 (2004).
- [130] M. Lewenstein, A. Sanpera, V. Ahufinger, B. Damski, A. Sen De, and U. Sen, *Ultracold Atomic Gases in Optical Lattices: Mimicking Condensed Matter Physics and Beyond*, Adv. Phys. **56**, 243 (2007).
- [131] O. Morsch, J. H. Müller, M. Cristiani, D. Ciampini, and E. Arimondo, *Bloch Oscillations and Mean-Field Effects of Bose-Einstein Condensates in 1D Optical Lattices*, Phys. Rev. Lett. **87**, 140402 (2001).
- [132] H. Moritz, T. Stöferle, M. Köhl, and T. Esslinger, *Exciting Collective Oscillations in a Trapped 1D Gas*, Phys. Rev. Lett. **91**, 250402 (2003).
- [133] H. P. Büchler, G. Blatter, and W. Zwerger, *Commensurate-Incommensurate Transition of Cold Atoms in an Optical Lattice*, Phys. Rev. Lett. **90**, 130401 (2003).
- [134] T. Stöferle, H. Moritz, C. Schori, M. Köhl, and T. Esslinger, *Transition from a Strongly Interacting 1D Superfluid to a Mott Insulator*, Phys. Rev. Lett. **92**, 130403 (2004).
- [135] M. Köhl, H. Moritz, T. Stöferle, C. Schori and T. Esslinger, *Superfluid to Mott Insulator Transition in One, Two, and Three Dimensions*, J. Low Temp. Phys. **138**, 635 (2005).
- [136] I. B. Spielman, W. D. Phillips, and J. V. Porto, *Mott-Insulator Transition in a Two-Dimensional Atomic Bose Gas*, Phys. Rev. Lett. **98**, 080404 (2007).
- [137] B. Paredes, A. Widera, V. Murg, O. Mandel, S. Fölling, I. Cirac, G. V. Shlyapnikov, T. W. Hänsch, and I. Bloch, *Tonks-Girardeau Gas of Ultracold Atoms in an Optical Lattice*, Nature (London) **429**, 277 (2004).
- [138] T. Kinoshita, T. R. Wenger, and D. S. Weiss, *Observation of a One-Dimensional Tonks-Girardeau Gas*, Science **305**, 1125 (2004).
- [139] Z. Hadzibabic, P. Krüger, M. Cheneau, B. Battelier, and J. Dalibard, *Berezinskii-Kosterlitz-Thouless Crossover in a Trapped Atomic Gas*, Nature (London) **441**, 1118 (2006).
- [140] A. Sørensen and K. Molmer, *Spin-Spin Interaction and Spin Squeezing in an Optical Lattice*, Phys. Rev. Lett. **83**, 2274 (1999).
- [141] L. -M. Duan, E. Demler, and M. D. Lukin, *Controlling Spin Exchange Interactions of Ultracold Atoms in Optical Lattices*, Phys. Rev. Lett. **91**, 090402 (2003).
- [142] J. K. Pachos and M. B. Plenio, *Three-Spin Interactions in Optical Lattices and Criticality in Cluster Hamiltonians*, Phys. Rev. Lett. **93**, 056402 (2004).
- [143] J. J. García-Ripoll, M. A. Martin-Delgado, and J. I. Cirac, *Implementation of Spin Hamiltonians in Optical Lattices*, Phys. Rev. Lett. **93**, 250405 (2004).
- [144] L. -M. Duan, *Controlling Ultracold Atoms in Multi-Band Optical Lattices for Simulation of Kondo Physics*, Europhys. Lett. **67**, 721 (2004).

- [145] B. Paredes, C. Tejedor, and J. I. Cirac, *Fermionic Atoms in Optical Superlattices*, Phys. Rev. A **71**, 063608 (2005).
- [146] B. Damski, J. Zakrzewski, L. Santos, P. Zoller, and M. Lewenstein, *Atomic Bose and Anderson Glasses in Optical Lattices*, Phys. Rev. Lett. **91**, 080403 (2003).
- [147] H. P. Büchler, M. Hermele, S. D. Huber, M. P. A. Fisher, and P. Zoller, *Atomic Quantum Simulator for Lattice Gauge Theories and Ring Exchange Models*, Phys. Rev. Lett. **95**, 040402 (2005).
- [148] B. Paredes and J. I. Cirac, *From Cooper Pairs to Luttinger Liquids with Bosonic Atoms in Optical Lattices*, Phys. Rev. Lett. **90**, 150402 (2003).
- [149] W. Hofstetter, J. I. Cirac, P. Zoller, E. Demler, and M. D. Lukin, *High-Temperature Superfluidity of Fermionic Atoms in Optical Lattices*, Phys. Rev. Lett. **89**, 220407 (2002).
- [150] S. Trebst, U. Schollwöck, M. Troyer, and P. Zoller, *D-Wave Resonating Valence Bond States of Ultracold Fermionic Atoms in Optical Lattices*, Phys. Rev. Lett. **96**, 250402 (2006).
- [151] S. Peil, J. V. Porto, B. Laburthe Tolra, J. M. Obrecht, B. E. King, M. Subbotin, S. L. Rolston, and W. D. Phillips, *Patterned Loading of a Bose-Einstein Condensate into an Optical Lattice*, Phys. Rev. A **67**, 051603(R) (2003).
- [152] O. Mandel, M. Greiner, A. Widera, T. Rom, T. W. Hänsch, and I. Bloch, *Controlled Collisions for Multi-Particle Entanglement of Optically Trapped Atoms*, Nature (London) **425**, 937 (2003).
- [153] K. Winkler, G. Thalhammer, F. Lang, R. Grimm, J. Hecker Denschlag, A. J. Daley, A. Kantian, H. P. Büchler, and P. Zoller, *Repulsively Bound Atom Pairs in an Optical Lattice*, Nature (London) **441**, 853 (2006).
- [154] S. Fölling, F. Gerbier, A. Widera, O. Mandel, T. Gericke, and I. Bloch, *Spatial Quantum Noise Interferometry in Expanding Ultracold Atom Clouds*, Nature (London) **434**, 481 (2005).
- [155] M. Schellekens, R. Hoppeler, A. Perrin, J. Viana Gomes, D. Boiron, A. Aspect, and C. I. Westbrook, *Hanbury Brown Twiss Effect for Ultracold Quantum Gases*, Science **310**, 648 (2005).
- [156] E. Altman, E. Demler, and M. D. Lukin, *Probing Many-Body States of Ultracold Atoms via Noise Correlations*, Phys. Rev. A **70**, 013603 (2004).
- [157] D. Jaksch, H. -J. Briegel, J. I. Cirac, C. W. Gardiner, and P. Zoller, *Entanglement of Atoms via Cold Controlled Collisions*, Phys. Rev. Lett. **82**, 1975 (1999).
- [158] T. Calarco, H. -J. Briegel, D. Jaksch, J. I. Cirac, and P. Zoller, *Quantum Computing with Trapped Particles in Microscopic Potentials*, Fortschr. Phys. **48**, 945 (2000).
- [159] G. K. Brennen, C. M. Caves, P. S. Jessen, and I. H. Deutsch, *Quantum Logic Gates in Optical Lattices*, Phys. Rev. Lett. **82**, 1060 (1999).

-
- [160] G. K. Brennen, I. H. Deutsch, and P. S. Jessen, *Entangling Dipole-Dipole Interactions for Quantum Logic with Neutral Atoms*, Phys. Rev. A **61**, 62309 (2000).
- [161] J. Mompart, K. Eckert, W. Ertmer, G. Birkel, and M. Lewenstein, *Quantum Computing with Spatially Delocalized Qubits*, Phys. Rev. Lett. **90**, 147901 (2003).
- [162] J. K. Pachos and P. L. Knight, *Quantum Computation with a One-Dimensional Optical Lattice*, Phys. Rev. Lett. **91**, 107902 (2003).
- [163] E. Charron, E. Tiesinga, F. Mies, and C. Williams, *Optimizing a Phase Gate Using Quantum Interference*, Phys. Rev. Lett. **88**, 077901 (2002).
- [164] D. Jaksch, J. I. Cirac, P. Zoller, S. Rolston, R. Côté, and M. D. Lukin, *Fast Quantum Gates for Neutral Atoms*, Phys. Rev. Lett. **85**, 2208 (2000).
- [165] O. Mandel, M. Greiner, A. Widera, T. Rom, T. W. Hänsch, and I. Bloch, *Coherent Transport of Neutral Atoms in Spin-Dependent Optical Lattice Potentials*, Phys. Rev. Lett. **91**, 010407 (2003).
- [166] T. Calarco, U. Dorner, P. Julienne, C. Williams, and P. Zoller, *Quantum Computations with Atoms in Optical Lattices: Marker Qubits and Molecular Interactions*, Phys. Rev. A **70**, 012306 (2004).
- [167] E. Jane, G. Vidal, W. Dür, P. Zoller, and J. I. Cirac, *Simulation of Quantum Dynamics with Quantum Optical Systems*, Quantum Inform. Comput. **3**, 15 (2003).
- [168] E. M. Purcell, *Spontaneous Emission Probabilities at Radio Frequencies*, Phys. Rev. **69**, 681 (1946).
- [169] P. Goy, J. M. Raimond, M. Gross, and S. Haroche, *Observation of Cavity-Enhanced Single-Atom Spontaneous Emission*, Phys. Rev. Lett. **50**, 1903 (1983).
- [170] D. J. Heinzen, J. J. Childs, J. E. Thomas, and M. S. Feld, *Enhanced and Inhibited Visible Spontaneous Emission by Atoms in a Confocal Resonator*, Phys. Rev. Lett. **58**, 1320 (1987).
- [171] D. J. Heinzen and M. S. Feld, *Vacuum Radiative Level Shift and Spontaneous-Emission Linewidth of an Atom in an Optical Resonator*, Phys. Rev. Lett. **59**, 2623 (1987).
- [172] E. T. Jaynes and F. W. Cummings, *Comparison of Quantum Semiclassical Radiation Theories with Application to the Beam Maser*, Proc. IEEE **51**, 89 (1963).
- [173] D. Kleppner, *Inhibited Spontaneous Emission*, Phys. Rev. Lett. **47**, 233 (1981).
- [174] D. Meschede, H. Walther, and G. Müller, *One-Atom Maser*, Phys. Rev. Lett. **54**, 551 (1985).
- [175] M. Brune, J. M. Raimond, P. Goy, L. Davidovich, and S. Haroche, *Realization of a Two-Photon Maser Oscillator*, Phys. Rev. Lett. **59**, 1899 (1987).
- [176] G. Rempe, H. Walther, and N. Klein, *Observation of Quantum Collapse and Revival in a One-Atom Maser*, Phys. Rev. Lett. **58**, 353 (1987).

- [177] G. Rempe, F. Schmidt-Kaler, and H. Walther, *Observation of Sub-Poissonian Photon Statistics in a Micromaser*, Phys. Rev. Lett. **64**, 2783 (1990).
- [178] M. Weidinger, B. T. H. Varcoe, R. Heerlein, and H. Walther, *Trapping States in the Micromaser*, Phys. Rev. Lett. **82**, 3795 (1990).
- [179] O. Benson, G. Raithel, and H. Walther, *Quantum Jumps of the Micromaser Field: Dynamic Behavior Close to Phase Transition Points*, Phys. Rev. Lett. **72**, 3506 (1994).
- [180] M. Brune, F. Schmidt-Kaler, A. Maali, J. Dreyer, E. Hagley, J. M. Raimond, and S. Haroche, *Quantum Rabi Oscillation: A Direct Test of Field Quantization in a Cavity*, Phys. Rev. Lett. **76**, 1800 (1996).
- [181] M. Brune, E. Hagley, J. Dreyer, X. Maître, A. Maali, C. Wunderlich, J. M. Raimond, and S. Haroche, *Observing the Progressive Decoherence of the “Meter” in a Quantum Measurement*, Phys. Rev. Lett. **77**, 4887 (1996).
- [182] B. T. H. Varcoe, S. Brattke, M. Weidinger, and H. Walther, *Preparing Pure Photon Number States of the Radiation Field*, Nature (London) **403**, 743 (2000).
- [183] S. Brattke, B. T. H. Varcoe, and H. Walther, *Generation of Photon Number States on Demand via Cavity Quantum Electrodynamics*, Phys. Rev. Lett. **86**, 3534 (2001).
- [184] R. J. Thompson, G. Rempe, and H. J. Kimble, *Observation of Normal-Mode Splitting for an Atom in an Optical Cavity*, Phys. Rev. Lett. **68**, 1132 (1992).
- [185] G. T. Foster, L. A. Orozco, H. M. Castro-Beltran, and H. J. Carmichael, *Quantum State Reduction and Conditional Time Evolution of Wave-Particle Correlations in Cavity QED*, Phys. Rev. Lett. **85**, 3149 (2000).
- [186] H. Mabuchi, Q. A. Turchette, M. S. Chapman, and H. J. Kimble, *Real-Time Detection of Individual Atoms Falling Through a High-Finesse Optical Cavity*, Opt. Lett. **21**, 1393 (1996).
- [187] P. Münstermann, T. Fischer, P. W. H. Pinkse, and G. Rempe, *Single Slow Atoms from an Atomic Fountain Observed in a High-Finesse Optical Cavity*, Opt. Comm. **159**, 63 (1999).
- [188] J. A. Sauer, K. M. Fortier, M. S. Chang, C. D. Hamley, and M. S. Chapman, *Cavity QED with Optically Transported Atoms*, Phys. Rev. A. **69**, 051804(R) (2004).
- [189] C. J. Hood, M. S. Chapman, T. W. Lynn, and H. J. Kimble, *Real-Time Cavity QED with Single Atoms*, Phys. Rev. Lett. **80**, 4157 (1998).
- [190] P. Münstermann, T. Fischer, P. Maunz, P. W. H. Pinkse, and G. Rempe, *Dynamics of Single-Atom Motion Observed in a High-Finesse Cavity*, Phys. Rev. Lett. **82**, 3791 (1999).
- [191] C. J. Hood, T. W. Lynn, A. C. Doherty, A. S. Parkins, and H. J. Kimble, *The Atom-Cavity Microscope: Single Atoms Bound in Orbit by Single Photons*, Science **287**, 1447 (2000).

-
- [192] P. W. H. Pinkse, T. Fischer, P. Maunz, and G. Rempe, *Trapping an Atom with Single Photons*, Nature (London) **404**, 365 (2000).
 - [193] J. Ye, D. W. Vernooy, and H. J. Kimble, *Trapping of Single Atoms in Cavity QED*, Phys. Rev. Lett. **83**, 4987 (1999).
 - [194] J. McKeever, J. R. Buck, A. D. Boozer, A. Kuzmich, H. -C. Nägerl, D. M. Stamper-Kurn, and H. J. Kimble, *State-Insensitive Cooling and Trapping of Single Atoms in an Optical Cavity*, Phys. Rev. Lett. **90**, 133602 (2003).
 - [195] T. Puppe, I. Schuster, P. Maunz, K. Murr, P. W. H. Pinkse, and G. Rempe, *Trapping and Observing Single Atoms in a Blue-Detuned Intracavity Dipole Trap*, Phys. Rev. Lett. **99**, 013002 (2007).
 - [196] P. Horak, G. Hechenblaikner, K. M. Gheri, H. Stecher, and H. Ritsch, *Cavity-Induced Atom Cooling in the Strong Coupling Regime*, Phys. Rev. Lett. **79**, 4974 (1997).
 - [197] G. Hechenblaikner, M. Gangl, P. Horak, and H. Ritsch, *Cooling an Atom in a Weakly Driven High-Q Cavity*, Phys. Rev. A **58**, 3030 (1998).
 - [198] P. Domokos, P. Horak, and H. Ritsch, *Semiclassical Theory of Cavity-Assisted Atom Cooling*, J. Phys. B: At. Mol. Opt. Phys. **34**, 187 (2001).
 - [199] P. Domokos and H. Ritsch, *Mechanical Effects of Light in Optical Resonators*, J. Opt. Soc. Am. B **20**, 1098 (2003).
 - [200] P. Maunz, T. Puppe, I. Schuster, N. Syassen, P. W. H. Pinkse, and G. Rempe, *Cavity Cooling of a Single Atom*, Nature (London) **428**, 50 (2004).
 - [201] V. Vuletić and S. Chu, *Laser Cooling of Atoms, Ions, or Molecules by Coherent Scattering*, Phys. Rev. Lett. **84**, 3787 (2000).
 - [202] A. Griessner, D. Jaksch, and P. Zoller, *Cavity-Assisted Nondestructive Laser Cooling of Atomic Qubits*, J. Phys. B **37**, 1419 (2004).
 - [203] V. Vuletić, H. W. Chan, and A. T. Black, *Three-Dimensional Cavity Doppler Cooling and Cavity Sideband Cooling by Coherent Scattering*, Phys. Rev. A **64**, 033405 (2001).
 - [204] P. Domokos, A. Vukics, and H. Ritsch, *Anomalous Doppler-Effect and Polariton-Mediated Cooling of Two-Level Atoms*, Phys. Rev. Lett. **92**, 103601 (2004).
 - [205] S. Zippilli, G. Morigi, and H. Ritsch, *Cooling Trapped Atoms in Optical Resonators*, Phys. Rev. Lett. **95**, 143001 (2005).
 - [206] S. Nußmann, K. Murr, M. Hijlkema, B. Weber, A. Kuhn, and G. Rempe, *Vacuum-Stimulated Cooling of Single Atoms in Three Dimensions*, Nature Physics **1**, 122 (2005).
 - [207] A. Hemmerich, *Quantum Entanglement in Dilute Optical Lattices*, Phys. Rev. A **60**, 943 (1999).
 - [208] M. Gangl and H. Ritsch, *Cold Atoms in a High-Q Ring Cavity*, Phys. Rev. A **61**, 043405 (2000).

-
- [209] B. Nagorny, Th. Elsässer, H. Richter, A. Hemmerich, D. Kruse, C. Zimmermann, and Ph. W. Courteille, *Optical Lattice in a High-Finesse Ring Resonator*, Phys. Rev. A **67**, 031401 (2003).
- [210] H. W. Chan, A. T. Black, and V. Vuletić, *Observation of Collective-Emission-Induced Cooling of Atoms in an Optical Cavity*, Phys. Rev. Lett. **90**, 063003 (2003).
- [211] B. Nagorny, T. Elsässer, and A. Hemmerich, *Collective Atomic Motion in an Optical Lattice Formed Inside a High-Finesse Cavity*, Phys. Rev. Lett. **91**, 153003 (2003).
- [212] D. Kruse, C. von Cube, C. Zimmermann, and Ph. W. Courteille, *Observation of Lasing Mediated by Collective Atomic Recoil*, Phys. Rev. Lett. **91**, 183601 (2003).
- [213] J. Klinner, M. Lindholdt, B. Nagorny, and A. Hemmerich, *Normal Mode Splitting and Mechanical Effects of an Optical Lattice in a Ring Cavity*, Phys. Rev. Lett. **96**, 023002 (2006).
- [214] S. Slama, G. Krenz, S. Bux, C. Zimmermann, and Ph. W. Courteille, *Cavity-Enhanced Superradiant Rayleigh Scattering with Ultracold and Bose-Einstein Condensed Atoms*, Phys. Rev. A **75**, 063620 (2007).
- [215] S. Slama, S. Bux, G. Krenz, C. Zimmermann, and Ph. W. Courteille, *Superradiant Rayleigh Scattering and Collective Atomic Recoil Lasing in a Ring Cavity*, Phys. Rev. Lett. **98**, 053603 (2007).
- [216] P. Domokos and H. Ritsch, *Collective Cooling and Self-Organization of Atoms in a Cavity*, Phys. Rev. Lett. **89**, 253003 (2002).
- [217] S. Zippilli, G. Morigi, and H. Ritsch, *Suppression of Bragg Scattering by Collective Interference of Spatially Ordered Atoms with a High-Q Cavity Mode*, Phys. Rev. Lett. **93**, 123002 (2004).
- [218] A. T. Black, H. W. Chan, and V. Vuletić, *Observation of Collective Friction Forces Due to Spatial Self-Organization of Atoms: From Rayleigh to Bragg Scattering*, Phys. Rev. Lett. **91**, 203001 (2003).
- [219] M. Hennrich, T. Legero, A. Kuhn, and G. Rempe, *Vacuum-Stimulated Raman Scattering Based on Adiabatic Passage in a High-Finesse Optical Cavity*, Phys. Rev. Lett. **85**, 4872 (2000).
- [220] A. Kuhn, M. Hennrich, and G. Rempe, *Deterministic Single-Photon Source for Distributed Quantum Networking*, Phys. Rev. Lett. **89**, 067901 (2002).
- [221] J. McKeever, A. Boca, A. D. Boozer, R. Miller, J. R. Buck, A. Kuzmich, and H. J. Kimble, *Deterministic Generation of Single Photons from One Atom Trapped in a Cavity*, Science **303**, 1992 (2004).
- [222] M. Keller, B. Lange, K. Hayasaka, W. Lange, and H. Walther, *Continuous Generation of Single Photons with Controlled Waveform in an Ion-Trap Cavity System*, Nature (London) **431**, 1075 (2004).

- [223] J. M. Raimond, M. Brune, and S. Haroche, *Manipulating Quantum Entanglement with Atoms and Photons in a Cavity*, Rev. Mod. Phys. **73**, 565 (2001).
- [224] L. -M. Duan and H. J. Kimble, *Scalable Photonic Quantum Computation through Cavity-Assisted Interactions*, Phys. Rev. Lett. **92**, 127902 (2004).
- [225] J. I. Cirac, P. Zoller, H. J. Kimble, and H. Mabuchi, *Quantum State Transfer and Entanglement Distribution Among Distant Nodes in a Quantum Network*, Phys. Rev. Lett. **78**, 3221 (1997).

Part I

Ultracold Atoms in Optical Lattices Enclosed in an Optical Cavity

CHAPTER 2

BACKGROUND: COLD ATOMS IN OPTICAL LATTICES

Systems of cold atoms, loaded into optical lattices, open up the possibility to engineer model Hamiltonians, known from condensed matter physics, like Hubbard lattice models as the Bose-Hubbard model. In solid state systems these models are rather hard to test, whereas quantum optical systems are relatively simple and, which is an essential feature, tunable and offer therefore a plethora of applications to test fundamental condensed matter models.

In this chapter the basic properties of the physics of cold atoms in optical lattices are presented in a condensed form. We begin with an outline of the physics of a single atom in an optical lattice, where we review the energy band structure of the lattice potential, the Bloch and the Wannier functions, which serve as localized ground state functions for atoms in optical lattices. In the last section, we switch to several particles and derive the Bose-Hubbard model for cold atoms in optical lattices. This model is the basis for the subsequent efforts in this thesis. In chapter 3 we generalize this model to atoms enclosed in optical cavities, where the optical lattice, in addition to a “classical” lattice, as presented here in this chapter, is generated by the resonator itself.

2.1 Optical Lattices

Optical lattices are periodic potentials, created by the interaction of neutral atoms with the interference pattern of intersecting laser beams. The origin of the array of potential wells lies in the dependence of the interaction energy of the internal atomic states on the light intensity. The interference pattern of intersecting laser light causes a periodically varying intensity, leading to optical potential wells for the neutral atoms. These wells are separated by the order of the laser wavelength.

2.1.1 Optical Potentials - The AC-Stark Shift

The interaction of neutral atoms with light consists of two different processes. First, there is the absorption of a photon followed by the stimulated emission of a photon. This is the conservative part of the interaction, caused by the interaction of the light field with the induced dipole moment of the atom and leads to a shift of the energy levels of the atoms, the so-called *light shift* or *AC-Stark shift*. On the other hand an absorption process can also be followed by a spontaneous emission of a photon. This leads to the dissipative part of the interaction. Although this emission process is random in time and direction, it can induce a net force on the atom. On average the recoil momentum on the atom of the emitted photon is zero, while the direction of the momentum of the absorbed photons is always along the laser beam. This effect is widely used in Doppler cooling techniques.

Let us now consider a classical, single-mode laser light with frequency ω_l and wavenumber k_l forming a one-dimensional standing wave $\mathbf{E}(x, t) = E_l(x) \cos(\omega_l t - \phi) \boldsymbol{\epsilon}$, created by counter-propagating laser beams, schematically depicted in Fig. 2.1.

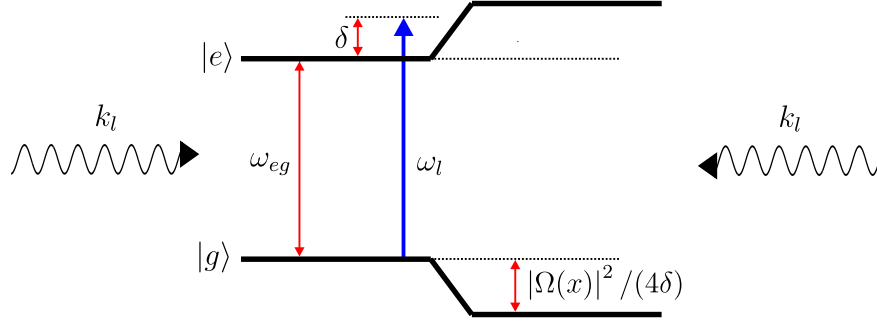


Figure 2.1. Scheme of the interaction of a two-level atom with ground state $|g\rangle$ and excited state $|e\rangle$, energetically separated by $\hbar\omega_{eg}$, with a standing wave laser field with frequency ω_l and wavenumber k_l . The detuning of the laser and the atomic transition frequency is given by $\delta = \omega_l - \omega_{eg}$. This leads to the so-called AC-Stark shift $\hbar |\Omega(x)|^2 / (4\delta)$ of the levels (2.7).

Here $E_l(x)$ is the amplitude of the electric field and $\boldsymbol{\epsilon}$ is the polarization vector. This light field interacts with a two-level atom with ground state $|g\rangle$ and excited state $|e\rangle$, with energy difference $\hbar\omega_{eg}$. Let us assume that the ground state energy is zero, i.e. $E_g = 0$. Thus, the interaction energy in the electric-dipole approximation reads as follows [1]:

$$\begin{aligned} H &= H_A + H_I \\ &= \frac{\hat{p}^2}{2m} + \hbar\omega_{eg}|e\rangle\langle e| - \mathbf{d} \cdot \mathbf{E}(\hat{x}). \end{aligned} \quad (2.1)$$

Here m is the atom mass, \hat{p} and \hat{x} is the atomic momentum and position operator, respectively. Note that in the electric dipole approximation \hat{x} corresponds to the atom's center of mass. \mathbf{d} is the dipole operator. Due to the odd parity of \mathbf{d} the interaction Hamiltonian can be written as

$$H_I = -\frac{\hbar\Omega(\hat{x})}{2} \left[e^{-i(\omega_l t - \phi)} \sigma_+ + e^{-i(\omega_l t - \phi)} \sigma_- \right] - \frac{\hbar\Omega^\dagger(\hat{x})}{2} \left[e^{i(\omega_l t - \phi)} \sigma_+ + e^{i(\omega_l t - \phi)} \sigma_- \right]. \quad (2.2)$$

Here $\Omega(\hat{x}) = E_l(\hat{x})\langle e|\mathbf{d}\cdot\boldsymbol{\epsilon}|g\rangle$ is the Rabi frequency. The operators σ_+ and $\sigma_- = \sigma_+^\dagger$ denote the well known Pauli matrices

$$\sigma_+ \equiv |e\rangle\langle g| = \begin{pmatrix} 0 & 1 \\ 0 & 0 \end{pmatrix}, \quad \sigma_- \equiv |g\rangle\langle e| = \begin{pmatrix} 0 & 0 \\ 1 & 0 \end{pmatrix}.$$

Physically the terms in the first bracket of (2.2) correspond to rising the atom from the ground state $|g\rangle$ to the excited state $|e\rangle$ and to lowering the atom from $|e\rangle$ to $|g\rangle$ by absorbing a photon from the laser field. The terms in the second bracket correspond to an atomic transition from $|g\rangle$ to $|e\rangle$ and a transition from $|e\rangle$ to $|g\rangle$ by emitting a photon. The first

and the last of these processes are resonant, whereas the other two processes are off-resonant and can be neglected as follows: Firstly, we choose a rotating frame to remove the time dependence, by means of a unitary transformation $|\tilde{\psi}\rangle = U(t)|\psi\rangle$, where $U = \exp(i\omega_l t|e\rangle\langle e|)$. This corresponds to a new Hamiltonian $\tilde{H} = UHU^\dagger + i\hbar\left(\frac{d}{dt}U\right)U^\dagger$, which is in our case

$$\tilde{H}_I = -\hbar\delta|e\rangle\langle e| - \frac{\hbar\Omega(\hat{x})}{2} \left[e^{i\phi}\sigma_+ + e^{i\phi}e^{-2i\omega_l t}\sigma_- \right] - \frac{\hbar\Omega^\dagger(\hat{x})}{2} \left[e^{-i\phi}e^{2i\omega_l t}\sigma_+ + e^{-i\phi}\sigma_- \right], \quad (2.3)$$

where $\delta = \omega_l - \omega_{eg}$ is the detuning of the light field from the atomic resonance frequency. For times $t \gg 1/\omega_l$, the time average of the time-dependent terms is approximately zero, such that we can safely neglect them. This is known as the rotating wave approximation. Omitting the tilde, the approximative interaction Hamiltonian is

$$H_I = -\hbar\delta|e\rangle\langle e| - \frac{\hbar\Omega(\hat{x})}{2}e^{i\phi}\sigma_+ - \frac{\hbar\Omega^\dagger(\hat{x})}{2}e^{-i\phi}\sigma_-. \quad (2.4)$$

The energy eigenvalues of this Hamiltonian are

$$E = -\frac{\hbar\delta}{2} \pm \frac{\hbar}{2}\sqrt{\delta^2 + |\Omega(x)|^2}. \quad (2.5)$$

For large detuning $|\delta| \gg \omega$, where the population in the excited state, and hence the saturation parameter, $s \approx |\Omega(x)|^2/(2\delta^2)$, is very small, the energy eigenvalues reduce to

$$E \approx -\frac{\hbar\delta}{2} \pm \frac{\hbar\delta}{2} \left[1 + \frac{1}{2} \left(\frac{|\Omega(x)|}{\delta} \right)^2 \right]. \quad (2.6)$$

The shift of the eigenvalues due to the interaction with the light field is the second term in square brackets and is called AC-Stark shift. As the calculations above show, it corresponds to the conservative part of the interaction and varies spatially via $\Omega(x)$. This light shift can be interpreted as a potential

$$V = -\frac{\hbar|\Omega(x)|^2}{4\delta} \quad (2.7)$$

for the atom in the ground state, in which it is most of the time in the low saturation limit. This defines the optical potential. For red detuning $\delta < 0$, the minima of the potentials are the maxima of the Rabi frequency $\Omega(x)$, i.e. the intensity maxima. For blue detuning, $\delta > 0$, to the contrary, the atoms are repelled from points with high intensity, since the potential minima correspond to the points with the lowest intensity.

2.1.2 Spontaneous Emission

In reality, the excited state will decay by emitting photons spontaneously. As aforementioned, there exists a dissipative force originating from to this spontaneous emission process, beside the conservative dipole force. There are several possibilities to treat this process, for instance the description with a stochastic Schrödinger equation [2] or via the interaction with an external reservoir and a master equation (see Sec. 3.1.3). For the moment we limit ourselves to a more phenomenological treatment and add a non-hermitian part to the Hamiltonian (2.4)

$$H' = H - i\frac{\gamma}{2}|e\rangle\langle e|, \quad (2.8)$$

where $\gamma = |\langle e|\mathbf{d}\cdot\boldsymbol{\epsilon}|g\rangle|^2\omega_{eg}^3/(3\pi\epsilon_0\hbar c^3)$ is the spontaneous emission rate for a two-level atom [3]. For large detuning, the light shift, which can also be calculated with second order perturbation theory, is now a complex number $\Delta E = \hbar|\Omega(x)|^2/[4(\delta - i\gamma/2)] = V(x) + i\Gamma_{\text{eff}}$. The real part corresponds to the optical potential, whereas the imaginary part describes the non-conservative part, the spontaneous emission. The dissipation term

$$\Gamma_{\text{eff}} = \frac{\hbar|\Omega(x)|^2\gamma}{8\delta^2} \quad (2.9)$$

is proportional to δ^{-2} and can therefore be safely neglected for large detuning $|\delta| \gg \Omega$, compared to the conservative part $V \sim \delta^{-1}$. Note that the spontaneous emission rate is enhanced for red detuned optical lattices, since it increases with increasing light intensity.

2.1.3 Lattice Geometry

In order to create periodic arrays of optical potentials, several laser beams have to be overlapped. The simplest possible pattern is a one-dimensional lattice, generated by two counter-propagating laser beams, which produce a single standing wave $E_l(x) = E_0 \cos(k_l x)$. In this case, the lattice potential (2.7) is simply given by

$$V = -\frac{\hbar\Omega_0^2}{4\delta} \cos^2(k_l x) = V_0 \cos^2(k_l x), \quad (2.10)$$

where $\Omega_0 = E_0\langle e|\mathbf{d}\cdot\boldsymbol{\epsilon}|g\rangle$. The main difference to periodic potentials in solid crystals is the tunability of the potential. On the one hand the potential depth V_0 depends on the laser intensity $|E_0|^2$, on the other hand the potential minima can be moved and made state-dependent by the use of laser polarizations. Optical lattices in higher dimensions are generated basically with the same method, by superimposing standing laser fields in other directions. Varying the geometry and polarizations opens up a large variety of possibilities of lattice properties. See for instance [4–7]. Note, that another advantage compared to crystalline periodic potentials is the much less number of imperfections in optical lattices and the exceptional isolation from the environment, leading to long coherence times of the atomic dynamics.

2.2 A Single Particle in an Optical Lattice

In this section we will review some standard results of the physics of a single particle in a periodic potential. For simplicity we consider only a single spatial dimension, such as the optical potentials, derived in section 2.1.1. For large detuning or on times where spontaneous emission can be neglected the time evolution of a single particle is given by the Hamiltonian

$$H = \frac{\hat{p}^2}{2m} + V_0 \cos^2(k_l \hat{x}). \quad (2.11)$$

The lattice constant is given by $a = \pi/k_l$. The main consequences of (2.11), like the energy band structure or Brillouin zones, are due to the periodicity of the potential (see Fig. 2.2).

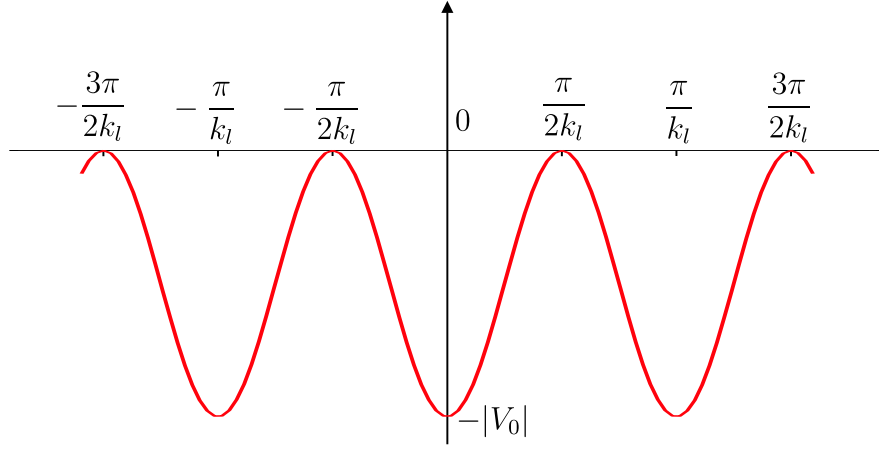


Figure 2.2. Periodic potential $V_0 \cos^2(k_l x)$ with $V_0 < 0$, corresponding to a one-dimensional optical lattice.

2.2.1 Harmonic Oscillator Approximation

When the optical lattice is sufficiently deep and the particle is trapped in one of the potential wells, the potential can be expanded, leading to a harmonic potential

$$V = \frac{m\omega_{\text{HO}}^2 x^2}{2} \quad \text{with} \quad \omega_{\text{HO}} = \Omega_0 k_l \sqrt{\frac{\hbar}{2|\delta|m}} = 2\sqrt{\frac{|V_0|E_R}{\hbar^2}}. \quad (2.12)$$

Here E_R denotes the recoil frequency, i.e. $E_R = \hbar^2 k_l^2 / (2m)$. In this case the ground state wavefunction of the particle is simply given by the Harmonic Oscillator wave functions

$$\varphi_{\text{HO}}(x) = \sqrt{\frac{1}{x_0 \sqrt{\pi}}} e^{-x^2/(2x_0^2)}. \quad (2.13)$$

The size of the ground state is characterized by the oscillator length $x_0 = \sqrt{\hbar/(m\omega_{\text{HO}})}$, or $k_l x_0 = (|V_0|/E_R)^{-1/4}$. A necessary condition for the validity of this approximation, is that the depth of the lattice is large enough. This is fulfilled for $x_0 \ll a$. Later we will construct the localized eigenfunctions of the complete lattice and calculate certain matrix elements thereof. Using this harmonic approximation reduces of course much the complexity of the calculation of these matrix elements. In Sec. 2.3 we will investigate the validity of the harmonic approximation in this context.

2.2.2 Bloch Functions

The potential in (2.11) is invariant under translations $x \rightarrow x + la$ for $l \in \mathbb{Z}$. Therefore, if $\phi(x)$ is a time-independent solution of the corresponding, also $\phi(x + na)$ solves the Schrödinger equation corresponding to the Hamiltonian

$$\left[-\frac{\hbar^2}{2m} \frac{d^2}{dx^2} + V_0 \cos^2(k_l x) \right] \phi(x) = E \phi(x). \quad (2.14)$$

This is the Mathieu equation [8]. The periodicity condition on the solutions, which, in the physical context, are called Bloch functions, implies, that they are of the following form:

$$\phi_q^{(n)}(x) = e^{iqx} u_q^{(n)}(x). \quad (2.15)$$

The parameter q is called quasimomentum and is restricted to the first Brillouin zone, i.e. $q \in [-\pi/a, \pi/a]$. The number n is the energy band index, since for a given q there are several solutions of (2.14). The functions $u_q^{(n)}(x)$ have the same periodicity as the lattice potential, $u_q^{(n)}(x + la) = u_q^{(n)}(x)$ for $l \in \mathbb{Z}$. They are eigenfunctions of the Hamiltonian

$$H_q = \frac{(\hat{p} + q)^2}{2m} + V_0 \cos^2(k_l \hat{x}). \quad (2.16)$$

This is known as Bloch's Theorem [9, 10]. Due to the periodicity given by the lattice, things get much easier, when we use Fourier expansions. For instance, the function $u_q^{(n)}(x)$ can be written as

$$u_q^{(n)}(x) = \frac{1}{\sqrt{2\pi}} \sum_{j \in \mathbb{Z}} c_j^{(n,q)} e^{i2k_l x j}. \quad (2.17)$$

Note that the factor 2 in the exponent is due to the squared cosine potential. The eigenvalue equation corresponding to the Hamiltonian (2.16) is now an equation for the coefficients $c_j^{(n,q)}$

$$\sum_{j' \in \mathbb{Z}} H_{jj'} c_{j'}^{(n,q)} = E_q^{(n)} c_j^{(n,q)} \text{ with } H_{jj'} = \begin{cases} [2j + q/(\hbar k_l)]^2 E_R + V_0/2 & \text{if } j' = j \\ V_0/4 & \text{if } j' = j \pm 1 \\ 0 & \text{otherwise} \end{cases} \quad (2.18)$$

By restricting to a finite value of coefficients, i.e. $-J \leq j \leq J$, this problem can be readily solved. Note that already relatively small values of J ($J \approx 10$) provide for accurate results. In Fig. 2.3 the energy band structure $E_q^{(n)}$ as a function of q for the periodic lattice potential is depicted. In Fig. 2.3(a), there is no lattice potential present, i.e. $V_0 = 0$. Here, the quadratic spectrum of free particles is observable. For deeper lattices, the lower bands, $E_q^{(n)} < 0$, correspond to bound states, while higher energy bands still belong to free particles. For deep enough lattices, e.g. as in Fig. 2.3(c), the energy gap between the two lowest bands is nearly constant and approximately given by $\hbar\omega_{\text{HO}}$. Very cold atoms correspond to energies much smaller than this value, which makes it possible to restrict the system to the lowest Bloch band.

2.2.3 Wannier Functions

The Bloch functions (2.15) are invariant under translations by integer multiples of the lattice constant. This is shown in Fig. 2.4, where we plot the probability density for the Bloch function $\phi_0^{(0)}(x)$ of the lowest band ($n = 0$) for $q = 0$ and several lattice depths. If the lattice is absent ($V_0 = 0$), the solutions are plane waves, leading to a homogeneous probability distribution. This is not suitable to describe particles, localized at a certain well of the optical lattice. Hence, by superimposing Bloch functions with different quasi-momenta, one is able to construct proper wavefunctions for localized particles.

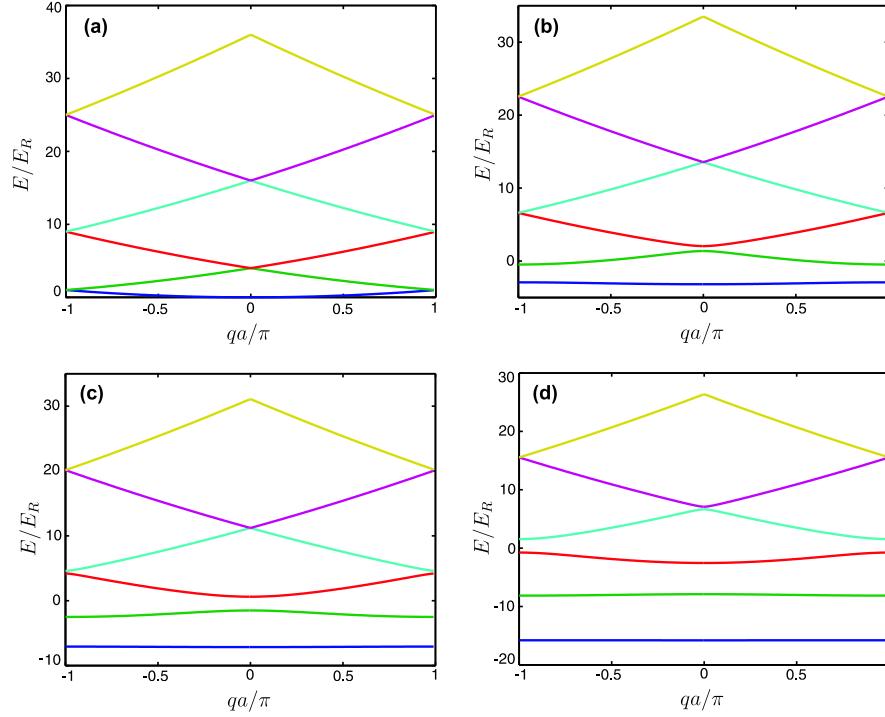


Figure 2.3. Energy band structure as a function of the quasimomentum for $V_0 \cos^2(k_l x)$ with $V_0 < 0$. The lattice constant is given by $a = \pi/k_l$. For a potential depth of (a) $V_0 = 0$ the energy spectrum is quadratic and corresponds to free particles. For deeper lattices, (b) $V_0 = -5E_R$ and (c) $V_0 = -10E_R$, the lower lying energy bands ($E_q^{(n)} < 0$) correspond to bound states. In (d), for $V_0 = -20E_R$, three bound states occur.

Such a family of orthonormal solutions of (2.14) which form a complete basis of the Hilbert space, corresponding to the particle's external degrees of freedom, are the Wannier functions [9, 10]. In principle the Wannier function mostly located at site x_j , corresponding to the n -th energy band, is defined - up to a normalization constant N - as the following superposition of Bloch functions:

$$w_n(x - x_j) = \frac{1}{\sqrt{N}} \int_{-\pi/a}^{\pi/a} dq \phi_q^{(n)}(x) e^{-iqx_j}. \quad (2.19)$$

Since the Bloch functions are unique only up to an arbitrary complex phase, the definition (2.19) is also not unique. Nevertheless, Kohn showed [11] that there exists only one choice of phases, such that the Wannier functions $w_n(x)$ (i) are real for each band, (ii) fall off exponentially, i.e. $|w_n(x)| \sim e^{-h_n x}$ for large $|x|$ with $h_n > 0$, and (iii) are either symmetric (for even n) or antisymmetric (for odd n) around the potential minima. The Wannier functions corresponding to this choice of phases, which we will use in the following, are known as *maximally localized* Wannier functions. In order to obtain these kind of Wannier functions, we have to choose the phases of $\phi_q^{(n)}(x)$ as follows [11]: For even band index n and also for the lowest energy band ($n = 0$), choose $\phi_q^{(n)}(0) \in \mathbb{R}$ and such that $q \mapsto \phi_q^{(n)}(0)$ is an analytic

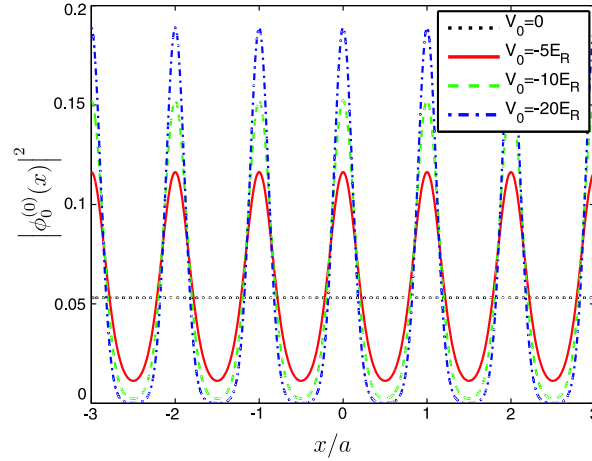


Figure 2.4. Probability distribution of the Bloch functions for the lowest band and zero quasimomentum, $|\phi_0^{(0)}(x)|^2$ for a lattice depth of $V_0 = 0$ (dotted, black line), $V_0 = -5E_R$ (solid, red line), $V_0 = -10E_R$ (dashed, green line) and $V_0 = -20E_R$ (dashed-dotted, blue line). If the lattice is absent, the particles are free, which implies a homogeneous probability distribution. The deeper the lattice gets, the more the wave function gets localized in every lattice well.

function. This can be ensured by choosing an equal sign for all coefficients in the Fourier sum (2.17). Then $w_n(x - x_j)$ are symmetric around x_j and real. For odd n , on the other hand, choosing $\phi_q^{(n)}(0)$ purely imaginary, and imposing the same smoothness condition on the Bloch functions lead to real but antisymmetric Wannier functions.

Since we restrict our investigations to very cold atoms, we only have to deal with Wannier functions of the lowest energy band. Examples of this Wannier functions are plotted in Fig. 2.5(a). Here we plotted $w_0(x)$ for $V_0 = -5E_R$ and $V_0 = -10E_R$. The deeper potential provides better localized wavefunctions. In Fig. 2.5(b) we depict the asymptotic behavior of the $n = 0$ Wannier functions on a logarithmic scale and compare it with their approximations by groundstate wavefunctions of harmonic oscillators (2.13). The deeper the potential, the better is this approximation. Nevertheless, $\log(|w_n(x)|)$ decreases linearly, whereas the harmonic oscillator functions are Gaussians, and show a quadratic behavior on a logarithmic scale.

2.3 The Bose-Hubbard Model

Originally, the Bose-Hubbard model was used to study systems in condensed matter theory, like electrons in periodic crystalline structures. For instance, Fisher et al. [12] were the first to investigate the phase diagram of the Bose-Hubbard Hamiltonian at temperature $T = 0$. The application of this model to cold atoms in optical lattices was firstly discussed by Jaksch et al. [13], which envisioned a wide variety of promising applications of AMO physics in the physics of condensed matter. Although this model is nowadays commonly used, we exhibit

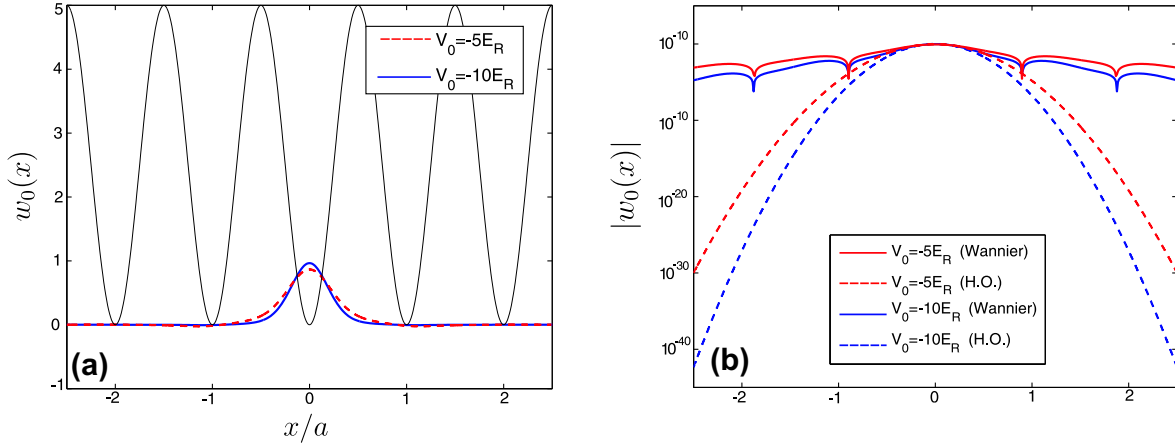


Figure 2.5. (a) Wannier functions $w_0(x)$ for $V_0 = -5E_R$ (dashed, red line) and $V_0 = -10E_R$ (solid, blue line). The lattice potential $V = -5E_R \cos^2(k_l x)$ is indicated with the thinner line. (b) Logarithmic absolute value of the Wannier functions $w_0(x)$ for $V_0 = -5E_R$ (red line) and $V_0 = -10E_R$ (blue line). The corresponding approximations by harmonic oscillator functions (2.13) are the dashed lines. Clearly one sees the decay $\propto e^{-|x|}$ for the Wannier functions, whereas the harmonic oscillator decay $\propto e^{-x^2}$.

its naive derivation, since a generalization of the Bose-Hubbard model (see chapters 5 and 6) to cold atoms in cavities, where the optical lattice is generated by the resonator, is the basis of our work in this thesis.

2.3.1 Microscopic Derivation of the Bose-Hubbard Hamiltonian

We consider two-level atoms in a one-dimensional optical lattice, consisting of M lattice sites, generated by counter-propagating laser light. A single atom is described by the Hamiltonian (2.11). Restricting the dynamics to two-body interactions, the situation with several bosonic particles is described with the second quantized formalism [14] in the form:

$$H = \int_{\mathbb{R}} dx \Psi^\dagger(x) \left(-\frac{\hbar^2}{2m} \nabla^2 + V(x) \right) \Psi(x) + \frac{1}{2} \int_{\mathbb{R}} \int_{\mathbb{R}} dx dy \Psi^\dagger(x) \Psi^\dagger(y) U(x, y) \Psi(x) \Psi(y). \quad (2.20)$$

Here $\Psi(x)$ denotes the field operator for the bosonic particles, $V(x) = V_0 \cos^2(k_l x) + V_T(x)$ is the external potential for the single particle, which consists of the lattice potential $V_0 \cos^2(k_l x)$ and an additional external trapping potential $V_T(x)$ (e.g. a magnetic parabolic potential). $U(x, y)$ denotes the two-body interaction. In the regime of cold temperatures, the only significant contribution to $U(x, y)$ are s-wave collisions, reducing the two-body interactions to contact interactions

$$U(x, y) = g_{1D} \delta(x - y), \quad (2.21)$$

where the coupling parameter g_{1D} is a function of a one-dimensional s-wave scattering length g_{1D} [15], the only parameter describing the two-body interaction. This means, only particles located at the same lattice well, interact significantly via $U(x, y)$. Note that in real-world

situations, the one-dimensional lattice is in principle only quasi one-dimensional, arising from a very tight confinement in the other two dimensions. In the 3D-case the contact interaction term is modeled by a pseudopotential [16]

$$U(\mathbf{x}) = \frac{4\pi\hbar^2 a_s}{m} \delta^3(\mathbf{x}) = g\delta^3(\mathbf{x}), \quad (2.22)$$

where m is the mass of the atoms and a_s denotes the s-wave scattering length. The integration in the second term of (2.20) has then to be performed over $\mathbb{R}^3 \times \mathbb{R}^3$. For tight axial confinement, which is necessary in order to consider one-dimensional optical lattices (and therefore the one-dimensional integration in the first term of (2.20)), the 3D-interaction can be reduced to a one-dimensional coupling strength g_{1D} [15].

In order to derive the Bose-Hubbard model, we expand the field operators in the Wannier basis

$$\Psi(x) = \sum_{i=1}^M \sum_{n=0}^{\infty} w_n(x - x_i) b_{n,i}, \quad (2.23)$$

where $b_{n,i}$ is the bosonic annihilation operator for a particle in the energy band n , located at site i , i.e. trapped in the lattice well around the potential minimum at x_i . As a first approximation we assume, such a low temperature T , that the corresponding energy is much lower than the energy gap between the two lowest Bloch bands, approximately given by $\hbar\omega_{\text{HO}}$. In addition, we assume that this applies also for the mean interaction energies $g_{1D}\langle\hat{n}_i\rangle$, where $\langle\hat{n}_i\rangle$ is the mean number of atoms at an arbitrary site i . If this is the case, we can restrict the second sum in (2.23) to the lowest energy band $n = 0$,

$$\Psi(x) = \sum_{i=1}^M w(x - x_i) b_i, \quad (2.24)$$

where $w(x) \equiv w_0(x)$ and $b_i \equiv b_{0,i}$. Replacing the field operators in (2.20) by this expression, we obtain the following Hamiltonian:

$$H = \sum_{k,l} E_{kl} b_k^\dagger b_l + V_0 \sum_{k,l} J_{kl} b_k^\dagger b_l + \sum_{k,l} V_{kl} b_k^\dagger b_l + \frac{1}{2} \sum_{i,j,k,l} U_{ijkl} b_i^\dagger b_j^\dagger b_k b_l, \quad (2.25)$$

where the first order matrix elements are given by

$$E_{kl} = \int_{\mathbb{R}} dx w(x - x_k) \left(-\frac{\hbar^2}{2m} \nabla^2 \right) w(x - x_l), \quad (2.26a)$$

$$J_{kl} = \int_{\mathbb{R}} dx w(x - x_k) \cos^2(kx) w(x - x_l), \quad (2.26b)$$

$$V_{kl} = \int_{\mathbb{R}} dx w(x - x_k) V_T(x) w(x - x_l). \quad (2.26c)$$

The matrix elements for the on-site interaction reads as

$$U_{ijkl} = g_{1D} \int_{\mathbb{R}} dx w(x - x_i) w(x - x_j) w(x - x_k) w(x - x_l). \quad (2.27)$$

The separation of the matrix elements for the kinetic energy (E_{kl}) and for the potential energy ($J_{kl}V_0$) is artificial here and they can be simply added. If an optical cavity with an intracavity quantum field is present this is no longer true. Therefore we retain this separation here.

Next, we assume that the variation of the additional external potential over the size of a single lattice well is negligible, i.e. $V_T(x)w(x-x_i) = V_T(x_i)w(x-x_i)$. Therefore, due to the orthonormality of the Wannier functions, the contribution of the external potential amounts to a discretized energy shift

$$V_{kl} = V_T(x_k) \int_{\mathbb{R}} dx w(x-x_k)w(x-x_l) = V_T(x_k)\delta_{kl} = \varepsilon_k\delta_{kl}. \quad (2.28)$$

The on-site elements J_{kk} and E_{kk} are independent of the lattice site k , and are therefore denoted by E_0 and J_0 , respectively. The off-site elements $J_{k,l}$ E_{kl} for $k \neq l$ are symmetric with respect to the lattice sites, and describe tunneling to other wells. Here we can safely restrict to hopping between neighboring sites (this is known as the tight-binding approximation). Since the next-nearest elements are typically two orders of magnitude smaller than the nearest-neighbor term [see Fig. 2.6(a) and Fig. 2.6(b)] they can safely be neglected. This means, E_{kl} and J_{kl} with $|k-l| > 1$ are omitted, and we denote the neighboring tunneling elements $E_{l,l+1}$ and $J_{l,l+1}$ by E and J , respectively.

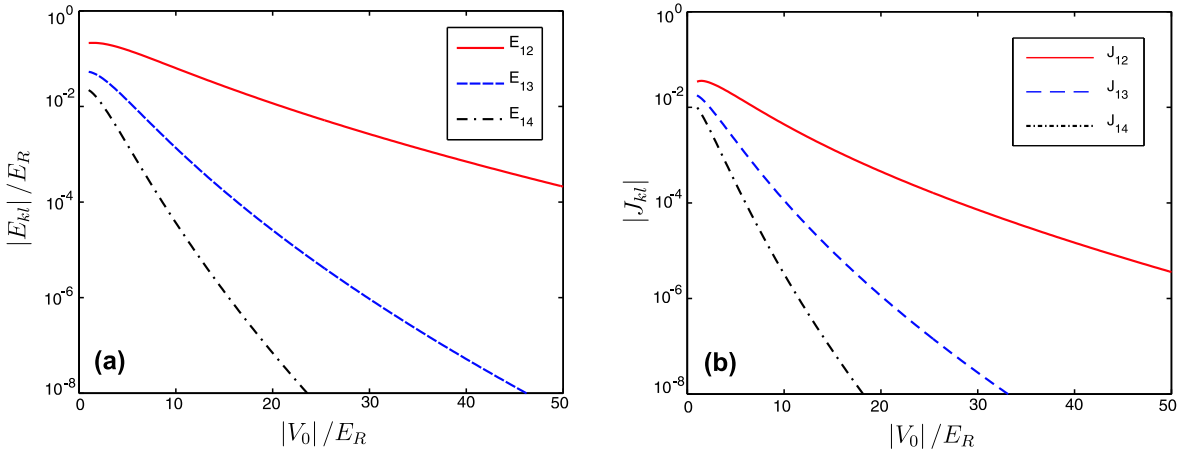


Figure 2.6. (a) Tunneling matrix elements for the kinetic energy for the nearest neighbors E/E_R (red, solid line), where $E \equiv E_{12}$, for the next-to-nearest neighbors E_{13}/E_R (blue, dashed line) and for the third neighbors E_{14}/E_R (black, dashed-dotted line) along one dimension as a function of the potential depth. (b) The same for the tunneling matrix element of the potential energy $J \equiv J_{12}$ (red, solid line), J_{13} (blue, dashed line) and J_{14} (black, dashed-dotted line). The nearest neighbor elements are at least two orders of magnitude larger and dominate.

Similar approximations can be performed for the on-site interaction matrix elements (2.27). Here, only U_{ijkl} with $i = j = k = l$ have to be taken into account since the pure overlap integrals of Wannier functions with at least one Wannier function sited at a

neighboring well are more than two orders of magnitude smaller than U_{kkkk} for an arbitrary k (See Fig. 2.7). Obviously, this matrix element is even smaller if one Wannier function is located at a next-to-neighboring well.

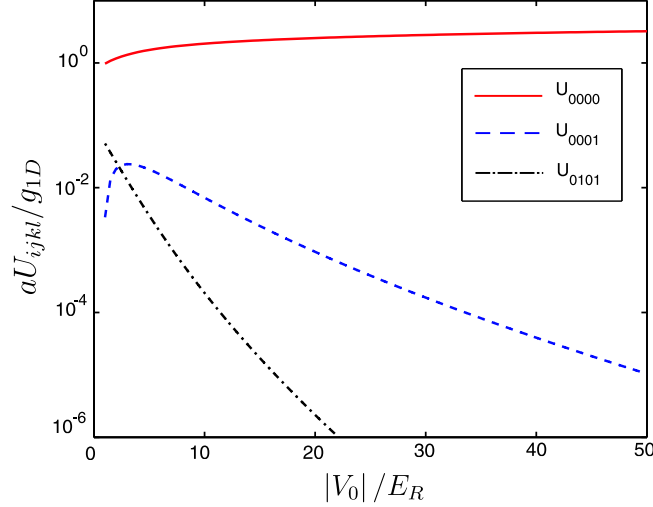


Figure 2.7. On-site interaction energy $U \equiv U_{0000}$ (red, solid line) in units of g_{1D}/a compared with nearest neighbor elements U_{0101} (blue, dashed line) and U_{0001} (black, dashed-dotted line) along one dimension as a function of the potential depth. The latter ones are negligible, since they are at least two orders of magnitude smaller.

Finally, combining all these approximations, we obtain the Bose-Hubbard Hamiltonian

$$H = (E_0 + J_0 V_0) \sum_{i=1}^M \hat{n}_i + (E + J V_0) \sum_{\langle i,j \rangle} b_i^\dagger b_j + \frac{U}{2} \sum_{i=1}^M \hat{n}_i (\hat{n}_i - 1) + \sum_{i=1}^M \varepsilon_i \hat{n}_i, \quad (2.29)$$

where $\hat{n}_i = b_i^\dagger b_i$ is the number operator for particles at site i , M is the number of wells and $\langle i, j \rangle$ denotes the summation over neighboring sites i and j . Note, that for a fixed number of particles, which we will assume, i.e. $\hat{N} = \sum_{i=1}^M \hat{n}_i = N \mathbf{1}$ the first sum is just a global energy shift and can be omitted. If an additional external trap is absent, which we will also assume in the following chapters, (2.29) reduces to

$$H = (E + J V_0) \sum_{\langle i,j \rangle} b_i^\dagger b_j + \frac{U}{2} \sum_{i=1}^M \hat{n}_i (\hat{n}_i - 1). \quad (2.30)$$

Note that in the absence of an external trapping potential, we can directly map the total tunneling matrix element $E + J V_0$ to the bandstructure. For $U = 0$ we have the usual tight-binding Hamiltonian [10]. The single-particle eigenstates of this model have the form

$$|\psi\rangle = \sum_{n=1}^M e^{i\alpha n} b_n^\dagger |0\rangle. \quad (2.31)$$

The constant α is determined by periodic boundary conditions $\alpha l = 2\pi M$, which we impose. Here l is an integer number. Applying the tight-binding Hamiltonian on $|\psi\rangle$ with eigenvalue E_α brings us to the relation

$$2(E + JV_0) = E_\alpha. \quad (2.32)$$

Obviously the total tunneling matrix element can then simply be found as

$$E + JV_0 = \frac{\max(E_q^{(0)}) - \min(E_q^{(0)})}{4}. \quad (2.33)$$

The zero denotes the lowest energy band. The hopping matrix element can thus be easily calculated from the Bloch band. Unfortunately this method does not work for the kinetic energy and the potential matrix element separately. Another approximation method is based on the Mathieu functions, solving also the single-particle Hamiltonian (2.11). For deep enough lattices, the matrix element is approximately given by [17]

$$E + JV_0 = \frac{4}{\sqrt{\pi}} E_R \left(\frac{|V_0|}{E_R} \right)^{3/4} e^{-2\sqrt{|V_0|/E_R}}. \quad (2.34)$$

The validity of this expression is shown in Fig. 2.8(f), where we compare the so estimated value of the tunneling element with the exact one, derived with Wannier functions. Nevertheless, the same disadvantage as above comes here into play.

For deep lattices it is also possible to approximate the Wannier functions by groundstate wavefunctions of harmonic oscillators (2.13), which allows for analytic expressions of the matrix elements (2.26) and (2.27):

$$E_0 = \frac{\hbar^2}{4mx_0^2}, \quad (2.35a)$$

$$E = \frac{\hbar^2}{4mx_0^2} \left(1 - \frac{\pi^2}{2k_l^2 x_0^2} \right) e^{-\pi^2/(4k_l^2 x_0^2)}, \quad (2.35b)$$

$$J_0 = \frac{1 + e^{-k_l^2 x_0^2}}{2}, \quad (2.35c)$$

$$J = \frac{1 - e^{-k_l^2 x_0^2}}{2} e^{-\pi^2/(4k_l^2 x_0^2)}, \quad (2.35d)$$

$$U = \frac{g_{1D}}{\sqrt{2\pi}x_0}. \quad (2.35e)$$

Here $x_0 = \sqrt{\hbar/(m\omega_{\text{HO}})} = 1/k \cdot (|V_0|/E_R)^{-1/4}$ is the width of the harmonic oscillator ground state. In Fig. 2.8 we compare the various matrix elements, on-site and off-site, for kinetic and potential energy as well as the on-site interaction U , calculated with the Wannier functions and with the harmonic oscillator approximation, as a function of the relative potential depth $|V_0|/E_R$. The on-site elements from both methods are converging, which is not the case for the off-site elements. Here, the harmonic oscillator elements always underestimate the real matrix elements. The reason for this behavior is the much stronger decrease of the Gauss functions than of the Wannier functions [see Fig. 2.5(b)].

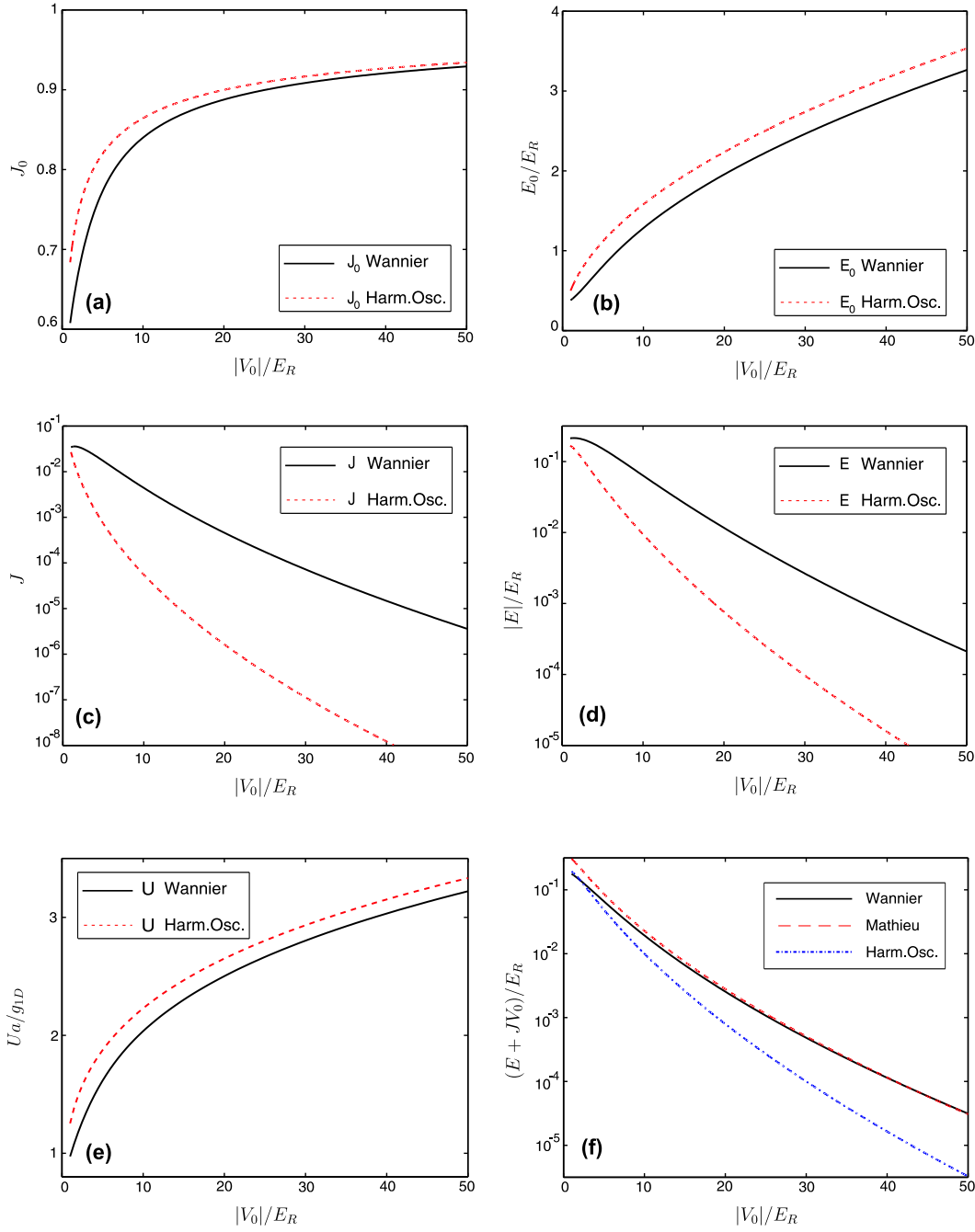


Figure 2.8. (a) On-site matrix elements of the kinetic energy E_0/E_R , calculated with Wannier functions (solid line) and with groundstate functions of a harmonic oscillator (2.13) (dashed line). (b) The same for the dimensionless on-site matrix element of the potential energy J_0 . (c) Tunneling matrix element of the kinetic energy E/E_R with Wannier functions (solid line) and oscillator functions (dashed-line). (d) The same as (c) for the potential energy J . (e) On-site interaction U in units of g_{1D}/a , for Wannier function (solid line) and harmonic oscillator functions (dashed line). (f) Tunneling matrix element of the total energy $(E + JV_0)/E_R$ calculated with Wannier functions (solid line), harmonic oscillator functions (dashed-dotted line), and the approximation by the Mathieu function (2.34) (dashed line). All quantities are plotted as functions of $|V_0|/E_R$.

2.3.2 The Superfluid State and the Mott Insulator State

In the Hamiltonian (2.30) there is a competition between the tunneling matrix element $E + JV_0$, which is essentially the kinetic energy element E , as we can see in Fig. 2.8(c) and (d), which tries to delocalize the particles and the interaction term U , which attempts to localize the particles and keeping the particle number fluctuations small. Essentially two parameters characterize the system, the average particle density $n = N/M$ and the ratio between interaction and hopping $U/(E + JV_0)$. Two main regimes exist for the system. On the one hand, the system can be either in a *superfluid* phase, where the single-particle wave functions are delocalized over the lattice. On the other hand, the system can be in the *Mott insulator* phase, where the particles are localized on single lattice sites. One of the first investigations in this direction was the study of the phase diagram of the Bose-Hubbard model by Fisher et al. [12], which we schematically depict in Fig. 2.9. At that time, however, an experimental verification seemed far out of reach. One of the main advantages of the realization of the Bose-Hubbard model with cold atoms in optical lattices, is the tunability of the ratio $U/(E + JV_0)$ via the power of the lattice lasers. A lot of investigation on this subject has now been done and also the first experimental realization of the Mott-insulator to superfluid phase transition in the seminal work by Greiner et al. [18] has been performed. For a review of the current status of the research on the field see [7].

Let us first consider the regime, where the kinetic energy dominates over the on-site interaction, i.e. $U/(E + JV_0) \rightarrow 0$. In this limit the ground state of the system is a superfluid state, which in the case of a lattice with M sites and N particles can be written as

$$|\text{SF}\rangle = \frac{1}{\sqrt{N!}} \left(\frac{1}{M} \sum_{i=1}^M b_i^\dagger \right)^N |0\rangle, \quad (2.36)$$

where $|0\rangle = |0, \dots, 0\rangle$ denotes the state of an empty lattice. In this state all atoms occupy the same single-particle wavefunction, which is delocalized over the lattice. This macroscopic occupation of one state realizes a Bose-Einstein condensate (BEC). Particle number fluctuations in a site i , $(\Delta \hat{n}_i)^2 = \langle \hat{n}_i^2 \rangle - \langle \hat{n}_i \rangle^2$ are large and scale as the average density N/M . Furthermore, the systems shows long-range off-diagonal coherence.

As $U/(E + JV_0)$ and hence the interaction energy increases, the particles repel each other more and more. This impedes the tunneling of particles to a neighboring site, since the necessary kinetic energy for this process is insufficient to negotiate the repulsion energy. When the particle density n is equal to one, the ground state of the systems, consists of a single localized particle in every well. Generally, a necessary condition for such a Mott insulator state, is an integer mean particle density. For $(E + JV_0)/U \rightarrow 0$ the ground state of the system is the Mott insulator state

$$|\text{MI}\rangle = \prod_{i=1}^M |n\rangle_i \quad (2.37)$$

for $n = N/M \in \mathbb{N}$. This state has no particle number fluctuations and the off-diagonal coherences decay exponentially with the distance of the respective sites.

In Fig. 2.9 we show this in the schematic picture of the Bose-Hubbard phase diagram, in the grand canonical ensemble for fixed mean number of particles $\bar{n} = \langle \hat{N} \rangle / M$ via a chemical

potential μ . The lobes correspond to the Mott insulator phases, with $n = 1, 2, \dots$ particles in every lattice site. In this lobes, particle number fluctuations vanish. We can also observe, that for non-integer $\bar{n} \notin \mathbb{N}$, even for $U \ll (E + JV_0)$, the system is not in the Mott insulating regime. A small fraction of particles remain superfluid on top of the Mott insulator core, this is the regime between the Mott lobes, indicated by the solid line $\langle \hat{n} \rangle = 1 + \varepsilon$ in Fig. 2.9. For $E + JV_0 = 0$ the necessary energy to increase the average particle density by one is just the on-site interaction energy U . Therefore the elongation of each lobe at the ordinate is just U .

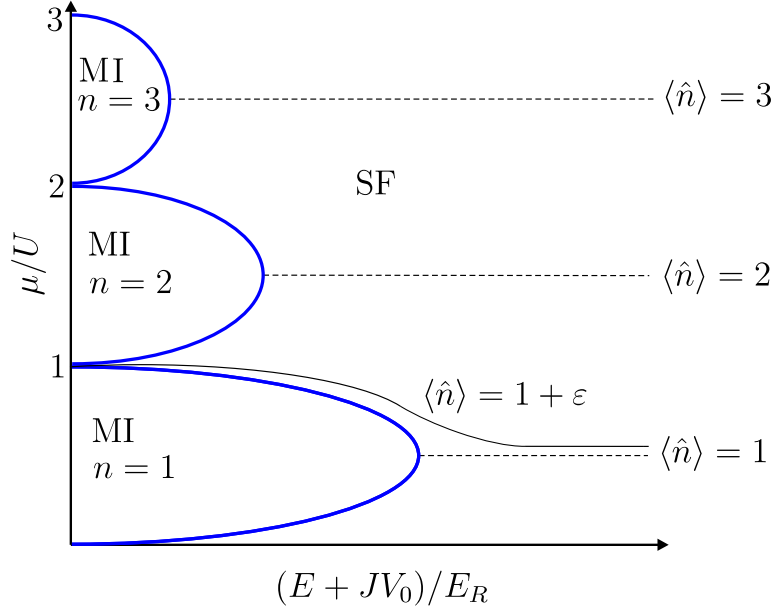


Figure 2.9. Schematic phase diagram for the Bose-Hubbard model (2.29) at zero temperature without external trap, i.e. $\varepsilon_i = 0$ for all i . The Mott lobes indicate regimes, where the particles are in the Mott insulating regime, with fixed number of $n = 1, 2, \dots$ particles per site.

The transition from the Mott insulator phase to the superfluid phase realizes a so-called quantum phase transition, i.e. a phase transition at zero temperature. We will not discuss the quantum statistical features of this system in greater detail, instead we refer the interested reader for instance to [19].

Bibliography

- [1] C. Cohen-Tannoudji, in *Les Houches, Session LIII, 1990 - Fundamental Systems in Quantum Optics*, edited by J. Dalibard, J. M. Raimond, and J. Zinn-Justin (Elsevier Science Publishers B. V., Amsterdam, 1992).
- [2] C. W. Gardiner and P. Zoller, *Quantum Noise*, 3rd Ed., (Springer, Berlin, 2005).
- [3] C. Cohen-Tannoudji, J. Dupont-Roc, and G. Grynberg, *Atom-Photon Interactions: Basic Processes and Applications*, (John Wiley and Sons, New York, 1998).

-
- [4] P. S. Jessen and I. H. Deutsch, *Optical Lattices*, Adv. At. Mol. Opt. Phys. **37**, 95 (1996).
 - [5] P. B. Blakie and C. W. Clark, *Wannier States and Bose-Hubbard Parameters for 2D Optical Lattices*, J. Phys. B **37**, 1391 (2004).
 - [6] D. Jaksch and P. Zoller, *The Cold Atom Hubbard Toolbox*, Ann. Phys. **315**, 52 (2005).
 - [7] M. Lewenstein, A. Sanpera, V. Ahufinger, B. Damski, A. Sen De, and U. Sen, *Ultracold Atomic Gases in Optical Lattices: Mimicking Condensed Matter Physics and Beyond*, Adv. Phys. **56**, 243 (2007).
 - [8] M. Abramovitz and I. A. Stegun, *Handbook of Mathematical Functions with Formulas, Graphs, and Mathematical Table*, (Dover, 1972).
 - [9] N. W. Ashcroft and N. D. Mermin, *Solid State Physics*, International Ed., (Holt Rinehart and Winston, 1987).
 - [10] C. Kittel, *Introduction to Solid State Physics*, 8th Ed., (John Wiley and Sons, New York, 2004).
 - [11] W. Kohn, *Analytic Properties of Bloch Waves and Wannier Functions*, Phys. Rev. **115**, 809 (1959).
 - [12] M. P. A. Fisher, P. B. Weichmann, G. Grinstein, and D. S. Fisher, *Boson Localization and the Superfluid-Insulator Transition*, Phys. Rev. B **40**, 546 (1989).
 - [13] D. Jaksch, C. Bruder, J. I. Cirac, C. W. Gardiner, and P. Zoller, *Cold Bosonic Atoms in Optical Lattices*, Phys. Rev. Lett. **81**, 3108 (1998).
 - [14] See, for example, A. Galindo and P. Pascual, *Quantum Mechanics II*, (Springer, Berlin, 1990).
 - [15] M. Olshanii, *Atomic Scattering in the Presence of an External Confinement and a Gas of Impenetrable Bosons*, Phys. Rev. Lett. **81**, 938 (1998).
 - [16] See, for example, K. Huang, *Statistical Mechanics*, (Wiley, New York 1987).
 - [17] W. Zwerger, *Mott-Hubbard Transition of Cold Atoms in Optical Lattices*, J. Opt. B **5**, 9 (2003).
 - [18] M Greiner, O. Mandel, T. W. H'ansch, and IBloch, *Quantum Phase Transition from a Superfluid to a Mott Insulator in a Gas of Ultracold Atoms*, Nature (London), **415**, 39 (2002).
 - [19] S. Sachdev, *Quantum Phase Transitions*, (Cambridge University Press, 1999).

CHAPTER 3

BACKGROUND: BASICS OF CAVITY QUANTUM ELECTRODYNAMICS (CQED)

In chapter 2 we briefly reviewed some of the main features of the theory of cold atoms in optical lattices and discussed the physical applications thereof, allowing for an experimental realization of the Mott insulator to superfluid phase transition.

In this chapter we will deal with another versatile quantum optical system. Optical cavities turned out to be a useful tool to significantly enhance the interaction between matter and light on a fundamental quantum level, providing for a variety of applications in AMO physics. Moreover, in the strong coupling regime, a backaction mechanism of the intracavity light field on the motion of atoms inside the resonator and vice versa exists. Hence, atom and cavity has to be considered as a single entity, the atom-cavity system. A number of impressive results based on this complex interaction has been predicted and experimentally verified in the last years.

In this chapter on basic essentials of cavity QED, we first present some general properties of cavities, followed by a discussion of the Jaynes-Cummings Hamiltonian [1], describing the interaction of an atom with a single mode of the cavity. Next we introduce dissipation, namely spontaneous emission of photons from atoms and loss of cavity photons to the system, which is now also coherently driven. Then we discuss how to eliminate the excited state of the two-level atom from the dynamics, to obtain an effective Hamiltonian, which is the crucial element in the description of the resonator-generated optical lattice, as a generalization of the optical lattices, discussed in the previous chapter. Furthermore, we briefly show how to add an additional far-detuned dipole trap (classical optical lattice), not influenced by the cavity mode, as an additional, useful element of the model. Finally, we consider motion transverse to the cavity axis (up to here only motion along the cavity axis will be allowed), which leads to a slight variation in the corresponding Hamiltonian.

3.1 Atoms in Optical Cavities

This section is devoted to recapitulate the important properties of optical cavity resonators. We start with a discussion about classical resonators, followed by introducing ideal (lossless) quantum cavities, i.e. atoms inside the resonator are coupled to the quantized intracavity field. Finally we add dissipation to the system, in order to describe more realistic situations.

3.1.1 Optical Cavities

We consider a Fabry-Perot resonator, consisting of two highly reflective mirrors, where monochromatic light is coupled in at one mirror, and the transmitted intensity is measured

at the opposite mirror. In order to achieve a simple illustration, we assume the mirrors to be flat and parallel with an axial distance of L (x -direction). An incident plane wave $E_{\text{in}} = E_0 \cos(kx)$ leaks into the empty cavity via one of the mirrors, as depicted in Fig. 3.1.

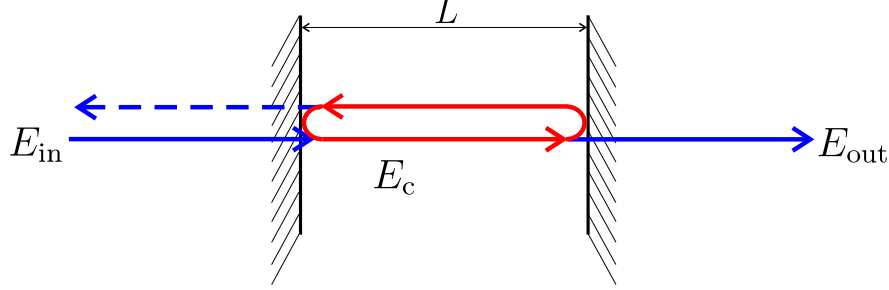


Figure 3.1. Schematic diagram of a Fabry-Perot type resonator, consisting of two parallel mirrors with distance L . On the left mirror light is coupled in, on the right mirror it leaks out of the resonator, where it is detected.

Generally, the normal modes of an empty cavity are defined as the solutions of the Helmholtz equation

$$\left(\nabla^2 + \frac{\omega^2}{c^2}\right) u(\mathbf{x}) = 0, \quad (3.1)$$

which fulfill appropriate boundary conditions, corresponding to the specific mirror geometry. The electric field is a superposition of the eigenmodes $u_{nmk}(\mathbf{x})$ with eigenfrequencies ω_{nmk} . In our one-dimensional example this is fairly easy, since the electric field has to vanish at the mirror, we obtain

$$u_n(x) = \sin\left(\frac{\pi n}{L}x\right) \quad \text{and} \quad \omega_n = \frac{n\pi c}{L} \quad \text{for } n \in \mathbb{N} \quad (3.2)$$

Two consecutive longitudinal modes of the resonator are characterized by consecutive mode numbers n , which are typically very large. The corresponding difference in frequency is called *free spectral range*

$$\nu_{\text{FSR}} \equiv \frac{\omega_{n+1} - \omega_n}{2\pi} = \frac{c}{2L} \quad (3.3)$$

The transmitted light has a maximum, when its frequency corresponds to one of the eigenfrequencies. Hence, two peaks in the transmission signal are separated by ν_{FSR} . If the mirrors are not of this perfect (and idealistic) form, the mode functions are much more complicated and of course in reality three-dimensional. This implies the appearance of transverse modes, i.e. modes with transverse (here y - and z -direction) intensity dependence, like the transverse-electro-magnetic modes TEM_{nm} . In a cavity formed by two spherical mirrors, the most fundamental mode is the TEM_{00} mode [2]. This mode is also called *Gaussian mode*, since - near the cavity center - its radial dependence is that of a Gaussian function¹

$$u_{00}(\mathbf{x}) = \sin(kx)e^{-(y^2+z^2)/w_0^2}, \quad (3.4)$$

¹In the rest of this thesis, though, we will use $\cos(kx)$ instead of the sin-function. This amounts just in an addition of a global phase and makes physically no difference. With the cosine, we have a potential well at $x = 0$.

where the beam radius $w(x) = w_0 \sqrt{1 + 4x^2/(k^2 w_0^4)}$ at the cavity center ($x = 0$) is called waist of the cavity and $k = 2\pi/\lambda$ is the mode wavenumber. Here we omitted the longitudinal mode number, which precisely has to be taken into account via λ . For a symmetric cavity the waist can be calculated [3]:

$$w_0^2 = \frac{L}{k} \sqrt{\frac{2R-L}{L}}. \quad (3.5)$$

Here, R is the radius of curvature of the mirror. For a confocal cavity ($R = L$) this reduces to $w_0^2 = L/k$. The mode volume of the cavity is the integral of the squared modulus of the corresponding mode function, i.e.

$$V = \int_{\mathbb{R}^3} d^3\mathbf{x} |u_{00}(\mathbf{x})|^2 \approx \frac{\pi w_0^2}{4} L, \quad (3.6)$$

if we assume that the edges of the cavity mirrors at $x = 0$ and $x = L$ are impenetrable, resulting in a vanishing mode function for $x < 0$ and $x > L$.

Let us now come back to our simplified plane mirror model and assume, that both mirrors have a reflectivity \mathcal{R} , a transmittivity \mathcal{T} and a loss rate \mathcal{L} , resulting from absorption and scattering in the mirror medium. Furthermore we assume, that the cavity is enclosed by a vacuum, i.e. the index of refraction is one. At any of the two mirrors the relation $\mathcal{R} + \mathcal{T} + \mathcal{L} = 1$ must hold. According to Airy's formula, the total transmittivity of the resonator is [4]

$$\mathcal{T}_{\text{cav}} = \frac{\mathcal{T}^2}{(1 - \mathcal{R})^2 + 4\mathcal{R} \sin^2(kL)} \quad (3.7)$$

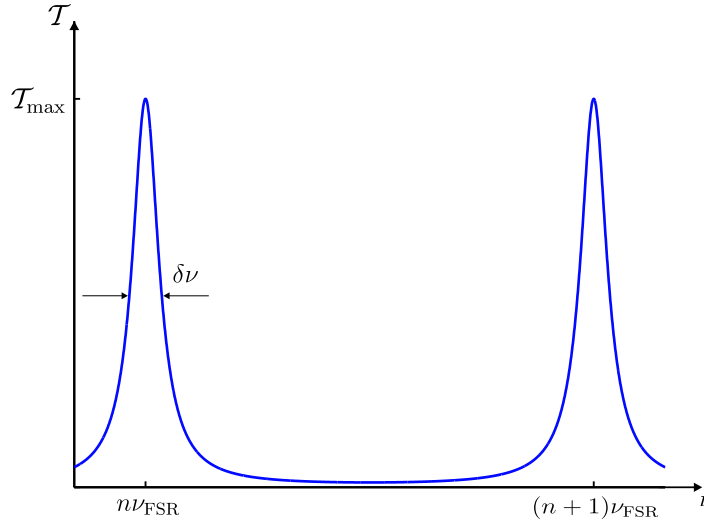


Figure 3.2. Transmittivity of the Fabry-Perot resonator corresponding to (3.7) as a function of the frequency of the incoming light. The distance between the peaks of the Lorentzians is called the free spectral range ν_{FSR} . The linewidth (FWHM) $\delta\nu$ defines the cavity decay rate κ .

When the frequency of the incoming field is on resonance with one of the longitudinal modes ($kL = 2\pi n$), this expression presumes its maximum $\mathcal{T}_{\text{max}} = \mathcal{T}^2/(1 - \mathcal{R})^2$. Expanding

the \sin -function in the denominator of (3.7), which is possible for wavenumbers $k = \omega/c$ close to one of the mode frequencies, we obtain a Lorentz profile for (3.7) around the peak at $\nu = n\nu_{\text{FSR}}$ (see Fig. 3.2)

$$\mathcal{T}_{\text{cav}} \approx \frac{\mathcal{T}_{\text{max}}}{1 + 4 \left(\frac{\mathcal{F}}{\nu_{\text{FSR}}} \right)^2 (\Delta\nu)^2}, \quad (3.8)$$

where $\Delta\nu = \nu - n\nu_{\text{FSR}}$. Here we defined a very important characteristic parameter for resonators, the finesse \mathcal{F} by

$$\mathcal{F} = \frac{\pi\sqrt{\mathcal{R}}}{1 - \mathcal{R}}. \quad (3.9)$$

Note, that the finesse solely depends on the reflectivity of the mirror and gives a measure for the resolutions of the light field in the resonator, before it leaks out of the cavity. From this Lorentzian we can easily read off the width (FWHM) $\delta\nu = \kappa/\pi$ (κ is therefore known as the cavity loss rate)

$$\delta\nu = \frac{\kappa}{\pi} = \frac{\nu_{\text{FSR}}}{\mathcal{F}}. \quad (3.10)$$

Finally the quality factor, or Q -factor, of a resonator at resonance is defined as 2π times the ratio of stored energy in the cavity to energy loss per oscillation period, i.e.

$$Q = 2\pi \frac{W}{\Delta W} = \omega \frac{W}{P_L}, \quad (3.11)$$

where W is the energy, stored in the resonator, $\Delta W = \tau P_L$ the energy loss per oscillation period (duration τ) and $P_L = -\frac{dW}{dt}$ the energy loss per unit time. Using the decay constant of the resonator, $\kappa = P_L/W$, we obtain:

$$Q = \frac{\omega}{\kappa} = 2\pi n \frac{\nu_{\text{FSR}}}{\kappa} = 2n\mathcal{F}. \quad (3.12)$$

Here, n denotes the number of the longitudinal mode.

We conclude this section with an overview of current state-of-the-art numbers, which experimental cavity QED groups have achieved. The group of Jeff Kimble at Caltech [5] use a cavity with a length of $L = 42.2\mu\text{m}$, waist $w_0 = 20\mu\text{m}$ and mirrors with a curvature radius of $R = 20\text{cm}$. The finesse has a value of $\mathcal{F} = 4.2 \times 10^5$ and at a cavity frequency of $\omega = 2.211\text{MHz}$ (corresponding to the D2 line of atomic Caesium $\lambda = 852.4\text{nm}$) a Q -factor of $Q = 8.584 \times 10^7$. In one of the most recent experiments in Gerhard Rempe's group at MPQ Garching [6] the cavity in use has a length of $L = 0.122\text{mm}$ and a waist of $w_0 = 29\mu\text{m}$. They operate at a frequency of $\omega = 2.416\text{MHz}$, corresponding to $\lambda = 780.2\text{nm}$. The finesse of the cavity is $\mathcal{F} = 4.4 \times 10^5$ and its quality factor $Q = 1.282 \times 10^8$.

3.1.2 The Jaynes-Cummings Hamiltonian

We consider here a single two-level atom, interacting with a single mode of the quantized electromagnetic field, first investigated by Jaynes [1]. This model is a reasonable approximation for an atom interacting with the field inside an optical resonator without losses. In

principle, the procedure is similar to the case of the interaction with a classical field, presented in Sec. 2.1.1. A single one-dimensional standing wave quantized mode with frequency ω_c is given by [7]

$$\mathbf{E}(\mathbf{x}) = i\sqrt{\frac{\hbar\omega_c}{2\varepsilon_0 V}}u(\mathbf{x})a\boldsymbol{\epsilon} + \text{h.c.} \quad (3.13)$$

Here V denotes the quantization volume and $u(\mathbf{x})$ the mode function of the cavity mode (3.6). The annihilation operator of a photon of the considered mode is given by $a \equiv \hat{a}$, whereas a^\dagger corresponds to the creation of a cavity photon. Near the center of a confocal, Fabry-Perot cavity the mode function in axial direction (here: x -direction) is cosine-like, whereas in transverse direction, the mode function decays as a Gaussian,

$$u(\mathbf{x}) = \cos(kx)e^{-(y^2+z^2)/w_0^2}. \quad (3.14)$$

In the following, we will neglect the transversal dependence and assume the region of interaction is exactly in the center of the cavity. We assume the ground state energy of the atom to be zero ($E_g = 0$), and use the electromagnetic dipole and long-wavelength approximation. Then the Hamiltonian for a single atom, interacting with a single quantized mode is given by

$$\begin{aligned} H &= H_A + H_F + H_I \\ &= \frac{\hat{p}^2}{2m} + \hbar\omega_{eg}|e\rangle\langle e| + \hbar\omega_c \left(a^\dagger a + \frac{1}{2} \right) - i\hbar g(\hat{x}) \left(a - a^\dagger \right) \otimes (\sigma_+ + \sigma_-), \end{aligned} \quad (3.15)$$

where $g(\hat{x}) = \langle e|\mathbf{d}\cdot\boldsymbol{\epsilon}|g\rangle \cos(k\hat{x})\sqrt{\omega_c/(2\varepsilon_0 V\hbar)}$ denotes the coupling strength. The other notations are the same as in Sec. 2.1.1. Again the interaction Hamiltonian H_I consists of two resonant terms $\sigma_+ \otimes a$, $\sigma_- \otimes a^\dagger$, and two non-resonant terms $\sigma_+ \otimes a^\dagger$, $\sigma_- \otimes a$. The first correspond to a transition of the atom $|g\rangle \rightarrow |e\rangle$ accompanied by the annihilation of a photon of the field mode and a transition $|e\rangle \rightarrow |g\rangle$, together with the creation of a photon, both of these processes are energy conserving. The latter ones correspond to a transition of the atom $|g\rangle \rightarrow |e\rangle$ accompanied by the emission of a photon of the field mode and a transition $|e\rangle \rightarrow |g\rangle$, together with the annihilation of a photon. They are highly off-resonant and do not conserve energy. Therefore we can safely neglect them (rotating wave approximation). Finally the Hamiltonian, after a simple energy shift reads as follows:

$$H = \frac{\hat{p}^2}{2m} + \hbar\omega_{eg}|e\rangle\langle e| + \hbar\omega_c a^\dagger a - i\hbar g(\hat{x}) \left(\sigma_+ a - \sigma_- a^\dagger \right). \quad (3.16)$$

This is the well known Jaynes-Cummings Hamiltonian. From this point on we omit the tensor product between operators acting on different Hilbert spaces. Let us briefly review the properties of this system, which can easily be solved analytically. If we neglect, for the moment, the translational degrees of freedom, the ground state of this system is $|g, 0\rangle$, where the atom is in its internal ground state and zero photons are present in the cavity. Generally the eigenstates are superpositions of $n+1$ photons in the cavity and the atom in the ground state, $|g, n+1\rangle$, and n photons in the cavity, but the atom in the excited state, $|e, n\rangle$. We formulate this as follows:

$$|+, n\rangle = \cos\theta_n|e, n\rangle + \sin\theta_n|g, n+1\rangle, \quad (3.17a)$$

$$|-, n\rangle = -\sin\theta_n|e, n\rangle + \cos\theta_n|g, n+1\rangle. \quad (3.17b)$$

The basis $\{|+, n\rangle, |-, n\rangle\}$ is called the *dressed states* basis. Within the rotating frame approximation, the Hamiltonian can be decomposed as a direct sum $H = \sum H_n$, where each H_n acts just in the manifold \mathcal{E}_n , spanned by the *bare states* basis $\{|g, n+1\rangle, |e, n\rangle\}$. The rotation angle θ_n is determined by the coupling $g(x)$ and the atom-cavity detuning $\Delta = \omega_c - \omega_{eg}$.

$$\tan 2\theta_n = -\frac{2g\sqrt{n+1}}{\Delta} \quad \text{with} \quad 0 \leq 2\theta_n \leq \pi, \quad (3.18)$$

which results in coefficients for the dressed states of

$$\cos \theta_n = \sqrt{\frac{\Omega_n + \Delta}{2\Omega_n}} \quad \text{and} \quad \sin \theta_n = \sqrt{\frac{\Omega_n - \Delta}{2\Omega_n}}, \quad (3.19)$$

where $\Omega_n = \sqrt{\Delta^2 + 4g^2(n+1)}$. Fig. 3.3 shows the correspondence between the dressed states and uncoupled bare states. The energy eigenvalues of the dressed states are

$$E_{\pm, n} = n\hbar\omega_c + \frac{\hbar(\omega_c + \omega_{eg})}{2} \pm \frac{\hbar}{2}\Omega_n. \quad (3.20)$$

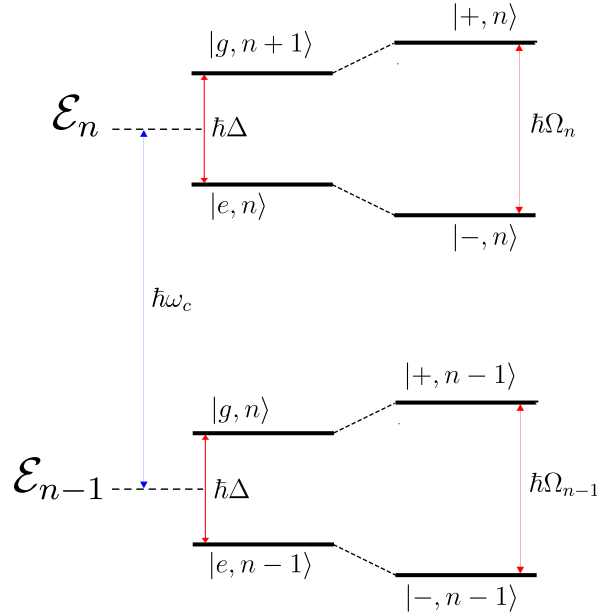


Figure 3.3. Schematic diagram of the uncoupled bare states (left) and the the dressed states (right), which are the eigenstates of the coupled system. The dressed states corresponding to n photons are forming manifolds \mathcal{E}_n , which are energetically well separated by the energy of one cavity photon $\hbar\omega_c$. The splitting of the dressed states within each manifold depends on n via Ω_n .

The coupling with the light mode induces a light shift, as in the case of the interaction with a classical light field. This energy splitting $E_{+, n} - E_{-, n} = \hbar\Omega_n$ depends via $g = g(\hat{x})$ on the atomic position. The splitting of the lowest pair of energy levels, corresponding to $n = 0$,

is called *normal mode splitting* or *vacuum Rabi-splitting*. At resonance ($\Delta = 0$) its value is just given by the, spatial dependent, coupling strength $g(x)$

$$\Delta E_0(x) = 2\hbar g(x) \quad (3.21)$$

This normal mode is visible, when the atom is strongly interacting with the a single photon of the cavity, which implies that the coupling constant is larger than the corresponding linewidths, i.e. $g_0 \gg (\gamma, \kappa, \tau^{-1})$, where τ is the interaction time of the atom and the cavity mode. g_0 denotes the maximum of the coupling constant. Meeting these criteria experimentally is a very hard and complicated task, especially for cavities of optical frequencies. The first who observed the normal mode splitting in the optical regime were Thompson et al. [8]. The opposite limit $\kappa \gg g$ is called bad-cavity limit. Recent experimental numbers are, for instance, $(g_0, \kappa, \gamma)/2\pi = (34, 4.1, 2.5)$ MHz in Kimble's group [5], while at the MPQ in Garching the group of Rempe applies $(g_0, \kappa, \gamma)/2\pi = (16, 1.4, 3)$ MHz in the blue-detuned dipole trap experiment [6].

For a not too large coupling constant, we can calculate approximate energy shifts of the eigenstates of (3.16), using time-independent perturbation theory.

$$\Delta E \approx -\hbar g^2(x) \frac{n+1}{\Delta} \quad \text{for } |g, n+1\rangle, \quad (3.22a)$$

$$\Delta E \approx +\hbar g^2(x) \frac{n+1}{\Delta} \quad \text{for } |e, n\rangle. \quad (3.22b)$$

Therefore we are in a similar situation as in the classical model before (2.7), with the difference, that the depth of the cavity-induced lattice now depends on the number of photons in the cavity mode. In Figure 3.4 we schematically depict the dependence of the energy spectrum on the axial position of the atom, within one well. Since the energy is increasing with n this energy spectrum is known as the Jaynes-Cummings ladder. Since dissipative effects play a crucial role in cavities, we postpone a more detailed discussion of the resonator-generated lattice, after an introduction of lossy channels and coherent driving schemes to the cavity. Note that here at least one photon has to be present to realize this potential. The state $|g, 0\rangle$ experiences no energy shift. Other models exist, where also an empty cavity can induce trapping potentials [9].

3.1.3 Open Systems - Dissipation

The Jaynes-Cummings Hamiltonian, derived in the previous section, describes closed systems and therefore does not take into account any losses whatsoever. This simplification is in most experimental situations too crude and interactions of the system with the environment cannot be ignored. From the various possible loss channels, only two are of major importance for our studies. Our system is assumed to be coupled to the environment via spontaneous emission of photons from the atoms and via loss of photons from the cavity. Not only that these damping mechanisms allow to gain information about the system, i.e. the atoms and the intracavity field, they also provide the necessary channel to transport entropy out of the system, a basic requirement to perform cavity cooling.

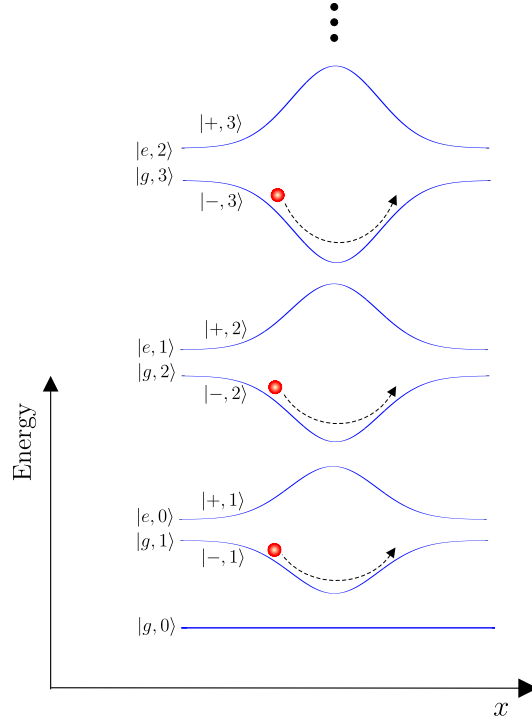


Figure 3.4. Axial dependence of the energy eigenvalues (3.22) within one well of the lattice potential, generated by the cavity. The depth of these wells is increasing with increasing n (number of photons in the cavity), therefore this energy spectrum is called Jaynes-Cummings ladder.

Beside these losses, we consider two coherent pumping laser fields, both with frequency ω_p (see Fig. 3.5). One of these driving lasers is directly impinging on the atoms, the other pumping field excites the cavity modes, by directly injecting a laser beam through one of the cavity mirrors. The interaction of the atoms with this coherent pumping field can be modeled by an interaction with a classical field (see Sec. 2.1.1). In the rotating frame approximation, the corresponding Hamiltonian is [cf. (2.2) and (2.4)]

$$H_{AP} = -i\hbar h(\hat{\mathbf{x}})\zeta (\sigma_+ e^{-i\omega_p t} - \sigma_- e^{i\omega_p t}). \quad (3.23)$$

$h(\mathbf{x})$ denotes the mode function of the pump laser and ζ its strength. They are given by $h(\hat{\mathbf{x}})\zeta = -iE_p(\hat{\mathbf{x}})\langle e|\mathbf{d}\cdot\boldsymbol{\epsilon}|g\rangle$. The laser field pumping the atoms is formed by a broad standing wave, transversally to the cavity axis, i.e. $E_p(\hat{\mathbf{x}}) = E_p \cos(k_p \hat{y})$. Since we are only interested in the dynamics in the direction of the cavity axis, we can neglect the spatial dependence of the pumping field, and without loss of generality, we can set $h(\mathbf{x}) \equiv 1$. This driving field will often be referred to as the “atom pump”.

In addition, also the cavity mode is coherently excited by a driving laser field, with strength η and the same frequency ω_p , in order to get rid of the time dependencies of both of the driving fields, simultaneously. In the following this will be often called the “cavity

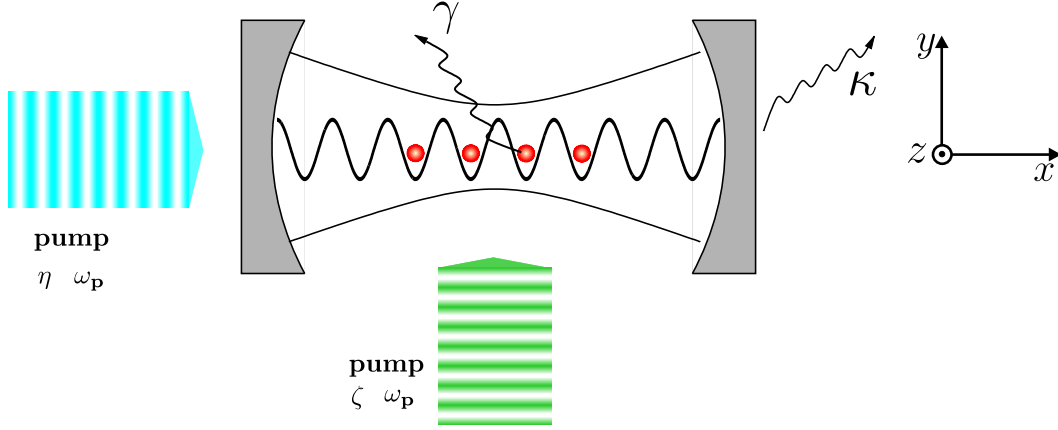


Figure 3.5. Scheme of atoms in a cavity, interacting with a single cavity mode. The system is coupled to a reservoir via cavity loss, characterized by the loss rate κ and spontaneous emission from photons, described by the spontaneous emission rate γ . Furthermore, two pump lasers, both with the same frequency ω_p but different strength, are coherently driving the system.

pump". The Hamiltonian, describing this contribution is

$$H_{CP} = -i\hbar\eta \left(ae^{i\omega_p t} - a^\dagger e^{-i\omega_p t} \right). \quad (3.24)$$

Although, in principle, η and ζ can be chosen complex, to describe other relative phases, which also allows for interesting effects [10], we restrict in this work on real η and ζ . Altogether, the Hamiltonian describing the non-dissipative evolution of the system thus is

$$\begin{aligned} H_S &= H_A + H_F + H_I + H_{AP} + H_{CP} \\ &= \frac{\hat{p}^2}{2m} + \hbar\omega_{eg}|e\rangle\langle e| + \hbar\omega_c a^\dagger a - i\hbar g(\hat{x}) (\sigma_+ a - \sigma_- a^\dagger) \\ &\quad - i\hbar\zeta (\sigma_+ e^{-i\omega_p t} - \sigma_- e^{i\omega_p t}) - i\hbar\eta (ae^{i\omega_p t} - a^\dagger e^{-i\omega_p t}). \end{aligned} \quad (3.25)$$

To eliminate the time dependence, we perform a unitary transformation $|\tilde{\psi}\rangle = U(t)|\psi\rangle$, where $U = \exp[i\omega_p t(\sigma_+ \sigma_- + a^\dagger a)]$. This corresponds to a transformation $\tilde{H} = U H U^\dagger + i\hbar \left(\frac{d}{dt} U \right) U^\dagger$. Omitting the tilde we obtain

$$H_S = \frac{\hat{p}^2}{2m} - \hbar\Delta_a |e\rangle\langle e| - \hbar\Delta_c a^\dagger a - i\hbar g(\hat{x}) (\sigma_+ a - \sigma_- a^\dagger) - i\hbar\zeta (\sigma_+ - \sigma_-) - i\hbar\eta (a - a^\dagger), \quad (3.26)$$

where $\Delta_a = \omega_p - \omega_{eg}$ and $\Delta_c = \omega_p - \omega_c$ denote the atom-pump detuning and the cavity-pump detuning, respectively.

In order to develop a theoretical description for the interaction of a system \mathcal{S} with a reservoir \mathcal{R} , which form altogether a Hilbert space $\mathcal{H} = \mathcal{H}_S \otimes \mathcal{H}_R$. The system is then

described by the Hamiltonian H_S from (3.26). Typically the reservoir is modelled as a bath of independent harmonic oscillators with frequencies ω_k and a free-evolution Hamiltonian

$$H_R = \sum_{k=0}^{\infty} \left(c_k^\dagger c_k + \frac{1}{2} \right), \quad (3.27)$$

where c_k and c_k^\dagger are annihilation and creation operators for the reservoir excitations, respectively. For the interaction of the system variables with the reservoir, we use the rotating frame approximation. Then the atom-reservoir Hamiltonian is analogue to the Jaynes-Cummings Hamiltonian, but with many modes

$$H_{AR} = \sum_{k=0}^{\infty} g_{AR,k}(x) \left(\sigma_+ c_k + \sigma_- c_k^\dagger \right). \quad (3.28)$$

Similarly the Hamiltonian for the coupling of the reservoir modes to the cavity mode is in the same line as (3.24)

$$H_{CR} = \sum_{k=0}^{\infty} g_{CR,k} \left(a^\dagger c_k + a c_k^\dagger \right). \quad (3.29)$$

Here $g_{AR,k}(x)$ and $g_{CR,k}$ are the coupling strengths of the reservoir mode k with the atom and the cavity mode, respectively. The total evolution of the system, can be obtained by solving the von-Neumann equation for the density operator $\chi(t)$ and the total Hamiltonian $H = H_S + H_R + H_{AR} + H_{CR}$

$$\frac{d}{dt} \chi(t) = -\frac{i}{\hbar} [H, \chi] \quad (3.30)$$

Solving this equation for the huge system $\mathcal{S} \otimes \mathcal{R}$ is a very hard - and in our case unnecessary - task, since we are only interested in the dynamic of the atom-cavity system. Several approximations can be done, to reduce the analytical difficulties. On the one hand, interactions with the reservoir are - for quantum optical systems - typically very weak, such that excitations of higher than second order are negligible (Born-Approximation [11]). On the other hand, the influence of the small system on the huge reservoir can be safely neglected. Furthermore, the decay timescale for correlations in the reservoir is much smaller than in the system, causing that the reservoir state does not depend at all on the state of the system and has effectively no memory. This is - qualitatively - the meaning of the Markov approximation [11, 12], which we assume to be valid in our case. Altogether, we use both of these approximations and trace over the degrees of freedom of the reservoir, to obtain a density operator for the system under investigation

$$\rho = \text{tr}_R \{ \chi \}. \quad (3.31)$$

The resulting dynamical equation for the reduced density operator of the system, is called the *master equation*. We abandon a detailed derivation and refer to specific quantum optical literature, e.g. [11]. For the considered system and its dissipation channels it reads as:

$$\begin{aligned} \dot{\rho} = & -\frac{i}{\hbar} [H_S, \rho] - \gamma(\bar{n} + 1) (\sigma_+ \sigma_- \rho + \rho \sigma_+ \sigma_- - 2\sigma_- \rho \sigma_+) - \gamma\bar{n} (\sigma_- \sigma_+ \rho + \rho \sigma_- \sigma_+ - 2\sigma_+ \rho \sigma_-) \\ & - \kappa(\bar{n} + 1) \left(a^\dagger a \rho + \rho a^\dagger a - 2a \rho a^\dagger \right) - \kappa\bar{n} \left(a a^\dagger \rho + \rho a a^\dagger - 2a^\dagger \rho a \right), \end{aligned} \quad (3.32)$$

where γ is the spontaneous emission rate for the atoms (see Sec. 2.1.2) and κ the loss rate of cavity photons. The only influence of the state of the reservoir on the system is via the mean occupation number of its oscillator mode $\bar{n} \equiv \bar{n}(\omega_{eg}, T)$. For a reservoir at temperature T , the mean occupation of a mode k with frequency ω_k is [11]

$$\bar{n}(\omega_k, T) = \frac{1}{e^{\hbar\omega_k/(k_B T)} - 1}, \quad (3.33)$$

where k_B denotes Boltzmann's constant. At low temperatures and for optical frequencies, these numbers are very small, $\bar{n} \ll 1$. Since we constrain our investigations in the following to zero temperature, where the reservoir is in a vacuum state $|\text{vac}\rangle\langle\text{vac}|$, \bar{n} is exactly zero and the final master equation for the system reduces to

$$\dot{\rho} = -\frac{i}{\hbar}[H_S, \rho] + \mathcal{L}\rho. \quad (3.34)$$

The Liouvillian superoperator \mathcal{L} , describing spontaneous emission and cavity loss is given by

$$\mathcal{L}\rho = \mathcal{L}_\kappa\rho + \mathcal{L}_\gamma\rho = \kappa \left(2a\rho a^\dagger - a^\dagger a\rho - \rho a^\dagger a \right) + \gamma \left(2\sigma_- \rho \sigma_+ - \sigma_+ \sigma_- \rho - \rho \sigma_+ \sigma_- \right). \quad (3.35)$$

3.2 Resonator-Generated Optical Lattices

In chapter 2 we discussed how optical lattices can be generated with “classical” fields, i.e. laser fields with a very high photon number. In this case the AC-Stark shift generates optical potentials for atoms in the ground state, and by changing the geometry of the intersecting laser beams one can produce a broad variety of lattice geometries. In Sec. 3.1.2 we presented an analogue situation for atoms interacting with a single mode of a cavity. Nevertheless the AC-Stark shifts (3.22) are in this sense only valid for an ideal, lossless cavity. In this section we derive the lattice potential for a cavity, including dissipation via spontaneous emission and loss of cavity photons.

3.2.1 Adiabatic Elimination of the Excited States

In the Heisenberg picture, with an evolution determined by the Liouvillian (3.35) the operators for the internal atomic dynamics and the field obey the Heisenberg-Langevin equations

$$\dot{\sigma}_- = -\frac{i}{\hbar}[\sigma_-, H] - \gamma\sigma_- + \hat{\xi} = (i\Delta_a - \gamma)\sigma_- + g(\hat{x})\sigma_z a + \zeta\sigma_z + \hat{\xi}, \quad (3.36a)$$

$$\dot{\sigma}_+ = -\frac{i}{\hbar}[\sigma_+, H] - \gamma\sigma_+ + \hat{\xi}^\dagger = -(i\Delta_a + \gamma)\sigma_+ + g(\hat{x})\sigma_z a^\dagger + \zeta\sigma_z + \hat{\xi}^\dagger, \quad (3.36b)$$

$$\dot{a} = -\frac{i}{\hbar}[a, H] - \kappa a + \hat{\xi}_a = (i\Delta_c - \kappa)a + g(\hat{x})\sigma_- + \eta + \hat{\xi}_a. \quad (3.36c)$$

Here $\sigma_z \equiv |e\rangle\langle e| - |g\rangle\langle g| = [\sigma_+, \sigma_-]$ is the Pauli matrix for the z -component, which describes the inverse population. The noise operators $\hat{\xi}$, $\hat{\xi}^\dagger$, and $\hat{\xi}_a$ describe white noise [13]. Since, by assumption, the reservoir is at zero temperature and therefore in the vacuum state, their

expectation values vanish and we can neglect these noise terms. The mode function corresponds to a standing wave, Fabry-Perot cavity, i.e. $g(\hat{x}) = g_0 \cos(k\hat{x})$. When the cavity is only very weakly driven, the systems Hilbert space consists of the states $|g, 1\rangle$ or $|e, 0\rangle$, and contributions of other states can be neglected [14]. Hence,

$$\langle a\sigma_z \rangle = -\langle a \rangle. \quad (3.37)$$

Nevertheless, in situations where the excited state is very weakly populated, this relation holds at least approximately. This is the so-called *low-saturation regime*, where the saturation parameter $s = g_0^2/(\Delta_a^2 + \gamma^2)$ (see also Sec. 2.1.1) is very small, $s \ll 1$. This is a regime where typical quantum optical situations take place, and rather easily attainable, by choosing a large atom-pump detuning Δ_a . More generally, this method consists of replacing σ_z by its expectation value $\langle \sigma_z \rangle$, a technique called bosonisation [15], since the commutation relations for Pauli matrices are modified to bosonic commutation relations: $[\sigma_-, \sigma_+] = -\sigma_z \rightarrow -\langle \sigma_z \rangle$. Then the equations (3.36) become linear, and $\langle \sigma_z \rangle$, which is also called population inversion has only the role as a parameter, which has to be chosen self-consistently. Nevertheless, for low saturation, the population inversion can be well approximated by -1. In this regime the timescale of the ground state evolution is much longer than those of the excited state. Hence, we can set the derivatives in (3.36a) and (3.36b) to zero, as well as $\sigma_z = -1$. Then the excited state is adiabatically eliminated from the dynamics. The steady state values of the operators σ_\pm follow then self-explanatory

$$\sigma_- = -\frac{\zeta + g(\hat{x})a}{\gamma - i\Delta_a} \quad \text{and} \quad \sigma_+ = -\frac{\zeta + g(\hat{x})a^\dagger}{\gamma + i\Delta_a}. \quad (3.38)$$

After deriving these steady state “values” of these operators, we can proceed along two different lines. On the one hand, we can replace them in the equation for the field (3.36c), yielding

$$\dot{a} = [i\Delta_c - \kappa - (\Gamma_0 + iU_0) \cos^2(k\hat{x})] a + \eta - (\gamma_{\text{eff}} + i\eta_{\text{eff}}) \cos(k\hat{x}), \quad (3.39)$$

where we applied the specific form of the mode function $g(\hat{x}) = g_0 \cos(k\hat{x})$ and introduced the following abbreviations, characterizing the atom’s dispersive and absorptive influence on the cavity field:

$$U_0 = \frac{g_0^2 \Delta_a}{\gamma^2 + \Delta_a^2} \quad \text{and} \quad \Gamma_0 = \frac{g_0^2 \gamma}{\gamma^2 + \Delta_a^2}. \quad (3.40)$$

Here U_0 can be interpreted as the energy light shift per photon for the atom, which will be clarified with equation (3.42) and Γ_0 as the photon loss probability per atom through incoherent scattering. The other two terms are only relevant in the case, where the atoms are directly pumped and therefore reflect the influence of the atomic position on the field.

$$\gamma_{\text{eff}} = \frac{g_0 \zeta \gamma}{\gamma^2 + \Delta_a^2} \quad \text{and} \quad \eta_{\text{eff}} = \frac{g_0 \zeta \Delta_a}{\gamma^2 + \Delta_a^2}. \quad (3.41)$$

On the other hand, we can also replace σ_\pm by their steady state expressions (3.38) in the Hamiltonian (3.26) and in the spontaneous emission part of the Liouvillian (3.35). In this

way we obtain an effective Hamiltonian (choosing normal order for the field operators), which then solely depends on the atom's external degrees of freedom and the cavity field. Thus,

$$H_{\text{eff}} = \frac{\hat{p}^2}{2m} + \hbar U_0 \cos^2(k\hat{x}) a^\dagger a + \hbar \eta_{\text{eff}} \cos(k\hat{x}) (a + a^\dagger) - i\hbar \eta (a - a^\dagger). \quad (3.42)$$

Now the interpretation of U_0 is clear. This is the analogue of the classical AC-Stark light shift (2.10), per one photon ($\langle a^\dagger a \rangle = 1$). The terms corresponding to Γ_0 and γ_{eff} arise from the replacement in the Liouvillian \mathcal{L}_γ , which reads as

$$\mathcal{L}_{\gamma, \text{eff}} = \Gamma_0 \cos^2(k\hat{x}) (2a\rho a^\dagger - a^\dagger a\rho - \rho a^\dagger a) + \gamma_{\text{eff}} [a - a^\dagger, \rho]. \quad (3.43)$$

This method must - of course - lead also to the same dynamical equation as (3.39) for the field. This is easy to check by calculating

$$\frac{d}{dt} \langle a \rangle = \text{tr}\{\dot{\rho} a\} \quad \text{with} \quad \dot{\rho} = -\frac{i}{\hbar} [H_{\text{eff}}, \rho] + \mathcal{L}_\kappa \rho + \mathcal{L}_{\gamma, \text{eff}} \rho. \quad (3.44)$$

A major part of our work is the derivation of a generalized Bose-Hubbard model, which includes also resonator-generated optical lattices and the cavity as a dynamical element. This procedure requires a many-particle Hamiltonian in second quantization formalism (see Sec. 2.3.1). The implementation of (3.42) as the corresponding single-particle Hamiltonian provides a generalized Hamiltonian with adiabatically eliminated excited states. Nevertheless, it is also possible to use (3.26) as a single-particle Hamiltonian in the second quantization formalism and then eliminate the excited state of the atoms. This leads finally to the same Bose-Hubbard Hamiltonian (see chapter 6).

Finally we can make a useful approximation. In the rest of this thesis, we work in a regime far off resonance, i.e. $\Delta_a \gg \gamma$. Hence $U_0 \gg \Gamma_0$ and $\eta_{\text{eff}} \gg \gamma_{\text{eff}}$. This allows us to neglect spontaneous emission at all and set $\gamma = 0$ in the equations above.

3.2.2 Intracavity trapping potential

The trapping depth of the resonator-generated optical lattice depends on two quantities, the coupling strength U_0 and the number of photons in the cavity field. In order to have bound states, we have to reassure that this depth fulfills at least $V \geq 2E_R$. Experiments for $U_0 > E_R$, where atoms are trapped with just a single photon in the potential of the cavity field were successfully performed in the group of Kimble [16] and in the group of Rempe [17]. Although fascinating from a fundamental point of view, this setup involves short trapping times, not suitable for instance for quantum communication purposes. Also in the case of directly driven atoms, we consider only a weak cavity field (see chapter 6), where the above relation might not hold. Therefore we decouple the trapping from the QED interaction by introducing an additional “classical” potential along the cavity axis, allowing us to consider situations where bound states always exist and an expansion of the second-quantized Hamiltonian in a Wannier basis always makes sense.

This can be achieved by implementing an intracavity red-detuned, far off-resonance dipole trap (FORT) [18–20], along the cavity axis. This leads to a position-dependent AC-Stark Shift (2.7)

$$V_F(\mathbf{x}) = -\frac{\hbar g_F}{\omega_F - \omega_{eg}} \cos^2(k_F x) e^{-(x^2 + y^2)/w_0^2}, \quad (3.45)$$

where we assumed that the waist of the FORT field is equal to those of the cavity field, which is in fact a very accurate approximation. Experimentally, the external trapping laser frequency ω_F is mainly chosen to have a detuning of two free spectral ranges from the cavity frequency ω_c , such that it is in resonance with another mode of the cavity. Hence, the cavity field and the FORT field will not interfere perfectly constructive in the cavity and the coupling of the atom to the total electromagnetic field in the cavity differs from site to site of the cavity lattice. Nevertheless, for the experimentally applied detunings of two free spectral ranges, the coincidence of the cavity field wells and the FORT field wells in the vicinity of the center of the cavity is almost perfect [21], such that the exact value of ω_F is rather irrelevant. For a red-detuned trapping laser, the ground state experiences a negative shift, the excited state an equally large positive shift². Thus, we can extend the Hamiltonian (3.26) to

$$H_S = \frac{\hat{p}^2}{2m} - \hbar\Delta_a|e\rangle\langle e| + \hbar\Delta_F(\hat{x})(|e\rangle\langle e| - |g\rangle\langle g|) - \hbar\Delta_c a^\dagger a \quad (3.46)$$

$$\begin{aligned} & -i\hbar g(\hat{x})(\sigma_+ a - \sigma_- a^\dagger) - i\hbar\zeta(\sigma_+ - \sigma_-) - i\hbar\eta(a - a^\dagger) \\ & = \frac{\hat{p}^2}{2m} - \hbar\tilde{\Delta}_a\sigma_+\sigma_- - \hbar\Delta_F(\hat{x}) - \hbar\Delta_c a^\dagger a \\ & -i\hbar g(\hat{x})(\sigma_+ a - \sigma_- a^\dagger) - i\hbar\zeta(\sigma_+ - \sigma_-) - i\hbar\eta(a - a^\dagger), \end{aligned} \quad (3.47)$$

where $\Delta_F(x) = \omega_p - V_F(x)/\hbar$, resulting from the transition to the rotating frame and $\tilde{\Delta}_a = \Delta_a - 2\Delta_F(x)$. Note, that we again neglected the transverse part of the mode functions, assuming the atom to be in the radial center of the cavity. In experiments this has to be accomplished by additional transverse traps. Proceeding as above with the elimination of the excited states (large detuning) leads to identical expressions for the steady-states of σ_\pm , except the replacement $\Delta_a \rightarrow \tilde{\Delta}_a$. Following the lines of Sec. 3.2.1, we obtain an extended effective Hamiltonian, after an energy shift of $\hbar\omega_p$

$$\tilde{H}_{\text{eff}} = \frac{\hat{p}^2}{2m} + \hbar\tilde{U}_0 \cos^2(k\hat{x})a^\dagger a + V_{\text{cl}} \cos^2(k_F\hat{x}) + \hbar\tilde{\eta}_{\text{eff}} \cos(k\hat{x})(a + a^\dagger) - i\hbar\eta(a - a^\dagger), \quad (3.48)$$

where we defined the parameters as

$$\tilde{U}_0 = \frac{g_0^2 \tilde{\Delta}_a}{\gamma^2 + \tilde{\Delta}_a^2}, \quad \tilde{\eta}_{\text{eff}} = \frac{g_0 \zeta \tilde{\Delta}_a}{\gamma^2 + \tilde{\Delta}_a^2} \quad \text{and} \quad V_{\text{cl}} = -\frac{g_F}{\omega_F - \omega_{eg}}. \quad (3.49)$$

The suffix *cl* should emphasize, that this trapping potential is independent of the quantized cavity field with (eventually) few photons. Hence it could be interpreted as a “classical” potential. The form of the Liouvillian (3.43) remains unchanged. Only the denominators of γ_{eff} and Γ_0 have to be adapted, with the replacement of Δ_a by $\tilde{\Delta}_a$. We do not consider here the subtle question of the influence of the FORT field to cooling/heating issues or fluctuation processes. A detailed discussion can be found in [23].

For a reasonable choice of the FORT wavelength (e.g. $104k_F/2 = 102k/2$ [23]), an almost perfect agreement of the FORT wells and the cavity field wells can be found near the center of

²For certain species of atoms like Cesium it is possible to adjust the wavelength of the FORT laser λ_F by a few free spectral ranges to the “magic wavelength”, where the ground and the excited state are both shifted negatively. This allows state-insensitive cooling for these types of atoms. [22]

the cavity. Hence, in the vicinity of the center, we can replace k_F by the cavity wavenumber k . Here we can also neglect the spatial variation of the coupling strength across the wells of the FORT trap. In this sense Δ_a differs from $\tilde{\Delta}_a$ just by a constant. Thus, we can omit all the tildes in (3.48) and obtain as a final expression for the effective Hamiltonian:

$$H_{\text{eff}} = \frac{\hat{p}^2}{2m} + \left(V_{\text{cl}} + \hbar U_0 a^\dagger a \right) \cos^2(k\hat{x}) + \hbar \eta_{\text{eff}} \cos(k\hat{x}) \left(a + a^\dagger \right) - i\hbar \eta \left(a - a^\dagger \right). \quad (3.50)$$

Recently, the group of Rempé was able to experimentally realize a blue-detuned intracavity dipole trap [6]. Here, the atoms are repelled from the intensity maximum of the trapping field and instead attracted to antinodes of the field. This has the advantage that the Stark shift for all levels are small, leading to free-space-like properties of the atom, except for the strong coupling to the cavity mode. This is an ideal setup to test our model. Similar like above, a suitable choice of longitudinal modes (in this case, the detuning is three free spectral ranges from the main cavity mode), leads to a good matching of trap intensity minima and cavity field maxima, in the center region of the cavity. Furthermore this setup allows to avoid difficulties with issues like cavity-enhanced heating.

3.3 Transverse Motion

Up to now we took only one-dimensional motion along the cavity axis into account. When the cavity is pumped, driving the mode along the cavity axis, only forces along this axis are exerted. A coherently pumped atom, on the other hand, scatters photons from the pumping field, which impinges perpendicular to the cavity axis on the atom, into the cavity mode. Hence, forces in both directions are exerted. Nevertheless, Vukics [10] has showed that cross effects between the two direction have almost no influence on the dynamical properties of the system, allowing for an independent study of both directions. In the last part of this thesis (chapter 11 and 12) we consider the motion of the atom transversally to the cavity axis, in the direction of the laser beams, which excites the atom. This requires some slight variations in the effective Hamiltonian, which we will derive in this section.

Our model again consists of a two-level atom, interacting with a single, standing wave mode of a cavity field. We apply a single coherent laser field, which pumps directly the atom and forms a broad standing wave in y -direction, i.e. transversally to the cavity axis (see Fig. 3.6). We do not consider cavity pumping and an additional classical lattice potential, here. Hence, the system Hamiltonian (3.26) is modified to

$$H_S = \frac{\hat{p}_y^2}{2m} - \hbar \Delta_a |e\rangle\langle e| - \hbar \Delta_c a^\dagger a - i\hbar g(\hat{x}) \left(\sigma_+ a - \sigma_- a^\dagger \right) - i\hbar \zeta h(\hat{y}) (\sigma_+ - \sigma_-), \quad (3.51)$$

where $g(x) = g_0 \cos(k\hat{x})$ is the mode function of the cavity mode and \hat{p}_y is the momentum operator in y -direction. We assume that the atom remains near the center of the cavity and neglect the transverse Gaussian profile of the mode function. The transverse mode function of the pumping laser is denoted $h(\hat{y}) = \cos(k_p \hat{y})$. Note that the coupling strength of the atom to this laser field is implemented in the constant ζ . The Liouvillian superoperators for cavity decay and spontaneous emission (3.35) remain the same, as for motion along the cavity axis.

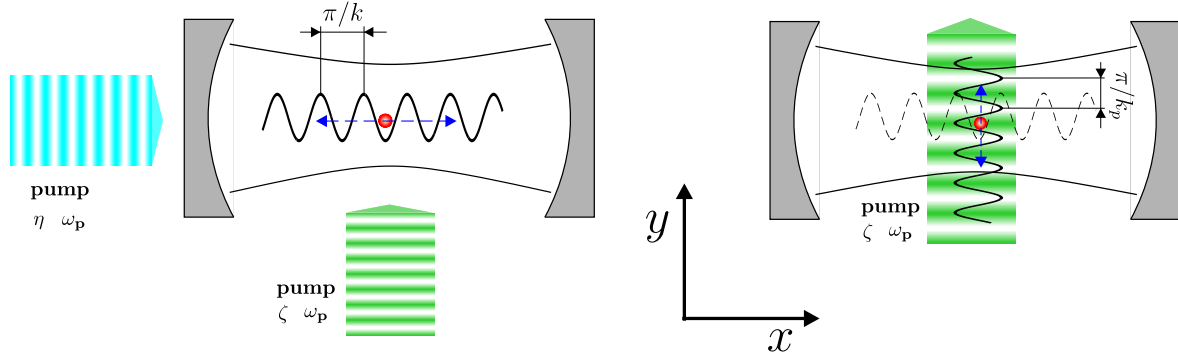


Figure 3.6. Left: In this setup we investigate the motion of the atom along the cavity axis (x -direction), in the optical lattice, generated by the resonator (lattice constant $a = \pi/k$). Here we consider driving of the atom and/or the cavity mode with a coherent laser field. Right: Here we consider motion of the atom transversally to the cavity axis (y -direction), in the lattice, built up by the pumping laser (lattice constant $a = \pi/k_p$).

Since we only have to take into account the motion along the y -axis, the value of the x -position of the atom does not matter and without loss of generality we can set $\cos(k\hat{x}) = 1$. After adiabatic elimination of the excited state, analogue to Sec. 3.2.1, we obtain the following steady state expressions

$$\sigma_- = -\frac{\zeta \cos(k_p \hat{y}) + g_0 a}{\gamma - i\Delta_a} \quad \text{and} \quad \sigma_+ = -\frac{\zeta \cos(k_p \hat{y}) + g_0 a^\dagger}{\gamma + i\Delta_a}. \quad (3.52)$$

We replace the σ_\pm operators in (3.51), yielding an effective Hamiltonian, describing atomic motion along the y -direction and the cavity field evolution

$$H_{\text{eff}} = \frac{\hat{p}_y^2}{2m} - \hbar(\Delta_c - U_0)a^\dagger a + V_0 \cos^2(k_p \hat{y}) + \text{sgn}(U_0)\sqrt{\hbar U_0 V_0} \cos(k_p \hat{y}) (a + a^\dagger), \quad (3.53)$$

where $V_0 = \hbar\zeta^2\Delta_a/(\gamma^2 + \Delta_a^2)$ is the lattice potential, associated with the driving laser field. This is a standard optical lattice potential through the AC-Stark shift in the sense of Sec. 2.1.1, independent of the photon number $a^\dagger a$ in the cavity. As we will see, this is a convenient simplification, when it comes to second quantization and the calculation of the matrix elements in the Wannier basis.

Obviously we also have to replace σ_\pm in the Liouvillian corresponding to spontaneous emission

$$\mathcal{L}_{\gamma, \text{eff}} = \Gamma_0 (2a\rho a^\dagger - a^\dagger a\rho - \rho a^\dagger a) + \gamma_{\text{eff}} \cos(k_p \hat{y}) [a - a^\dagger, \rho]. \quad (3.54)$$

These are now the ingredients of the von-Neumann equation, determining the evolution of our system's density operator. We limit, however, our investigations to a regime, where the frequency of the pumping laser is far detuned from the atomic transition frequency, $\Delta \gg \gamma$. Hence, we can again neglect spontaneous emission and all terms associated with it.

Bibliography

- [1] E. T. Jaynes and F. W. Cummings, *Comparison of Quantum Semiclassical Radiation Theories with Application to the Beam Maser*, Proc. IEEE **51**, 89 (1963).
- [2] F. K. Kneubühl and M. W. Sigrist, *Laser*, 5. Auflage (Teubner, 2006).
- [3] H. Kogelnik and T. Li, *Laser Beams and Resonators*, Appl. Opt. **5**, 1550 (1966).
- [4] E. Hecht, *Optik*, (Addison-Wesley, 1994).
- [5] R. Miller, T. E. Northup, K. M. Birnbaum, A. Boca, A. D. Boozer, and H. J. Kimble, *Trapped Atoms in Cavity QED: Coupling Quantized Light and Matter*, J. Phys. B: At. Mol. Opt. Phys. **38**, 551 (2005).
- [6] T. Puppe, I. Schuster, P. Maunz, K. Murr, P. W. H. Pinkse, and G. Rempe, *Trapping and Observing Single Atoms in a Blue-Detuned Intracavity Dipole Trap*, Phys. Rev. Lett. **99**, 013002 (2007).
- [7] See, for example, M. Orszag, *Quantum Optics*, (Springer, 2000).
- [8] R. J. Thompson, G. Rempe, and H. J. Kimble, *Observation of Normal-Mode Splitting for an Atom in an Optical Cavity*, Phys. Rev. Lett. **68**, 1132 (1992).
- [9] C. Schön and J. I. Cirac, *Trapping Atoms in the Vacuum Field of a Cavity*, Phys. Rev. A **67**, 043813 (2003).
- [10] A. Vukics, P. Domokos, and H. Ritsch, *Multidimensional and Interference Effects in Atom Trapping by a Cavity Field*, J. Opt. B: Quant. Semiclass. Opt. **6**, 143 (2004).
- [11] See, for example, C. Cohen-Tannoudji, J. Dupont-Roc, and G. Grynberg, *Atom-Photon Interactions: Basic Processes and Applications* (John Wiley and Sons, New York, 1992).
- [12] See, for example, C. W. Gardiner and P. Zoller, *Quantum Noise*, 3rd Ed., (Springer, Berlin, 2005).
- [13] P. Domokos and H. Ritsch, *Mechanical Effects of Light in Optical Resonators*, J. Opt. Soc. Am. B **20**, 1098 (2003).
- [14] G. Hechenblaikner, M. Gangl, P. Horak, and H. Ritsch, *Cooling an Atom in a Weakly Driven High-Q Cavity*, Phys. Rev. A **58**, 3030 (1998).
- [15] I. Protsenko, P. Domokos, V. Lefèvre-Seguin, J. Hare, J. M. Raimond, and L. Davidovich, *Quantum Theory of a Thresholdless Laser*, Phys. Rev. A **59**, 1667 (1999).
- [16] C. J. Hood, T. W. Lynn, A. C. Doherty, A. S. Parkins, and H. J. Kimble, *The Atom-Cavity Microscope: Single Atoms Bound in Orbit by Single Photons*, Science **287**, 1447 (2000).
- [17] P. W. H. Pinkse, T. Fischer, P. Maunz, and G. Rempe, *Trapping an Atom with Single Photons*, Nature (London) **404**, 365 (2000).

- [18] J. Ye, D. W. Vernooy, and H. J. Kimble, *Trapping of Single Atoms in Cavity QED*, Phys. Rev. Lett. **83**, 4987 (1999).
- [19] P. Maunz, T. Puppe, I. Schuster, N. Syassen, P. W. H. Pinkse, and G. Rempe, *Cavity Cooling of a Single Atom*, Nature (London) **428**, 50 (2004).
- [20] J. A. Sauer, K. M. Fortier, M. S. Chang, C. D. Hamley, and M. S. Chapman, *Cavity QED with Optically Transported Atoms*, Phys. Rev. A **69**, 051804 (2004).
- [21] D. W. Vernooy, *Cold Atoms in Cavity QED for Quantum Information Processing*, PhD thesis, (California Institute of Technology, Pasadena, 2000.)
- [22] J. McKeever, J. R. Buck, A. D. Boozer, A. Kuzmich, H.-C. Nägerl, D. M. Stamper-Kurn, and H. J. Kimble, *State-Insensitive Cooling and Trapping of Single Atoms in an Optical Cavity*, Phys. Rev. Lett. **90**, 133602 (2003).
- [23] S. J. van Enk, J. McKeever, H. J. Kimble, and J. Ye, *Cooling of a Single Atom in an Optical Trap Inside a Resonator*, Phys. Rev. A **64**, 013407.

CHAPTER 4

PUBLICATION

Quantum Motion of Laser-Driven Atoms in a Cavity Field[†]

Optics Communications **243**, 145 (2004)

C. Maschler and H. Ritsch

*Institut für theoretische Physik, Universität Innsbruck,
A-6020 Innsbruck, Austria*

We investigate the quantum motion of coherently driven ultracold atoms in the field of a damped high- Q optical cavity mode. The laser field is chosen far detuned from the atomic transition but close to a cavity resonance, so that spontaneous emission is strongly suppressed but a coherent field builds up in the resonator by stimulated scattering. On one hand the shape of the atomic wave function determines the field dynamics via the magnitude of the scattering and the effective refractive index the atoms create for the mode. The mode intensity on the other hand determines the optical dipole force on the atoms. The system shows rich coupled atom-field dynamics including self-organisation, self trapping, cooling or heating. In the limit of deep trapping we are able to derive a system of closed, coupled equations for a finite set of atomic expectations values and the field. This allows to determine the self consistent ground state of the system as well as the eigenfrequencies and damping rates for excitations.

4.1 Introduction

Cooling and trapping of neutral atoms to temperatures close to quantum degeneracy has now become a standard experimental tool [1]. Laser fields so far-off resonance that they induce almost no spontaneous emission but still create significant forces have proven an ideal tool to manipulate and control this atoms in a well defined way [2]. Most spectacular applications include the formation of optical lattices for such atoms [3, 4] or quasi 1D traps. In most cases the back action of the atoms on the field can be largely neglected, although it was theoretically predicted almost from the beginning, that the atoms could influence the fields as a sort of dynamic refractive index [5]. In principle this implies a fairly complicated dynamical extension of the theoretical models as we now have a time dependent potential in the atomic Hamiltonian, which (nonlocally) depends on the atomic wavefunction itself. Although some important effects of atomic back action on the field (enhanced directional

[†]The author of the present thesis performed all the calculations in this publication.

scattering) for detuned fields were investigated by Ketterle already some time ago [7], these effects are very small for current atomic densities and the large atom-field detunings used for dipole trapping. However, the situation changes dramatically if the fields involved are not freely propagating but enclosed in a high- Q optical resonator [8–10], where the effective atom-field interaction per atom and per photon is strongly enhanced. On one hand this allows to create much deeper and larger potentials for a given laser power [11]. On the other hand the atomic back action on the field yields valuable information on the atomic time evolution [12]. As this information is obtained nondestructively it allows as well for subsequent controlled manipulation of the cold atoms (BEC). Proposed applications of this coupled dynamics range from energy extraction (damping) from the atomic cloud via cavity decay [9], unification of two condensates into one via cavity coupling [10] to the controlled generation of macroscopic atomic superposition states via cavity scattering [13]. In all of these cases the atoms were assumed to be moving in so far-off resonance driven cavity mode, that they basically act as a dynamic refractive index. During the motion one finds a large refractive index if the atoms are close to antinodes and almost no effect, when they sit around a node of the mode.

Here we generalize the situation to the case, where the coherent driving field is directly applied to the atoms instead of pumping the mode. They can be mathematically related to each other by a amplitude shift transformation of the field mode operator [14]. Such a transformation does not exist for a quantum description of atomic motion. As the atom now has a position distribution no single effective field shift can be found, which transforms the interaction Hamiltonian in the desired way. This leads to genuinely different dynamics.

In the case of coherent driving of only the atoms, all the photons in the cavity mode are created through scattering on the atoms. Hence, the shape of the atomic wavefunction not only determines the refractive index but also the effective pump amplitude of the cavity mode.

The importance of this new system property can be seen fairly easy in the generic case of a transverse plane wave pump field and a single standing wave cavity mode with sinusoidal mode function along the cavity axis. For a homogenous distribution of the atoms no photons will be coherently scattered into the mode as the contributions from the negative and positive parts of the mode cancel each other. If the atoms, however, are localized around an antinode of the field one gets very strong scattering into the mode and the field intensity scales as the square of the number of atoms. This effect implies a very interesting bistable self trapping and self organization effect of the atoms in the case when they can be treated as classical point particles and red atom field detuning [15], for which strong experimental evidence has been found recently [16]. Cavity cooling for a single atom has been recently also experimentally demonstrated by Rempe and coworkers [23]. Very intriguing dynamical phenomena of coupled atom field dynamics have also been observed in ring cavities ranging from strong common acceleration [17] to collective transverse oscillations [18].

Even more intriguing effects can be expected in the quantum regime, where two macroscopically distinct ground states of the system should exist. In the following we will investigate this in a simplified 1D model, which allows some analytical treatment but still contains a lot of the essential physics. This work is organized as follows: In Sec. 4.2 we develop our model of the quantum motion of a single driven two-level atom in high- Q cavity mode. In Sec. 4.3 we show that in the low temperature, deep trapping limits the dynamics relates to a quantized

oscillator with time dependent frequency, for which analytic solutions exists for many cases. This allows to determine ground state properties. In the following we use the Hamiltonian to derive a closed set of coupled equations for the field amplitude and a finite set of certain atomic expectation values. These can be easily numerically integrated. In Sec. 4.4 we numerically solve these equations for a wider range of parameters to determine the damping (cooling) rates in the system and compare the two cases of atom and cavity pumping.

4.2 Model

Let us consider a two-level atom with mass m and transition frequency ω_a strongly interacting with a single standing wave cavity mode of frequency ω_c . The atom is also coupled to a coherent laser field with frequency ω_p and strength ζ from the side of the cavity as depicted in Fig. 4.1. Alternatively the cavity is coherently driven at ω_p with amplitude η . At this point we will include both driving terms in the Hamiltonian, although for the examples we will only use one at a time.

The Hamiltonian of the system using the rotating-wave and the electric-dipole approximation is

$$H = \frac{p^2}{2m} - \hbar\Delta_a\sigma^+\sigma^- - \hbar\Delta_c a^\dagger a - i\hbar g(x) (\sigma^+ a - \sigma^- a^\dagger) - i\hbar(\mathbf{x})\zeta (\sigma^+ - \sigma^-) - i\eta (a - a^\dagger), \quad (4.1)$$

where $\Delta_a = \omega_p - \omega_a$ is the detuning of the pump laser from atomic resonance and $\Delta_c = \omega_p - \omega_c$ is the detuning from the cavity. ζ and η denote the pumping strengths of the external driving fields (Fig. 4.1).

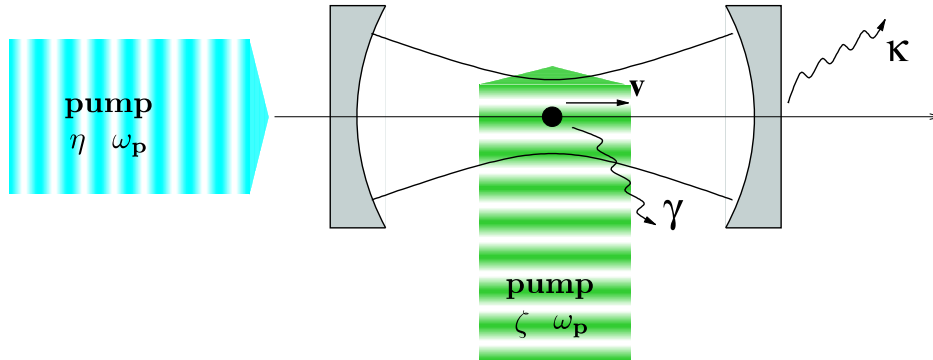


Figure 4.1. Scheme of an atom inside a cavity driven by two external lasers. The atom is directly driven with pump strengths ζ and frequency ω_p . An additional laser with strength η drives the cavity.

The mode functions of the cavity mode and the pump laser, which forms a broad standing wave transverse to the cavity are given by $g(x) = g_0 \cos(kx)$ and $h(\mathbf{x}) = h(y) = h_0 \cos(k_p y)$, respectively.

In addition we include two types of dissipation processes namely cavity loss at rate κ and spontaneous emission of the atom at rate γ . Using a standard technique in quantum optics we treat this incoherent processes as interaction with an external heat bath so that we get the following well known master equation for the density operator ϱ [24].

As we are mainly interested in the limit of very large atom-pump detunings, where spontaneous emission is strongly suppressed and the forces are governed by the dipole force of the fields, we neglect the recoil induced radiation pressure force on the atom. In fact due to the symmetries of cavity mode and pump its average value is zero and the corresponding momentum diffusion can be expected to be very small. Hence we get

$$\dot{\varrho}(t) = \frac{1}{i\hbar} [H, \varrho(t)] + \mathcal{L}\varrho(t), \quad (4.2)$$

where the Liouvillian reads as

$$\mathcal{L}\varrho(T) = \kappa \left(2a\varrho(t)a^\dagger - a^\dagger a\varrho(t) - \varrho(t)a^\dagger a \right) + \gamma \left(2\sigma^- \varrho(t)\sigma^+ - \sigma^+ \sigma^- \varrho(t) - \varrho(t)\sigma^+ \sigma^- \right) \quad (4.3)$$

The corresponding Heisenberg equation for the atomic polarization then reads

$$\dot{\sigma}^- = i\Delta_a \sigma^- + g(x)\sigma_z a + \zeta h(\mathbf{x})\sigma_z - \gamma \sigma^- \quad (4.4)$$

In a similar way we obtain

$$\dot{a} = i\Delta_c a + g(x)\sigma^- - \kappa a + \eta. \quad (4.5)$$

Here, we restrict ourselves to a regime of low saturation, such that we can adiabatically eliminate the excited atomic state. In addition we assume a coherent field amplitude $\alpha = \langle a \rangle$ much bigger than one, i.e., $|\alpha| \gg 1$, which allows us to treat the coherent cavity field amplitude as a classical c-number quantity [19].

Despite all these simplifications we are still left with an effective Hamiltonian, which does not allow a direct analytic solution. Hence in order to get some first insight we resort to a further simplification step and consider the case, where the atoms are well localized in position space around the field antinodes, where they see a potential minimum. This allows to expand the optical potential around the antinode $kx = -\pi$, so that the cavity mode locally creates a harmonic potential. Of course we have to do a self consistency check on our parameters at the end to see whether this approximation stays valid during time evolution.

Finally we obtain

$$H_{\text{eff}} = \frac{p^2}{2m} - \hbar\Delta_c |\alpha(t)|^2 + \hbar U_0 |\alpha(t)|^2 (1 - k^2 x^2) + 2\hbar\eta_{\text{eff}} h(y) \left(-1 + \frac{k^2 x^2}{2} \right) \text{Re}(\alpha(t)) + 2\hbar\eta \text{Im}(\alpha(t)). \quad (4.6)$$

Taking the average value with respect to the atomic degrees of freedom, the equation for the field amplitude then reads

$$\dot{\alpha}(t) = [i\Delta_c - \kappa - (\Gamma_0 + iU_0) (1 - k^2 \langle x^2 \rangle)] \alpha(t) - (\gamma_{\text{eff}} + i\eta_{\text{eff}}) h(y) \left(1 - \frac{k^2 \langle x^2 \rangle}{2} \right) + \eta. \quad (4.7)$$

In the above equations the magnitude of the dispersive and absorptive influence of the atom on the cavity field scales with the parameters [20]

$$U_0 = \frac{g_0^2 \Delta_a}{\Delta_a^2 + \gamma^2} \quad \text{and} \quad \Gamma_0 = \frac{g_0^2 \gamma}{\Delta_a^2 + \gamma^2}. \quad (4.8)$$

U_0 can be easily interpreted as the light shift per photon, which the atom experiences at an antinode, while Γ_0 gives the photon loss probability per atom through incoherent scattering. As mentioned above the transverse pump field impinging on the atoms implies a position dependent pumping term which scales with the parameters

$$\gamma_{\text{eff}} = \frac{g_0 \zeta \gamma}{\Delta_a^2 + \gamma^2} \quad \text{and} \quad \eta_{\text{eff}} = \frac{g_0 \zeta \Delta_a}{\Delta_a^2 + \gamma^2}. \quad (4.9)$$

As we work in the far-off resonance regime we have $U_0 \gg \Gamma_0$ and $\eta_{\text{eff}} \gg \gamma_{\text{eff}}$, so that we can safely neglect spontaneous emission, i.e., $\gamma = 0$ for our first discussion of the dynamics in the following.

4.3 System Dynamics

4.3.1 Mapping to an oscillator with time dependent frequency

Looking at the effective Hamiltonian (4.6) one sees that it can be rewritten as the Hamiltonian of a harmonic oscillator

$$H = \frac{p^2}{2m} + \frac{m\omega^2(t)x^2}{2} + f(t) \quad (4.10)$$

with time-dependent frequency

$$\omega(t) = k \sqrt{\frac{2\hbar}{m}} \sqrt{-U_0 |\alpha(t)|^2 + \eta_{\text{eff}} \hbar(y) \text{Re}(\alpha(t))}. \quad (4.11)$$

The third term $f(t)$ in Eq. (4.10) only amounts to a global time dependent phase and we do not have to take it into account in detail. Of course the central problem is that we do not have an prescribed form of $\alpha(t)$, which has to be dynamically determined. One interesting limit here corresponds to the case of instant reaction of the field to the atom for large κ , for which we arrive at a nonlinear Schrödinger equation. Here we will not pursue this limit in more detail as we have the use of high- Q cavities in mind.

To solve such problems Lewis and Riesenfeld have developed a method to express the dynamic solution of (4.10) in terms of time parameterized oscillator eigenfunctions [6, 21] for any given $\omega(t)$. Their method requires to solve an extra c-number differential equation, the so-called Ermakov equation

$$\ddot{r}(t) + \omega^2(t)r(t) = \frac{1}{mr^3(t)} \quad (4.12)$$

to explicitly find the desired time dependent solution. This is even analytically possible in several cases and the solutions are then related to the harmonic oscillator eigenfunctions for any time t through the relation

$$\psi_n(x, t) = \frac{1}{n! 2^n \sqrt{\pi \hbar}} \frac{\exp[i\beta_n(t)]}{\sqrt{r(t)}} H_n\left(\frac{x}{r(t)\sqrt{\hbar}}\right) \exp\left[i\frac{m}{2\hbar}\left(\frac{\dot{r}(t)}{r(t)} + \frac{i}{mr^2(t)}\right)x^2\right], \quad (4.13)$$

where $\beta_n(t)$ reads

$$\beta_n(t) = -\frac{1}{\hbar} \int_0^t \left[\frac{\hbar(n+1/2)}{mr^2(t')} - f(t') \right] dt'. \quad (4.14)$$

In our case we do not have an explicit form of $\omega(t)$ and so we cannot derive an explicit analytical answer. However, the numerical solution of the full dynamics can be simply found by solving a single ordinary differential equation for $r(t)$ in parallel with finding the light field dynamics. This is fairly easily possible, as one can express the values of atomic operators needed to solve the light field equation simply in terms of $r(t)$ for any given n . If the atom is initially in the ground state $\psi_0(x, 0)$ with respect to the momentary field intensity, this relation reads

$$\langle x^2(t) \rangle = \frac{\hbar}{2} r^2(t) \quad (4.15)$$

$$\langle p^2(t) \rangle = \frac{\hbar}{2} r^{-2}(t) + \frac{\hbar m^2}{2} \dot{r}^2(t). \quad (4.16)$$

Similar results hold for initial conditions of higher n . Note that due to the influence of atomic expectation values on the field dynamics, which feed back to the atomic time evolution, the problem is not linear. Hence if we decompose the initial condition into a harmonic oscillator basis, we cannot solve the dynamics separately for each basis state and then add up the contributions. Instead we numerically have to find the solution independently for each initial condition. From the form of the solutions one sees immediately, that the shape of the wavefunction does not change, if one starts with an oscillator eigenfunction. An initially prepared Gaussian wave packet stays Gaussian all the time and only its width changes. This is important, if we start with a steady state and then change one of the operating parameters like pump strength or detuning. Here the wavefunction always corresponds to the same oscillator eigenstate and we only get a time dependent width and phase of the wavefunction.

Of course during time evolution we have to check, whether this width stays consistent with the harmonic approximation for the potential. From the time dependent solution we can then extract all desired quantities as the kinetic or the total mean energy of the atom to characterize the cooling and relaxation properties of our system. Of course by looking for solutions with time independent r we can search for steady states and find properties of the ground state of the coupled system. To illustrate this at an example, we solve (4.7) and (4.12) in the case where the pump light is directly applied to the atom, i.e., $\eta = 0$ and $\eta_{\text{eff}} \neq 0$. For simplicity we start with a superposition of only few oscillator eigenstates. As initial basis we choose the eigenstates corresponding to the momentary eigenfrequency $\omega(0)$ derived from the chosen initial value of the field amplitude $\alpha(0)$.

Hence we have to set $r(0) = [m\omega(0)]^{-1/2}$ and $\dot{r}(0) = 0$. The operating parameters $\Delta_c = -10\kappa$ and $U_0 = -5\kappa$ are chosen in a way that the light field creates an attractive potential for the atoms and we get cooling in the corresponding classical model [19]. As a simple but nontrivial example we choose an even superposition of the ground state and the first excited state $\psi(x, 0) = \frac{1}{\sqrt{2}} [\psi_0(x, 0) + \psi_1(x, 0)]$ and a very weak initial value of the field $\alpha(0) = 1$.

The expectation values of the position operator (center of mass) and position operator squared (proportional to the potential energy) than explicitly read

$$\langle x(t) \rangle = \sqrt{\frac{\hbar}{2}} r(t) \cos [\beta_0(t) - \beta_1(t)] \quad (4.17)$$

$$\begin{aligned} &= \sqrt{\frac{\hbar}{2}} r(t) \cos \left[\frac{1}{m} \int_0^t r^{-2}(\tau) d\tau \right] \\ \langle x^2(t) \rangle &= \hbar r^2(t). \end{aligned} \quad (4.18)$$

The corresponding numerical solution is shown in Fig. 4.2. As expected the atom starts to oscillate in the potential and induces corresponding field oscillations with some delay. Clearly the dissipative character of the atomic motion is visible. Interestingly after some initial adjustments, the motion of the center of mass is only very weakly damped, whereas the average potential energy proportional to $\langle x^2(t) \rangle$ and the field amplitude $\alpha(t)$ tend to a stationary value. So after some time the atom oscillates in a self generated deep potential well with an almost constant field. The slow damping of the center of mass motion is connected to the fact that $\langle x(t) \rangle$ does not directly enter in the field equation. In contrast to classical mechanics, quantum mechanics allows states where $\langle x^2(t) \rangle$ is constant despite of oscillating $\langle x(t) \rangle$. Effectively we see that the system dynamically traps and localizes itself close to a field antinode.

4.3.2 Coupled equations for atomic expectation values and the field

Using the method developed above allows in principle to obtain the time dependent wave-function of the system for any given initial condition. However, the method is a bit involved to apply in general. Applying it to a broad Gaussian wave packet with an initial width much larger than the ground state requires many basis states to be included in the dynamics. Although from this we then can calculate all possible observables, the whole procedure can be rather inefficient. In particular one is often interested only in the time evolution of a few key quantities as energy, localization and field. It turns out that similar to the semiclassical model [22], it is more efficient to use the effective Hamiltonian (4.6) directly to derive a coupled system of differential equations for the field and the desired expectation values directly. After some algebra within the harmonic approximation one finds the following equations for the squared atomic position and momentum observables:

$$\frac{d}{dt} \alpha(t) = [i\Delta_c - \kappa - iU_0 (1 - k^2 \langle x^2 \rangle)] \alpha(t) + i\eta_{\text{eff}} \hbar(y) (1 - k^2 \langle x^2 \rangle / 2) + \eta \quad (4.19a)$$

$$\frac{d}{dt} \langle x^2 \rangle = \frac{1}{m} \langle xp + px \rangle \quad (4.19b)$$

$$\frac{d}{dt} \langle xp + px \rangle = \frac{2}{m} \langle p^2 \rangle + 4k^2 \hbar \langle x^2 \rangle [U_0 |\alpha(t)|^2 - \eta_{\text{eff}} \hbar(y) \text{Re}(\alpha(t))] \quad (4.19c)$$

$$\frac{d}{dt} \langle p^2 \rangle = 2k^2 \hbar \langle xp + px \rangle [U_0 |\alpha(t)|^2 - \eta_{\text{eff}} \hbar(y) \text{Re}(\alpha(t))] \quad (4.19d)$$

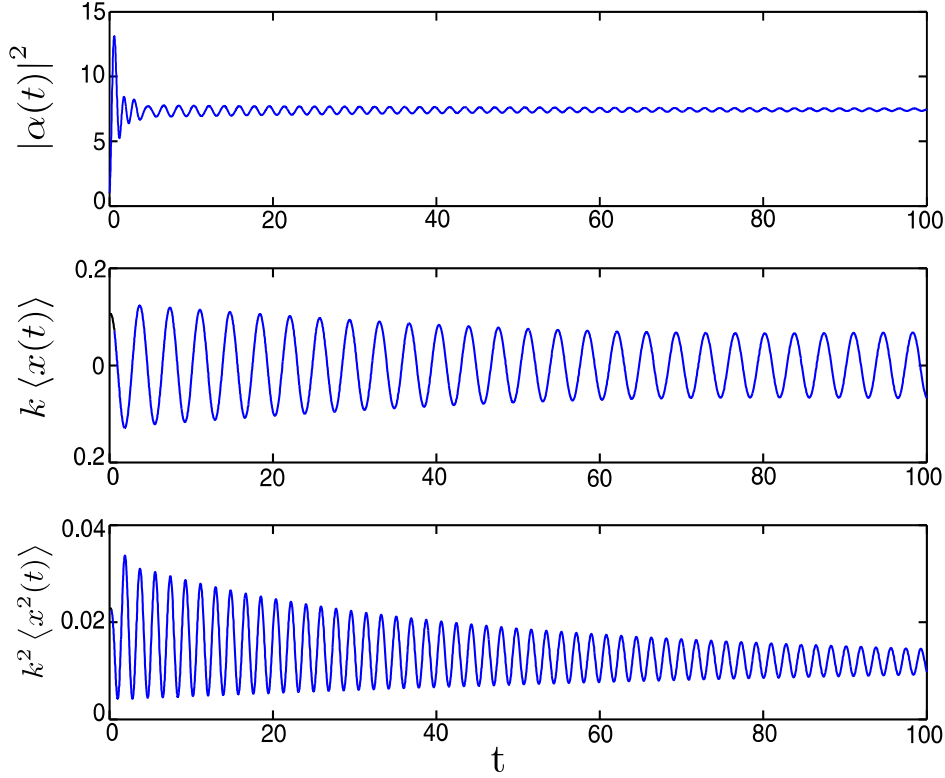


Figure 4.2. Numerical solution of the field equation (4.7) and the Ermakov equation (4.12) for the directly driven atom. The initially prepared state is $\psi(x,0) = \frac{1}{\sqrt{2}} [\psi_0(x,0) + \psi_1(x,0)]$. The parameters are $\kappa = 1$, $\eta_{\text{eff}}^2 = 200$, $\Delta_c = -10$ and $U_0 = -5$.

Again this system is not analytically solvable, but surprisingly it is closed, finite and fairly easy to solve numerically, independent of the precise form of the initial wavefunction. Let us again first consider the case of coherent pumping applied directly to the atom, i.e. $\eta = 0$ and $\eta_{\text{eff}} \neq 0$. A typical numerical solution of the time evolution is shown in Fig. 4.4. As above after some relaxation oscillations the system reaches a quasi steady state. Again we have chosen parameters implying cooling in the classical case. Note that the solution obeys the limitations set by the Heisenberg uncertainty relation in the quantum dynamics.

4.3.3 Steady state properties

Before we discuss the parameter dependence of the dynamics in more detail, we derive some simple results on stationary states of this system. Interestingly by setting (4.19a) and (4.19c) to zero one immediately sees, that there is no unique solution for the steady state equations. For any given value of $\langle x_s^2 \rangle$ exists a corresponding value of $\langle p_s^2 \rangle$, such that the system is in a steady state. Hence we have different stable states despite the fact that the system is coupled to a zero temperature bath via the cavity modes. Only if we impose the extra condition, that the steady state is a Heisenberg limited Gaussian wave packet like the ground state of an oscillator, the solution becomes unique and we have

$$\langle x^2 \rangle = \frac{b^2}{2} \quad \text{and} \quad \langle p^2 \rangle = \frac{\hbar^2}{2b^2}, \quad (4.20)$$

where b is a solution of the equation:

$$\frac{\hbar}{b^2 m} = -2k^2 \left[U_0 |\alpha_s|^2 - \eta_{\text{eff}} \hbar(y) \text{Re}(\alpha_s) \right] b^2. \quad (4.21)$$

The corresponding stationary field amplitude then reads

$$\alpha_s = -i \frac{(1 - k^2 b^2/4) \eta_{\text{eff}} \hbar(y)}{i\Delta_c - \kappa - iU_0(1 - k^2 b^2/2)}. \quad (4.22)$$

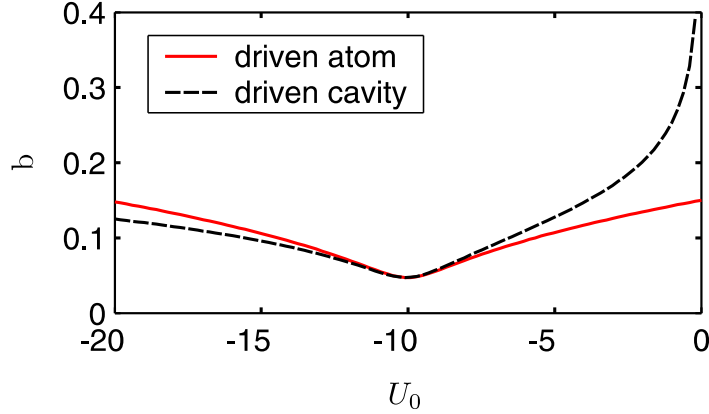


Figure 4.3. Width b of the stationary oscillator ground state for $\Delta_c = -10\kappa$, depending on U_0 . The other parameters are $\kappa = 1$ and $\eta_{\text{eff}}^2 = 200\kappa$. The solid line corresponds to the directly driven atom, the dashed dotted line corresponds to the laser-driven cavity.

In Fig. 4.3 we plot the width of the system ground state b as a function of the coupling strength U_0 for negative pump cavity detuning $\Delta_c = -10\kappa$. We see a fairly weak dependence of b on U_0 while the corresponding stationary photon number shown in Fig. 4.6 shows a sharp peak, when we hit resonance. Note, that there is only one physically acceptable solution of (4.21). In principle this equation has two positive roots b^2 but we have to exclude one of them, because it corresponds to a width much larger than the wavelength invalidating the harmonic approximation for the potential.

For comparison we now consider the case of cavity pumping as well, i.e., we set $\eta_{\text{eff}} = 0$ and $\eta \neq 0$. This makes the equations a bit simpler. Using (4.6) we can again derive an analogous system of nonlinear differential equations as above.

Assuming that the stationary state is a Gaussian state with width b , we can uniquely solve the steady state equations for b and get

$$\frac{\hbar^2}{mb^2} = -2k^2 \hbar U_0 |\alpha_s|^2 b^2. \quad (4.23)$$

Here the corresponding stationary field value is

$$\alpha_s = -\frac{\eta}{i[\Delta_c - U_0(1 - k^2 b^2/2)] - \kappa}. \quad (4.24)$$

For comparison b for this case is also shown in Fig. 4.3 (dash-dotted line). Note that while for strong coupling $U_0 \gg \kappa$ the values pretty much agree, we observe a significant difference in the ground state width for small $|U_0|$. To facilitate the comparison we have chosen η in such a way (see the next section) as to minimize the difference in the maximum steady photon number $|\alpha_s|^2$ in the two cases (see Fig. 4.6). Although being a bit artificial this conditions allows to compare the dynamical aspects of the two cases over a wide range of parameters.

4.4 Cavity cooling in the quantum regime

In the next step, we try to investigate the dissipative behavior of the coupled atom field dynamics and see how the cavity damping can be used to extract energy from the system. For red detuning ($\Delta_a < 0$) the atom is pushed towards the field antinode, where the atom interacts maximally with the field. Hence in order to allow dynamic localization of the wavefunction one has to extract energy from the motion. In the classical version of the model there are parameter regimes where one gets heating and others where one has an effective friction force for the atomic motion. The regime of heating could be useful as well for the tailored generation of motional excitations.

Here we will concentrate in the cooling regime, which appears for $\Delta_c < U_0 < 0$, as only this regime allows capturing and stable trapping. To this end we have to resort to numerical simulations for some characteristic cases. In Fig. 4.4 we show such a numerical solution of (4.19a) - (4.19d) for $\Delta_c = -10$ and $U_0 = -5$. We assume a rather broad initial position distribution $\langle x^2 \rangle \approx (\lambda/2)^2$ and choose $\langle p^2 \rangle$ according to the Heisenberg minimum uncertainty relation. We see that after some damped oscillations, the width of the position distributions tends to a stationary state much smaller than the initial condition. Hence the atoms trap themselves close to an antinode. At the same time the field and momentum width reach nonzero steady states as well. Note that the field intensity inside the resonator increases very rapidly and is entirely due to coherent scattering from the atoms. The behavior is qualitative similar, but still different from the case of direct light injection into the cavity. The numerical solution is shown in Fig 4.5. Clearly the position dependent scattering only present in the first case leads to a much more pronounced damping and atom field coupling.

Obviously the parameters characterizing the pump strengths η_{eff} and η are inherently different. Hence to compare both setups we have to use some method to relate the two cases in order to facilitate a useful comparison. Here we have chosen η in a way that the stationary photon number reached in the case $\Delta_c = U_0$ coincides in both cases. It is interesting, that in this case the stationary photon numbers for different values of Δ_c and U_0 are also very similar for a large range of parameters. For the chosen parameters the largest relative difference between both photon numbers in the case of Fig. 4.6 is $5 \cdot 10^{-3}$. This property allows us now to quantify the difference in the damping rates and atomic localization for a large range of parameters.

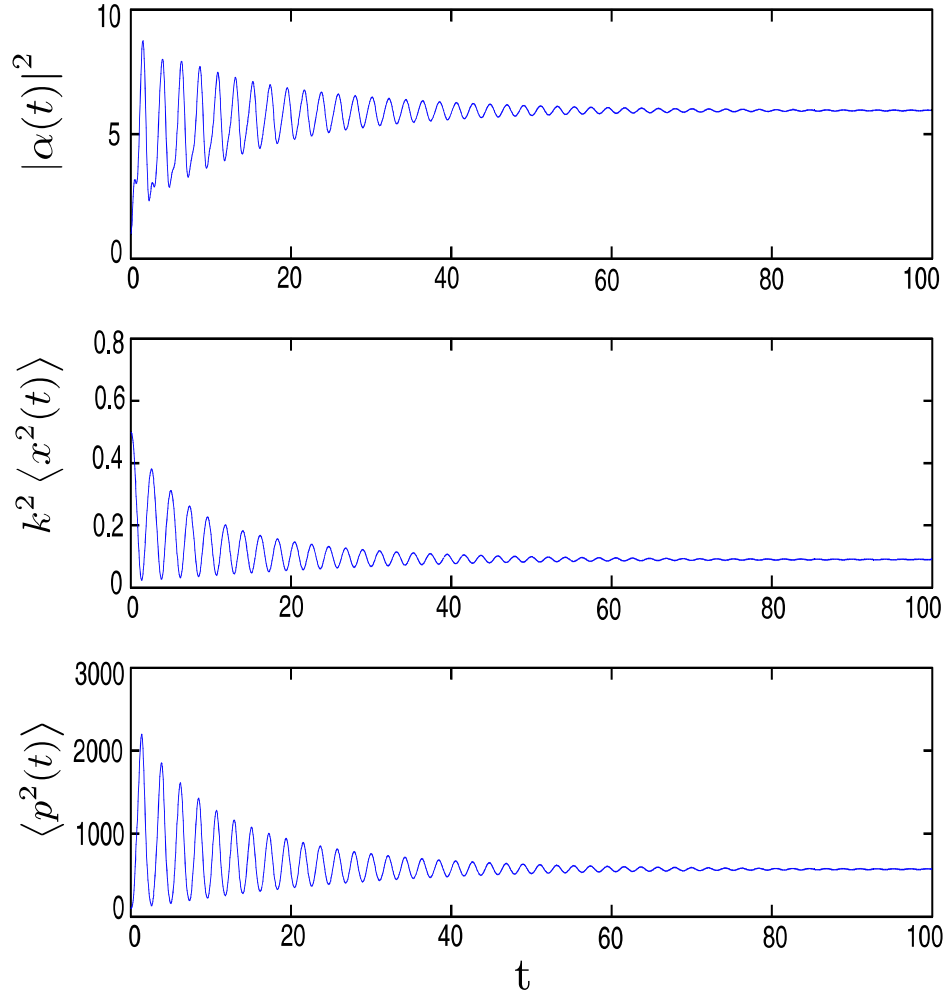


Figure 4.4. Numerical Solutions for the directly driven atom. (a) Intensity $|\alpha(t)|^2$ of the cavity field and (b),(c) Variances of x and p , respectively. The parameters in this case are $\kappa = 1$, $\eta_{\text{eff}}^2 = 200$, $\Delta_c = -10$ and $U_0 = -5$.

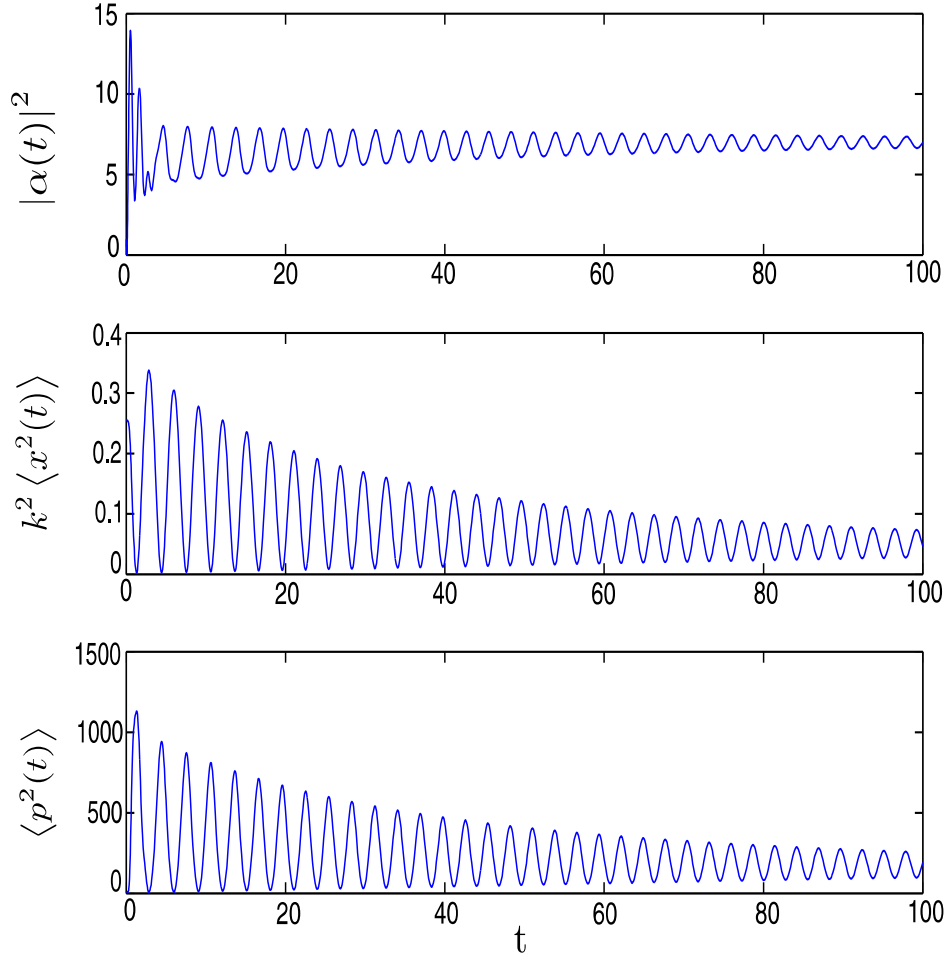


Figure 4.5. Numerical solution for the atom inside the laser-driven cavity. (a) Intensity $|\alpha(t)|^2$ of the cavity field and (b),(c) Variances of x and p , respectively. The parameters in this case are also $\kappa = 1$, $\Delta_c = -10$ and $U_0 = -5$, whereas η is chosen in the described way for $\eta_{\text{eff}}^2 = 200$.

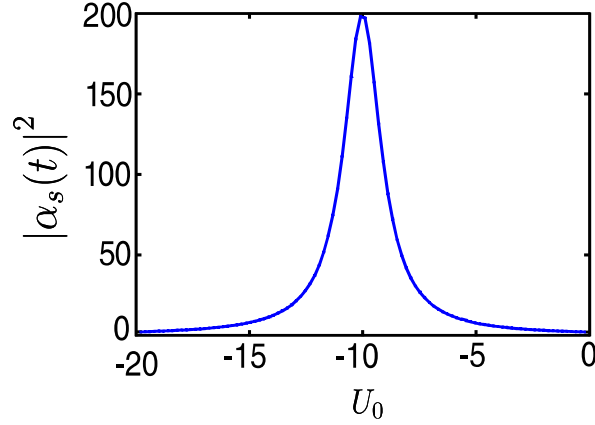


Figure 4.6. Stationary photon number $|\alpha_s(t)|^2$ of the cavity field for the laser-driven cavity and the cavity with directly driven atom, in the case of the harmonic ground state, whose width depends on U_0 and Δ_c . The parameters are $\kappa = 1$, $\Delta_c = -10$ and $\eta_{\text{eff}}^2 = 200$. We choose η , such that both photon numbers coincide for $\Delta_c = U_0$.

To quantify the cooling efficiency we fit the time dependence of the cycle averaged energy of the atom

$$E = \frac{1}{2m} \langle p^2 \rangle + \frac{m\omega^2(t)}{2} \langle x^2 \rangle, \quad (4.25)$$

to an exponential decay, from which we then read off a damping rate. Here $\omega(t)$ is the time-dependent trap frequency. Although quantum dynamical aspects of the cavity field are in principle physically very interesting, we have to limit our parameter space here to large enough photon numbers $|\alpha_s|^2 > 1$ to legitimate the semiclassical approximation for the field.

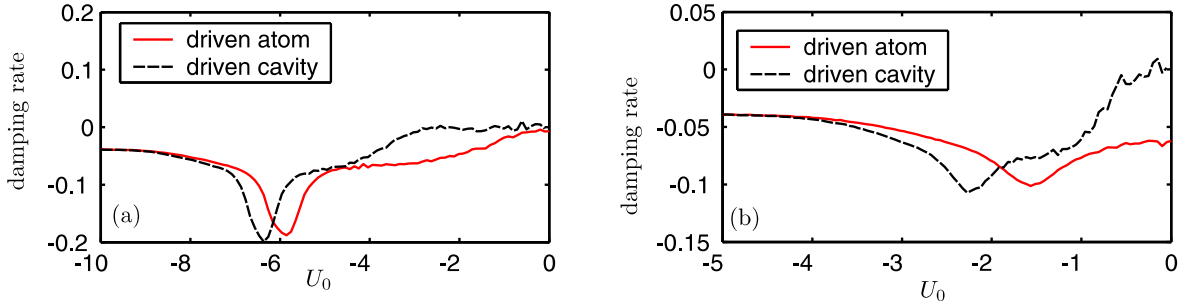


Figure 4.7. Numerically calculated damping parameters for (a) $\Delta_c = -10$ and (b) $\Delta_c = -5$ for the directly driven atom (solid line) and the driven cavity (dash-dotted line). The parameters are $\kappa = 1$, $\eta_{\text{eff}}^2 = 200$ and η as described in Fig. 4.6.

As obvious from Fig. 4.7 for large $|\Delta_c|$ we find a strong resonant enhancement of the damping rate around $U_0 \approx \Delta_c/2$. In general for large detuning and large $|U_0|$ (strong coupling) the difference between driving the atom or the mode is not very pronounced. However, for smaller $|U_0|$, which is the regime more easily attainable experimentally, driving directly the

atom shows improved damping and capturing than using a laser-driven cavity. The domain of strong cooling broadens for smaller $|\Delta_c|$.

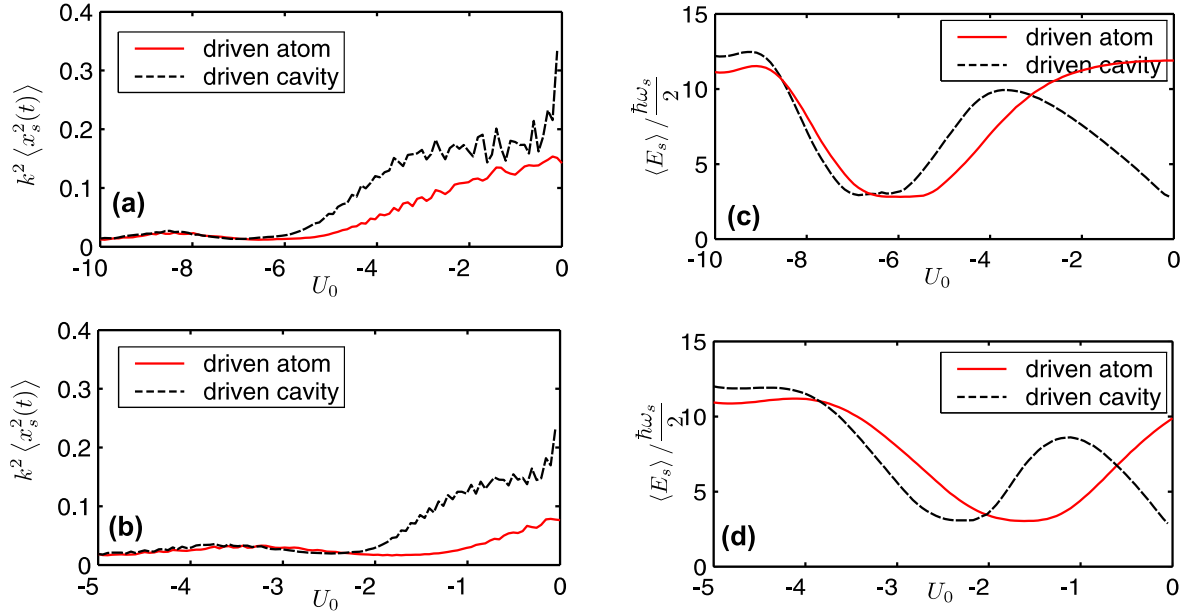


Figure 4.8. Numerically calculated variance of the position of the atom in the stationary states (a) $\Delta_c = -10$ and (b) $\Delta_c = -5$ for the directly driven atom (solid line) and the driven cavity (dash-dotted line). Numerically calculated relation of the stationary energy of the atom relative to the ground state energy of a harmonic oscillator with steady-state frequency for (c) $\Delta_c = -10$ and (d) $\Delta_c = -5$ for the directly driven atom (solid line) and the driven cavity (dash-dotted line). Other parameters are the same as in Fig. 4.7.

In Fig. 4.8(a)-(b) we calculate the stationary variance of the atomic position distribution. Again we observe good localization for large $|U_0|$ in both cases, whereas the directly driven atom is significantly better localized for smaller $|U_0|$. Note that achieving the same photon number requires a much stronger laser for atom driving, which could in practice limit its applicability. A second important quantity to characterize the performance of the cooling is the final temperature of the atom. In the quantum regime we have to compare the stationary energy of the atom relative to the ground state energy of a harmonic oscillator with equivalent steady-state frequency. Note that as our potential is time dependent a direct comparison of the final energies as a function of various parameters makes much less sense. Interestingly as seen from Fig. 4.8(c)-(d) the average excitation can reach very low values clearly in the quantum regime. For the chosen parameters and initial conditions we, however, do not get efficient ground state cooling. Again for small $|U_0|$ we see the largest differences between atom and cavity driving.

In practice there are several other possibilities to optimize damping and cooling for a given geometry. For a fixed detuning we can e.g. optimize the pump strength η_{eff} as a function of coupling strength U_0 . We find that the maximum value of the damping rate only weakly depends on η_{eff} . Nevertheless the maximum damping occurs at significantly lower values of

$|U_0|$, as we show in Fig. 4.9.

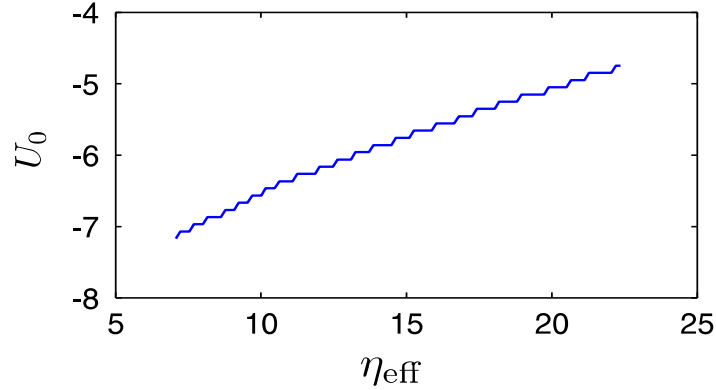


Figure 4.9. Value of U_0 where the damping rate reaches its maximum in the case of the driven atom for $\Delta_c = -10$ and $\kappa = 1$.

The above considerations are valid for fairly large atomic excitations as long as the harmonic approximation for the potential is valid. As has been emphasized before [9] in the regime of very weak excitations from the ground state, one can approximate the excitation spectrum of the atom through linearization analytically. This allows us to check the reliability of our numerical predictions at least qualitatively. Following a standard procedure we set: $\alpha(t) = \alpha_0 + \delta\alpha(t)$ and $\psi(x, t) = e^{-i\mu t} [\psi_0(x) + \delta\psi(x, t)]$, where μ is the energy of the ground state, i.e. $\mu = \hbar\omega_0/2 + \hbar U_0 |\alpha_0|^2 + 2\hbar\eta_{\text{eff}} h(y) \text{Re}(\alpha_0)$ for the driven atom and $\mu = \hbar\omega_0/2 + \hbar U_0 |\alpha_0|^2$ for the laser-driven cavity. By making the ansatz

$$\begin{aligned}\delta\psi(x, t) &= e^{-\gamma t} [e^{-i\nu t} \delta\psi_+(x) + e^{i\nu t} \delta\psi_-(x)^*], \\ \delta\alpha(t) &= e^{-\gamma t} [e^{-i\nu t} \delta\alpha_+(t) + e^{i\nu t} \delta\alpha_-(t)^*],\end{aligned}\tag{4.26}$$

we then obtain a linear system of equations for the eigenvalues $\omega = \gamma - i\nu$ and for the excitation eigenstates $\delta\alpha_{\pm}(t)$ and $\delta\psi_{\pm}(x)$. In the harmonic approximation, the cavity field only couples the ground state of the harmonic oscillator ψ_0 and the second excited state ψ_2 . For the excitations we hence can assume that our Hilbert space for the atomic wavefunction is spanned by these two states, which reduces the eigenvalue problem to a 6×6 linear system. Two of the eigenvalues are in both cases zero. The remaining characteristic polynomial then reads:

$$\begin{aligned}0 &= (4\omega_0^2 - \omega^2) [-\Delta_c + U_0 (1 + \omega_r/\omega_0) - i\kappa - \omega] \\ &\quad \times [-\Delta_c + U_0 (1 + \omega_r/\omega_0) + i\kappa + \omega] - 16 \frac{\omega_r^2}{\omega_0} \\ &\quad \times [-\Delta_c + U_0 (1 + \omega_r/\omega_0)] |\alpha_0 U_0 + \eta_{\text{eff}} h(y)/2|^2,\end{aligned}\tag{4.27}$$

where $\omega_r = \hbar k^2/(2m)$. Note that the characteristic polynomial in the case of a laser-driven cavity is very similar and can be obtained by setting $\eta_{\text{eff}} = 0$ and inserting the proper value for α_0 .

In both cases ω_0 is the ground state frequency of a harmonic oscillator (4.11) for the two different driving schemes. The imaginary part of one of the eigenvalues can be interpreted

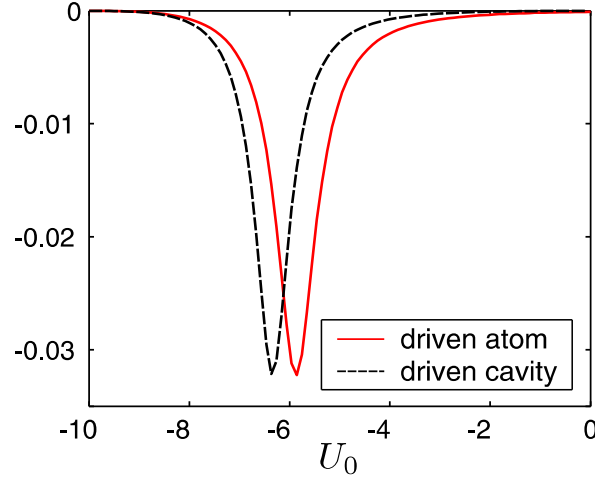


Figure 4.10. Numerically calculated imaginary part of one of the eigenvalues of (4.27) for the directly driven atom (solid line) and for the driven cavity (dash-dotted line). The parameters are $\Delta_c = -10$, $\kappa = 1$, $\eta_{\text{eff}}^2 = 200$ and η as described in Fig. 4.6.

as energy loss and has to be compared to our numerically obtained damping rates. When we plot this for a certain value of Δ_c we obtain qualitatively the same behavior as in Fig. 4.7. This can be seen in Fig. 4.10. Hence the weak excitations seem to be damped by the same mechanisms.

4.5 Conclusions

Enclosing the far-off resonance laser field to manipulate ultracold atoms in a high- Q cavity has many new and important dynamical quantities. Cavity decay opens a new decay channel for motional energy (entropy) without the detrimental effects of ordinary spontaneous emission. In this way the atom can dynamically trap and cool itself, which could be very important for coherent loading of optical microtraps. In particular by applying the driving field directly to the atom we can significantly enhance the localization and cooling properties of the system. At the same time monitoring the cavity output field will then give a direct observable on the number and temperature of the loaded atoms. By proper choice of parameters one can also create controlled excitations and manipulate the wave function in a well defined way.

Acknowledgments

This project was supported by the Austrian FWF under grants P13435 and S1512.

Bibliography

- [1] see e.g. *Bose-Einstein Condensation*, L. Pitaevskii and S. Stringari, Oxford, Clarendon Press, 2003.
- [2] R. Grimm, M. Weidemller, and Yu. B. Ovchinnikov, *Adv. At. Mol. Opt. Phys.* **42**, 95 (2000).
- [3] M. Greiner, O. Mandel, T. Esslinger, T.W. Hänsch, and I. Bloch, *Nature* **415**, 39 (2002).
- [4] D. Jaksch, C. Bruder, J. I. Cirac, C.W. Gardiner, and P. Zoller, *Phys. Rev. Lett.* **81**, 3108 (1998).
- [5] M. Holzmann and J. Audretsch, *Europhys. Lett.* **40**, 31 (1997).
- [6] H. R. Lewis and W. B. Riesenfeld, *J. Math. Phys.* **10**, 1458 (1969).
- [7] J. Stenger, S. Inouye, D.M. Stamper-Kurn, A.P. Chikkatur, D.E. Pritchard, and W. Ketterle, *Appl. Phys. B* **69**, 347 (1999).
- [8] P. Horak, G. Hechenblaikner, K. M. Gheri, H. Stecher, and H. Ritsch, *Phys. Rev. Lett.* **79**, 4974 (1997).
- [9] P. Horak and H. Ritsch, *Phys. Rev. A* **63**, 023603(R) (2001).
- [10] D. Jaksch, S. Gardiner, K. . Schulze, J. Cirac, and P. Zoller, *Phys. Rev. Lett.* **86**, 4773 (2001).
- [11] A. Mosk, S. Jochim, H. Moritz, Th. Elsässer, M. Weidemller, and R. Grimm, *Opt. Lett.* **26**, 1837 (2001).
- [12] P. Horak, S. M. Barnett, and H. Ritsch, *Phys. Rev. A* **61**, 033609 (2000).
- [13] P. Horak and H. Ritsch, *Eur. Phys. J. D* **13**, 279 (2001).
- [14] W. Ren, J. D. Cresser, and H. J. Carmichael, *Phys. Rev. A* **46**, 7162 (1992).
- [15] P. Domokos and H. Ritsch, *Phys. Rev. Lett.* **89**, 253003, (2002).
- [16] H. W. Chan, A.T. Black, and V. Vuletic, *Phys. Rev. Lett.* **90**, 063003 (2003).
- [17] D. Kruse, C. von Cube, C. Zimmermann, and P. W. Courteille, *Phys. Rev. Lett.* **91**, 183601 (2003).
- [18] B. Nagorny, T. Elsässer, and A. Hemmerich, *Phys. Rev. Lett.* **91**, 153003 (2003).
- [19] P. Domokos, P. Horak, and H. Ritsch, *J. Phys. B* **34**, (2001).
- [20] P. Domokos and H. Ritsch, *J. Opt. Soc. Am. B* **20**, 1098 (2003).
- [21] I. A. Pedrosa, *Phys. Rev. A* **55**, 3219 (1997).
- [22] M. Gangl and H. Ritsch, *Phys. Rev. A* **61**, 011402(R) (2000).

- [23] P. Maunz, T. Puppe, I. Schuster, N. Syassen, P. W. H. Pinkse, and G. Rempe, *Nature* **428**, 50 (2004).
- [24] C. W. Gardiner, P. Zoller, *Quantum noise 2nd Ed.*, Springer, Berlin (2000).

CHAPTER 5

PUBLICATION

Cold Atom Dynamics in a Quantum Optical Lattice Potential[†]

Physical Review Letters **95**, 260401 (2005)

C. Maschler and H. Ritsch

*Institut für theoretische Physik, Universität Innsbruck,
A-6020 Innsbruck, Austria*

We study a generalized cold atom Bose Hubbard model, where the periodic optical potential is formed by a cavity field with quantum properties. On the one hand the common coupling of all atoms to the same mode introduces cavity mediated long range atom-atom interactions and on the other hand atomic backaction on the field introduces atom-field entanglement. This modifies the properties of the associated quantum phase transitions and allows for new correlated atom-field states including superposition of different atomic quantum phases. After deriving an approximative Hamiltonian including the new long range interaction terms we exhibit central physical phenomena at generic configurations of few atoms in few wells. We find strong modifications of population fluctuations and next-nearest neighbor correlations near the phase transition point.

Laser fields can nowadays be routinely used to create tailored optical potentials for ultra-cold neutral atoms [1]. Loading an atomic BEC into such a periodic standing light pattern allows to experimentally implement systems, which are well described by a Bose Hubbard Hamiltonian with externally controllable parameters [2–4]. In some recent spectacular experiments the predicted Mott-insulator to superfluid quantum phase transition has been observed [5]. As the light fields are normally intense and strongly detuned from any atomic transition, their properties can be safely approximated by prescribed classical fields independent of the atomic state. However, this is invalid if they are confined within an optical resonator. For a sufficient atom number N and atom-field coupling g the fields become dynamical quantities depending on the atoms. In addition in a high- Q cavity the quantum properties of the field get important and the atoms move in quantized potentials [6, 7]. Ultimately this allows different states of the lattice field (e.g. different photon numbers) to be quantum correlated with different quantum phases of the atoms. As a striking example the atoms could be in a superposition of a Mott insulator and a superfluid state connected with a different cavity field amplitudes. Even in the classical field limit of high photon numbers all atoms see the same field state and thus we get new long range atom-atom interactions.

[†]The author of the present thesis performed all the calculations in this publication.

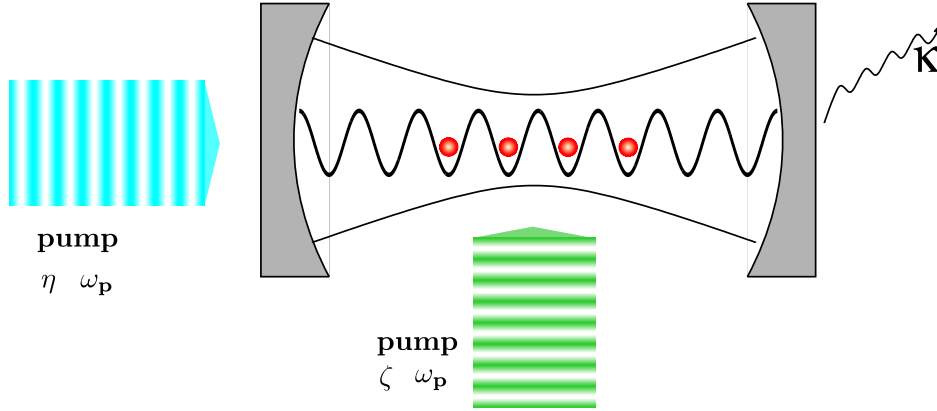


Figure 5.1. Sketch of the setup. N two-level atoms, strongly interacting with a single standing wave mode of an optical cavity, are coherently driven by a laser field via the cavity mirrors.

Interestingly the idea of implementing such combination of cavity QED and a BEC has experimentally made such rapid progress recently, that its success can be expected very soon [8].

In this work we discuss the basic physical properties of such a generalized model of ultracold atoms in a periodic potential generated by a quantized field mode. In a first step we derive an approximate Hamiltonian analogous to the Bose Hubbard Hamiltonian including a quantized potential. Its basic physical implications are then exhibited in two cases: (a) a strongly damped cavity, where the field dynamics can be adiabatically eliminated, which leads to a rescaling of the coupling parameters and new long range atom-atom coupling terms and (b) a dynamical model where the field is approximated by its time dependent expectation value derived from a dynamical equation containing atomic expectation values.

Model: Let us consider N two-level atoms with mass m and transition frequency ω_a strongly interacting with a single standing wave cavity mode of frequency $\omega_c \ll \omega_a$. The system is coherently driven by a laser field with frequency $\omega_p \approx \omega_c$ through the cavity mirror with amplitude η . Alternatively the atoms are illuminated transversally to the cavity axes (see Fig. 5.1) with amplitude ζ .

Including damping, the dynamics is given by the master equation for the atom field density operator $\dot{\rho} = \frac{1}{i\hbar}[H, \rho] + \mathcal{L}\rho$, where the Liouvillian \mathcal{L} models dissipation. For large atom-pump detuning spontaneous emission is negligible and cavity loss κ will be the dominant dissipative process, i.e., $\mathcal{L}\rho = \kappa(2a\rho a^\dagger - a^\dagger a\rho - \rho a^\dagger a)$. Here a is the annihilation operator for a cavity photon.

As convenient choice we rewrite the Hamiltonian in a second quantized form, where the direct interaction between the atoms is modeled by a pseudopotential and characterized by the s-wave scattering length a_s :

$$H = \int d^3x \Psi^\dagger(\mathbf{x}) H_0 \Psi(\mathbf{x}) + \frac{1}{2} \frac{4\pi a_s \hbar^2}{m} \int d^3x \Psi^\dagger(\mathbf{x}) \Psi^\dagger(\mathbf{x}) \Psi(\mathbf{x}) \Psi(\mathbf{x}). \quad (5.1)$$

Here $\Psi(\mathbf{x})$ is the field operator for the atoms and H_0 is the single-particle Hamiltonian in rotating-wave and dipole approximation:

$$H_0 = \frac{p^2}{2m} - \hbar \Delta_a \sigma^+ \sigma^- - \hbar \Delta_c a^\dagger a - i \hbar g(x) (\sigma^+ a - \sigma^- a^\dagger) - i \hbar h(\mathbf{x}) \zeta (\sigma^+ - \sigma^-) - i \hbar \eta (a - a^\dagger), \quad (5.2)$$

where $\Delta_a = \omega_p - \omega_a$ and $\Delta_c = \omega_p - \omega_c$ is the atom-pump and cavity-pump detuning, respectively. Along the cavity axis (x-direction) the atom-field coupling is set to $g(x) = g_0 \cos(kx)$, while the transverse laser beam forms a standing wave with amplitude $h(\mathbf{x}) = h_0 \cos(k_y y)$ in the y-direction, where we set $y = 0$ for our 1D-considerations. In the regime of low saturation [9] (large Δ_a) adiabatic elimination of the excited atomic state in (5.2) then leads to:

$$H_0 = \frac{p^2}{2m} + \cos^2(kx) (\hbar U_0 a^\dagger a + V_{\text{cl}}) - \hbar \Delta_c a^\dagger a - i \hbar \eta (a - a^\dagger) + \hbar \eta_{\text{eff}} \cos(kx) (a + a^\dagger). \quad (5.3)$$

The important parameter $U_0 = g_0^2/\Delta_a$ here is the optical lattice depth per photon [6] and also gives the refractive index of one atom at an antinode. The term containing $\eta_{\text{eff}} = g_0 h_0 \zeta/\Delta_a$ represents an effective pump through atomic scattering into the mode. Along x the cavity field forms an optical lattice potential with period $\lambda/2$ and depth $\hbar U_0 a^\dagger a$. For the sake of generality we add an extra classical potential V_{cl} as well.

To derive a generalized Bose-Hubbard Hamiltonian we expand the Bloch states of a single atom inside the lattice using localized Wannier functions [10] and rewrite the field operators in Eq. (5.1) in these functions, keeping only the lowest vibrational state at each site (lowest band) $\Psi(\mathbf{x}) = \sum_i b_i w(\mathbf{x} - \mathbf{x}_i)$ to get:

$$H = \sum_{k,l} E_{k,l} b_k^\dagger b_l + (\hbar U_0 a^\dagger a + V_{\text{cl}}) \sum_{k,l} J_{k,l} b_k^\dagger b_l + \hbar \eta_{\text{eff}} (a + a^\dagger) \sum_{k,l} \tilde{J}_{k,l} b_k^\dagger b_l - i \hbar \eta (a - a^\dagger) + \frac{U}{2} \sum_k b_k^\dagger b_k (b_k^\dagger b_k - 1) - \hbar \Delta_c a^\dagger a. \quad (5.4)$$

The operators b_k^\dagger (b_k) correspond to the creation (annihilation) of an atom at site k and the on-site interaction of two atoms is given by $U = \frac{4\pi a_s \hbar^2}{m} \int d^3x |\psi(\mathbf{x})|^4$. As the nonlinear part of the nearest-neighbor interaction is typically two orders of magnitude smaller than the on-site interaction it is neglected as usually. In contrast to the classical field case [3] the appearance of the cavity field operator does not allow to reassemble all hopping terms to a single expression. To be still able to proceed analytically we assume a weak dependence

of $w(x)$ on the cavity photon number. Although the opposite limit might even contain more interesting physics, we will concentrate on this limit to be able to proceed analytically. Explicitly the coupling matrix elements read:

$$E_{k,l} = \int d^3x w(\mathbf{x} - \mathbf{x}_k) \left(-\frac{\hbar^2}{2m} \nabla^2 \right) w(\mathbf{x} - \mathbf{x}_l), \quad (5.5a)$$

$$J_{k,l} = \int d^3x w(\mathbf{x} - \mathbf{x}_k) \cos^2(kx) w(\mathbf{x} - \mathbf{x}_l), \quad (5.5b)$$

$$\tilde{J}_{k,l} = \int d^3x w(\mathbf{x} - \mathbf{x}_k) \cos(kx) w(\mathbf{x} - \mathbf{x}_l). \quad (5.5c)$$

These matrix elements are symmetric, i.e., $E_{k,l} = E_{l,k}$, $J_{k,l} = J_{l,k}$ and $\tilde{J}_{k,l} = \tilde{J}_{l,k}$ and the on-site elements $E_{k,k}$ and $J_{k,k}$ are independent of k . As the next-nearest neighbor terms are typically two orders of magnitude smaller than the nearest-neighbor amplitudes they are omitted too. Note that in the case of transverse pumping two adjacent wells acquire different depths since the \cos in (5.3) changes sign periodically, which implies $\tilde{J}_{k,k} = -\tilde{J}_{k+1,k+1}$. The Hamiltonian (5.4) now reads:

$$\begin{aligned} H = E_0 \hat{N} + E \hat{B} + \left(\hbar U_0 a^\dagger a + V_{\text{cl}} \right) \left(J_0 \hat{N} + J \hat{B} \right) + \hbar \eta_{\text{eff}} \left(a + a^\dagger \right) \tilde{J}_0 \sum_k (-1)^{k+1} \hat{n}_k \\ - \hbar \Delta_c a^\dagger a - i \hbar \eta \left(a - a^\dagger \right) + \frac{U}{2} \sum_k \hat{n}_k (\hat{n}_k - 1), \end{aligned} \quad (5.6)$$

where we introduced $\hat{N} = \sum_k \hat{n}_k = \sum_k b_k^\dagger b_k$ (number operator) and $\hat{B} = \sum_k \left(b_{k+1}^\dagger b_k + h.c. \right)$ (jump operator). E_0, J_0 and \tilde{J}_0 are on-site matrix elements, whereas E and J are the site-to-site hopping elements. The Hamiltonian (5.6) is a central result of this work and gives the starting point to discuss the physics below.

Lets first look at the light field dynamics and write down the corresponding Heisenberg equation:

$$\dot{a} = \left[i \left(\Delta_c - U_0 \left(J_0 \hat{N} + J \hat{B} \right) \right) - \kappa \right] a + \eta - i \eta_{\text{eff}} \tilde{J}_0 \sum_k (-1)^{k+1} \hat{n}_k. \quad (5.7)$$

We see that the quantum state of the field depends not only on the number of atoms \hat{N} but also on coherences via \hat{B} . Particularly interesting effects can also be expected from the last term describing transverse pumping as the corresponding operator has an alternating sign for neighboring wells. Hence it vanishes exactly for a Mott insulator state, while it gives a nonzero contribution for a superfluid state. Nevertheless we will concentrate here on the more simple setup pumping acts via a cavity mirror and set $\eta_{\text{eff}} = 0$ below.

Bad cavity limit: The common interaction of all atoms with the same field implies a complicated dynamics. Luckily in typical setups the field damping rate κ is the fastest time

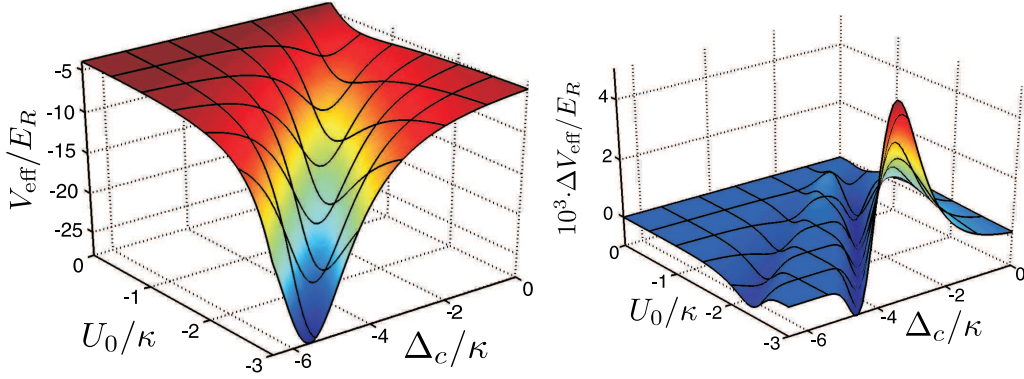


Figure 5.2. (a) Numerically found average potential depth $V_{\text{eff}} = V_{\text{cl}} + \hbar U_0 \langle a^\dagger a \rangle$ of the ground state of (5.6) for $N = 2$ atoms in two wells. (b) Relative error in this potential using expansion (5.9). The parameters are $\eta = 2\kappa$, $V_{\text{cl}} = -4E_R$ and the scattering length is $a_s = 0.1E_R$.

scale in the system. This allows to eliminate the cavity degrees of freedom by formally solving equation (5.7) for $a = \eta/[\kappa - i(\Delta_c - U_0(J_0\hat{N} + J\hat{B}))]$ and inserting this back to (5.4). As \hat{N} commutes with \hat{B} this gives no ordering problem. For a fixed atom number $N = \langle \hat{N} \rangle$ we then expand a to second order in the small tunneling matrix element J :

$$a \approx \frac{\eta}{\kappa - i\Delta'_c} \left[1 - \frac{iU_0J}{\kappa - i\Delta'_c} \hat{B} - \frac{U_0^2J^2}{(\kappa - i\Delta'_c)^2} \hat{B}^2 \right], \quad (5.8)$$

where $\Delta'_c = \Delta_c - U_0J_0N$ is a rescaled detuning, so that we have:

$$H = \left[E + J \left(V_{\text{cl}} - \hbar U_0 \eta^2 \frac{\kappa^2 - \Delta_c'^2}{(\kappa^2 + \Delta_c'^2)^2} \right) \right] \hat{B} - 3\hbar U_0^2 \eta^2 \Delta'_c \frac{3\kappa^2 - \Delta_c'^2}{(\kappa^2 + \Delta_c'^2)^3} J^2 \hat{B}^2 + \frac{U}{2} \sum_k \hat{n}_k (\hat{n}_k - 1). \quad (5.9)$$

Obviously H now contains cavity induced rescaling of the tunnel coupling proportional to \hat{B} as well as nonlocal correlated two atom hopping terms proportional to \hat{B}^2 mediating long range interactions. In Fig. 5.2 we show the excellent agreement of the field calculated from the expansion (5.8) compared to a full numerical inversion within a large parameter range as used below. Note that the matrix elements still weakly depend on the depth of the optical potential via $\langle \hat{B} \rangle$ but as J is small they can be approximated neglecting the \hat{B} -term and setting $J_0 = 1$ in the field expectation value $\alpha^0 = \eta/[\kappa - i(\Delta_c - NU_0)]$.

Lets now discuss some key physics. In the simplest case of a single particle in two wells the symmetric and antisymmetric superpositions of the atom in either site are eigenstates with an energy difference

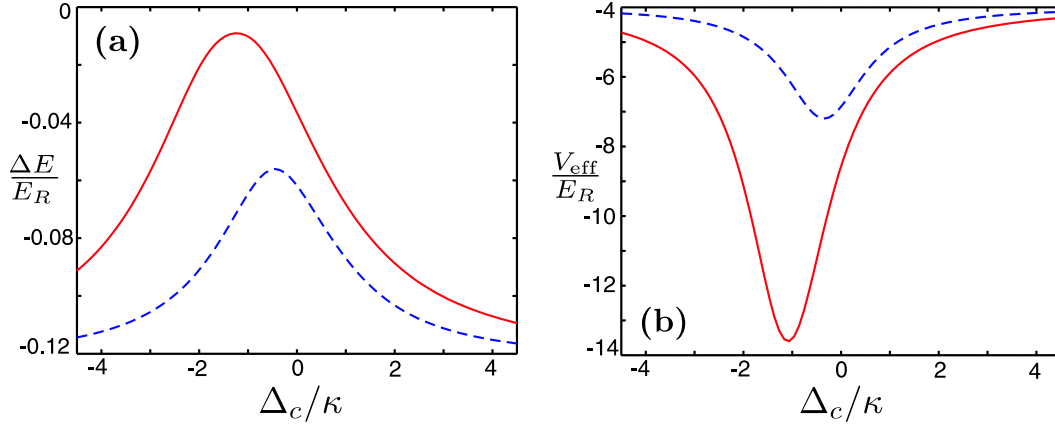


Figure 5.3. (a) Energy difference ΔE as function of Δ_c for a single atom in two wells for $U_0 = -1.2\kappa$ (solid line) and $U_0 = -0.4\kappa$ (dashed line). The associated lattice depth is shown in (b). The other parameters are $\eta = 2\kappa$ and $V_{\text{cl}} = -4E_R$.

$$\Delta E = 2 \left[E + J \left(V_{\text{cl}} - \hbar U_0 \eta^2 \frac{\kappa^2 - \Delta_c'^2}{(\kappa^2 + \Delta_c'^2)^2} \right) \right], \quad (5.10)$$

strongly depending on the cavity parameters (see Fig. 5.3a). Hence detuning gives a handle to control the tunnel coupling and atom confinement (Fig. 5.3b). Note that the symmetric and antisymmetric eigenstate are associated with different field amplitudes (lattice depths).

Adding more atoms the interaction term comes to play and the ground state of the system is a superposition of different atomic configurations. Here the cavity parameters influence the position and shape of the well known Mott-insulator superfluid transition [2–4]. An important quantum feature appears for fields where the uncertainty in the photon number is not negligible. For an average photon number \bar{n} generating a potential depth close to the phase transition point the photon numbers $\bar{n} \pm 1$ are then associated to different atomic phases, so that the ground state contains atomic states of different phases correlated with the corresponding photon number. Even for a system being dominantly in the insulator phase, photon number fluctuations then allow the atoms to jump. This is shown in Fig. 5.4a for 4 particles in 4 wells. Here we compare the site occupation probabilities as a function of scattering length for a purely classical and a quantum potential where the photon number uncertainty allows hopping even in the insulator regime. This behaviour can be enhanced or reduced through cavity mediated interaction as shown in Fig. 5.4b, where we plot the atom number fluctuations in one well as a function of a_s for different atom-cavity detunings and compare it to the classical field case. Clearly the atom number fluctuations are enhanced on one side of the cavity resonance and suppressed on the other.

The appearance of long range 4 particle interactions mediated by the \hat{B}^2 -term in (5.9) can be seen by comparing the density-density correlation functions $\langle n_i n_j \rangle$ [11] for nearest and

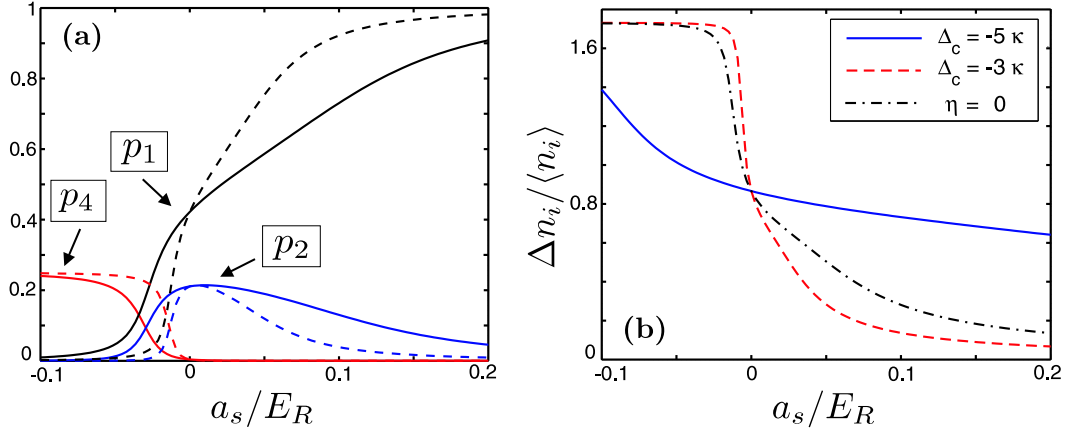


Figure 5.4. (a) Occupation probabilities p_i for i atoms in one well as function of scattering length for the ground state of 4 atoms in 4 wells. The parameters are $U_0 = -\kappa$ and $\Delta_c = -3.75\kappa$ and $V_{\text{eff}} = \hbar U_0 \langle a^\dagger a \rangle = -4E_R$. For comparison the dashed lines correspond to an equivalent classical potential, i.e., $\langle a^\dagger a \rangle = 0$ and $V_{\text{cl}} = -4E_R$. (b) Fluctuations of atom number in one well as a function of a_s for different cavity detunings $\Delta_c = -5\kappa$ (solid line), $\Delta_c = -3\kappa$ (dashed line) and a classical field (dashed-dotted line).

next nearest neighbor sites. Depending on cavity parameters as shown in Fig. 5.5a each of the two correlations can be enhanced or reduced with respect to the classical potential case.

Coupled atom-field dynamics in the semiclassical limit: As final point we turn to the classical field limit of the coupled Hamiltonian (5.6) for fixed N and large photon number. Here the field is approximately in a coherent state $|\alpha\rangle$ and the system is assumed to evolve as a product state $|\Phi\rangle = |\psi\rangle \otimes |\alpha(t)\rangle$. The Heisenberg equation (5.7) for the field then reduces to a classical equation for α containing expectation values of atomic operators:

$$\dot{\alpha}(t) = \left[i \left(\Delta_c - U_0 \langle \psi | J_0 \hat{N} + J \hat{B} | \psi \rangle \right) - \kappa \right] \alpha(t) + \eta, \quad (5.11a)$$

$$i\hbar \frac{d}{dt} |\psi\rangle = \left[E + J \left(V_{\text{cl}} + \hbar U_0 |\alpha(t)|^2 \right) \right] \hat{B} |\psi\rangle + \frac{U}{2} \sum_k \hat{n}_k (\hat{n}_k - 1) |\psi\rangle. \quad (5.11b)$$

$\alpha(t)$ is then inserted back into the atomic Hamiltonian like a classical time dependent potential V_{cl} [9, 12]. Similar to the case of a time dependent Gross-Pitaevskii equation [12] the corresponding Schrödinger equation can be solved simultaneously, where the matrix elements E, J have to be recalculated in each time step.

Although the factorizing assumption is in general doubtful and one has to check the dynamical restriction to the lowest band, this procedure gives a first insight in the dynamical behavior of the model. As a generic example we show the time evolution of the uncertainty of the site occupation number starting with a 'superfluid' state at $t = 0$, when the onsite interaction is turned on. Fig. 5.5b shows that in contrast to a fixed external potential the dynamic cavity field leads to a damping of the fluctuations approaching a Mott insulator state.

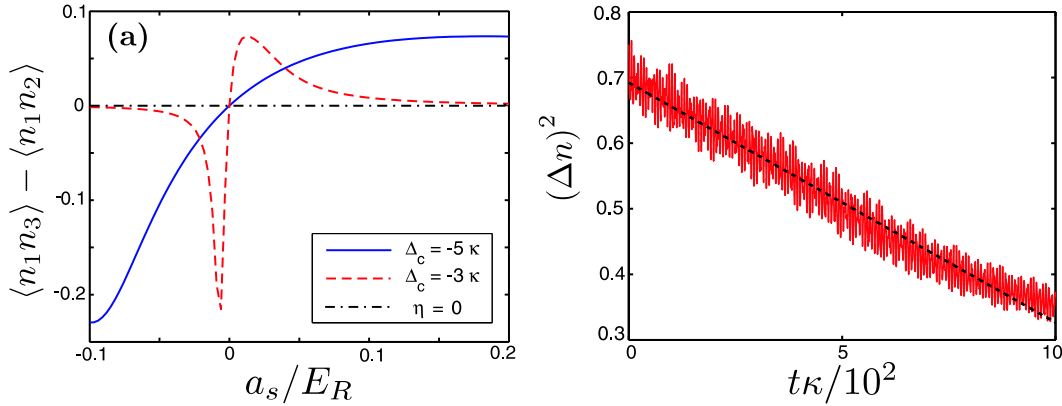


Figure 5.5. (a) Difference of the density-density correlation functions: $\langle n_1 n_3 \rangle - \langle n_1 n_2 \rangle$. Parameters are as in Fig. 5.4b. (b) Dynamical evolution of atom number fluctuations in one well starting from an interaction free ground state and a sudden turn on of onsite-interaction. A linear fit is depicted by the dashed line. Here we chose $U_0 = -\kappa$, $\Delta_c = -4.2\kappa$, $V_{cl} = 0$, $a_s = 3E_R$ and η such that $V_{eff} = -4E_R$.

In summary we have shown that a dynamical quantum optical potential for ultracold atoms invokes a wealth of new physics. The effects are pronounced in the limit of strong coupling and small photon numbers but long range interactions persist even in the bad cavity limit within a classical field approximation. The considered systems are in range of current experimental capabilities and should allow to control and study new quantum phases.

Acknowledgments: We thank G. Moriggi, M. Lewenstein and P. Domokos for helpful discussions. Funded by the Austrian Science Fund FWF - P17708.

Bibliography

- [1] See e.g. *Laser Manipulation of Atoms and Ions*, ed. by E. Arimondo and W. D. Phillips, Varenna Summer School, 1991 (North-Holland, Amsterdam 1992).
- [2] M. P. A. Fisher *et al.*, Phys. Rev. B **40**, 546 (1989).
- [3] D. Jaksch *et al.*, Phys. Rev. Lett. **81**, 3108 (1998); D. Jaksch and P. Zoller, Ann. Phys. **315**, 52 (2005).
- [4] W. Zwerger, J. Opt. B **5**, S9 (2003).
- [5] M. Greiner *et al.*, Nature **415**, 39 (2002).
- [6] P. Domokos and H. Ritsch, J. Opt. Soc. Am. B **20**, 1098 (2003).
- [7] A. Griessner, D. Jaksch, and P. Zoller, J. Phys. B **37**, 1419 (2004).
- [8] B. Nagorny, T. Elsässer, and A. Hemmerich, Phys. Rev. Lett. **91**, 153003 (2003); J. A. Sauer *et al.*, Phys. Rev. A **69**, 051804 (2004).

-
- [9] C. Maschler and H. Ritsch, Opt. Comm. **243**, 145 (2004).
 - [10] C. Kittel, *Quantum Theory of Solids*, John Wiley & Sons, (New York 1963).
 - [11] T. D. Kühner, S. R. White, and H. Monien, Phys. Rev. B **61**, 12474 (2000).
 - [12] P. Horak and H. Ritsch, Phys. Rev. A **63**, 23603 (2001).

CHAPTER 6

PUBLICATION

Ultracold Atoms in Optical Lattices Generated by Quantized Light Fields[†]

arXiv: quant-ph/0710.4220 (submitted to European Journal of Physics D)

C. Maschler¹, I. B. Mekhov^{1,2}, and H. Ritsch¹

- 1) *Institut für theoretische Physik, Universität Innsbruck,
A-6020 Innsbruck, Austria*
2) *St. Petersburg State University, Faculty of Physics,
St. Petersburg, Russia*

We study an ultracold gas of neutral atoms subject to the periodic optical potential generated by a high- Q cavity mode. In the limit of very low temperatures, cavity field and atomic dynamics require a quantum description. Starting from a cavity QED single atom Hamiltonian we use different routes to derive approximative multiparticle Hamiltonians in Bose-Hubbard form with rescaled or even dynamical parameters. In the limit of large enough cavity damping the different models agree. Compared to free space optical lattices, quantum uncertainties of the potential and the possibility of atom-field entanglement lead to modified phase transition characteristics, the appearance of new phases or even quantum superpositions of different phases. Using a corresponding effective master equation, which can be numerically solved for few particles, we can study time evolution including dissipation. As an example we exhibit the microscopic processes behind the transition dynamics from a Mott insulator like state to a self-ordered superradiant state of the atoms, which appears as steady state for transverse atomic pumping.

6.1 Introduction

Laser light, far red detuned from an atomic resonance, is nowadays a standard tool in experimental quantum optics to create tunable optical potentials [1] which can be loaded with ultracold atoms to provide for a plethora of possibilities to study quantum properties of many-body strongly correlated systems [2]. The high level of microscopic understanding and extensive control of the light fields and atoms allow to implement genuine models like e.g. the Bose-Hubbard (BH) model [3, 4]. Initially originating from condensed matter physics [5]

[†]The author of the present thesis performed all the calculations in this publication. I. M. acted as a discussion partner of all the aspects of this work.

it has been used to study the Mott insulator to superfluid phase transition [6] in detail and in real time. Adjusting several of the lattice parameters as the intensity and the configuration of the lattice lasers provides a versatile toolbox of techniques to control the dynamics of the atoms in the lattice [7]. Moreover, the collisional properties of the certain types of atoms can be tailored by means of magnetic [8] or optical [9] Feshbach resonances. Using extra confinement it was even possible to observe the Mott insulator to superfluid transition in 1D [10, 11] and 2D [12], followed by other spectacular demonstrations of condensed matter physics phenomena as the realization of a Tonks gas in 1D [13, 14] and the Berezinskii-Kosterlitz-Thouless phase transition in 2D [15]. Theoretically many more proposals to apply these methods to spin systems and investigate further fascinating properties of strongly correlated systems were put forward (see [16] for a review).

In all of these approaches, the light fields were approximated by classical, externally prescribed fields independent of the atoms. This requires intense light, far detuned from any atomic transition. Of course this assumption holds no longer if the light, which generates the optical lattice, is enhanced by an optical resonator. In this case - given a sufficient atom number N and atom-field coupling g - the field itself becomes a dynamical quantity [17] depending on the atomic distribution. As all atoms are coupled to the same field modes, this immediately introduces substantial long range interactions, which cannot be ignored as in free space. In specially designed cases this force induces coherently driven atoms to self-organize in regular patterns as predicted in Ref. [18, 19] and subsequently experimentally verified [20].

In addition, in a high- Q optical resonator relatively low photon numbers are sufficient to induce strong forces. This was demonstrated by trapping an atom in the field of just a single photon [21, 22]. Hence the inevitable photon number fluctuations induced by cavity damping induce force fluctuations on the atoms inducing diffusion. At the same time as cavity photon loss constitutes a dissipation channel, it can also carry out energy and entropy of the system. This opens possibilities for cooling of atomic motion [23–26], as demonstrated by beautiful experiments in the group of Rempe [27, 28]. Since this cooling mechanism does not require the existence of closed optical cycles it could even be used for qubits [29] or to damp quantum oscillations or phase fluctuations of a BEC coupled to a cavity field [30, 31].

For low photon numbers the quantum properties of the light field get important as well and the atoms are now moving in different quantized potentials determined by the cavity photon number. Quantum mechanics of course allows for superpositions of photon numbers invoking superpositions of different optical potentials for the atoms. First simplified models to describe this new physics were recently proposed by us [32] and in parallel by other authors [33]. As the intracavity field itself depends on the atomic state (phase), different atomic quantum states are correlated with different states of the lattice field with differing photon number distributions. In this way quantum mechanics allows for the creation of very exotic atom-field states, like a superposition of a Mott-insulator and superfluid phase, each thereof correlated with a different photon number. Some quite exotic looking phase diagrams for this system were already discussed in Ref. [33]. Without resorting to the full complex dynamics of the system, the quantum correlations between the field and the atomic wavefunctions open the possibility of non-destructively probing the atomic state by weak scattering of coherent light into the cavity mode [34] and carefully analyzing its properties [35].

It is quite astonishing, that experimental progress in the recent years has made such systems experimentally accessible and at present already several experimental groups succeeded

in loading a BEC into a high- Q optical cavity [36–39]. A reliable analysis of these experiments has made more thorough theoretical studies of systems mandatory.

In this work we concentrate on the study of an ultracold gas in optical lattices including the quantum nature of the lattice potential generated from a cavity field. This extends and substantiates previous studies and predictions on such a system by us [32] as well as other authors [33]. Here we limit ourselves to the case of a high- Q cavity which strongly enhances a field sufficiently red detuned from any atomic transition to induce an optical potential without significant spontaneous emission. In particular we address two different geometric setups, where either the cavity mode is directly driven through one mirror, or the atoms are coherently excited by a laser and scatter light into the cavity mode. The cavity potential can also be additionally enhanced by some extra conservative potential applied at a different frequency [40, 41]. These two generic cases leads to quite different physical behavior and allow to discuss several important aspects of the underlying physics.

This paper is organized as follows. Sec. 6.2 is devoted to a systematic presentation of our model and various simplifying approximations as adiabatic elimination of the excited states of the atoms and subsequent formulation of an effective multi-particle Hamiltonian in second quantized form. In section 6.3, we specialize on the simplest generic case of a coherently driven cavity and approximate the corresponding Hamiltonian by adiabatic elimination of the cavity field. We investigate the properties thereof, corresponding to the influence of the cavity on the Mott-insulator to superfluid quantum phase-transition and identify the regime of validity for the elimination of the cavity field. Finally, we compare these results with the dynamics of the full master equation. In Sec. 6.4 we study the more complex case of atoms coherently driven by a laser field transversal to the cavity axis, where it is much harder to find valid analytical simplifications and one has to resort to numerical studies of few particle dynamics. Finally, we conclude in Sec. 6.5.

6.2 Model

We start with N two-level atoms with mass m and transition frequency ω_{eg} strongly interacting with a single standing wave cavity mode of frequency ω_c . We also consider coherent driving of the atoms at frequency ω_p and strength ζ and the cavity with amplitude η (see Fig. 6.1). Note that in the specific examples later we will consider only one pump laser beam at a time.

Using the rotating-wave and electric-dipole approximation, we can describe a single atom of this system by the Jaynes-Cummings Hamiltonian [42]

$$H^{(1)} = H_A^{(1)} + H_R^{(1)} + H_{Int}^{(1)}. \quad (6.1)$$

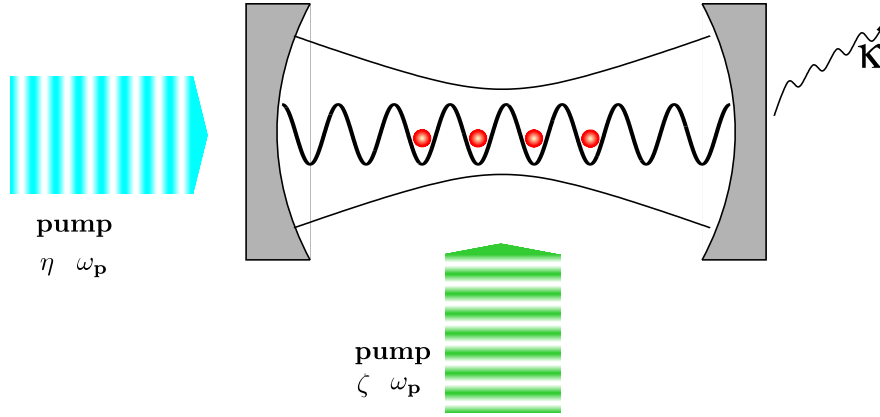


Figure 6.1. (color online). Scheme of atoms inside an optical cavity, driven by two external lasers.

Explicitly the different Hamiltonians for the atoms, the field mode and the interaction read:

$$H_A^{(1)} = \frac{\hat{\mathbf{p}}^2}{2m} + V_e(\mathbf{x})\sigma^+\sigma^- + V_g(\mathbf{x})\sigma^-\sigma^+ + \hbar\omega_{VG}\sigma^+\sigma^- - i\hbar h(\mathbf{x})\zeta (\sigma^+e^{-i\omega_p t} - \sigma^-e^{i\omega_p t}), \quad (6.2a)$$

$$H_R^{(1)} = \hbar\omega_c a^\dagger a - i\hbar\eta (ae^{i\omega_p t} - a^\dagger e^{-i\omega_p t}), \quad (6.2b)$$

$$H_{Int}^{(1)} = -i\hbar g(\mathbf{x}) (\sigma^+ a - \sigma^- a^\dagger). \quad (6.2c)$$

Here $h(\mathbf{x})$ denotes the mode-function of the transverse pump field, $g(\mathbf{x})$ denotes the cavity mode function and the field operator a describes the annihilation of a cavity photon with frequency ω_c . The transition frequency of the atom is given by ω_{eg} . $V_e(\mathbf{x})$ and $V_g(\mathbf{x})$ are external trapping potentials for the atom in the excited and the ground state, respectively. In order to change to slowly varying variables we apply a unitary transformation with operator $U(t) = \exp[i\omega_p t (\sigma^+\sigma^- + a^\dagger a)]$, such that we end up with the following single-particle Hamiltonian, using the same symbols for the transformed quantities:

$$H_A^{(1)} = \frac{\hat{\mathbf{p}}^2}{2m} + V_e(\mathbf{x})\sigma^+\sigma^- + V_g(\mathbf{x})\sigma^-\sigma^+ - \hbar\Delta_a\sigma^+\sigma^- - i\hbar h(\mathbf{x})\zeta (\sigma^+ - \sigma^-), \quad (6.3a)$$

$$H_R^{(1)} = -\hbar\Delta_c a^\dagger a - i\hbar\eta (a - a^\dagger), \quad (6.3b)$$

$$H_{Int}^{(1)} = -i\hbar g(\mathbf{x}) (\sigma^+ a - \sigma^- a^\dagger), \quad (6.3c)$$

where $\Delta_c = \omega_p - \omega_c$, $\Delta_a = \omega_p - \omega_{eg}$ denotes the detunings of the cavity and the atomic transition frequency from the pumping field frequency. In order to describe the situation for N atoms, we use the single-particle Hamiltonian of Eq. (6.1) and (6.3) in second quantization formalism[43], i.e.,

$$H = H_A + H_R + H_{A-R} + H_{A-P} + H_{A-A}. \quad (6.4)$$

The terms in this expression correspond to the single particle terms in (6.2) and (6.3). Hence, H_A and H_R model the free evolution of the atomic and the field variables, respectively. They

read as:

$$H_A = \int d^3\mathbf{x} \left[\Psi_g^\dagger(\mathbf{x}) \left(-\frac{\hbar^2}{2m} \nabla^2 + V_g(\mathbf{x}) \right) \Psi_g(\mathbf{x}) + \Psi_e^\dagger(\mathbf{x}) \left(-\frac{\hbar^2}{2m} \nabla^2 - \hbar\Delta_a + V_e(\mathbf{x}) \right) \right] \Psi_e(\mathbf{x}), \quad (6.5)$$

where $\Psi_g(\mathbf{x})$ and $\Psi_e(\mathbf{x})$ denotes the atomic field operators for annihilating an atom at position \mathbf{x} in the ground state and the excited state, respectively. They obey the usual bosonic commutation relations

$$\left[\Psi_f(\mathbf{x}), \Psi_{f'}^\dagger(\mathbf{x}') \right] = \delta^3(\mathbf{x} - \mathbf{x}') \delta_{f,f'} \quad (6.6a)$$

$$\left[\Psi_f(\mathbf{x}), \Psi_{f'}(\mathbf{x}') \right] = \left[\Psi_f^\dagger(\mathbf{x}), \Psi_{f'}^\dagger(\mathbf{x}') \right] = 0, \quad (6.6b)$$

for $f, f' \in \{e, g\}$. The field operator remains unchanged, i.e., $H_R = -\hbar\Delta_c a^\dagger a - i\hbar\eta(a - a^\dagger)$. The two-body interaction is modeled by a short-range pseudopotential [44], characterized by the s-wave scattering length a_s , leading to a Hamiltonian

$$H_{A-A} = \frac{U}{2} \int d^3\mathbf{x} \Psi_g^\dagger(\mathbf{x}) \Psi_g^\dagger(\mathbf{x}) \Psi_g(\mathbf{x}) \Psi_g(\mathbf{x}), \quad (6.7)$$

where $U = 4\pi a_s \hbar^2/m$. The coupling of the cavity field with the atoms inside the cavity is given by

$$H_{A-R} = -i\hbar \int d^3\mathbf{x} \Psi_g^\dagger(\mathbf{x}) g(\mathbf{x}) a \Psi_e(\mathbf{x}) + \text{h.c.}, \quad (6.8)$$

whereas the interaction with the laser beam, which coherently drives the atoms, reads

$$H_{A-P} = -i\hbar\zeta \int d^3\mathbf{x} \Psi_g^\dagger(\mathbf{x}) h(\mathbf{x}) \Psi_e(\mathbf{x}) + \text{h.c.}. \quad (6.9)$$

Let us now calculate the Heisenberg equations for the various field operators, starting with the operator for the excited state, i.e.,

$$\frac{\partial \Psi_e(\mathbf{x})}{\partial t} = i \left[\frac{\hbar}{2m} \nabla^2 - \frac{V_e(\mathbf{x})}{\hbar} + \Delta_a \right] \Psi_e(\mathbf{x}) - [g(\mathbf{x}) + \zeta h(\mathbf{x})] \Psi_g(\mathbf{x}). \quad (6.10)$$

The first term corresponds to the free evolution of the atomic state, whereas the second term describes the absorption of a cavity photon or a pump photon together with the annihilation of a ground state atom. Similarly, the equation for the ground state operator reads:

$$\frac{\partial \Psi_g(\mathbf{x})}{\partial t} = i \left[\frac{\hbar}{2m} \nabla^2 - \frac{V_g(\mathbf{x})}{\hbar} - \frac{U}{\hbar} \Psi_g^\dagger(\mathbf{x}) \Psi_g(\mathbf{x}) \right] \Psi_g(\mathbf{x}) + [g(\mathbf{x}) + \zeta h(\mathbf{x})] \Psi_e(\mathbf{x}). \quad (6.11)$$

Finally, the Heisenberg equation for the cavity field operator is given by:

$$\frac{\partial a}{\partial t} = i\Delta_c a + \eta + \int d^3\mathbf{x} g(\mathbf{x}) \Psi_g^\dagger(\mathbf{x}) \Psi_e(\mathbf{x}). \quad (6.12)$$

Again, the first term corresponds to the free field evolution, whereas the last two terms are driving terms of the cavity field.

As we want to treat temperatures close to $T = 0$ we have to avoid heating and the model only makes sense for very weak atomic excitation, where there is only negligible spontaneous emission. In this limit we can adiabatically eliminate the excited states from the dynamics of our system. This requires large atom-pump detunings Δ_a , where we also can neglect the kinetic energy term and the trapping potential in (6.10) compared to Δ_a . Necessarily, we assume that the field operators $\Psi_g(\mathbf{x})$ and a vary on a much slower time scale than the $1/\Delta_a$ terms, such that we obtain:

$$\Psi_e(\mathbf{x}, t) = -\frac{i}{\Delta_a} [\zeta h(\mathbf{x}) + g(\mathbf{x})a(t)] \Psi_g(\mathbf{x}, t). \quad (6.13)$$

Inserting this expression for $\Psi_e(\mathbf{x})$ into (6.11) and (6.12) leads then to:

$$\begin{aligned} \frac{\partial \Psi_g(\mathbf{x})}{\partial t} = i \left[\frac{\hbar}{2m} \nabla^2 - \frac{V_g(\mathbf{x})}{\hbar} - \frac{\zeta^2 h^2(\mathbf{x})}{\Delta_a} - \frac{g^2(\mathbf{x})}{\Delta_a} a^\dagger a \right. \\ \left. - \frac{\zeta h(\mathbf{x}) g(\mathbf{x})}{\Delta_a} (a + a^\dagger) - \frac{U}{\hbar} \Psi_g^\dagger(\mathbf{x}) \Psi_g(\mathbf{x}) \right] \Psi_g(\mathbf{x}), \end{aligned} \quad (6.14)$$

$$\frac{\partial a}{\partial t} = i \left[\Delta_c - \frac{1}{\Delta_a} \int d^3 \mathbf{x} g^2(\mathbf{x}) \Psi_g^\dagger(\mathbf{x}) \Psi_g(\mathbf{x}) \right] a - \frac{i\zeta}{\Delta_a} \int d^3 \mathbf{x} h(\mathbf{x}) \Psi_g^\dagger(\mathbf{x}) \Psi_g(\mathbf{x}) + \eta. \quad (6.15)$$

The central trick is now to find an effective Hamiltonian H_{eff} which leads to the same dynamics as given by Eq. (6.14) and (6.15). Thus this Hamiltonian has to obey:

$$i\hbar \frac{\partial \Psi_g(\mathbf{x})}{\partial t} = [\Psi_g(\mathbf{x}), H_{\text{eff}}] \quad \text{and} \quad i\hbar \frac{\partial a}{\partial t} = [a, H_{\text{eff}}]. \quad (6.16)$$

From this we can easily read off a possible effective Hamiltonian of the form:

$$\begin{aligned} H_{\text{eff}} = \int d^3 \mathbf{x} \Psi_g^\dagger(\mathbf{x}) \left\{ -\frac{\hbar^2}{2m} \nabla^2 + V_g(\mathbf{x}) \right. \\ \left. + \frac{\hbar}{\Delta_a} \left[\zeta^2 h^2(\mathbf{x}) + g^2(\mathbf{x}) a^\dagger a + \zeta h(\mathbf{x}) g(\mathbf{x}) (a + a^\dagger) \right] \right\} \Psi_g(\mathbf{x}) \\ + \frac{U}{2} \int d^3 \mathbf{x} \Psi_g^\dagger(\mathbf{x}) \Psi_g^\dagger(\mathbf{x}) \Psi_g(\mathbf{x}) \Psi_g(\mathbf{x}) - i\hbar \eta (a - a^\dagger) - \hbar \Delta_c a^\dagger a. \end{aligned} \quad (6.17)$$

The corresponding single particle Hamiltonian, which leads to this second quantized Hamiltonian is [45]:

$$H_{\text{eff}}^{(1)} = \frac{\mathbf{p}^2}{2m} + V_g(\mathbf{x}) + \frac{\hbar}{\Delta_a} \left[\zeta^2 h^2(\mathbf{x}) + g^2(\mathbf{x}) a^\dagger a + \zeta h(\mathbf{x}) g(\mathbf{x}) (a + a^\dagger) \right] - i\hbar \eta (a - a^\dagger) - \hbar \Delta_c a^\dagger a. \quad (6.18)$$

This simplified effective atom-field Hamiltonian will be the basis of our further considerations. It is, however, still much too complex for a general solution and we will have to make further simplifying assumptions. Hence at this point we will restrict ourselves to 1D motion along the cavity axis. In an experimental setup this could be actually realized by a deep radial trapping potential, but we think that at least qualitatively the model should also capture the essential physics if some transverse motion of the particles was allowed. As

one consequence this assumption requires a rescaling of the effective two-body interaction strength [46], which enters as an open parameter in our model anyway.

Mathematically we thus end up with a one-dimensional optical lattice, which is partly generated by the resonator field and superimposed onto a prescribed extra trapping potential $V_g(\mathbf{x}) = V_g(x)$. The mode function of the cavity along the axis is approximated by $g(\mathbf{x}) = g(x) = g_0 \cos(kx)$ and the transverse laser beam forms a broad standing wave $h(\mathbf{x}) = h_0 \cos(k_y y)$, which in our one-dimensional considerations ($y = 0$) is just a constant term that we can eventually omit in (6.17).

As we consider external pumping of atoms and mode, we essentially treat an open system and we have to deal with dissipation as well. Such dissipation processes are modeled by Liouvillian terms \mathcal{L} appearing in the master equation for the atom-field density operator, i.e.,

$$\dot{\varrho} = \frac{1}{i\hbar}[H_{\text{eff}}, \varrho] + \mathcal{L}\varrho. \quad (6.19)$$

As mentioned above, we assume large atom-pump detuning Δ_a , suppressing spontaneous emission to a large extent. However, we still have to deal with the cavity loss κ , which will thus be the dominant dissipation process. Hence the corresponding Liouvillian using a standard quantum optics approach [49] reads:

$$\mathcal{L}\varrho = \kappa \left(2a\varrho a^\dagger - a^\dagger a\varrho - \varrho a^\dagger a \right). \quad (6.20)$$

Equivalently in the corresponding Heisenberg equation for the field operator, cavity loss leads to damping terms and fluctuations, so that it then reads:

$$\begin{aligned} \dot{a} = & \left\{ i \left[\Delta_c - \frac{g_0^2}{\Delta_a} \int dx \Psi_g^\dagger(x) \cos^2(kx) \Psi_g(x) \right] - \kappa \right\} a \\ & - i \frac{\zeta g_0 \hbar_0}{\Delta_a} \int dx \Psi_g^\dagger(x) \cos(kx) \Psi_g(x) + \eta + \Gamma_{in}. \end{aligned} \quad (6.21)$$

Since we will be mainly interested in normally ordered quantities and assume vacuum ($T=0$) outside the cavity, the input noise operators Γ_{in} will not enter in the dynamics, such that we will omit them later.

Let us proceed and transform the Hamiltonian in a more commonly known form. Following standard procedures, one constructs maximally localized eigenfunctions at each site and expands the atomic field operator $\Psi_g(x)$ in terms of single atom Wannier functions [48]

$$\Psi_g(x) = \sum_n \sum_k b_{n,k} w_n(x - x_k), \quad (6.22)$$

where $b_{n,k}$ corresponds to the annihilation of a particle in the n -th energy band at site k . Since we assume the involved energies to be much smaller than the excitation energies to the second band, we are able to keep only the lowest vibrational state in the Wannier expansion, i.e., $\Psi_g(x) = \sum_k b_k w(x - x_k)$, where $w(x) = w_0(x)$. This yields to the following Hamiltonian:

$$\begin{aligned} H = & \sum_{k,l} E_{kl} b_k^\dagger b_l + \left(\hbar U_0 a^\dagger a + V_{\text{cl}} \right) \sum_{k,l} J_{kl} b_k^\dagger b_l + \hbar \eta_{\text{eff}} \left(a + a^\dagger \right) \sum_{k,l} \tilde{J}_{kl} b_k^\dagger b_l - i \hbar \eta \left(a - a^\dagger \right) \\ & + \frac{1}{2} \sum_{i,j,k,l} U_{ijkl} b_i^\dagger b_j^\dagger b_k b_l - \hbar \Delta_c a^\dagger a, \end{aligned} \quad (6.23)$$

where the addendum eff of the Hamiltonian is omitted. Here we introduced an important characteristic parameter of atomic cavity QED, namely the refractive index U_0 of a single atom at an antinode, which is given by $U_0 = g_0^2/\Delta_a$. It gives the frequency shift of the cavity mode induced by a single atom at an antinode and also corresponds to the optical lattice depth for an atom per cavity photon [17]. Similarly, the parameter $\eta_{\text{eff}} = g_0 h_0 \zeta / \Delta_a$ describes the position dependent effective pump strength of the cavity mode induced by the scattered light from a single atom at an antinode.

Note that in contrast to a free space lattice the Wannier state expansion, Eq. 6.22 is a rather formal procedure here, as the potential depth and thus the Wannier functions depend on the cavity field and thus in principle are dynamic quantities, which have to be determined consistently. This is of course consequently also true for the various coupling parameters in the Hamiltonian. The above model thus can only be valid as long as the single band approximation stays valid during the system dynamics. In particular in the case, where the atoms are trapped solely by the cavity field [21, 22] this is not valid for very low photon numbers.

In principle this problem can be circumvented by adding an additional external trapping potential $V_g(x)$ to the model, which guarantees a minimum potential depth even in the case of zero cavity photons. Practically this is feasible, for instance, with a far detuned, off-resonant dipole trap (FORT) [50], i.e., $V_g(x) = V_{\text{cl}} \cos^2(k_F x)$, where k_F denotes the wave number of the FORT field. In the experimental realization, the frequency of the corresponding laser field ω_F is only very few free spectral ranges separated from the main cavity frequency ω_c [27, 51, 52]. Hence, in the vicinity of the cavity center, the coincidence of the FORT field and the cavity field is very good, and we can replace in good agreement $\cos^2(k_F x)$ with $\cos^2(kx)$.

Let us remark here that by including this extra potential we have saved our model and allowed for further analytical analysis of the dynamics, but we also have thrown out a great deal of interesting physics already. Actually, for very few atoms one still can solve the full Hamiltonian without the restriction to the lowest bands by quantum Monte Carlo wave-function simulations. Some early results of such simulations can be found in Ref. [55, 56]. However, this is not the subject of this work and we will proceed here with the effective lattice model under the assumption of a deep enough extra potential or strong enough cavity fields.

Note that in (6.23), in contrast to the case of the Bose-Hubbard model in a classical optical lattice, where the matrix elements of the potential and kinetic energy can be merged, here two separate parts exist due to the presence of the cavity field operators in the Hamiltonian. Explicitly they read as:

$$E_{kl} = \int dx w(x - x_k) \left(-\frac{\hbar^2}{2m} \nabla^2 \right) w(x - x_l), \quad (6.24a)$$

$$J_{kl} = \int dx w(x - x_k) \cos^2(kx) w(x - x_l), \quad (6.24b)$$

$$\tilde{J}_{kl} = \int dx w(x - x_k) \cos(kx) w(x - x_l). \quad (6.24c)$$

The on-site elements J_{kk} and E_{kk} are independent of the lattice site k , whereas \tilde{J}_{kl} changes sign periodically, i.e., $\tilde{J}_{kk} = -\tilde{J}_{k+1,k+1}$ due to the cos, which has twice the periodicity of

the lattice. This also accounts for $\tilde{J}_{k,k+1} = 0$. Note that the existence of this term implies that two adjacent wells acquire different depths forcing us to reassure that for the case of the directly pumped atom $\eta_{\text{eff}}(a + a^\dagger) \cos(kx)$ is only a small perturbation of the lattice. As the next-nearest elements are typically two orders of magnitude smaller than the nearest-neighbor term [3] they can safely be neglected (tight-binding approximation). Furthermore, in the case of the nonlinear interaction matrix elements,

$$U_{ijkl} = g_{1D} \int dx w(x - x_i) w(x - x_j) w(x - x_k) w(x - x_l) \quad (6.25)$$

we can omit the off-site terms since they are also typically two orders of magnitude smaller than the on-site interaction matrix elements. Note that g_{1D} is the one-dimensional on-site interaction strength, originating from an adjustment of the scattering length a_s , due to the transversal trapping [46]. As a central result of our studies we therefore obtain a generalized Bose-Hubbard Hamiltonian:

$$\begin{aligned} H = & E_0 \hat{N} + E \hat{B} + \left(\hbar U_0 a^\dagger a + V_{\text{cl}} \right) \left(J_0 \hat{N} + J \hat{B} \right) + \hbar \eta_{\text{eff}} (a + a^\dagger) \tilde{J}_0 \sum_k (-1)^{k+1} \hat{n}_k \\ & - \hbar \Delta_c a^\dagger a - i \hbar \eta (a - a^\dagger) + \frac{U}{2} \sum_k \hat{n}_k (\hat{n}_k - 1), \end{aligned} \quad (6.26)$$

where the nonlinear on-site interaction is characterized by $U = \frac{4\pi a_s \hbar^2}{m} \int dx |w(x)|^4$. In addition, we introduced the number operator $\hat{N} = \sum_k \hat{n}_k = \sum_k b_k^\dagger b_k$ and the jump operator $\hat{B} = \sum_k (b_{k+1}^\dagger b_k + h.c.)$. The site-independent on-site matrix elements are labeled E_0, J_0 and \tilde{J}_0 , whereas E and J are the site-to-site hopping elements. Note that for strong classical intracavity fields and no transverse pump we recover the standard Bose-Hubbard Hamiltonian.

Finally, let us remark that we now can also rewrite the field Heisenberg Eq. (6.21) in the above terms, which gives:

$$\dot{a} = \left\{ i \left[\Delta_c - U_0 \left(J_0 \hat{N} + J \hat{B} \right) \right] - \kappa \right\} a + \eta - i \eta_{\text{eff}} \tilde{J}_0 \sum_k (-1)^{k+1} \hat{n}_k. \quad (6.27)$$

Here we clearly see that besides the number operator \hat{N} for the atoms also the coherence properties via the operator \hat{B} and statistics via \hat{n}_k plays a decisive role in the field dynamics. As this field acts back on the atomic motion, interesting and complex coupled dynamics can be expected from this model, which was partly already discussed in [32, 33] and will be elucidated more in the remainder of this work.

6.3 Cavity pump

Let us now turn to the conceptually simplest case and restrict the pumping only to the cavity, where a only single mode is coherently excited (*cavity pumping*). This mode will generate an optical potential in addition to the prescribed external potential. For large enough photon numbers the external potential can be even omitted and the particles are trapped solely by

the cavity field. As essential ingredient in the dynamics, the identical coupling of all atoms to this same field mode induces a long-range interaction between the atoms independent of their positions. Setting $\eta_{\text{eff}} = 0$, the Hamiltonian (6.26) is reduced to:

$$H = E_0 \hat{N} + E \hat{B} + \left(\hbar U_0 a^\dagger a + V_{\text{cl}} \right) \left(J_0 \hat{N} + J \hat{B} \right) - \hbar \Delta_c a^\dagger a - i \hbar \eta \left(a - a^\dagger \right) + \frac{U}{2} \hat{C}. \quad (6.28)$$

Here we introduced $\hat{C} = \sum_k \hat{n}_k (\hat{n}_k - 1)$ for the operator of the two-body on-site interaction. Still we see that the corresponding Heisenberg equation for the cavity field:

$$\dot{a} = \left\{ i \left[\Delta_c - U_0 \left(J_0 \hat{N} + J \hat{B} \right) \right] - \kappa \right\} a + \eta. \quad (6.29)$$

depends on photon number and coherence. For very weak fields this yields an atom statistics dependent cavity transmission spectrum, which was studied in some detail in Ref. [35]. Here we go one step further and study the dynamical back action of the field onto atomic motion and field mediated atom-atom interaction, which appear at higher photon number. As the model is still rather complex we need some further approximations at this point in order to catch some qualitative insight.

6.3.1 Field-eliminated Hamiltonian

Although the influence of the cavity field on the atoms is equal on all particles, their common interaction generates a dynamics much more complex than for a Bose-Hubbard model with prescribed external potential. This is more analogous to real solid state physics where the state of the electrons also acts back on the potentials. To exhibit the underlying physics, we will now derive an approximate Hamiltonian, which solely depends on particle variables by adiabatically eliminating the field (6.28). This should be valid when the damping rate κ of the cavity generates a faster time scale than the external atomic degrees of freedom. Actually as tunneling is mostly a very slow process (much slower than the recoil frequency), this will be almost always the case in practical experimental setups. To this end, we simply equate (6.29) to zero and obtain formally $a = \eta / \{ \kappa - i [\Delta_c - U_0 (J_0 \hat{N} + J \hat{B})] \}$. In the following we constrain ourselves to the case of a fixed number of atoms, i.e., $\hat{N} = N \mathbf{1}$. The very small tunneling matrix element J can be used as an expansion parameter, leading to:

$$a \approx \frac{\eta}{\kappa - i \Delta'_c} \left[\mathbf{1} - i \frac{U_0 J}{\kappa - i \Delta'_c} \hat{B} - \frac{(U_0 J)^2}{(\kappa - i \Delta'_c)^2} \hat{B}^2 \right], \quad (6.30)$$

where we introduced a shifted detuning $\Delta'_c = \Delta_c - U_0 N$.

In order to obtain an effective Hamiltonian, where the cavity degrees of freedom are eliminated, we replace the field terms in (6.28), by the steady state expressions (6.30), as well as in the Liouville super operator (6.20). Note, that this is more appropriate than the naive approach of a replacement just in the Hamiltonian, as has been done in our former work [32]. If we consider terms up to order $\propto J^2$, the exchange in the Hamiltonian yields:

$$H_{\text{ad}} = (E + J V_{\text{cl}}) \hat{B} + \frac{U}{2} \hat{C} + \frac{\hbar U_0 J \eta^2}{\kappa^2 + \Delta'^2_c} \left(\frac{\Delta'^2_c - \kappa^2}{\kappa^2 + \Delta'^2_c} \hat{B} - \frac{3 U_0 J \Delta'_c}{\kappa^2 + \Delta'^2_c} \hat{B}^2 \right). \quad (6.31)$$

Next, we apply the same procedure to the Liouville equation - again up to terms $\propto J^2$ - we obtain an adiabatic Liouville operator:

$$\mathcal{L}_{\text{ad}}\varrho = -i\frac{2U_0J\kappa^2\eta^2}{(\kappa^2 + \Delta'_c)^2} \left[\hat{B} + \frac{2\Delta'_cU_0J}{\kappa^2 + \Delta'^2_c} \hat{B}^2, \varrho \right] + \frac{\kappa U_0^2 J^2 \eta^2}{(\kappa^2 + \Delta'_c)^2} \left(2\hat{B}\varrho\hat{B} - \hat{B}^2\varrho - \varrho\hat{B}^2 \right). \quad (6.32)$$

The Lindblad terms in the second line are real, corresponding to dissipation, whereas the first, imaginary term corresponds to a unitary time evolution and has therefore to be added to the adiabatic Hamiltonian, i.e.,

$$H_{\text{ad}} \rightarrow H_{\text{ad}} + \frac{2\hbar U_0 J \kappa^2 \eta^2}{(\kappa^2 + \Delta'^2_c)^2} \left(\hat{B} + \frac{2\Delta'_c U_0 J}{\kappa^2 + \Delta'^2_c} \hat{B}^2 \right).$$

Altogether, we end up with a Hamiltonian, where the cavity field has been eliminated:

$$H_{\text{ad}} = (E + JV_{\text{cl}})\hat{B} + \frac{U}{2}\hat{C} + \frac{\hbar U_0 J \eta^2}{\kappa^2 + \Delta'_c} \left(\hat{B} + \frac{U_0 J \Delta'_c}{\kappa^2 + \Delta'^2_c} \frac{\kappa^2 - 3\Delta'^2_c}{\kappa^2 + \Delta'^2_c} \hat{B}^2 \right). \quad (6.33)$$

The loss rate of the cavity is described by the remaining dissipative part of (6.32):

$$\mathcal{L}_{\text{ad}}\varrho = \frac{\kappa U_0^2 J^2 \eta^2}{(\kappa^2 + \Delta'_c)^2} \left(2\hat{B}\varrho\hat{B} - \hat{B}^2\varrho - \varrho\hat{B}^2 \right). \quad (6.34)$$

Note, that the above adiabatic elimination procedure is not completely unambiguous due to ordering freedom. Nevertheless it should give a qualitatively correct first insight. An alternative way of deriving an effective Hamiltonian, depending solely on particle observable is similar to (6.16) and (6.17). This amounts to a replacement of the field variables with (6.30) in the Heisenberg equation for the external atomic degrees of freedom, which read as follows:

$$\dot{b}_k = \frac{1}{i\hbar} \left[\left(E + JV_{\text{cl}} + \hbar U_0 J a^\dagger a \right) (b_{k-1} + b_{k+1}) - U \hat{n}_k b_k \right]. \quad (6.35)$$

A naive replacement of the field operator a and its adjoint a^\dagger by (6.30) in the above expression leads to an equation for \dot{b}_k , which cannot be generated from an effective adiabatic Hamiltonian in the form $\dot{b}_k = -i/\hbar [b_k, H_{\text{ad}}]$. Hence, before substituting the adiabatic field operators, we have to symmetrize the expression containing the field term in (6.35) in the form

$$\dot{b}_k = -\frac{i}{\hbar} \left[(E + JV_{\text{cl}}) (b_{k-1} + b_{k+1}) - U \hat{n}_k b_k \right] - \frac{i\hbar U_0 J}{2} \left[a^\dagger a (b_{k-1} + b_{k+1}) + (b_{k-1} + b_{k+1}) a^\dagger a \right]. \quad (6.36)$$

This form enables us to describe the dynamics of b_k by a Heisenberg equation with an effective Hamiltonian, which up to second order in J reads:

$$H_{\text{ad}} = (E + JV_{\text{cl}})\hat{B} + \frac{U}{2}\hat{C} + \frac{\hbar U_0 J \eta^2}{\kappa^2 + \Delta'_c} \left(\hat{B} + \frac{U_0 J \Delta'_c}{\kappa^2 + \Delta'^2_c} \hat{B}^2 \right). \quad (6.37)$$

The terms in the second line stem from the field terms in (6.36). Although this Hamiltonian looks a bit different from the first version derived before (6.33), their properties are - within

their regime of validity - in very good agreement as long as hopping is slow compared to damping.

To exhibit the physical content of this Hamiltonian one can look at its eigenstates. As first step we calculate the Mott insulator state [see Eq. (6.49)] fraction of the lowest energy state $|\psi\rangle$ of these two Hamiltonians, i.e., $p_{\text{MI}} = |\langle\psi|\text{MI}\rangle|^2$ (see also Fig. 6.4), as a function of the on-site interaction energy for different values of Δ'_c . This will indicate changes of position and behavior of the Mott insulator superfluid transition. as shown in Fig. 6.4. To compare the two approximate Hamiltonians in Fig. 6.2, we plot the difference of the Mott insulator fraction of the ground state of (6.33) and (6.37), as well as the difference of the steady state photon number. Obviously the two Hamiltonians, converge in the limit of large cavity decay κ . This can also be seen in Fig. 6.2, where the dashed-dotted line depicts the case of a smaller Δ'_c (which is equivalent to an enlarged κ), showing a strongly enhanced coincidence.

6.3.2 Field-eliminated density operator

Let us now use a further and somehow more systematic alternative approach to eliminate the cavity field dynamics from the system evolution directly from the Liouville equation by following a method proposed by Wiseman and Milburn [53], which is valid for large κ and low photon numbers. In this case we have

$$\left| \frac{\langle H_{at} \rangle}{\kappa} \right| \sim \left| \frac{\hbar U_0 \langle a^\dagger a \rangle}{\kappa} \right| = \varepsilon \ll 1, \quad (6.38)$$

where H_{at} is the atomic part of (6.28), i.e., $H_{at} = (E + V_{cl}J) \hat{B} + U\hat{C}/2$. Again the total atom number \hat{N} is supposed to be constant. This allows to expand the density operator in powers of ε , corresponding to states with increasing photon number:

$$\varrho = \varrho_0 \otimes |0\rangle_a \langle 0| + (\varrho_1 \otimes |1\rangle_a \langle 0| + h.c.) + \varrho_2 \otimes |1\rangle_a \langle 1| + (\varrho'_2 \otimes |2\rangle_a \langle 0| + h.c.) + O(\varepsilon^3). \quad (6.39)$$

Here ϱ_i are density operators for the particle variables, corresponding to the order i of magnitude in the expansion parameter ε . We substitute this expression into the Liouville equation (6.19) with the Hamiltonian from (6.28), which leads to the following set of equations:

$$\dot{\varrho}_0 = \frac{1}{i\hbar} [H_{at}, \varrho_0] - \eta (\varrho_1 + \varrho_1^\dagger) + 2\kappa \varrho_2 \quad (6.40a)$$

$$\begin{aligned} \dot{\varrho}_1 &= \frac{1}{i\hbar} [H_{at}, \varrho_1] - \eta (\sqrt{2}\varrho'_2 + \varrho_2 - \varrho_0) - \kappa \varrho_1 \\ &+ i \left[\Delta_c - U_0 (J_0 N + J\hat{B}) \right] \varrho_1 + \kappa O(\varepsilon^4) \end{aligned} \quad (6.40b)$$

$$\dot{\varrho}_2 = \frac{1}{i\hbar} [H_{at}, \varrho_2] + \eta (\varrho_1 + \varrho_1^\dagger) - 2\kappa \varrho_2 - iU_0 [J_0 N + J\hat{B}, \varrho_2] + \kappa O(\varepsilon^4) \quad (6.40c)$$

$$\dot{\varrho}'_2 = \frac{1}{i\hbar} [H_{at}, \varrho'_2] + \sqrt{2}\eta \varrho_1 - 2\kappa \varrho'_2 + 2i \left[\Delta_c - U_0 (J_0 N + J\hat{B}) \right] \varrho'_2 + \kappa O(\varepsilon^4) \quad (6.40d)$$

Now we adiabatically eliminate the off-diagonal elements ϱ_1 and ϱ'_2 . Setting their derivations in (6.40b) and (6.40d) to zero and neglecting terms with respect to the assumption (6.38), we obtain:

$$\varrho'_2 = \frac{\eta}{\sqrt{2}A} \varrho_1 + O(\varepsilon^3). \quad (6.41)$$

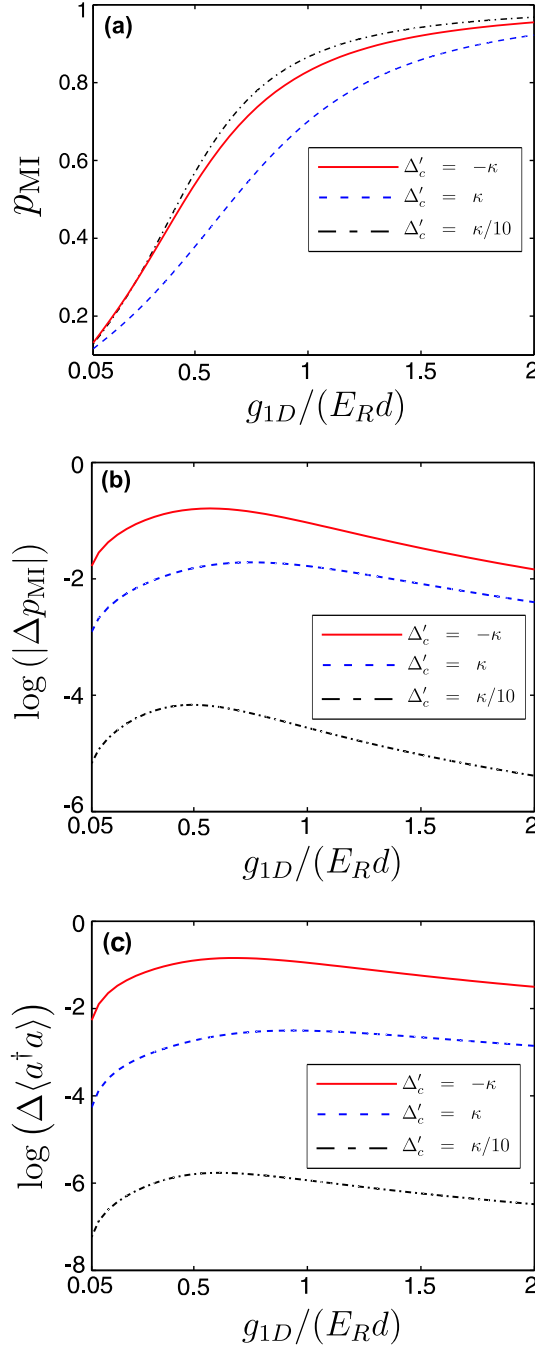


Figure 6.2. (color online) (a) Contribution of the Mott-insulator state to the ground state $p_{\text{MI}} = |\langle \psi | \text{MI} \rangle|^2$ of (6.37) as function of the 1D on-site interaction strength in units of $E_R d$ (d is the lattice constant) (b) Logarithmic difference of p_{MI} , calculated with the groundstate of (6.37) and (6.33). (c) Logarithmic difference of the adiabatically eliminated photon number $\langle \psi | a^\dagger a | \psi \rangle$ with a from (6.30) for the two different ground states. The parameters are $\kappa = 1/\sqrt{2}\omega_R$, $\eta = 2.35\omega_R$ and $\Delta'_c = -\kappa$ (red, solid line), $\kappa = 4\omega_R$, $\eta = 12.5\omega_R$ and $\Delta'_c = \kappa$ (blue, dashed line) and $\kappa = 4\omega_R$, $\eta = 10\omega_R$ and $\Delta'_c = -\kappa/10$ (black, dashed-dotted line). In any of the curves, we set $V_{\text{cl}} = 0$ and $U_0 = -\omega_R$. Here ω_R is the frequency corresponding to the recoil energy, i.e., $E_R = \hbar^2 k^2 / (2m) = \hbar \omega_R$.

This is consistent with the assumption $\varrho'_2 \sim O(\varepsilon^2)$. Here we defined $A = \kappa - i\Delta'_c + iU_0J\hat{B}$. Putting (6.41) into (6.40b) and neglecting the terms consistent with the order of the expansion, such that $\varrho_1 \sim O(\varepsilon)$, it follows that:

$$\varrho_1 = \frac{\eta}{A + \eta^2/A} (\varrho_0 - \varrho_2) + O(\varepsilon^4). \quad (6.42)$$

We simplify this expression, $\varrho_1 \approx \eta A^{-1}(\varrho_0 - \varrho_2)$, which is consistent with the above expansion and substitute it into (6.40a) and (6.40c):

$$\dot{\varrho}_0 = \frac{1}{i\hbar} [H_{at}, \varrho_0] + 2\kappa\varrho_2 - \eta^2 \left[A^{-1}(\varrho_0 - \varrho_2) + (\varrho_0 - \varrho_2) A^{\dagger-1} \right] \quad (6.43a)$$

$$\begin{aligned} \dot{\varrho}_2 &= \frac{1}{i\hbar} [H_{at}, \varrho_2] - iU_0 [J_0N + J\hat{B}, \varrho_2] - 2\kappa\varrho_2 \\ &+ \eta^2 \left[A^{-1}(\varrho_0 - \varrho_2) + (\varrho_0 - \varrho_2) A^{\dagger-1} \right]. \end{aligned} \quad (6.43b)$$

In order to formulate a master equation for the particle variables we have to use the reduced density operator, where we trace over the field variables, i.e., $\varrho_{at} = \text{tr}(\varrho) = \varrho_0 + \varrho_2 + O(\varepsilon^4)$. With (6.43a) and (6.43b) we see that:

$$\dot{\varrho}_{at} = \frac{1}{i\hbar} [H_{at}, \varrho_{at}] - iU_0 [J_0N + J\hat{B}, \varrho_2]. \quad (6.44)$$

As a further approximation, which is also consistent with the expansion order of the assumption (6.38), we set (6.43b) to zero and neglect $[H_{at}, \varrho_2]$ and all other terms smaller than $O(\varepsilon^3)$. Then we can express ϱ_2 through ϱ_0 :

$$\varrho_2 = \frac{\eta^2}{2\kappa} \left[A^{-1}\varrho_0 + \varrho_0 A^{\dagger-1} \right]. \quad (6.45)$$

Within this order of magnitude of ε we can replace ϱ_0 with ϱ_{at} , leading us finally to the following master equation for the reduced density operator of the particle variables:

$$\dot{\varrho}_{at} = \frac{1}{i\hbar} [H_{at}, \varrho_{at}] - i\frac{U_0\eta^2}{2\kappa} \left[J_0N + J\hat{B}, \left(A^{-1}\varrho_{at} + \varrho_{at} A^{\dagger-1} \right) \right]. \quad (6.46)$$

Note that this model also contains a damping part, since the operator A is not hermitian. Let us investigate this damping, by expanding the inverse of A up to first order in J , which is consistent with the order of magnitude in (6.46). Hence we replace A^{-1} and its adjoint in this equation by

$$A^{-1} \approx \frac{1}{\kappa - i\Delta'_c} \left(1 - i\frac{U_0J}{\kappa - i\Delta'_c} \hat{B} \right) \quad (6.47)$$

and its adjoint. Since we are restricted on a subspace of constant atom number, the Liouville equation reads as follows:

$$\dot{\varrho}_{at} = \frac{1}{i\hbar} \left[H_{at} + \frac{\hbar U_0\eta^2}{\kappa^2 + \Delta'^2_c} \left(J\hat{B} + \frac{U_0\Delta'_c J^2}{\kappa^2 + \Delta'^2_c} \hat{B}^2 \right), \varrho_{at} \right] - \frac{(JU_0\eta)^2}{2\kappa} \frac{\kappa^2 - \Delta'^2_c}{(\kappa^2 + \Delta'^2_c)^2} \left[\hat{B}, \left[\hat{B}, \varrho_{at} \right] \right]. \quad (6.48)$$

Obviously, the non-dissipative part of this equation agrees perfect with our adiabatically eliminated Hamiltonian (6.37) and the structure of the dissipative part is of the same Lindblad form as (6.34). Note that an expansion of A^{-1} to higher order in J would also provide us the correct next-order term of (6.37) plus an extra term in the Liouville-equation, which does not correspond to unitary time evolution, as described by a Hamiltonian. This confirms the usefulness of the naive elimination method, also used in Ref. [32]

6.3.3 Quantum phase transitions in an optical lattice

In section 6.3.1 we derived two approximate Hamiltonians (6.33) and (6.37) describing our system of cold atoms in an optical lattice. To a large extent they still implement the well known BH model, but with parameters controllable via cavity detuning and some additional nonlocal interaction terms. Let us now investigate their properties in some more detail. One of the key features of optical cavities is the feedback mechanism between atoms and cavity field. Hence, computations are a subtle issue, since the matrix elements in the BH Hamiltonian depend on the field amplitude, which itself depends on the atomic positions. In principle a rigorous treatment would consist of calculating the matrix elements (6.24) for every photon Fock state and treating the parameters of the BH model as operators. To avoid the full complexity of such an approach we will first assume only a weak dependence of the Wannier functions on the mean cavity photon number $\langle a^\dagger a \rangle$, which allows us to proceed analytically. For any set of operating parameters we then calculated the matrix elements in a self-consistent way replacing the photon number operator by its average in the iteration process. Explicitly this is implemented by starting from some initial guess $J_0^{(0)}, E_0^{(0)}, J^{(0)}, E^{(0)}$ in the Hamiltonian (6.37), from which we calculate the ground state $|\psi^{(0)}\rangle$. By use of this state we obtain an initial mean photon number $\langle \psi^{(0)} | a^\dagger a | \psi^{(0)} \rangle$, with the steady-state field operator (6.30). Now we can calculate the matrix elements $J_0^{(1)}, E_0^{(1)}, J^{(1)}, E^{(1)}$ again leading to a new ground state $|\psi^{(1)}\rangle$ and a new mean photon number $\langle \psi^{(1)} | a^\dagger a | \psi^{(1)} \rangle$. Proceeding iteratively, in most case the fixpoint is reached already after very few iterations and the system properties are then calculated with this self-consistent matrix elements. The convergence speed decreases near the resonance for the cavity photon number (cf. Fig. 6.3), which occurs for $\Delta_c = U_0 J_0 N - \kappa$, especially for large U_0 . Introducing some damping in the iteration procedure easily resolves this issue, though. As we mentioned already before, we restrict the model on a subspace \mathcal{H}_N

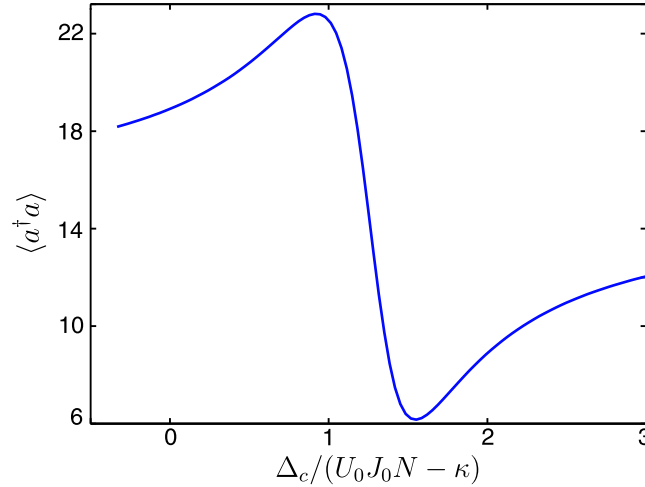


Figure 6.3. (color online). Self-consistent photon number in the case of four particles in four wells without on-site interaction. Parameters are $U_0 = -\omega_R$ and $\kappa = \omega_R$.

of a fixed total particle number N in an optical lattice of M sites. A basis of \mathcal{H}_N consists of the states $|N, 0, 0, \dots, 0\rangle, |N-1, 1, 0, \dots, 0\rangle, \dots, |0, 0, \dots, 0, N\rangle$. Since we are interested in

the quantum phase transition between the Mott insulator (MI) and the superfluid (SF) state occurring during the variation of certain external parameters, we investigate the contributions of these specific states to the ground state of the atomic system. The Mott insulator state is a product of Fock states with uniform density distribution, i.e.,

$$|\text{MI}\rangle = |n, n, \dots, n\rangle, \quad (6.49)$$

with $n = N/M$. In contrast, in a SF state each atom is delocalized over all sites. It is given by a superposition of Fock states, namely of all possible distribution of the atoms in the lattice sites, i.e.,

$$|\text{SF}\rangle = \sum_{k_1, k_2, \dots, k_M} \frac{N!}{\sqrt{M^N} \sqrt{k_1! k_2! \dots k_M!}} |k_1, k_2, \dots, k_M\rangle, \quad (6.50)$$

with $\sum_{i=1}^M k_i = N$. Although the density in the superfluid state is also uniform $\langle \hat{n}_i \rangle_{\text{SF}} = N/M$ and therefore equal to the Mott insulator state, its properties are fundamentally different. This manifests especially in the spectra and angle dependence of scattered light, providing for new, non-destructive probing schemes for the atomic phases [34, 35].

Let us now investigate the influence of the cavity on position and shape of the well-known “classical” MI-SF-transition [3–5]. To do so, we compare the two cases of a pure quantum field, i.e., $V_{cl} = 0$ in (6.37), and a classical field ($\eta = 0$) provided by V_{cl} for generating the optical potential. We choose η in such a way, that at zero on-site interaction, $g_{1D} = 0$, both potentials are equally deep. As depicted in Fig. 6.4, the influence of the cavity strongly depends on the detuning Δ_c . Two contributions arise from the quantum nature of the potential. On the one hand the potential depth and therefore the matrix elements depend on the atomic state. For a classical potential this is clearly not the case. On the other hand the cavity mediates long-range interactions via the field, which corresponds to the \hat{B}^2 -term in (6.37). If a potential depth near the phase transition point for the quantum case is associated with some certain average photon number \bar{n} , then $\bar{n} \pm 1$ are associated to different atomic phases. This means that the ground state of the quantized cavity field contains contributions of different atomic states, each of them correlated with the corresponding photon number. In this sense photon number fluctuations drive particle fluctuations. Depending on parameters the former or the latter effect contributes more. In Fig. 6.4 this is shown for four atoms in four wells, where we calculated the occupation probability for the Mott insulator $p_{\text{MI}} = |\langle \psi | \text{MI} \rangle|^2$ and the superfluid state $p_{\text{SF}} = |\langle \psi | \text{SF} \rangle|^2$ for the ground state $|\psi\rangle$ of (6.37) as a function of the dimensionless one-dimensional on-site interaction strength $g_{1D}/(dE_R)$ for a purely classical and a purely quantum case. For $\Delta_c - U_0 J_0 N = \kappa$, photon number fluctuations enhance particle fluctuations, shifting the superfluid to Mott insulator transition to higher values of the on-site interaction [Fig. 6.4(a)]. However, if we choose $\Delta_c - U_0 J_0 N = -\kappa$, the influence of the atomic state on the potential depth exceeds the cavity-mediated long-range interactions, strongly shifting the transition to lower values of g_{1D} [Fig. 6.4(b)]. Note, that for this behavior, the cavity loss rate must be - although within the bad cavity limit - small enough. For larger κ the quantum effects disappear and the ground states for classical and quantum potential coincide.

To correctly address the long-range interactions, corresponding to the \hat{B}^2 term in (6.37), we calculate the contribution of the Mott insulator state to the ground state of this adiabatic

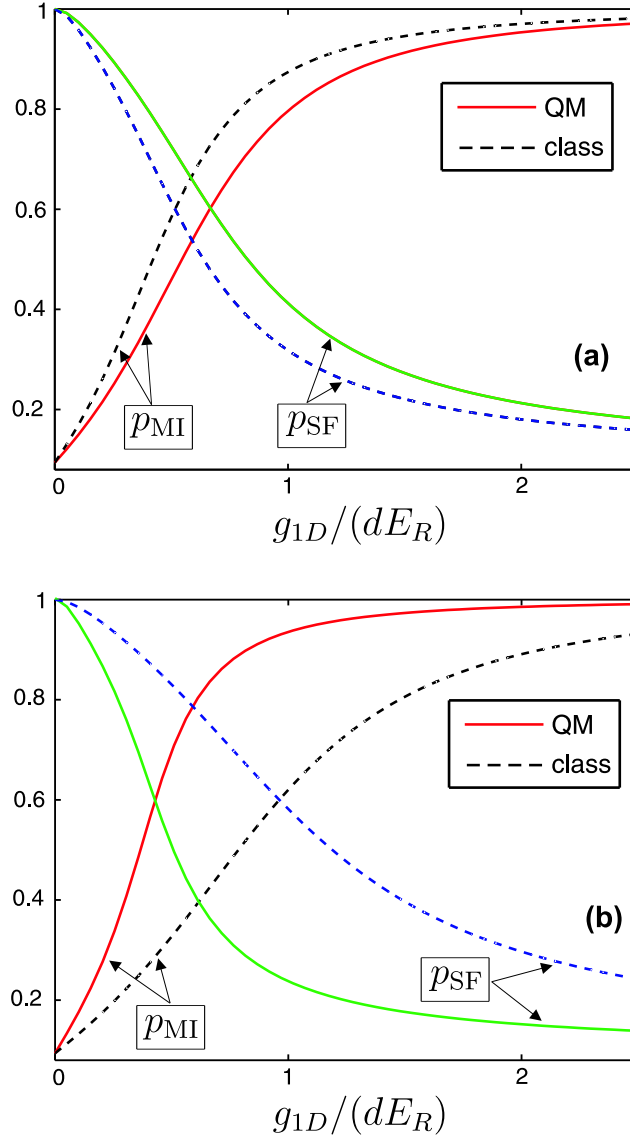


Figure 6.4. (color online) Cavity influence of the Mott insulator to superfluid transition by means of a comparison of the occupation probabilities p_{MI} and p_{SF} for a purely quantum field, i.e., $V_{cl} = 0$, and a purely classical field, i.e., $\eta = 0$, as a function of the dimensionless one-dimensional on-site interaction strength $g_{1D}/(dE_R)$. We choose η such that both potentials are of equivalent depth for zero on-site interaction ($g_{1D} = 0$). The quantum and classical case is depicted with solid and dashed lines, respectively. In (a) we set $(U_0, \kappa, \eta) = (-1, 1/\sqrt{2}, \sqrt{5.5})\omega_R$ and $\Delta_c - U_0 J_0 N = \kappa$. (b) The same as (a) but with $\Delta_c - U_0 J_0 N = -\kappa$.

Hamiltonian including and omitting the \hat{B}^2 part, respectively. Although, in the situation of Fig. 6.4(a) the net effect enhances the phase transition, the cavity mediates long-range coherence via \hat{B}^2 , which can be seen by enlarged particle number fluctuations as shown in Fig. 6.5. Although the effect is not too strong as it depends on J^2 it has infinite range and will get more important for large particle numbers.

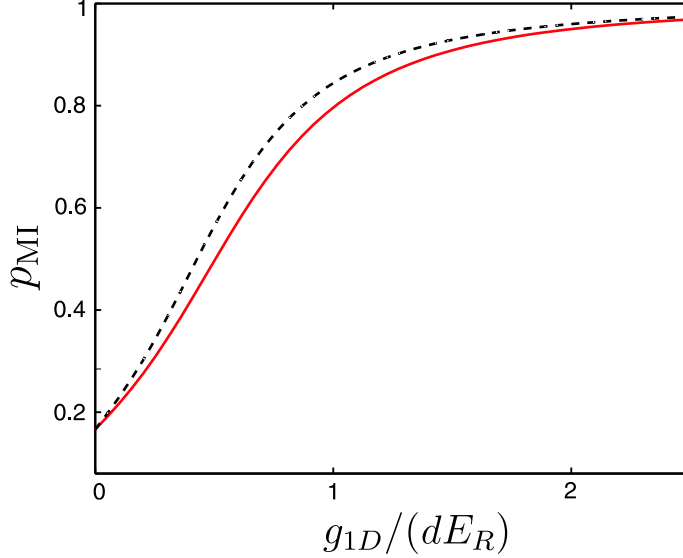


Figure 6.5. (color online) Influence of the long-range interaction on the Mott insulator to superfluid phase transition, mediated via the \hat{B}^2 term in (6.37). The solid line shows the probability for the Mott insulator state as a function of dimensionless one-dimensional on-site interaction strength $g_{1D}/(dE_R)$ for a purely quantum field, i.e., $V_{cl} = 0$. The dashed line corresponds to the probability for the same Hamiltonian, neglecting the \hat{B}^2 term. The parameters are the same as in Fig. 6.4(a).

Finally, we exhibit the transition from a cavity field with quantum properties towards a classical optical lattice. This relies on the assumption that a very bad cavity should be almost like no cavity and increasing κ , but keeping the potential depth constant, approaches the classical limit. Hence, the effects of the quantum natures and feedback of lattice potential should disappear and the ground states for classical and quantum potential coincide. The adiabatic eliminated Hamiltonian then has to approach the classical Bose-Hubbard Hamiltonian. This is shown in Fig. 6.6 for a system of four atoms in four wells, where we simultaneously increase κ and η , keeping $U_0\eta^2/\kappa^2 = -6E_R$ fixed. For every κ we calculated the value of the on-site interaction g_{1D} , where the contributions of the Mott state and the superfluid state to the ground state of (6.37) are equal, i.e., $|\langle\psi|MI\rangle| = |\langle\psi|SF\rangle|$. This is compared with the corresponding value of the interaction strength at the same intersection point of a purely classical Bose-Hubbard model with a potential depth of $V_{cl} = -6E_R$. We see that the transition occurs already at a cavity linewidth of only an order of magnitude larger than the recoil frequency, where the deviation is small already. Thus one needs quite good resonators to see the quantum shift in the phase transition.

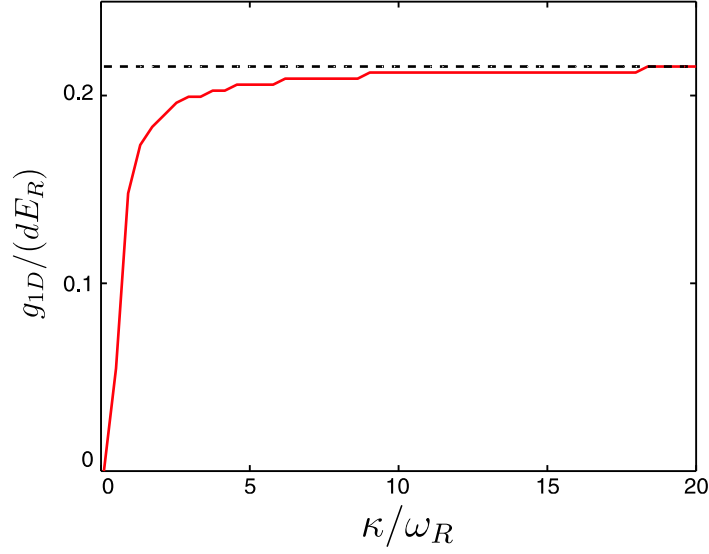


Figure 6.6. (color online) Value of the on-site interaction g_{1D} , where the contributions of the Mott state and the superfluid state to the ground state of (6.37) are equal, i.e., $|\langle\psi|\text{MI}\rangle| = |\langle\psi|\text{SF}\rangle|$, as a function of κ (solid line) for a system of four atoms in four wells. Simultaneously we increase η , such that $U_0\eta^2/\kappa^2 = -6E_R$ is fixed. Obviously, the corresponding value at the same intersection point of a purely classical Bose-Hubbard Hamiltonian with $V_{cl} = -6E_R$ is constant (dashed line). Parameters are $U_0 = -\omega_R$, $\kappa = 4\omega_R$ and $\Delta_C - U_0N = -\kappa$.

6.3.4 Comparison with the full dynamics of the master equation

Using the approximate adiabatic model with eliminated field we have found important changes in the physics so far. Even stronger effects are to be expected in the limit of less and less cavity damping and stronger atom field coupling. Let us now investigate some first signs of this and test the range of validity of the above model in this limit. To do so we have to resort to numerics and compare solutions of the full master equation (6.19) with the ground states of the adiabatically eliminated Hamiltonian (6.37). Obviously solving the full master equation is a numerically demanding task. Nevertheless, constraining to few atoms in few wells we are able to solve the equations and reveal the essential physical mechanisms. The limit of the band model description is of course reached for atoms coupled strongly to a cavity field with only very few photons and no additional classical potential V_d present. Here very strong changes in the tunneling amplitudes occur whenever a photon leaks out of the cavity and reduces the momentary potential depth. This leads to strongly enhanced particle hopping. For instance, one can think of the situations “one photon present” and “no photon present”, where the atoms can freely move within the cavity in the absence of an external trap. On the other hand one extra photon can almost block hopping. Note that in this case the ground state atomic configuration can be close to superfluid for a low photon number and close to an insulator state for a higher photon number. As our matrix elements depend only on the mean photon number $\langle a^\dagger a \rangle$, these differences cannot be taken into account in an adiabatic model.

We can explicitly show this behavior by reducing the coupling strength U_0 , but keeping the average potential depth fixed (equal matrix elements), by means of a higher average cavity photon number, which leads to strongly reduced photon number fluctuations. This is depicted in Fig. 6.7, where we show the tunneling behavior $\langle kx(t) \rangle$ of a single atom in a two well approximation. The atomic ground state of this system is the symmetric state $|\psi_0\rangle = (|l\rangle + |r\rangle)/\sqrt{2}$ having a mean position of $\langle kx \rangle_{\psi_0} = \pi/2$. Here, $|l\rangle$ ($|r\rangle$) means the left (right) of the two wells. Decreasing U_0 , increasing η and adjusting Δ_c , yields different mean photon numbers $\langle a^\dagger a \rangle$, but equal average lattice potential depth $V = U_0 \langle a^\dagger a \rangle$. (We do not consider an additional classical potential here.) If only few photons are present, we observe large fluctuations of the field and the system damps fast to the ground state. As the photon number increases, the potential approximates a classical potential as expected, where there is no dephasing. The (nearly) equal oscillation frequencies show that the matrix elements coincide for the different photon numbers. This is an interesting feature corresponding to the quantum nature of the potential. In contrast to the Bose-Hubbard model for a classical optical lattice, lattice depth and interaction strength are not the only important system parameters. Quantum fluctuations of the potential are an additional source of atomic fluctuations, playing an essential role in the evolution of the system. Obviously, if only an external potential is present and the atom is no longer coupled to the cavity field ($U_0 = 0$), the system is undamped, due to the lack of the only dissipation channel present, cavity loss. In this case the Hamiltonian (6.28) reduces to $H = (E + JV_d)\hat{B} + U/2\hat{C}$, and the atom, initially not in the symmetric state, oscillates between the left and right well. Note that a more rigorous treatment of operator-valued matrix elements - as described in the previous section - would be capable of describing this behavior correctly. Alternatively for few atoms Monte-Carlo wave function simulations of the full Hamiltonian could be performed, allowing for processes, where the particle leaves the lowest band [54].

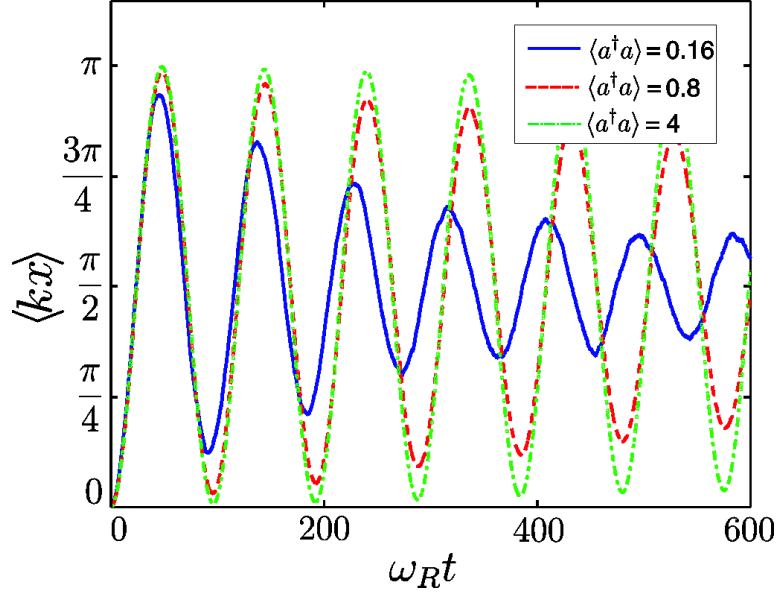


Figure 6.7. (color online) Mean position $\langle kx(t) \rangle$ of a single atom in two wells. We adjusted U_0, η, Δ_c in such a way, that the mean number of cavity photons increases, but the lattice depth stays nearly constant: $V = \hbar U_0 \langle a^\dagger a \rangle = -8E_R$. Starting with $(U_0, \eta, \kappa) = (-50, 10, 25)$ (in units of ω_R) and $\Delta_c = J_0 U_0$, followed by a successive reduction of U_0 by a factor of 5, together with an increase of η by a factor of $\sqrt{5}$ and a proper adjustment of Δ_c , this leads to mean photon numbers of 0.16 (solid line), 0.8 (dashed line), and 4 (dashed-dotted line). Initially, the atom is in the right well.

Obviously, this enhancement of atom fluctuations for low photon numbers also affects the dynamics of several atoms. We demonstrate this for the case of two atoms in two wells. We assume strong coupling with few cavity photons and a strong on-site interaction, which - in principle - inhibits tunneling and drives the system deeply into the Mott insulator regime. However, starting from a state slightly perturbed from the ground state of the adiabatically eliminated Hamiltonian (6.37), the system does not evolve towards this Mott-like ground state but towards some other, drastically different state. Increasing the photon number, while keeping the lattice depth constant, reduces the atom fluctuations and keeps the system near its adiabatic ground state. This is shown in Fig. 6.8(a), where the probability for the system being in the Mott insulator regime $p_{\text{MI}} = |\psi_{\text{MI}}(t)|^2$ is plotted. Again we observe that, the larger the intracavity photon number is, the more the potential approaches a purely classical one and the more significant the ground state probabilities of (6.37) are. Hence we see that including the photon number fluctuations strongly suppresses the Mott insulator state by allowing the particles to hop during photon number fluctuations. This is also a strong restriction for the use of our adiabatic model Hamiltonian, where only average photon numbers enter the model parameters.

Qualitatively this behavior is already indicated by the form of the dissipative part of adiabatically eliminated Liouvillian (6.34). This superoperator does not affect the superfluid state, which is the ground state in the case of zero interaction, i.e., $\mathcal{L}_{\text{ad}}\varrho = 0$ for $\varrho = |\text{SF}\rangle\langle\text{SF}|$. Other states are significantly altered, leading to a non-unitary evolution for $U \neq 0$.

Clearly, some added external classical potential diminishes this problem as it can ensure the existence of a bound state, independent of the number of cavity photons, giving an upper limit to the hopping rate. This is demonstrated in Fig. 6.8(b), where a classical potential of $V_{cl} = -5E_R$ is added. Here for $\langle a^\dagger a \rangle = 1.44$ the deviations from the adiabatic ground state are of the same order as for $V_{cl} = 0$ for $\langle a^\dagger a \rangle = 4.8$ [Fig. 6.8(a)]. Nevertheless, for not too leaky cavities (κ is in an intermediate regime), the regime of validity of the adiabatically eliminated Hamiltonian (6.37) is limited to case where either a large purely classical potential or a large photon number is given.

Finally, we investigate the other limit of validity, where a rather large external classical potential, but only a very low photon number is given, i.e., a weakly driven cavity. Here the ground state properties of our model resemble to a very high degree those of the ordinary Bose-Hubbard model. As mentioned above, an atomic ensemble interacting with a purely classical potential, has no channels of dissipation in the absence of spontaneous emission. So unless we prepare the system in its groundstate, it will show undamped oscillation. In strong contrast the coupling of the atoms to an even small intracavity field with a very low photon number opens a dissipation channel. Although the enhancement of atom number fluctuations due to fluctuation induced tunneling is small, this damping still can drive the system into a steady state, very closely to the adiabatic ground state of (6.37). This is shown in Fig. 6.9 for the case of two atoms in two wells. Here we prepare, for different values of on-site interaction, the atoms in a state perturbed from the ground state of (6.37) with initially no photon in the cavity and a given value of the classical potential $V_{cl} = -10E_R$. For $g_{1D} = 0$, the ground state is the superfluid state, so Fig. 6.9(a) is the generalization of Fig. 6.7 to two atoms. Although the photon number is only $\langle a^\dagger a \rangle = 1.3 \times 10^{-4}$, the system is driven into its ground state. For increasing interaction strength, the Mott insulator state becomes more and more favored. Still, the interaction with the tiny intracavity field enables damping of the atomic

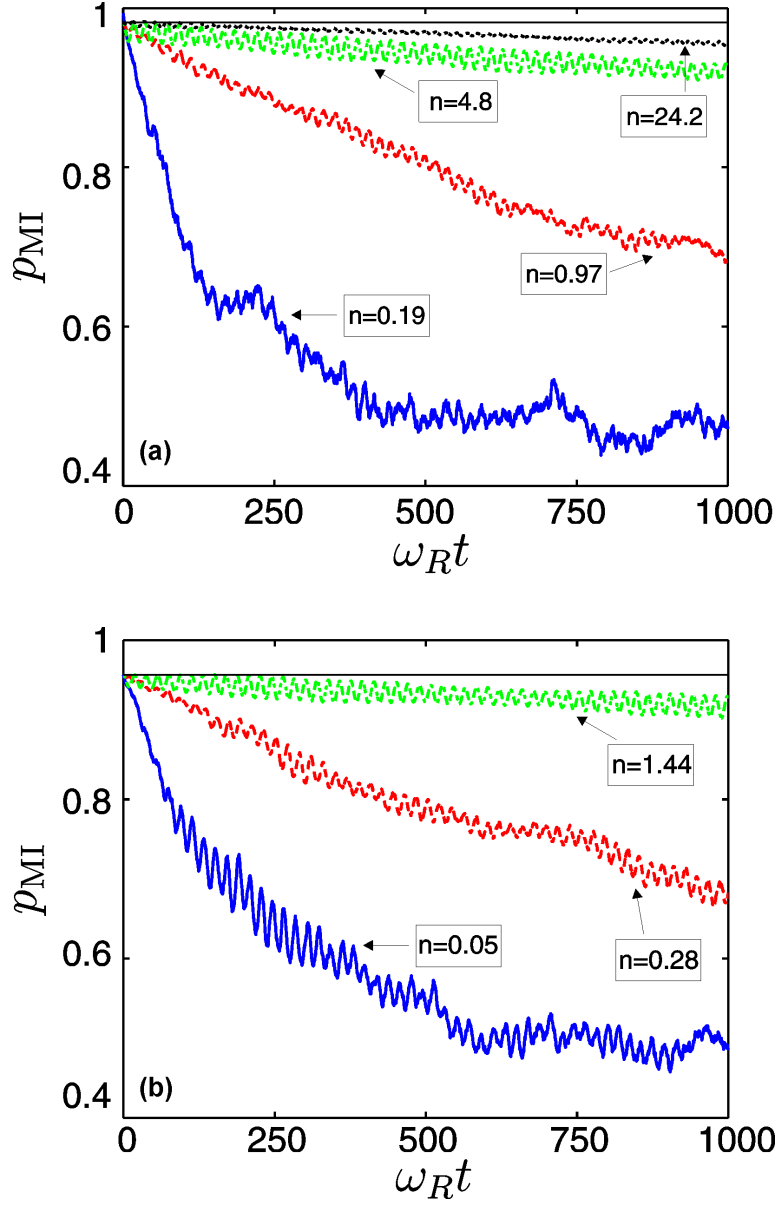


Figure 6.8. (color online) Probability of the Mott insulator state $|\psi_{\text{MI}}(t)|^2$ for two atoms in two wells. Parameters and procedure as in Fig. 6.7, but due to the second atom the photon numbers are increased. The on-site interaction is $U = 0.32E_R$. (a) $V_{cl} = 0$. The curves correspond to a mean photon number of 0.19 (solid line), 0.97 (dashed line), 4.8 (dashed-dotted line) and 24.2 (dotted line). (b) $V_{cl} = -5E_R$ and corresponding photon numbers of 0.05 (solid line), 0.28 (dashed line), 1.44 (dashed-dotted line).

evolution towards a steady state, very close to the adiabatic ground state.

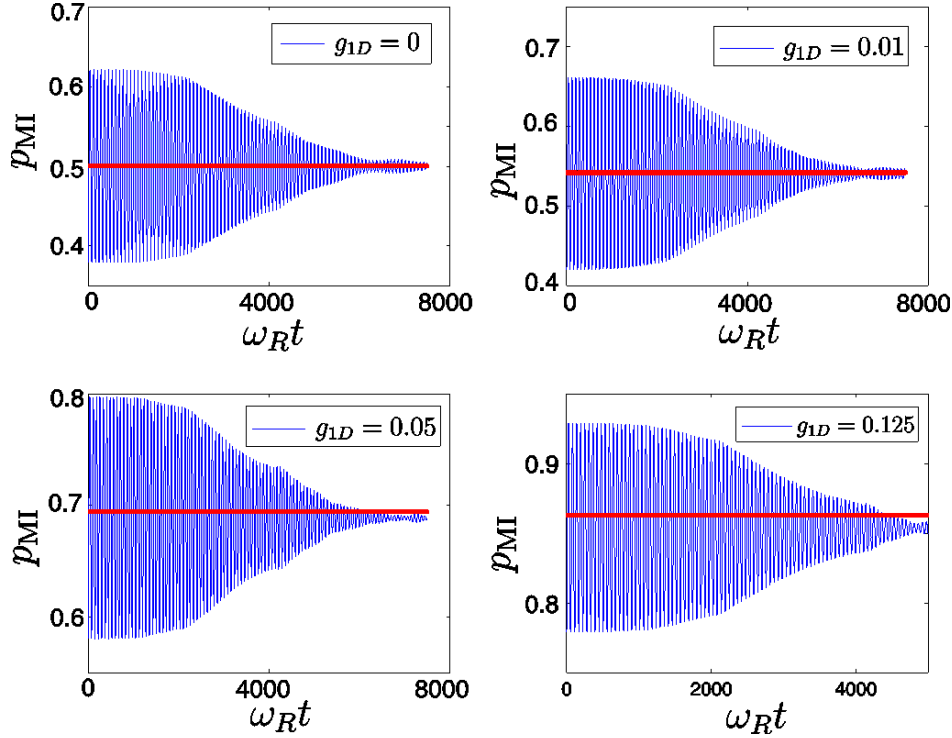


Figure 6.9. (color online) Probability of the Mott insulator state $|\psi_{\text{MI}}(t)|^2$ for two atoms in two wells for different on-site interaction. In (a) there is no interaction, i.e., $U = 0$, in (b) $U = 0.0065E_R$, in (c) $U = 0.0324E_R$ and in (d) $U = 0.081E_R$. Other parameters are $(U_0, \kappa, \eta, \Delta_c) = (-50, 25, 1, 0)$ (in units of ω_R), the classical potential is $V_{cl} = -10E_R$. The solid line in each subplot shows the corresponding ground state probability of (6.37) and the number of cavity photons is $\langle a^\dagger a \rangle = 1.3 \times 10^{-4}$.

This leads to the conclusion, that, although the cavity field may not lead to significant modifications of the ground state of the system, the cavity is a useful tool for faster preparing a system of atoms in its ground state by opening a dissipation channel, so that it decays towards an eigenstate of the adiabatically eliminated Hamiltonian (6.37).

6.4 Atom pumping

Let us now return to our starting Hamiltonian (6.26) and consider a second generic model, where the pump laser is not injected through the cavity mirrors, but directly illuminating the atoms. This rather small change has a drastic influence on the physical behavior of this system. In the case of cavity pumping, all atoms are simultaneously coupled to the same mode. In this way the cavity field depends on the atomic distribution and long range order interactions are mediated via the cavity field, influencing the Mott-insulator to superfluid phase transition. In the new geometry, only the directly excited atoms coherently scatter photons in

the cavity mode. Due to the position-dependent coupling, the scattered field amplitude and phase for each atom is strongly position dependent. Atoms located at nodes are not coupled to the field, leading to no scattering, whereas atoms at antinodes are maximally coupled, leading to maximum scattering. Atoms in adjacent wells are separated by half a wavelength and scatter with opposite phases, such that their contributions to the scattered field interfere destructively. Naively one would thus immediately conclude that atoms forming a state with a homogeneous density scatter no field at all so that nothing happens [34, 35]. Nevertheless, fluctuations of the density still can allow for some background scattering which should diminish for lower temperature. For suitable parameters the corresponding forces start to reorder the atoms towards a periodic pattern of the atoms, where scattering is strongly enhanced. This then deepens the optical potential, stabilizing the pattern in a self-organizing runaway process, semiclassically described in [18].

At $T = 0$ quantum fluctuations still can trigger this reorganization. To study this effect we assume the coherent pump field to form a broad plane wave propagating transversally to the cavity axis (see Fig. 6.1) replacing cavity pumping. This means that we set $\eta = 0$ and the Hamiltonian (6.26) for constant atom number N reads as follows:

$$H = (E + JV_{cl}) \hat{B} + \hbar(U_0 J_0 N - \Delta_c) a^\dagger a + \frac{U}{2} \hat{C} + \hbar U_0 J a^\dagger a \hat{B} + \hbar \eta_{\text{eff}} (a + a^\dagger) \tilde{J}_0 \hat{D}. \quad (6.51)$$

Here we introduced the operator $\hat{D} = \sum_k (-1)^{k+1} \hat{n}_k$ describing the difference in atom number between odd and even sites. The corresponding Heisenberg equation for the cavity field (6.27) reads as follows:

$$\dot{a} = \left\{ i \left[\Delta_c - U_0 \left(J_0 N + J \hat{B} \right) \right] - \kappa \right\} a - i \eta_{\text{eff}} \tilde{J}_0 \hat{D}. \quad (6.52)$$

Consequently the Heisenberg equation for the particle operators is:

$$\dot{b}_k = \left(E + JV_{cl} - iU_0 J a^\dagger a \right) (b_{k+1} + b_{k-1}) - i \eta_{\text{eff}} \tilde{J}_0 (a + a^\dagger) (-1)^{k+1} b_k + U \hat{n}_k b_k. \quad (6.53)$$

Hence we see that the occupation number difference drives the cavity field, which then in turn starts to dephase neighboring atom sites via the first term in the second line of Eq. (6.53). Note that this interesting part of the dynamics even survives for deeper lattices when J is negligibly small and \tilde{J} is of order unity. This will be discussed in more detail using various approximations below.

6.4.1 Field-eliminated Hamiltonian

Adiabatic elimination of the field variables is a bit more subtle here as compared to the cavity pump case discussed before. The scattering amplitude of light into the cavity mode here depends strongly on the atomic positions. Hence even small position changes have a large influence on the cavity field dynamics. The maximum photon number is established when all the atoms are well localized at either only odd or only even lattice sites. For red

atom field detuning this increases the lattice depth and forces the atoms into one of two stable patterns, where the wells where atoms are located are deeper than the empty ones. Hence this changes the translational periodicity of the optical lattice from $\lambda/2$ to λ . Such bistable behavior was observed by Vuletić and coworkers [20] and explained in a semiclassical treatment [18].

Let us now turn to a quantum treatment of atoms and field. Naive adiabatic elimination encounters a first difficulty, as the operators \hat{B}, \hat{D} do not commute, $[\hat{B}, \hat{D}] \neq 0$. Hence this already creates an ordering problem in the formal steady-state solution of (6.52), which gets even more difficult when it comes to the replacement of the field operators to obtain an effective Hamiltonian (6.51). Unfortunately also the second approach used in the case of cavity pumping, namely reading off an effective Hamiltonian from the particle operator Heisenberg equation does not resolve this problems. Replacing a with the steady-state expression in (6.53) leads to a rather complex form, so that there is no simple way to find a suitable effective Hamiltonian H_{ad} , with $i\hbar\dot{b}_k = [b_k, H_{\text{ad}}]$.

Hence we have to resort to the further approximation of neglecting the term $\hbar U_0 J a^\dagger a \hat{B}$, compared to JV_{cl} . This still leaves the most important part of the new physics, but reduces the field equation to the form:

$$\dot{a} = (i\Delta'_c - \kappa) a - i\eta_{\text{eff}} \tilde{J}_0 \hat{D}. \quad (6.54)$$

The steady-state solution of this equation is immediately at hand and free of ordering ambiguities of non-commuting operators.

$$a = \frac{i\eta_{\text{eff}} \tilde{J}_0}{i\Delta'_c - \kappa} \hat{D}. \quad (6.55)$$

Also the particle operator equation is much simpler within this approximation:

$$\dot{b}_k = (E + JV_{\text{cl}}) (b_{k-1} + b_{k+1}) - i\eta_{\text{eff}} \tilde{J}_0 (a + a^\dagger) (-1)^{k+1} b_k + U \hat{n}_k b_k. \quad (6.56)$$

In this form one then can find a well defined effective Hamiltonian only containing particle operators. Let us thus proceed as in Sec. 6.3.1 and simply substitute (6.55) and its adjoint into (6.51). This yields the effective Hamiltonian:

$$H_{\text{ad}} = (E + JV_{\text{cl}}) \hat{B} + \frac{U}{2} + \frac{\hbar \tilde{J}_0^2 \eta_{\text{eff}}^2 \Delta'_c}{\kappa^2 + \Delta'^2_c} \hat{D}^2. \quad (6.57)$$

Within first order in J the replacement of the field variables in the Liouvillean part of the master equation (6.20) in this case does not provide an extra terms to be included in the Hamiltonian. So the effective cavity decay induced dissipation on the atomic dynamics takes the simple and intuitive form:

$$\mathcal{L}_{\text{ad}} \varrho = \frac{\kappa \eta_{\text{eff}}^2 \tilde{J}_0^2}{\kappa^2 + \Delta'^2_c} \left(2\hat{D} \varrho \hat{D} - \hat{D}^2 \varrho - \varrho \hat{D}^2 \right). \quad (6.58)$$

Note that Eq. (6.57) with the replacement of the field operator by its steady-state expression also leads to the same time evolution as induced by (6.56) after symmetrizing with respect to the field terms. The two approaches thus lead to identical predictions, which we will exhibit in some more detail in the following.

6.4.2 Self-organization of atoms in an optical lattice

In this section we investigate the microscopic dynamics of self-ordering near zero temperature and compare the results of the general model Hamiltonian (6.51) and the corresponding effective Hamiltonian (6.57). In order to simplify things, we keep the approximation from above and neglect $JU_0 a^\dagger a$ in the model, i.e.,

$$H = (E + JV_{\text{cl}}) \hat{B} - \hbar \Delta'_c a^\dagger a + \frac{U}{2} \hat{C} + \hbar \eta_{\text{eff}} \tilde{J}_0 \hat{D} (a + a^\dagger), \quad (6.59)$$

with $\Delta'_c = \Delta_c - U_0 J_0 N$. Let us point out here, that the Hamiltonian in this approximative form is equivalent to a Hamiltonian describing 1D motion along an optical lattice transverse to the cavity axis. Such a lattice can e.g. be generated by the pump laser itself as it was studied in [55, 56] to investigate the onset of the self-organization process [18–20] at zero temperature.

Similar to that case, the effective Hamiltonian Eq. (6.59) for moderate coupling reproduces quite well the results of a full Monte-Carlo wavefunction simulation. We have checked this for a rather small system of two atoms in two wells with periodic boundary conditions. This is the minimal system to study self-organization but in general sufficient to capture the physics. In this special case the operator \hat{B} simply couples the ordered $|11\rangle$ state to the state $1/\sqrt{2}(|20\rangle + |02\rangle)$, while the operator \hat{D}^2 leaves all the basis states $\{|11\rangle, |20\rangle, |02\rangle\}$ unchanged. It simply leads to a relative energy shift. Hence starting from a perfectly ordered atomic state (the analog of the Mott insulator state) the Hamiltonian part of the time evolution of the system couples it to the symmetric superposition of ordered states. In an adiabatic limit those ordered states are correlated with a coherent field $\pm\alpha$ in the cavity. Thus without damping the evolution would simply read:

$$|\psi(t)\rangle = \cos(2\omega t) |11, 0\rangle + \frac{i \sin(2\omega t)}{\sqrt{2}} (|20, 2\alpha\rangle + |02, -2\alpha\rangle). \quad (6.60)$$

where the frequency ω is given by the $(E + JV_{\text{cl}})/\hbar$. Here $|11, 0\rangle$ is the state with one atom in each well and zero photons, whereas $|20, \alpha\rangle$ ($|02, -\alpha\rangle$) corresponds to the state with both atoms in the left (right) well, and the cavity field being in a coherent state with amplitude 2α (-2α). The factor 2 is due to constructive interference of the fields, scattered by the ordered atoms. In the Mott state, the scattering fields cancel each other.

Note that such an entangled superposition of different atomic states and fields cannot be reproduced by any classical or mean field evolution and requires a genuine quantum description. If on-site interaction is added the amplitude of this oscillations decreases due to extra relative different phase changes of the self-ordered and the Mott state.

Of course we now have to add the effect of dissipation via cavity loss. We will see that even single cavity photon decay events strongly perturb the system evolution. This can be immediately seen by applying the photon annihilation operator to the entangled atom-field state, i.e.,

$$|\psi(t)'\rangle \propto a|\psi(t)\rangle \propto |20, 2\alpha\rangle - |02, -2\alpha\rangle. \quad (6.61)$$

This procedure projects out the Mott contributions to the state as they are connected to zero photons. Surprisingly in addition it also blocks further tunneling by introducing a minus sign between the two ordered states. At this point coherent atomic time evolution stops until a second photon escapes and re-establishes the plus sign. This then allows tunnel coupling back to the Mott insulator state again. In this sense self-ordering is an instantaneous projective process here, where the cavity acts as measurement apparatus asking a sort of yes/no ordering question.

The fact, that for transverse pumping the adiabatic field state associated to the Mott insulator is an intracavity vacuum decouples this state from further dynamics even in the presence of dissipation. This creates numerical difficulties and prohibits an approximation of the dissipative dynamics by the adiabatic ground state values of (6.57) only. As soon as a photon leaks out of the cavity, the contribution of the Mott-insulator state is canceled, no matter how large it, corresponding to a given on-site interaction, might be. Hence, every initial state evolves into a superposition of the ordered states and the ground state values of the effective Hamiltonian do not make much sense. Nevertheless, including the damping via the effective Liouvillean (6.58) approximately reveals the complete dynamics. In Fig. 6.10 we show the results of a Monte-Carlo simulation of the dynamics of the Mott and the superfluid contribution, corresponding to (6.59) and compare it with a solution of the master equation, consisting of the Hamiltonian (6.57) and Liouvillean (6.58), where the field variables are eliminated. Furthermore, the restriction of the Hilbert space to the two states of (6.61) and $|11, 0\rangle$, allows for a proof of the accuracy of our assumption, concerning the fast evolution of the cavity field. We use the coefficients $c(t), \tilde{c}(t)$ (calculated with the Monte Carlo simulation) of $|\psi(t)\rangle = \tilde{c}(t)|11, 0\rangle + c(t)(|20, 2\alpha\rangle \pm |02, -2\alpha\rangle)$ to construct a purely atomic state $|\varphi(t)\rangle = \tilde{c}(t)|11\rangle + c(t)(|20\rangle \pm |02\rangle)$. Then the mean photon number, calculated with the effective photon operator (6.55) agrees very well with the real mean photon number, i.e.,

$$\frac{\eta_{\text{eff}}^2 \tilde{J}_0^2}{\Delta_c'^2 + \kappa^2} \langle \varphi(t) | \hat{D}^2 | \varphi(t) \rangle \approx \langle \psi(t) | a^\dagger a | \psi(t) \rangle. \quad (6.62)$$

6.5 Conclusions

Based on an approximative Bose-Hubbard type model descriptions, we have shown that quantum characteristics of light fields generating optical potentials lead to shifts in quantum phase transition points and play a decisive role in the microscopic dynamics of the transition process. While many physical aspects can be already captured by effective Hamiltonians with rescaled parameters, cavity mediated long-range interactions also play an important role and add a new nonlocal element to optical lattices dynamics for atoms. In that context even small modifications in the setup, from cavity pump to transverse pump, have a drastic influence on the behavior of the system on a microscopic level. We have seen that the Bose-Hubbard Hamiltonian for the former system can, in a certain parameter regime, be significantly simplified by adiabatically eliminating the field variables. Although the cavity has influence on its shape, the Mott insulator to superfluid phase transition occurs similar to classical optical lattices. For transverse pumping this is not the case. Here, the fields scattered by the atoms in the uniform Mott state cancel and completely suppress scattering. In parallel new ordered states with maximal coupling of pump and cavity field appear and

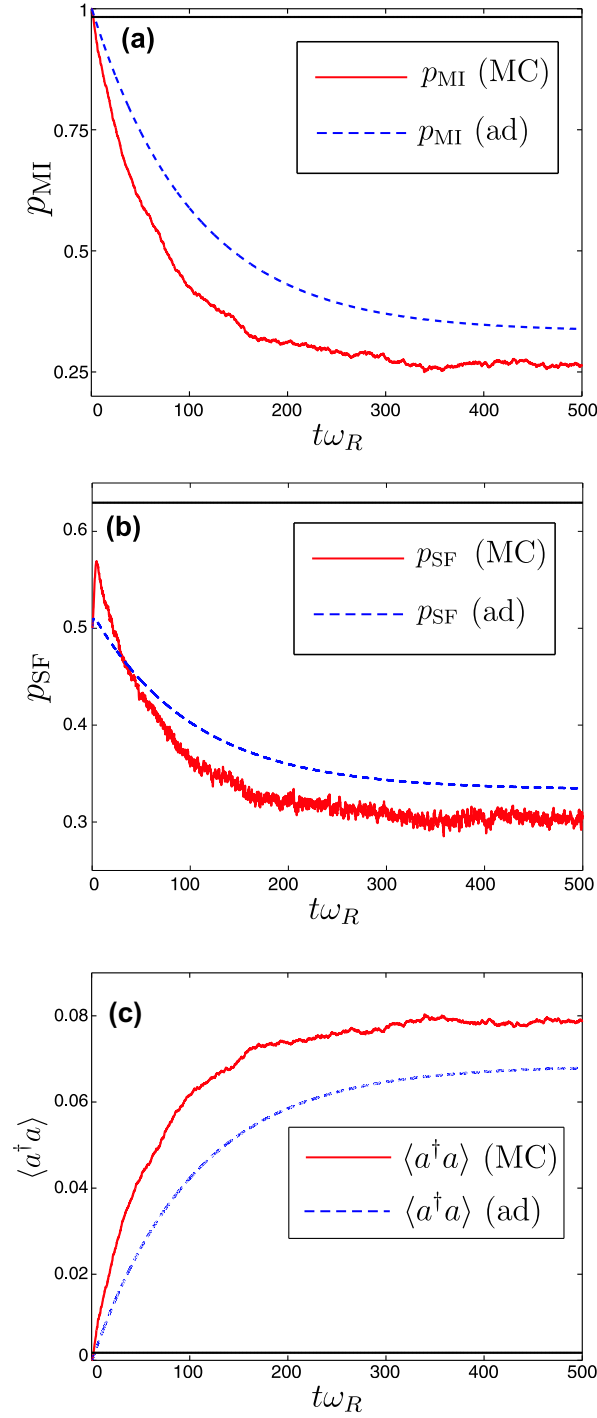


Figure 6.10. (color online) (a) Contribution of the Mott insulator state p_{MI} in a system of two atoms in two wells. The solid line shows the results of a Monte-Carlo simulation, corresponding to (6.59) with dissipation via cavity loss. The dashed line depicts the solution of a master equation with effective Hamiltonian (6.57) and Liouvillean (6.58). The constant line, shows the ground state value of this contribution of the effective Hamiltonian. (b) The same for the contribution of the superfluid state p_{SF} . (c) shows analogue results for the mean photon number. Parameters are $V_{\text{cl}} = -10E_R$, $(\kappa, U_0, \eta_{\text{eff}}) = (4, -0.1, 1)\omega_R$ and $\Delta_c = U_0 J_0 N + \kappa$.

the dynamics favors a superposition of these two ordered states correlated with coherent field states with phase difference π . Hence the dynamics generates strong atom field entanglement and large effective optical nonlinearities even in the limit of linear weak field scattering.

Of course the various approximations used to derive our effective Hamiltonians still leave a lot of room for improvements and we could only touch a very small part of the physical effects and possibilities contained in these model. Fortunately the experimental progress in this field is spectacularly fast and several groups now have set up optical lattices with cavity fields [36–39] and intriguing potential applications of such systems were already proposed [57], so that one can expect a fast and exciting further development of this field.

Acknowledgments

The authors would like to thank M. Lewenstein, G. Morigi, S. Fernández-Vidal, A. Micheli, and A. Vukics for useful discussions. This work was funded by the Austrian Science Fund (P17709 and S1512). After completion of this work we became aware of related parallel work by M. Lewenstein and coworkers, which treats many aspects of this model in the thermodynamic limit [58].

Bibliography

- [1] See e.g. *Laser Manipulation of Atoms and Ions*, ed. by E. Arimondo and W. D. Phillips, Varenna Summer School, 1991 (North-Holland, Amsterdam 1992).
- [2] I. Bloch, *Nature Physics* **1**, 23 (2005); I. Bloch and M. Greiner, *Adv. At. Mol. Opt. Phys.* **52**, 1 (2005).
- [3] D. Jaksch, C. Bruder, J. I. Cirac, C. W. Gardiner, and P. Zoller, *Phys. Rev. Lett.* **81**, 3108 (1998);
- [4] W. Zwerger, *J. Opt. B* **5**, 9 (2003).
- [5] M. P. A. Fisher, P. B. Weichman, G. Grinstein, and D. S. Fisher, *Phys. Rev. B* **40**, 546 (1989).
- [6] M. Greiner, O. Mandel, T. Esslinger, T. W. Hänsch, and I. Bloch, *Nature (London)* **415**, 39 (2002); M. Greiner, O. Mandel, T. W. Hänsch and I. Bloch, *Nature (London)* **419**, 51 (2002).
- [7] D. Jaksch and P. Zoller, *Ann. Phys.* **315**, 52 (2005).
- [8] S. Inouye, M. R. Andrews, J. Stenger, H. -J. Miesner, D. M. Stamper-Kurn and W. Ketterle, *Nature (London)* **392**, 151 (1998).
- [9] M. Theis, G. Thalhammer, K. Winkler, M. Hellwig, G. Ruff, R. Grimm, and J. Hecker Denschlag, *Phys. Rev. Lett.* **93**, 123001 (2004).

- [10] T. Stöferle, H. Moritz, C. Schori, M. Köhl, and T. Esslinger, Phys. Rev. Lett. **92**, 130403 (2004).
- [11] M. Köhl, H. Moritz, T. Stöferle, C. Schori and T. Esslinger, J. Low Temp. Phys. **138**, 635 (2005).
- [12] I. B. Spielman, W. D. Phillips, and J. V. Porto, Phys. Rev. Lett. **98**, 080404 (2007).
- [13] B. Paredes, A. Widera, V. Murg, O. Mandel, S. Fölling, I. Cirac, G. V. Shlyapnikov, T. W. Hänsch and I. Bloch, Nature (London) **429**, 277 (2004).
- [14] T. Kinoshita, T. R. Wenger, and D. S. Weiss, Science **305**, 1125 (2004).
- [15] Z. Hadzibabic, P. Krüger, M. Cheneau, B. Battelier, and J. Dalibard, Nature (London) **441**, 1118 (2006).
- [16] M. Lewenstein, A. Sanpera, V. Ahufinger, B. Damski, A. Sen De, and U. Sen, Adv. Phys. **56**, 243 (2007).
- [17] P. Domokos and H. Ritsch, J. Opt. Soc. Am. B **20**, 1098 (2003).
- [18] P. Domokos and H. Ritsch, Phys. Rev. Lett. **89**, 253003 (2002).
- [19] S. Zippilli, G. Morigi, and H. Ritsch, Phys. Rev. Lett. **93**, 123002 (2004).
- [20] A. T. Black, H. W. Chan, and V. Vuletić, Phys. Rev. Lett. **91**, 203001 (2003).
- [21] P. W. H. Pinkse, T. Fischer, P. Maunz, and G. Rempe, Nature (London) **404**, 365 (2000).
- [22] C. J. Hood, T. W. Lynn, A. C. Doherty, A. S. Parkins, and H. J. Kimble, Science **287**, 1447 (2000).
- [23] P. Horak, G. Hechenblaikner, K. M. Gheri, H. Stecher, and H. Ritsch, Phys. Rev. Lett. **79**, 4974 (1997); G. Hechenblaikner, M. Gangl, P. Horak, and H. Ritsch, Phys. Rev. A **58**, 3030 (1998).
- [24] V. Vuletić, H. W. Chan, and A. T. Black, Phys. Rev. A **64**, 033405.
- [25] P. Domokos, A. Vukics, and H. Ritsch, Phys. Rev. Lett. **92**, 103601 (2004).
- [26] S. Zippilli, G. Morigi, and H. Ritsch, Phys. Rev. Lett. **95**, 143001 (2005).
- [27] P. Maunz, T. Puppe, I. Schuster, N. Syassen, P. W. H. Pinkse, and G. Rempe, Nature (London) **428**, 50 (2004).
- [28] S. Nußmann, K. Murr, M. Hijkema, B. Weber, A. Kuhn, and G. Rempe, Nature Physics **1**, 122 (2005).
- [29] A. Griessner, D. Jaksch, and P. Zoller, J. Phys. B **37**, 1419 (2004).
- [30] P. Horak, S. M. Barnett, and H. Ritsch, Phys. Rev. A **61**, 033609 (2000).

- [31] D. Jaksch, S. A. Gardiner, K. Schulze, J. I. Cirac, and P. Zoller, Phys. Rev. Lett. **86**, 4733 (2001).
- [32] C. Maschler and H. Ritsch, Phys. Rev. Lett. **95**, 260401 (2005).
- [33] J. Larsson, B. Damski, G. Morigi, and M. Lewenstein, arXiv:cond-mat/0608335.
- [34] I. B. Mekhov, C. Maschler, and H. Ritsch, Phys. Rev. Lett. **98**, 100402 (2007); I. B. Mekhov, C. Maschler, and H. Ritsch, Phys. Rev. A (accepted).
- [35] I. B. Mekhov, C. Maschler, and H. Ritsch, Nature Physics **3**, 319 (2007).
- [36] A. Öttl, S. Ritter, M. Köhl, and T. Esslinger, Phys. Rev. Lett. **95** 090404 (2005); T. Bourdel, T. Donner, S. Ritter, A. Öttl, M. Köhl, and T. Esslinger, Phys. Rev. A **73** 43602 (2006).
- [37] P. Treutlein, D. Hunger, S. Camerer, T. W. Hänsch, and J. Reichel, Phys. Rev. Lett. **99**, 140403 (2007); Y. Colombe, T. Steinmetz, G. Dubois, F. Linke, D. Hunger, and J. Reichel, arXiv:quant-ph/0706.1390.
- [38] S. Slama, G. Krenz, S. Bux, C. Zimmermann, and Ph. W. Courteille, Phys. Rev. A **75**, 063620 (2007).
- [39] S. Gupta, K. L. Moore, K. W. Murch, and D. M. Stamper-Kurn, arXiv:quant-ph/0706.1052.
- [40] J. McKeever, J. R. Buck, A. D. Boozer, A. Kuzmich, H. -C. Nägerl, D. M. Stamper-Kurn, and H. J. Kimble, Phys. Rev. Lett. **90**, 133602 (2003).
- [41] T. Puppe, I. Schuster, P. Maunz, K. Murr, P. W. H. Pinkse, and G. Rempe, Phys. Rev. Lett. **99**, 013002 (2007).
- [42] E. T. Jaynes and F. W. Cummings, Proc. IEEE **51**, 89 (1963).
- [43] See, for example, A. Galindo and P. Pascual, *Quantum Mechanics II*, (Springer, Berlin, 1990).
- [44] K. Huang, *Statistical Mechanics*, (John Wiley & Sons, New York, 1987).
- [45] It is also possible, to eliminate the excited state first in the single particle dynamics, which leads to the same expression (6.18) and then implement this expression in second quantization formalism.
- [46] M. Olshanii, Phys. Rev. Lett. **81**, 938 (1998).
- [47] C. Maschler and H. Ritsch, Phys. Rev. Lett. **95**, 260401 (2005).
- [48] C. Kittel, *Quantum Theory of Solids*, (John Wiley & Sons, New York, 1963).
- [49] See, for example, C. W. Gardiner and P. Zoller, *Quantum Noise*, 3rd Ed. (Springer, Berlin, 2005).

-
- [50] R. Grimm, M. Weidemüller, and Y. B. Ovchinnikov, *Adv. At. Mol. Opt. Phys.* **42**, 95 (2000).
 - [51] J. Ye, D. W. Vernooy, and H. J. Kimble, *Phys. Rev. Lett.* **83**, 4987 (1999).
 - [52] J. A. Sauer, K. M. Fortier, M. S. Chang, C. D. Hamley, and M. S. Chapman, *Phys. Rev. A* **69**, 051804 (2004).
 - [53] H. M. Wiseman and G. J. Milburn, *Phys. Rev. A* **47**, 642 (1993).
 - [54] A. Vukics and H. Ritsch, *Eur. J. Phys. D* **44**, 585 (2007).
 - [55] C. Maschler, H. Ritsch, A. Vukics, and P. Domokos, *Opt. Comm.* **273**, 446 (2007).
 - [56] A. Vukics, C. Maschler, and H. Ritsch, *New J. Phys.* **9**, 255 (2007).
 - [57] D. Meiser, J. Ye, and M. J. Holland, *arXiv:quant-ph/0707.3834*.
 - [58] J. Larson, S. Fernández-Vidal, G. Morigi, and M. Lewenstein, *arXiv:cond-mat/0710.3047*.

Part II

Probing Atomic Phases in Optical Lattices

CHAPTER 7

PUBLICATION

Cavity Enhanced Light Scattering in Optical Lattices to Probe Atomic Quantum Statistics[†]

Physical Review Letters **98**, 100402 (2007)

I. B. Mekhov^{1,2}, C. Maschler¹, and H. Ritsch¹

1) *Institut für theoretische Physik, Universität Innsbruck,
A-6020 Innsbruck, Austria*

2) *St. Petersburg State University, V. A. Fock Institute of Physics,
St. Petersburg, Russia*

Different quantum states of atoms in optical lattices can be nondestructively monitored by off-resonant collective light scattering into a cavity. Angle resolved measurements of photon number and variance give information about atom-number fluctuations and pair correlations without single-site access. Observation at angles of diffraction minima provides information on quantum fluctuations insensitive to classical noise. For transverse probing, no photon is scattered into a cavity from a Mott insulator phase, while the photon number is proportional to the atom number for a superfluid.

Studies of ultracold atoms in optical lattices link various disciplines. Fundamental quantum many-body theories, formulated initially for condensed matter, can be tested in better controllable atomic systems [1], e.g., strongly correlated phases, quantum simulators. Such studies influence different areas [1]: quantum information processing, ultracold collisions, exotic molecules, etc.

While mean-field approaches describe only the average atomic density, the main goal is to study quantum properties of these gases. They are most prominent in lattices, where one has phase transitions between states of similar density but radically different quantum fluctuations.

Standard methods to measure quantum properties are based on matter-wave interference of atoms released from a trap [2] destroying the system. “Bragg spectroscopy” using stimulated matter-wave scattering by laser pulses proved successful [3, 4] but destructive.

[†]The primary contribution of the author of the present thesis performed to this publication was the installation of the model and the calculation of certain generic examples and statistical quantities (cf. Table 7.1). He also acted as a discussion partner on all other aspects of the work.

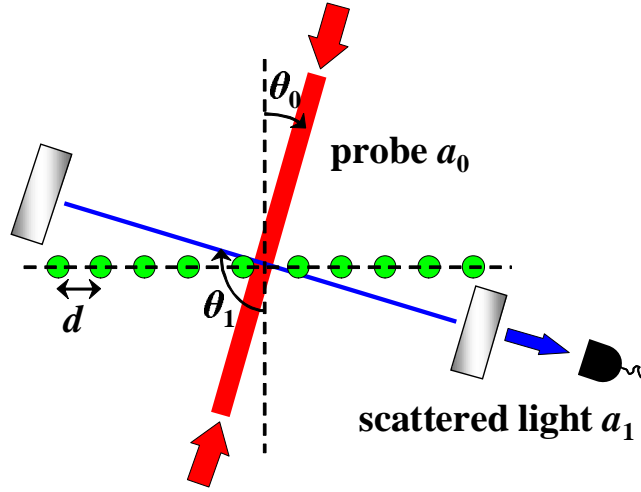


Figure 7.1. Setup: A lattice is illuminated by a probe at the angle θ_0 which is scattered into a cavity at θ_1 .

Alternative less destructive methods observing scattered light were proposed mainly for homogeneous Bose-Einstein condensates (BEC) [5–8], but not yet implemented.

Here we show that specifically for periodic lattices, light scattering can help to overcome experimental difficulties. In contrast to homogeneous BECs, scattering from a lattice allows to determine local and nonlocal correlations without single-atom optical access using the suppression of strong classical scattering at Bragg minima and monitoring much richer angular distributions. This looks extremely useful for studying phase transitions between, e.g., Mott insulator (MI) and superfluid (SF) states, without destruction, since various quantum phases show even qualitatively distinct scattering.

Joining two fields, cavity quantum electrodynamics (QED) and ultracold gases, will enable new investigations of both light and matter at ultimate quantum levels, which only recently became experimentally possible [9].

Our model is based on nonresonant interaction, not relying on a particle level structure. Thus it also applies to molecular physics, where new quantum phases were obtained [10]. It can be also applied for semiconductors [11], as, e.g., were used for BEC of exciton-polaritons [12].

Model. We consider N two-level atoms in an optical lattice with M sites. A region of $K \leq M$ sites is illuminated by probe light which is scattered into another mode (cf. Fig. 7.1). Although, each mode could be a freely propagating field, we will consider cavity modes whose geometries (i.e. axis directions or wavelengths) can be varied. A related manybody

Hamiltonian is given by

$$H = \sum_{l=0,1} \hbar \omega_l a_l^\dagger a_l + \int d^3 \mathbf{r} \Psi^\dagger(\mathbf{r}) H_{a1} \Psi(\mathbf{r}), \quad (7.1a)$$

$$H_{a1} = \frac{\mathbf{p}^2}{2m_a} + V_{\text{cl}}(\mathbf{r}) + \hbar g_0^2 \sum_{l,m=0,1} \frac{u_l^*(\mathbf{r}) u_m(\mathbf{r}) a_l^\dagger a_m}{\Delta_{ma}}, \quad (7.1b)$$

where a_0 (a_1) are the annihilation operators of the probe (scattered) light with the frequencies $\omega_{0,1}$, wave vectors $\mathbf{k}_{0,1}$, and mode functions $u_{0,1}(\mathbf{r})$; $\Psi(\mathbf{r})$ is the atom-field operator. In the effective single-atom Hamiltonian H_{a1} , \mathbf{p} and \mathbf{r} are the momentum and position operators of an atom of mass m_a trapped in a classical potential $V_{\text{cl}}(\mathbf{r})$; g_0 is the atom–light coupling constant. We consider the field-atom detunings $\Delta_{la} = \omega_l - \omega_a$ larger than the spontaneous emission rate and Rabi frequencies. Thus, in H_{a1} the adiabatic elimination of the upper state was used.

Assuming weak fields $a_{0,1}$, we expand $\Psi(\mathbf{r})$ in Eq. (7.1a) using localized Wannier functions corresponding to $V_{\text{cl}}(\mathbf{r})$ and keep only the lowest vibrational state at each site: $\Psi(\mathbf{r}) = \sum_{i=1}^M b_i w(\mathbf{r} - \mathbf{r}_i)$, where b_i is the atom annihilation operator at site with coordinate \mathbf{r}_i . Substituting this in Eq. (7.1a), one can get a generalized Bose-Hubbard Hamiltonian [1] including light scattering. However, in contrast to our previous work [13] and “Bragg spectroscopy” [4], we do not consider lattice excitations here and focus on scattering from atoms in a prescribed state.

Neglecting atomic tunneling, the Hamiltonian reads:

$$H = \sum_{l=0,1} \hbar \omega_l a_l^\dagger a_l + \hbar g_0^2 \sum_{l,m=0,1} \frac{a_l^\dagger a_m}{\Delta_{ma}} \left(\sum_{i=1}^K J_{i,i}^{lm} \hat{n}_i \right), \quad (7.2)$$

where $\hat{n}_i = b_i^\dagger b_i$. We define the operator of the atom number at illuminated sites as $\hat{N}_K = \sum_{i=1}^K \hat{n}_i$. For a deep lattice the coefficients $J_{i,i}^{lm} = \int d\mathbf{r} w^2(\mathbf{r} - \mathbf{r}_i) u_l^*(\mathbf{r}) u_m(\mathbf{r})$ reduce to $J_{i,i}^{lm} = u_l^*(\mathbf{r}_i) u_m(\mathbf{r}_i)$ neglecting atom spreading, which can be studied even by classical scattering [14].

The Heisenberg equation for the scattered light in the frame rotating with ω_0 ($\Delta_{01} = \omega_0 - \omega_1$) thus reads:

$$\dot{a}_1 = i \left[\Delta_{01} - \frac{g_0^2}{\Delta_{1a}} \sum_{i=1}^K |u_1(\mathbf{r}_i)|^2 \hat{n}_i \right] a_1 - i \frac{g_0^2 a_0}{\Delta_{0a}} \sum_{i=1}^K u_1^*(\mathbf{r}_i) u_0(\mathbf{r}_i) \hat{n}_i - \kappa a_1, \quad (7.3)$$

where κ is the cavity decay rate and a_0 will be assumed a classical field given by a c-number constant.

Light properties. Though the dispersion shift of a cavity mode is sensitive to atom statistics through \hat{n}_i , we assume it is much smaller than κ or Δ_{01} . A stationary solution of Eq. (7.3) for a_1 and photon number then reads

$$a_1 = C\hat{D}, \quad n_{ph} = a_1^\dagger a_1 = |C|^2 \hat{D}^* \hat{D}, \quad \hat{D} = \sum_{i=1}^K A_i \hat{n}_i, \quad (7.4)$$

with $C \equiv ig_0^2 a_0 / [\Delta_{0a}(i\Delta_{01} - \kappa)]$ and the coefficients $A_i(\theta_0, \theta_1) \equiv u_1^*(\mathbf{r}_i) u_0(\mathbf{r}_i)$. This expression of the light operators through the atomic ones is a central result here.

For a 1D lattice of period d and atoms trapped at $x_m = md$ ($m = 1, 2, \dots, M$) the mode functions are $u_{0,1}(\mathbf{r}_m) = \exp(imk_{0,1x}d)$ for traveling and $u_{0,1}(\mathbf{r}_m) = \cos(mk_{0,1x}d)$ for standing waves with $k_{0,1x} = |\mathbf{k}_{0,1}| \sin \theta_{0,1}$ (cf. Fig. 7.1). For the atomic quantum state we use the assumptions: (i) the mean atom number at all sites is $\langle \hat{n}_i \rangle = n = N/M$ ($\langle \hat{N}_K \rangle = N_K \equiv nK$) and (ii) the pair correlations $\langle \hat{n}_i \hat{n}_j \rangle$ are identical for any $i \neq j$, which is valid for a deep lattice, and will be denoted as $\langle \hat{n}_a \hat{n}_b \rangle$ (with $a \neq b$).

Thus, $\langle a_1 \rangle \sim \langle \hat{D} \rangle = \sum_{i=1}^K A_i \langle \hat{n}_i \rangle = nA$ showing that the field amplitude only depends on the mean density and exhibits the angular distribution of classical diffraction $A(\theta_0, \theta_1) \equiv \sum_{i=1}^K A_i(\theta_0, \theta_1)$ with diffraction maxima and minima. The central point now is that the photon number (7.4) is not just the amplitude squared, but we get

$$\langle \hat{D}^* \hat{D} \rangle = \langle \hat{n}_a \hat{n}_b \rangle |A|^2 + (\langle \hat{n}^2 \rangle - \langle \hat{n}_a \hat{n}_b \rangle) \sum_{i=1}^K |A_i|^2, \quad (7.5a)$$

$$R(\theta_0, \theta_1) \equiv \langle \hat{D}^* \hat{D} \rangle - |\langle \hat{D} \rangle|^2 = \langle \delta \hat{n}_a \delta \hat{n}_b \rangle |A|^2 + (\langle \delta \hat{n}^2 \rangle - \langle \delta \hat{n}_a \delta \hat{n}_b \rangle) \sum_{i=1}^K |A_i|^2, \quad (7.5b)$$

where $\delta \hat{n}_i \equiv \hat{n}_i - n$ giving $\langle \delta \hat{n}_a \delta \hat{n}_b \rangle = \langle \hat{n}_a \hat{n}_b \rangle - n^2$, and $\langle \delta \hat{n}^2 \rangle$ equal to the variance $(\Delta n_i)^2 = \langle \hat{n}_i^2 \rangle - n^2$. Thus, the intensity is sensitive to atomic quantum statistics via the density-density correlations $\langle \hat{n}_i \hat{n}_j \rangle$ different for particular states. Besides the classical angle dependence $|A|^2$, the second term in Eq. (7.5a) reflects fluctuations and has a completely different dependence. Particularly in a lattice, scattering is sensitive not only to the periodic density, but also to periodic fluctuations, leading to the observable difference between states with and without nonlocal correlations. Analysis of quadrature variances gives results similar to analysis of the noise quantity R .

For two traveling waves, Eq. (7.5a) gives the structure factor considered in Ref. [7] on homogeneous BECs. We show that a more general form including standing waves gives new measurable quantities beyond structure factor.

The intensity fluctuations of the scattered light depend on the fourth moments of the atomic number operators and four-point density correlations $\langle \hat{n}_i \hat{n}_j \hat{n}_k \hat{n}_l \rangle$. For example the photon-number variance is given by

$$(\Delta n_{ph})^2 = \langle n_{ph}^2 \rangle - \langle n_{ph} \rangle^2 = |C|^4 (\langle |\hat{D}|^4 \rangle - \langle |\hat{D}|^2 \rangle^2) + |C|^2 \langle |\hat{D}|^2 \rangle. \quad (7.6)$$

To discuss examples of different scattering we summarize statistical properties of typical states in Table 7.1. For light scattering, the most classical state corresponding to pointlike

atoms is MI. Here the atom number at each site \hat{n}_i does not fluctuate and we have no pair correlations. Hence we see from Eq. (7.5a) that the zeros of classical diffraction [$A(\theta_0, \theta_1) = 0$] are zeros of light intensity.

	MI	SF	Coherent
$ \Psi\rangle$	$\prod_{i=1}^M n_i\rangle_i$	$\frac{1}{\sqrt{M^N N!}} (\sum_{i=1}^M b_i^\dagger)^N 0\rangle$	$e^{-\frac{N}{2}} \prod_{i=1}^M e^{\sqrt{\frac{N}{M}} b_i^\dagger} 0\rangle_i$
$\langle \hat{n}_i^2 \rangle$	n^2	$n^2(1 - 1/N) + n$	$n^2 + n$
$(\Delta n_i)^2$	0	$n(1 - 1/M)$	n
$\langle \hat{N}_K^2 \rangle$	N_K^2	$N_K^2(1 - 1/N) + N_K$	$N_K^2 + N_K$
$(\Delta N_K)^2$	0	$N_K(1 - K/M)$	N_K
$\langle \hat{n}_a \hat{n}_b \rangle$	n^2	$n^2(1 - 1/N)$	n^2
$\langle \delta \hat{n}_a \delta \hat{n}_b \rangle$	0	$-N/M^2$	0

Table 7.1. Various statistical quantities of typical quantum atomic states, namely the Mott insulator state, the coherent state and the superfluid state.

This is different for a SF where each atom is delocalized over all sites leading to number fluctuations at a given site and at $K < M$ sites; the atoms at different sites are anticorrelated. At a classical diffraction zero we still find a photon number proportional to the atom number N .

A coherent state approximates a SF but without pair correlations. In the limit $N, M \rightarrow \infty$, it well describes scattering from a small region ($K \ll M$) of a partially illuminated superfluid (SF_K). However, we proved that even in this limit it fails to describe scattering at angles of Bragg maxima from a large lattice region ($K \sim M$).

Example. Let us now show the most striking predictions of this model at the basic example of a probe transverse to the lattice ($\theta_0 = 0$, cf. Fig. 7.1). The scattered light is collected in a cavity along the lattice ($\theta_1 = \pi/2$) with atoms trapped at the antinodes ($d = \lambda/2$) [13, 15].

The operator $\hat{D} = \sum_{k=1}^K (-1)^{k+1} \hat{n}_k$ (7.4) here gives almost zero average field amplitude independently on the atomic state. This reflects the opposite phase of light scattered from atoms separated by $\lambda/2$ (diffraction minimum). However, the cavity photon-number is proportional to $\langle \hat{D}^* \hat{D} \rangle = (\langle \hat{n}^2 \rangle - \langle \hat{n}_a \hat{n}_b \rangle) K$ [cf. Eq. (7.5a)], which is determined by statistics of a particular state. Thus, atoms in a MI state scatter no photons, while a SF scatters number of photons proportional to the atom number:

$$\begin{aligned} \langle a_1 \rangle_{\text{MI}} &= \langle a_1 \rangle_{\text{SF}} = 0, \quad \text{but} \\ \langle a_1^\dagger a_1 \rangle_{\text{MI}} &= 0, \quad \langle a_1^\dagger a_1 \rangle_{\text{SF}} = |C|^2 N_K. \end{aligned}$$

Moreover, the photon number fluctuations $(\Delta n_{\text{ph}})^2$ are also different for various atomic states. In the MI state, the variance $(\Delta |D|^2)_{\text{MI}}^2 = \langle |\hat{D}|^4 \rangle_{\text{MI}} - \langle |\hat{D}|^2 \rangle_{\text{MI}}^2 = 0$, whereas in SF, there is a strong noise $(\Delta |D|^2)_{\text{SF}}^2 \approx 2N_K^2$.

Coupled light-matter dynamics in a cavity can lead to a new self-organized phase [15] with atoms trapped at every second site ($d = \lambda$), which gives $\hat{D} = \sum_{k=1}^K \hat{n}_k = \hat{N}_K$ (7.4). If this state is a MI with $d = \lambda$, the number of photons $\langle a_1^\dagger a_1 \rangle_{\text{Self-org}} = |C|^2 N_K^2$ is proportional to the atom number squared and has a superradiant character.

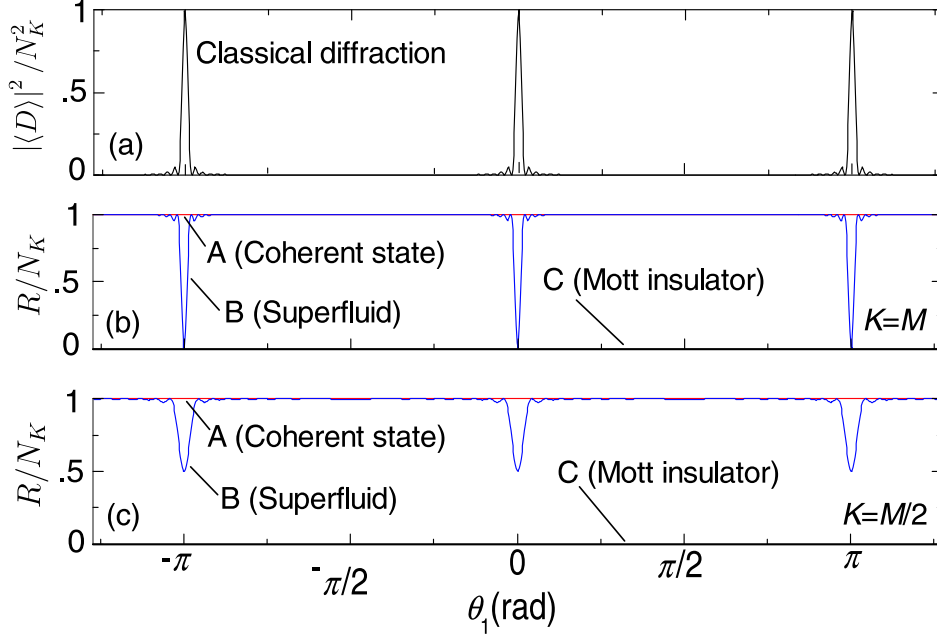


Figure 7.2. Intensity angular distributions for two traveling waves. (a) Intensity of classical diffraction; (b) noise quantity R (7.7) for coherent atomic state (constant 1, line A), SF with all sites illuminated $K = M$ (curve B), and MI state (constant 0, line C); (c) the same as in (b) but for partially illuminated SF with $K = M/2$. $N = M = 30$, $\theta_0 = 0$.

Angular distributions. We will quantitatively discuss angular intensity distributions for scattering between two traveling waves, where Eq. (7.5b) reduces to

$$R = \langle \delta \hat{n}_a \delta \hat{n}_b \rangle \frac{\sin^2(K\alpha_-/2)}{\sin^2(\alpha_-/2)} + (\langle \delta \hat{n}^2 \rangle - \langle \delta \hat{n}_a \delta \hat{n}_b \rangle) K. \quad (7.7)$$

While $|A|^2$ in the first term reproduces classical diffraction with $\alpha_- = k_{0x}d \sin \theta_0 - k_{1x}d \sin \theta_1$, the second term in Eq. (7.5b) is simply isotropic. Thus, the noise quantity is zero for MI, $R_{\text{MI}} = 0$, nonzero but isotropic for the coherent state, $R_{\text{Coh}} = N_K$, and angle dependent for a SF. In a SF, even small pair correlations $\langle \delta \hat{n}_a \delta \hat{n}_b \rangle = -N/M^2$ give a large contribution near diffraction maxima ($\alpha_- = 2\pi l, l = 0, 1, \dots$), where the geometric factor is K^2 , invalidating the coherent-state approximation.

Figure 7.2 displays those angular distributions. Classical diffraction $|\langle D \rangle|^2$ with the only possible zero-order maxima at $\theta_1 = 0, \pi$ ($d = \lambda_{0,1}/2$, $\theta_0 = 0$) is shown in Fig. 7.2(a). R for

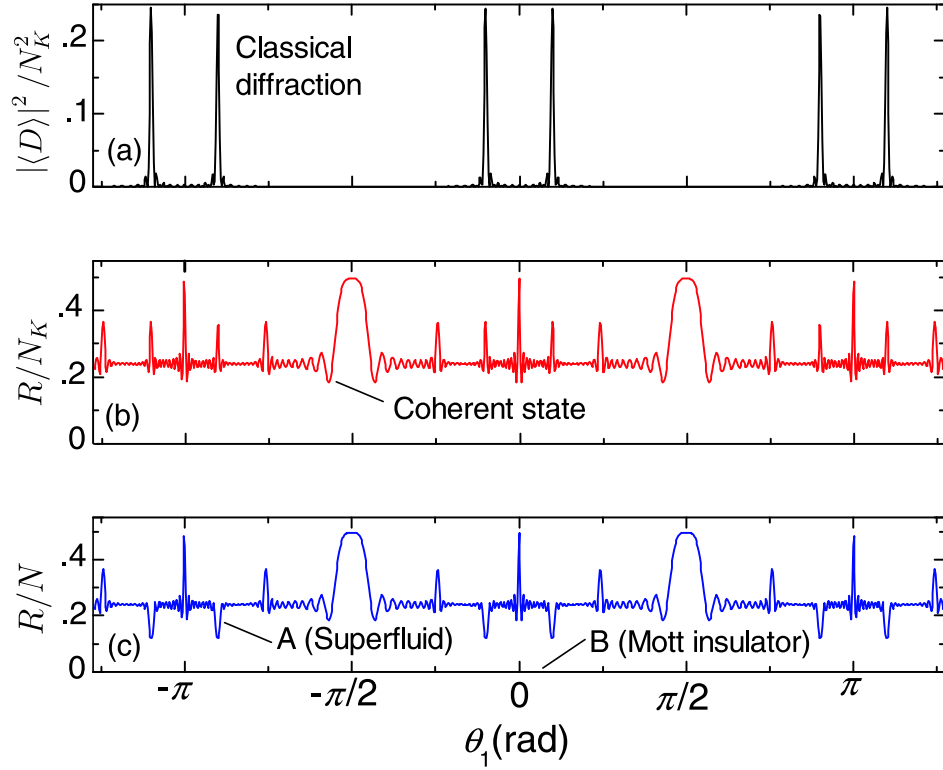


Figure 7.3. Intensity angular distributions for two standing-wave modes. (a) Intensity of classical diffraction; (b) noise quantity for coherent state; and (c) for SF (curve A) and MI (constant 0, line B). $N = M = K = 30$, $\theta_0 = 0.1\pi$.

the coherent and SF_K states are plotted in Figs. 7.2(b), (c). For MI, $R = 0$. In SF, there is a noise suppression at maxima, which is total for all sites illuminated, $K = M$, and partial for $K = M/2$.

In a maximum, \hat{D} (7.4), is reduced to \hat{N}_K . Thus, the field amplitude is determined by $N_K = nK$, the intensity depends on $\langle \hat{D}^* \hat{D} \rangle = \langle \hat{N}_K^2 \rangle$, while $R = (\Delta N_K)^2$ gives the atom number variance at K sites, which reflects the total and partial noise suppression in Figs. 7.2(b) and 7.2(c), since $\langle N_K \rangle$ fluctuates for $K < M$. In diffraction minima, the field is zero, but the intensity is proportional to $\langle \hat{n}^2 \rangle - \langle \hat{n}_a \hat{n}_b \rangle$. Under scattering of spatially incoherent light, the intensity is isotropic and proportional to $\langle \hat{n}^2 \rangle$.

So, in optical experiments, varying the geometry, the global statistics of K sites, local single-site statistics, and pair correlations can be obtained even without a single-site access. Thus, light scattering gives a way to distinguish between atomic states. As shown by Eq. (7.7) and Fig. 7.2, MI and SF_M states are different in diffraction minima and in incoherent light. They are indistinguishable in maxima. SF_M and coherent states differ in maxima only. MI and coherent state are different at any angles.

The noise quantity or photon statistics are different in orders of N_K for various states. Nevertheless, for large N_K , there could be practical problems to subtract large values in a

maximum. In Refs. [6], this even led to a conclusion about the state indistinguishability by intensity measurements. In contrast to homogeneous BECs, in lattices, this problem has a natural solution: measurements outside maxima are free of the strong classical-like part of scattering and thus directly reflect fluctuations.

A classical analogy of different light scattering consists in different density fluctuations. A quantum treatment gives a deeper insight. Superfluid state is a superposition of all possible multisite Fock states giving distributions of N atoms at M sites. Various Fock states become entangled to scattered light of different phases and amplitudes. In contrast to a classical case (and MI with the only multisite Fock state), light fields entangled to various distributions do not interfere with each other due to the orthogonality of the Fock states. This reflects the which way information and explains the zero amplitude but nonzero photon number in a diffraction minimum.

If at least one of the modes is a standing wave, the angle dependences become much richer. Besides new classical maxima given by $\alpha_{\pm} = k_{0x}d \sin \theta_0 \pm k_{1x}d \sin \theta_1$, the second, “noise,” term in Eqs. (7.5a) and (7.5b) is also not isotropic. It includes a sum of the geometric coefficients squared, which is equivalent to effective doubling of the lattice period (or light frequency doubling) leading to new features at angles, where classical diffraction predicts zero. In Fig. 7.3, a case of two standing waves is shown. Due to the effective period doubling (given by $2\alpha_{0,1} = 2k_{0,1x}d \sin \theta_{0,1}$ and $2\alpha_{\pm}$), new features at the angles of, e.g., effective first-order maxima appear, though classically only the zero-order maxima are still possible.

The angle dependence of the photon number variance $(\Delta n_{\text{ph}})^2$ determined by $(\Delta |D|^2)^2$ shows anisotropic features due to “period doubling” even for two traveling waves. For the coherent state, the light at a maximum displays strong noise $[(\Delta |D|^2)^2 = 4N_K^3 + 6N_K^2 + N_K]$ because $\langle |\hat{D}|^4 \rangle = N_K^4 + 6N_K^3 + 7N_K^2 + N_K$ and $\langle |\hat{D}|^2 \rangle = N_K^2 + N_K$, stronger than the isotropic component (N_K^2 in highest order of N_K) and new features at $\theta_1 = \pm\pi/2$ (for $\theta_0 = 0$, $2N_K^2$ in highest order of N_K). In SF_M , the noise at maxima can be suppressed, while at other angles it is nearly equal to that of the coherent state. In MI, $(\Delta |D|^2)^2 = 0$. Distinguishing between atomic states by light statistics is similar to that by the intensity.

In summary, we have shown that atomic quantum states can be nondestructively monitored by measuring scattered light. In contrast to homogeneous BECs, scattering from lattices exhibits advantageous properties: suppression of the classical scattering in Bragg minima, access to local and nonlocal correlations, angular distributions richer than classical diffraction. Also other optical phenomena and quantities depending nonlinearly on the atom number operators will reflect quantum atom statistics [16, 17], e.g., the dispersion of a medium will provide a spectral method of quantum state characterization. Exploiting quantum properties of light should be applicable to other Bragg spectroscopy setups.

Support by: Austrian Science Fund (P17709, S1512).

Bibliography

- [1] D. Jaksch *et al.*, Phys. Rev. Lett. **81**, 3108 (1998); I. Bloch, Nat. Phys. **1**, 23 (2005).
- [2] S. Fölling *et al.*, Nature **434**, 481 (2005); E. Altman, E. Demler, and M. Lukin, Phys. Rev. A **70**, 013603 (2004).

- [3] J. Stenger *et al.*, Phys. Rev. Lett. **82**, 4569 (1999).
- [4] T. Stöferle *et al.*, Phys. Rev. Lett. **92**, 130403 (2004).
- [5] L. You, M. Lewenstein, and J. Cooper, Phys. Rev. A **51**, 4712 (1995).
- [6] J. I. Cirac, M. Lewenstein, and P. Zoller, Phys. Rev. Lett. **72**, 2977 (1994); Z. Idziaszek, K. Rzazewski, and M. Lewenstein, Phys. Rev. A **61**, 053608 (2000).
- [7] J. Javanainen and J. Ruostekoski, Phys. Rev. A **52**, 3033 (1995); Phys. Rev. Lett. **91**, 150404 (2003).
- [8] M. G. Moore, O. Zobay, and P. Meystre, Phys. Rev. A **60**, 1491 (1999).
- [9] A. Öttl *et al.*, Phys. Rev. Lett. **95**, 090404 (2005); I. Teper, Y. Lin, and V. Vuletic, *ibid.* **97**, 023002 (2006).
- [10] T. Volz *et al.*, Nat. Phys. **2**, 692 (2006); K. Winkler *et al.*, Nature **441**, 853 (2006).
- [11] M. Kira and S. W. Koch, Phys. Rev. A **73**, 013813 (2006).
- [12] J. Kasprzak *et al.*, Nature **443**, 409 (2006).
- [13] C. Maschler and H. Ritsch, Phys. Rev. Lett. **95**, 260401 (2005).
- [14] S. Slama *et al.*, Phys. Rev. Lett. **94**, 193901 (2005); Phys. Rev. A **73**, 023424 (2006).
- [15] P. Domokos and H. Ritsch, Phys. Rev. Lett. **89**, 253003 (2002); A. Black, J. Thompson, and V. Vuletic, J. Phys. B **38**, S605 (2005).
- [16] After having finished this work, we became aware of a related research of P. Meystre. We are grateful for sending us the preprint quant-ph/0610029 and discussions.
- [17] I. Mekhov, C. Maschler, and H. Ritsch, in *Books of abstracts for XX Int. Conference on Atomic Physics, ICAP, Innsbruck, 2006*, p. 309 and conference web-site.

CHAPTER 8

PUBLICATION

Light Scattering from Ultracold Atoms in Optical Lattices as an Optical Probe of Quantum Statistics[†]

quant-ph/0702193 (accepted for publication in Physical Review A)

I. B. Mekhov^{1,2}, C. Maschler¹, and H. Ritsch¹

*1) Institut für theoretische Physik, Universität Innsbruck,
A-6020 Innsbruck, Austria*

*2) St. Petersburg State University, V. A. Fock Institute of Physics,
St. Petersburg, Russia*

We study off-resonant collective light scattering from ultracold atoms trapped in an optical lattice. Scattering from different atomic quantum states creates different quantum states of the scattered light, which can be distinguished by measurements of the spatial intensity distribution, quadrature variances, photon statistics, or spectral measurements. In particular, angle-resolved intensity measurements reflect global statistics of atoms (total number of radiating atoms) as well as local statistical quantities (single-site statistics even without an optical access to a single site) and pair correlations between different sites. As a striking example we consider scattering from transversally illuminated atoms into an optical cavity mode. For the Mott insulator state, similar to classical diffraction, the number of photons scattered into a cavity is zero due to destructive interference, while for the superfluid state it is nonzero and proportional to the number of atoms. Moreover, we demonstrate that light scattering into a standing-wave cavity has a nontrivial angle dependence, including the appearance of narrow features at angles, where classical diffraction predicts zero.

8.1 Introduction

Ever since the first generation of Bose-Einstein condensates (BEC), it has been a central task to study quantum properties of such degenerate gases. Surprisingly, it turned out that many properties are well explained by the Gross-Pitaevskii equation, which is an effective nonlinear single-particle equation and allows to calculate the evolution of the average atomic

[†]The primary contribution of the author of the present thesis performed to this publication was the installation of the model and the calculation of certain generic examples and statistical quantities (cf. Sections 8.5 and 8.6). He also acted as a discussion partner on all other aspects of the work.

density and phase. The density can be observed by simple absorption images after expansion, and the phase can be mapped onto density modulations in interferometric setups. The limited validity of such mean-field descriptions became apparent with the advent of optical lattices [1, 2], where one has quantum phase transitions between states of similar average density but radically different quantum fluctuations.

The majority of methods to characterize quantum properties of degenerate gases are based on matter-wave interference between atoms released from a trap in time-of-flight measurements [2–4], which destroys the system. Recently, a method of “Bragg spectroscopy” based on stimulated scattering of matter waves by laser pulses was applied to homogeneous BECs [5, 6] and atoms in lattices [7–10]. In this case, the measured quantities (e.g. structure factor), which carry information about density fluctuations, are also accessible via matter-wave interference. Although the scattered light and stimulated matter waves can be entangled and mutually carry the statistical information [11, 12], the laser fields are simply considered as a tool to stimulate matter waves.

In contrast to those works, the nondestructive methods based on measurements of light fields only, without destroying atoms, were proposed in Refs. [13–22] for homogeneous BECs in traps and optical lattices [23]. Here the average amplitude of the scattered light is solely determined by the average atomic density, while the photon number and other higher order field expectation values contain quantum statistical properties of atoms.

In this paper, we show that this is of even greater significance for atoms in lattices, where different quantum phases show qualitatively distinct light scattering [24]. In particular, linear scattering can create entangled states of light and manybody atomic states, exhibiting a nontrivial connection of the field amplitude and intensity. As a practical consequence, we demonstrate the possibility to distinguish between different quantum phases, e.g., Mott insulator (MI) and superfluid (SF), by measuring properties of a scattered off-resonant beam. This possibility is exhibited in several different ways involving simple intensity measurements, or more involved measurements of quadrature variances, photon statistics, as well as phase-sensitive or spectral measurements. A careful analysis of the scattered light provides information about global statistics (related to atom number at a lattice region illuminated by the probe), local quantities (reflecting statistics at a single site even without an optical single-site access), and pair correlations between different sites.

Note that we consider off-resonant and almost nondestructive light scattering, which in principle can be repeatedly or even continuously applied to the same sample. This is very different from noise spectroscopy in absorption images [3] where observations of quantum fluctuations of the atomic density were recently reported.

For homogeneous BECs [13–22], the scattered light was shown to consist of two contributions: the strong classical part insensitive to atomic fluctuations, and weaker one, which carries information about atom statistics. For a large atom number, the classical part completely dominates the second one, which, in some papers, even led to a conclusion about the impossibility of distinguishing between different atomic states by intensity measurements, and, hence, to a necessity to measure photon statistics.

In our work, we show that light scattering from atoms in optical lattices has essentially different and advantageous characteristics in contrast to scattering from homogeneous BECs. For example, the problem of suppressing the strong classical part of scattering has a natural

solution: in the directions of classical diffraction minima, the expectation value of the light amplitude is zero, while the intensity (photon number) is nonzero and therefore directly reflects density fluctuations. Furthermore, in an optical lattice, the signal is sensitive not only to the periodic density distribution, but also to the periodic distribution of density fluctuations, giving an access to even very small nonlocal pair correlations, which is possible by measuring light in the directions of diffraction maxima.

As free space light scattering from a small sample can be weak, it might be selectively enhanced by a cavity. The corresponding light scattering from an optical lattice exhibits a complicated angle dependence and narrow angle-resolved features appear at angles, where classical diffraction cannot exist. In experiments, such a nontrivial angle dependence can help in the separation between the signal reflecting atom statistics from a technical noise.

Joining the paradigms of two broad fields of quantum physics, cavity quantum electrodynamics (QED) and ultracold gases, will enable new investigations of both light and matter at ultimate quantum levels, which only recently became experimentally possible [25, 26]. Here we predict effects accessible in such novel setups.

Experimentally, diffraction (Bragg scattering) of light from classical atoms in optical lattices was considered, for example, in Refs. [27–29]. In our work, we are essentially focused on the properties of scattering from ultracold lattice atoms with quantized center-of-mass motion.

The paper is organized as follows. In Sec. II, a general theoretical model of light scattering from atoms in an optical lattice is developed taking into account atom tunneling between neighboring sites. In Sec. III, we significantly reduce the model to the case of a deep lattice and give a classical analogy of light diffraction on a quantum lattice. Section IV presents a relation between atom statistics and different characteristics of scattered light: intensity and amplitude, quadratures, photon statistics, and phase-sensitive and spectral characteristics. Properties of different atomic states are summarized in Sec. V.

In Sec. VI, we present a simple example of the model developed: light scattering from a lattice in an optical cavity pumped orthogonally to the axis. The main results are discussed in Sec. VII and summarized in Sec. VIII.

8.2 General model

We consider an ensemble of N two-level atoms in an optical lattice with M sites. Except the presence of a trapping lattice potential, atoms are illuminated by and scatter field modes at different directions. A possible experimental realization is shown in Fig. 8.1. Here, a lattice is illuminated by a “pump” beam, whereas measurements are carried out in one of the scattered modes, which is treated as a “probe.” Note that different experimental setups are possible: the modes can be either in free space, or selected by traveling- or standing-wave cavities, or even correspond to different modes of the same cavity. For definiteness, we will consider the case, where mode functions are determined by cavities, whose axes directions can be varied with respect to the lattice axis (the simplest case of two standing-wave cavities at angles θ_0 and θ_1 is shown in Fig. 8.1). Instead of varying the angles, the mode wavelengths can be varied with respect to the wavelength of a trapping beam. We also assume, that not all M

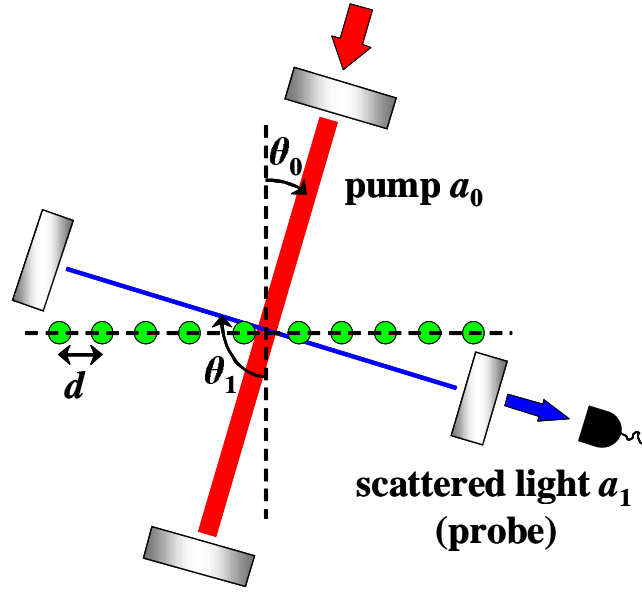


Figure 8.1. (Color online) Setup. Atoms in a lattice are illuminated by a pump wave at angle θ_0 ; scattered (probe) light is collected by a cavity at angle θ_1 and measured by a detector.

lattice sites are necessarily illuminated by additional modes, but some region with $K \leq M$ sites.

The manybody Hamiltonian in the second quantized form is given by

$$H = H_f + H_a, \quad (8.1a)$$

$$H_f = \sum_l \hbar \omega_l a_l^\dagger a_l - i \hbar \sum_l (\eta_l^* a_l - \eta_l a_l^\dagger), \quad (8.1b)$$

$$H_a = \int d^3 \mathbf{r} \Psi^\dagger(\mathbf{r}) H_{a1} \Psi(\mathbf{r}) + \frac{2\pi a_s \hbar^2}{m} \int d^3 \mathbf{r} \Psi^\dagger(\mathbf{r}) \Psi^\dagger(\mathbf{r}) \Psi(\mathbf{r}) \Psi(\mathbf{r}). \quad (8.1c)$$

In the field part of the Hamiltonian H_f , a_l are the annihilation operators of light modes with the frequencies ω_l , wave vectors \mathbf{k}_l , and mode functions $u_l(\mathbf{r})$, which can be pumped by coherent fields with amplitudes η_l . In the atom part, H_a , $\Psi(\mathbf{r})$ is the atomic matter-field operator, a_s is the s -wave scattering length characterizing the direct interatomic interaction, and H_{a1} is the atomic part of the single-particle Hamiltonian H_1 , which in the rotating-wave and dipole approximation has a form

$$H_1 = H_f + H_{a1}, \quad (8.2a)$$

$$H_{a1} = \frac{\mathbf{p}^2}{2m_a} + \frac{\hbar \omega_a}{2} \sigma_z - i \hbar g_0 \sum_l [\sigma^+ a_l u_l(\mathbf{r}) - \text{H. c.}] \quad (8.2b)$$

Here, \mathbf{p} and \mathbf{r} are the momentum and position operators of an atom of mass m_a and resonance frequency ω_a , σ^+ , σ^- , and σ_z are the raising, lowering, and population difference operators, g_0 is the atom–light coupling constant.

We will consider essentially nonresonant interaction where the light-atom detunings $\Delta_{la} = \omega_l - \omega_a$ are much larger than the spontaneous emission rate and Rabi frequencies $g_0 a_l$. Thus, in the Heisenberg equations obtained from the single-atom Hamiltonian H_1 (8.2), σ_z can be set to -1 (approximation of linear dipoles). Moreover, the polarization σ^- can be adiabatically eliminated and expressed via the fields a_l . An effective single-particle Hamiltonian that gives the corresponding Heisenberg equation for a_l can be written as $H_{1\text{eff}} = H_f + H_{a1}$ with

$$H_{a1} = \frac{\mathbf{p}^2}{2m_a} + V_{\text{cl}}(\mathbf{r}) + \hbar g_0^2 \sum_{l,m} \frac{u_l^*(\mathbf{r}) u_m(\mathbf{r}) a_l^\dagger a_m}{\Delta_{ma}}. \quad (8.3)$$

Here, we have also added a classical trapping potential of the lattice, $V_{\text{cl}}(\mathbf{r})$, corresponds to a strong classical standing wave. This potential can be, of course, derived from one of the modes $a_l = a_{\text{cl}}$ [in this case $V_{\text{cl}}(\mathbf{r}) = \hbar g_0^2 |a_{\text{cl}} u_{\text{cl}}(\mathbf{r})|^2 / \Delta_{\text{cla}}$], and it can scatter light into other modes. Nevertheless, at this point we will consider $V_{\text{cl}}(\mathbf{r})$ as an independent potential, which does not affect light scattering of other modes that can be significantly detuned from a_{cl} [i.e. the interference terms between a_{cl} and other modes are not considered in the last term of Eq. (8.3)]. The later inclusion of the light scattered by the trapping wave will not constitute a difficulty, due to the linearity of dipoles assumed in this model.

We will consider scattering of weak modes from the atoms in a deep lattice. So, the fields a_l are assumed much weaker than the field forming the potential $V_{\text{cl}}(\mathbf{r})$. To derive the generalized Bose–Hubbard Hamiltonian we expand the field operator $\Psi(\mathbf{r})$ in Eq. (8.1), using localized Wannier functions corresponding to $V_{\text{cl}}(\mathbf{r})$ and keeping only the lowest vibrational state at each site: $\Psi(\mathbf{r}) = \sum_{i=1}^M b_i w(\mathbf{r} - \mathbf{r}_i)$, where b_i is the annihilation operator of an atom at the site i with the coordinate \mathbf{r}_i . Substituting this expansion in Eq. (8.1) with H_{a1} (8.3), we get

$$H = H_f + \sum_{i,j=1}^M J_{i,j}^{\text{cl}} b_i^\dagger b_j + \hbar g_0^2 \sum_{l,m} \frac{a_l^\dagger a_m}{\Delta_{ma}} \left(\sum_{i,j=1}^K J_{i,j}^{lm} b_i^\dagger b_j \right) + \frac{U}{2} \sum_{i=1}^M b_i^\dagger b_i (b_i^\dagger b_i - 1), \quad (8.4)$$

where the coefficients $J_{i,j}^{\text{cl}}$ correspond to the quantum motion of atoms in the classical potential and are typical for the Bose-Hubbard Hamiltonian [1]:

$$J_{i,j}^{\text{cl}} = \int d\mathbf{r} w(\mathbf{r} - \mathbf{r}_i) \left(-\frac{\hbar^2 \nabla^2}{2m} + V_{\text{cl}}(\mathbf{r}) \right) w(\mathbf{r} - \mathbf{r}_j). \quad (8.5)$$

The coefficients $J_{i,j}^{lm}$ describe an additional contribution arising from the presence of light modes:

$$J_{i,j}^{lm} = \int d\mathbf{r} w(\mathbf{r} - \mathbf{r}_i) u_l^*(\mathbf{r}) u_m(\mathbf{r}) w(\mathbf{r} - \mathbf{r}_j). \quad (8.6)$$

In the last term of Eq. (8.4), only the on-site interaction was taken into account and $U = 4\pi a_s \hbar^2 / m_a \int d\mathbf{r} |w(\mathbf{r})|^4$.

As a usual approximation, we consider atom tunneling being possible only to the nearest neighbor sites. Thus, coefficients (8.5) do not depend on the site indices ($J_{i,i}^{\text{cl}} = J_0^{\text{cl}}$ and $J_{i,i\pm 1}^{\text{cl}} = J^{\text{cl}}$), while coefficients (8.6) are still index-dependent. The Hamiltonian (8.4) then reads

$$\begin{aligned} H = & H_f + J_0^{\text{cl}} \hat{N} + J^{\text{cl}} \hat{B} + \hbar g_0^2 \sum_{l,m} \frac{a_l^\dagger a_m}{\Delta_{ma}} \left(\sum_{i=1}^K J_{i,i}^{lm} \hat{n}_i \right) \\ & + \hbar g_0^2 \sum_{l,m} \frac{a_l^\dagger a_m}{\Delta_{ma}} \left(\sum_{\langle i,j \rangle} J_{i,j}^{lm} b_i^\dagger b_j \right) + \frac{U}{2} \sum_{i=1}^M \hat{n}_i (\hat{n}_i - 1), \end{aligned} \quad (8.7)$$

where $\langle i, j \rangle$ denotes the sum over neighboring pairs, $\hat{n}_i = b_i^\dagger b_i$ is the atom number operator at the i -th site, and $\hat{B} = \sum_{i=1}^M b_i^\dagger b_{i+1} + \text{H.c.}$ While the total atom number determined by $\hat{N} = \sum_{i=1}^M \hat{n}_i$ is conserved, the atom number at the illuminated sites, determined by $\hat{N}_K = \sum_{i=1}^K \hat{n}_i$, is not necessarily a conserved quantity.

The Heisenberg equations for a_l and b_i can be obtained from the Hamiltonian (8.7) as

$$\begin{aligned} \dot{a}_l = & -i \left(\omega_l + \frac{g_0^2}{\Delta_{la}} \sum_{i=1}^K J_{i,i}^{ll} \hat{n}_i + \frac{g_0^2}{\Delta_{la}} \sum_{\langle i,j \rangle} J_{i,j}^{ll} b_i^\dagger b_j \right) a_l - i g_0^2 \sum_{m \neq l} \frac{a_m}{\Delta_{ma}} \left(\sum_{i=1}^K J_{i,i}^{lm} \hat{n}_i \right) \\ & - i g_0^2 \sum_{m \neq l} \frac{a_m}{\Delta_{ma}} \left(\sum_{\langle i,j \rangle} J_{i,j}^{lm} b_i^\dagger b_j \right) + \eta \end{aligned} \quad (8.8a)$$

$$\begin{aligned} \dot{b}_i = & -\frac{i}{\hbar} \left(J_0^{\text{cl}} + \hbar g_0^2 \sum_{l,m} \frac{a_l^\dagger a_m}{\Delta_{ma}} J_{i,i}^{lm} + U \hat{n}_i \right) b_i - \frac{i}{\hbar} \left(J^{\text{cl}} + \hbar g_0^2 \sum_{l,m} \frac{a_l^\dagger a_m}{\Delta_{ma}} J_{i,i+1}^{lm} \right) b_{i+1} \\ & - \frac{i}{\hbar} \left(J^{\text{cl}} + \hbar g_0^2 \sum_{l,m} \frac{a_l^\dagger a_m}{\Delta_{ma}} J_{i,i-1}^{lm} \right) b_{i-1}. \end{aligned} \quad (8.8b)$$

In Eq. (8.8a) for the electromagnetic fields a_l , two last terms in the parentheses correspond to the phase shift of the light mode due to nonresonant dispersion (the second term) and due to tunneling to neighboring sites (the third one). The second term in Eq. (8.8a) describes scattering of all modes into a_l , while the forth term takes into account corrections to such scattering associated with tunneling due to the presence of additional light fields. In Eq. (8.8b) for the matter field operators b_i , the first term gives the phase of the matter-field at the site i , the second and third terms describe the coupling to neighboring sites.

It is important to underline that except for the direct coupling between neighboring sites, which is usual for the standard Bose–Hubbard model, Eqs. (8.8) also take into account long-range correlations between sites, which do not decrease with the distance and are provided by the common light modes a_l that are determined by the whole set of matter-field operators b_i .

8.3 Scattering from a deep lattice and classical analogy

We will significantly reduce the general model described by the Hamiltonian (8.7) and Heisenberg equations (8.8). In contrast to our previous paper [30] and works on so-called “Bragg spectroscopy” [7–10], we will not consider excitations of the lattice by light and stimulation of matter waves. The focus of the present paper is a study of properties of light scattered from the atoms in a prescribed quantum state, which is not necessarily the ground one. The main result is the demonstration of the possibility to distinguish between different atomic quantum states of different statistics by measuring light only.

We consider a very deep lattice formed by a strong classical potential $V_{\text{cl}}(\mathbf{r})$, so that the overlap between Wannier functions in Eqs. (8.5) and (8.6) is small and tunneling between neighboring sites is impossible ($J^{\text{cl}} = 0$ and $J_{i,j}^{\text{lm}} = 0$ for $i \neq j$). The on-site coefficients $J_{i,i}^{\text{lm}}$ (8.6) can be then approximated as $J_{i,i}^{\text{lm}} = u_l^*(\mathbf{r}_i)u_m(\mathbf{r}_i)$ neglecting details of the atomic localization, which are accessible even from the classical consideration [27–29].

For simplicity, we will consider scattering of a single classical mode a_0 (“pump”) considered as a given c-number quantity, into another mode a_1 with the relaxation rate κ included phenomenologically. The Heisenberg equation (8.8a) for the scattered light a_1 then reads

$$\dot{a}_1 = -i \left[\omega_1 + \frac{g_0^2}{\Delta_{1a}} \sum_{i=1}^K |u_1(\mathbf{r}_i)|^2 \hat{n}_i \right] a_1 - i \frac{g_0^2 a_0}{\Delta_{0a}} \left[\sum_{i=1}^K u_1^*(\mathbf{r}_i) u_0(\mathbf{r}_i) \hat{n}_i \right] - \kappa a_1 + \eta_1, \quad (8.9)$$

where we do not add the Langevin noise term, since we will be interested in normal ordered quantities only. In the Heisenberg equation for the matter-field operators b_i (8.8b), only the first term is nonzero. This term affects only the phase of the matter field, but not the atom number operators $\hat{n}_i = b_i^\dagger b_i$. Hence, though the the matter-field phase still depends on the common light mode, the operators \hat{n}_i , appearing in Eq. (8.9), are constant in time.

We assume that the dispersion shift of the cavity mode $g_0^2/\Delta_{1a} \sum_{i=1}^K |u_1(\mathbf{r}_i)|^2 \hat{n}_i$ is much smaller than κ or detuning between the pump and scattered light $\Delta_{01} = \omega_0 - \omega_1$. Thus, a stationary solution of Eq. (8.9) has a form

$$a_1 = C \hat{D}, \quad C \equiv -\frac{ig_0^2 a_0}{\Delta_{0a}(\kappa - i\Delta_{01})}, \quad (8.10a)$$

$$\hat{D} \equiv \sum_{i=1}^K u_1^*(\mathbf{r}_i) u_0(\mathbf{r}_i) \hat{n}_i, \quad (8.10b)$$

where we have also assumed no additional pumping ($\eta_1 = 0$) and replaced the operators $a_{0,1}(t)$ by their slowly varying envelopes $\tilde{a}_{0,1}(t)$ [$a_{0,1}(t) = \tilde{a}_{0,1} \exp(-i\omega_0 t)$] skipping in the following notations all tilde signs.

This expressing the light operators in terms of the atomic ones in Eq. (8.10) is a central result here, which we will use to study the properties of the scattered field.

In the following, we will consider a 1D lattice of the period d with atoms trapped at $x_m = md$ ($m = 1, 2, \dots, M$). The result for the field operator a_1 (8.10a) with the operator \hat{D}

(8.10b) has an analogy in classical diffraction. For scattering of a traveling wave a_0 in the direction of a traveling wave a_1 from a lattice with $\langle \hat{n}_i \rangle = n$ at each site, the expectation value of the field is given by

$$\langle a_1 \rangle = C \langle \hat{D} \rangle = C \sum_{m=1}^K e^{im\delta k_x d} \langle \hat{n}_m \rangle = C n e^{i(K+1)\alpha_-/2} \frac{\sin(K\alpha_-/2)}{\sin(\alpha_-/2)}, \quad (8.11)$$

where $\alpha_- = \delta k_x d$, and $\delta k_x = (\mathbf{k}_0 - \mathbf{k}_1)_x = k(\sin \theta_0 - \sin \theta_1)$ is the projection of the difference between two wave vectors on the lattice direction, $\theta_{0,1}$ are the angles between wave vectors and a vector normal to the lattice direction (cf. Fig. 8.1), $k = \omega/c$ for $\omega_0 = \omega_1 = \omega$.

Equation (8.11) simply describes classical diffraction of the traveling wave a_0 on a diffraction grating formed by equally spaced atoms with positions of diffraction maxima and minima (i.e. scattering angles θ_1) determined by the parameter α_- depending on the geometry of incident and scattered waves and diffraction grating through θ_0 , $|\mathbf{k}_{0,1}|$, and d . A more general form of the operator \hat{D} given by Eq. (8.10b) describes also diffraction of a standing wave a_0 into another mode a_1 , which can be formed, for example, by a standing-wave or ring optical cavity.

Equation (8.11) shows that the expectation value of the scattered field is sensitive only to the mean number of atoms per site n and reflects a direct analogy of light scattering from a classical diffraction grating. Nevertheless, the photon number (intensity) and photon statistics of the field a_1 are sensitive to higher moments of the number operators \hat{n}_i as well as to the quantum correlations between different lattice sites, which determines quantum statistical properties of ultracold atoms in an optical lattice and will be considered in the next sections.

8.4 Relation between quantum statistics of atoms and characteristics of scattered light

8.4.1 Probing quantum statistics by intensity and amplitude measurements

According to Eq. (8.10a), the expectation value of the photon number $a_1^\dagger a_1$ is proportional to the expectation value of the operator $\hat{D}^* \hat{D}$. We introduce coefficients $A_i(\theta_0, \theta_1)$ responsible for the geometry of the problem:

$$\begin{aligned} \hat{D} &= \sum_{i=1}^K A_i \hat{n}_i, \quad A_i(\theta_0, \theta_1) \equiv u_1^*(\mathbf{r}_i) u_0(\mathbf{r}_i), \\ A(\theta_0, \theta_1) &\equiv \sum_{i=1}^K A_i(\theta_0, \theta_1), \end{aligned} \quad (8.12)$$

where $u_{0,1}(\mathbf{r}_m) = \exp(imk_{0,1x}d + \phi_{0,1m})$ for traveling waves, and $u_{0,1}(\mathbf{r}_m) = \cos(mk_{0,1x}d + \phi_{0,1m})$ for standing waves ($m = 1, 2, \dots, M$), $k_{0,1x} = |\mathbf{k}_{0,1}| \sin \theta_{0,1}$, $\theta_{0,1}$ are the angles between

mode wave vectors and a vector normal to the lattice axis; in the plane-wave approximation, additional phases $\phi_{0,1m}$ are m -independent.

The expectation values of \hat{D} and $\hat{D}^*\hat{D}$ then read

$$\langle \hat{D} \rangle = \sum_{i=1}^K A_i \langle \hat{n}_i \rangle = nA, \quad (8.13a)$$

$$\langle \hat{D}^* \hat{D} \rangle = \sum_{i,j=1}^K A_i^* A_j \langle \hat{n}_i \hat{n}_j \rangle \quad (8.13b)$$

$$= \langle \hat{n}_a \hat{n}_b \rangle |A|^2 + (\langle \hat{n}^2 \rangle - \langle \hat{n}_a \hat{n}_b \rangle) \sum_{i=1}^K |A_i|^2, \quad (8.13c)$$

$$R(\theta_0, \theta_1) \equiv \langle \hat{D}^* \hat{D} \rangle - |\langle \hat{D} \rangle|^2 \\ = (\langle \hat{n}_a \hat{n}_b \rangle - n^2) |A|^2 + (\langle \hat{n}^2 \rangle - \langle \hat{n}_a \hat{n}_b \rangle) \sum_{i=1}^K |A_i|^2 \quad (8.13d)$$

$$= \langle \delta \hat{n}_a \delta \hat{n}_b \rangle |A|^2 + (\langle \delta \hat{n}^2 \rangle - \langle \delta \hat{n}_a \delta \hat{n}_b \rangle) \sum_{i=1}^K |A_i|^2. \quad (8.13e)$$

In Eqs. (8.13) we have used the following assumptions about the atomic quantum state $|\Psi\rangle$: (i) the expectation values of the atom number at all sites are the same, $\langle \hat{n}_i \rangle = n$, (ii) the nonlocal pair correlations between atom numbers at different sites $\langle \hat{n}_i \hat{n}_j \rangle$ are equal to each other for any $i \neq j$ and will be denoted as $\langle \hat{n}_a \hat{n}_b \rangle$ (with $a \neq b$). The latter assumption is valid for a deep lattice. We also introduced the fluctuation operators $\delta \hat{n}_i = \hat{n}_i - n$, which gives $\langle \delta \hat{n}^2 \rangle$ equal to the variance $(\Delta n_i)^2 = \langle \hat{n}_i^2 \rangle - n^2$.

Equation (8.13a) reflects the fact that the expectation value of the field amplitude (8.10a) is sensitive only to the mean atom numbers and displays the angle dependence of classical diffraction given by the factor $A(\theta_0, \theta_1)$, which depends on the mode angles and displays pronounced diffraction maxima and minima. Equation (8.13b) shows that the number of scattered photons (intensity) at some angle is determined by the density–density correlations. In the simplest case of two traveling waves, the prefactors $A_i^* A_j = \exp[i\delta k_x(x_j - x_i)]$ with $\delta k_x = k_{0x} - k_{1x}$. In this case, Eq. (8.13b) gives the so-called structure factor (function), which was considered in the works on light scattering from homogeneous BEC [17, 18]. Here we essentially focus on optical lattices. Moreover, it will be shown, that the more general Eq. (8.13b), which includes scattering of standing waves, contains new measurable features different from those of a usual structure factor.

Equation (8.13c) shows, that the angle dependence of the scattered intensity consists of two contributions. The first term has an angle dependence $|A(\theta_0, \theta_1)|^2$ identical to that of the expectation value of the field amplitude squared (8.13a). The second term is proportional to the quantity $\langle \hat{n}^2 \rangle - \langle \hat{n}_a \hat{n}_b \rangle$ giving quantum fluctuations and has a completely different angle dependence $\sum_{i=1}^K |A_i|^2$. The expression (8.13c) has a form similar to the one considered in papers [13, 15, 16] on light scattering from a homogeneous BEC, where the scattered intensity consisted of two parts: “coherent” (i.e. depending on the average density) and “incoherent” one (i.e. depending on the density fluctuations). Nevertheless, in the present case of a

periodic lattice, this similarity would be exact only in a particular case where there are no nonlocal pair correlations $\langle \hat{n}_a \hat{n}_b \rangle = n_a n_b = n^2$ ($\langle \delta \hat{n}_a \delta \hat{n}_b \rangle = 0$), which in general is not true and leads to observable difference between states with and without pair correlations.

Further insight into a physical role of nonlocal pair correlations can be obtained from Eqs. (8.13d) and (8.13e) for the “noise quantity” $R(\theta_0, \theta_1) \equiv \langle \hat{D}^* \hat{D} \rangle - |\langle \hat{D} \rangle|^2$, where we have subtracted the classical (averaged) contribution $|\langle \hat{D} \rangle|^2$ to the intensity $\langle \hat{D}^* \hat{D} \rangle$. Equation (8.13e) shows that, in the noise quantity, a term with the classical angular distribution $|A(\theta_0, \theta_1)|^2$ appears only if the pair correlations are nonzero. The physical meaning of this result is that, in an optical lattice, it is not only the density distribution that displays spatial periodic structure leading to diffraction scattering, but also the distribution of number fluctuations themselves. In the framework of our assumption about equal pair correlations, the spatial distribution of fluctuations $\langle \delta \hat{n}_a \delta \hat{n}_b \rangle$ can be either the same as the density distribution (with a lattice period d) or zero. In the former case, pair correlations contribute to the first term in Eqs. (8.13d) and (8.13e) with classical distribution $|A(\theta_0, \theta_1)|^2$, in the latter case, $\langle \delta \hat{n}_a \delta \hat{n}_b \rangle = 0$, and the only signal in the noise quantity is due to on-site fluctuations $\langle \delta \hat{n}^2 \rangle$ with a different angle dependence $\sum_{i=1}^K |A_i|^2$. Note that, in general, the spatial distribution of fluctuations can be different from that of the average density and can have a period proportional to the lattice period d . This will lead to additional peaks in the angular distribution of the noise quantity (8.13d), (8.13e). The generalization of those formulas is straightforward.

Even with spatially incoherent pump a_0 , the intensity of the scattered mode $a_1^\dagger a_1$ is sensitive to the on-site atom statistics. To model this situation, the quantum expectation value $\langle \hat{D}^* \hat{D} \rangle$ (8.13b) should be additionally averaged over random phases $\phi_{0,1m}$ appearing in the definition of mode functions in Eq. (8.12). In Eq. (8.13b), only terms with $i = j$ will then survive and the final result reads

$$\langle \hat{D}^* \hat{D} \rangle_{\text{inc}} = p_0 K \langle \hat{n}^2 \rangle, \quad (8.14)$$

where p_0 is equal to 1 for two traveling waves, 1/2 for a configuration with one standing wave, and 1/4, when both modes $a_{0,1}$ are standing waves.

8.4.2 Quadrature measurements

The photon number $a_1^\dagger a_1$ is determined by the expectation value $\langle \hat{D}^* \hat{D} \rangle$, whereas $\langle \hat{D} \rangle$ gives the field $\langle a_1 \rangle$ (8.10a). While photon numbers can be directly measured, a field $\langle a_1 \rangle$ measurement requires a homodyne scheme. Such a measurement then makes $\langle \hat{D} \rangle$ experimentally accessible. Actually for a quantum field only the expectation values of quadratures of a_1 that are Hermitian operators and can be measured. Using Eq. (8.10a) and the commutation relation $[a_1, a_1^\dagger] = 1$, the quadrature operator X_ϕ and its variance $(\Delta X_\phi)^2$ can be written as

$$X_\phi \equiv \frac{1}{2} (a_1 e^{-i\phi} + a_1^\dagger e^{i\phi}) = |C| \hat{X}_{\phi-\phi_C}^D, \quad (8.15a)$$

$$X_\phi^2 = \frac{1}{4} + |C|^2 (\hat{X}_{\phi-\phi_C}^D)^2, \quad (8.15b)$$

$$(\Delta X_\phi)^2 \equiv \langle X_\phi^2 \rangle - \langle X_\phi \rangle^2 = \frac{1}{4} + |C|^2 (\Delta X_{\phi-\phi_C}^D)^2, \quad (8.15c)$$

where $C = |C| \exp(i\phi_C)$ and the quadratures of \hat{D} are

$$\hat{X}_\beta^D \equiv \frac{1}{2} \left(\hat{D} e^{-i\beta} + \hat{D}^* e^{i\beta} \right), \quad (8.16a)$$

$$(\Delta X_\beta^D)^2 \equiv \langle (\hat{X}_\beta^D)^2 \rangle - \langle \hat{X}_\beta^D \rangle^2. \quad (8.16b)$$

In Eqs. (8.15), the phase ϕ is related to the homodyne reference phase, while ϕ_C is determined by the phase of the pump a_0 and parameters of the field-matter system [cf. Eq. (8.10a)]. Hence, the phase $\beta = \phi - \phi_C$ entering Eqs. (8.15) can be controlled by varying the phase difference between the pump and homodyne fields.

Using Eq. (8.12), the quadrature operator \hat{X}_β^D reads

$$\begin{aligned} \hat{X}_\beta^D &= \sum_{i=1}^K A_i^\beta \hat{n}_i, \quad A_i^\beta(\theta_0, \theta_1) \equiv |A_i| \cos(\phi_{A_i} - \beta), \\ A^\beta(\theta_0, \theta_1) &\equiv \sum_{i=1}^K A_i^\beta(\theta_0, \theta_1), \end{aligned} \quad (8.17)$$

where $A_i = |A_i| \exp(i\phi_{A_i})$, and we defined new quantities $A_i^\beta(\theta_0, \theta_1)$ and $A^\beta(\theta_0, \theta_1)$.

Since Eq. (8.17) for \hat{X}_β^D and Eq. (8.12) for \hat{D} have a similar structure, the Eqs. (8.13) for the quantities $\langle \hat{D} \rangle$, $\langle \hat{D}^* \hat{D} \rangle$, and R can be rewritten for the quantities $\langle \hat{X}_\beta^D \rangle$, $\langle (\hat{X}_\beta^D)^2 \rangle$, and $(\Delta X_\beta^D)^2$, respectively, with the change of parameters $A_i(\theta_0, \theta_1)$ and $A(\theta_0, \theta_1)$ to $A_i^\beta(\theta_0, \theta_1)$ and $A^\beta(\theta_0, \theta_1)$. Thus, the above discussion of Eqs. (8.13) can be repeated in terms of the quadrature operators with the only difference that coefficients $A_i^\beta(\theta_0, \theta_1)$ and $A^\beta(\theta_0, \theta_1)$ now depend also on the homodyne phase. An advantage of this reformulation is that the expectation value of the non-Hermitian operator a_1 , which determines $\langle \hat{D} \rangle$, is now replaced by the expectation value of the Hermitian operator X_ϕ , which is consistent with a procedure of measuring quadratures of the quantum field a_1 .

8.4.3 Photon number fluctuations

While the intensity of the scattered light is sensitive to the second moments of the number operators \hat{n}_i , quantum statistics of the field reflexes the forth-order moments. The variance $(\Delta n_{\text{ph}})^2$ of the photon number $n_{\text{ph}} = a_1^\dagger a_1$ is given by

$$\begin{aligned} (\Delta n_{\text{ph}})^2 &= \langle n_{\text{ph}}^2 \rangle - \langle n_{\text{ph}} \rangle^2 =: (\Delta n_{\text{ph}}^2) : + \langle n_{\text{ph}} \rangle \\ &= |C|^4 (\langle \hat{D}^{*2} \hat{D}^2 \rangle - \langle \hat{D}^* \hat{D} \rangle^2) + |C|^2 \langle \hat{D}^* \hat{D} \rangle, \end{aligned} \quad (8.18)$$

where $(\Delta n_{\text{ph}}^2) := \langle a_1^{\dagger 2} a_1^2 \rangle - \langle a_1^\dagger a_1 \rangle^2 = |C|^4 (\langle \hat{D}^{*2} \hat{D}^2 \rangle - \langle \hat{D}^* \hat{D} \rangle^2)$ is a normal ordered photon-number variance. Thus, the problem is reduced to measurements of the photon number

$|C|^2 \langle \hat{D}^* \hat{D} \rangle$ and quantity $|C|^4 \langle \hat{D}^{*2} \hat{D}^2 \rangle$, which after straightforward calculations is given by

$$\begin{aligned}
\langle \hat{D}^{*2} \hat{D}^2 \rangle &= \left| \sum_{i=1}^K A_i \right|^4 \langle n_a n_b n_c n_d \rangle \\
&+ 2 \left[\left(\sum_{i=1}^K |A_i|^2 A_i \right) \sum_{i=1}^K A_i^* + \text{c.c.} \right] (2 \langle n_a n_b n_c n_d \rangle - 3 \langle n_a^2 n_b n_c \rangle + \langle n_a^3 n_b \rangle) \\
&+ \left[\left(\sum_{i=1}^K A_i^2 \right) \left(\sum_{i=1}^K A_i^* \right)^2 + \text{c.c.} \right] (-\langle n_a n_b n_c n_d \rangle + \langle n_a^2 n_b n_c \rangle) \\
&+ 2 \left(\sum_{i=1}^K |A_i|^2 \right)^2 (\langle n_a n_b n_c n_d \rangle - 2 \langle n_a^2 n_b n_c \rangle + \langle n_a^2 n_b^2 \rangle) \\
&+ \left| \sum_{i=1}^K A_i^2 \right|^2 (\langle n_a n_b n_c n_d \rangle - 2 \langle n_a^2 n_b n_c \rangle + \langle n_a^2 n_b^2 \rangle) \\
&+ 4 \left| \sum_{i=1}^K A_i \right|^2 \sum_{i=1}^K |A_i|^2 (-\langle n_a n_b n_c n_d \rangle + \langle n_a^2 n_b n_c \rangle) \\
&+ \sum_{i=1}^K |A_i|^4 (-6 \langle n_a n_b n_c n_d \rangle + 12 \langle n_a^2 n_b n_c \rangle - 4 \langle n_a^3 n_b \rangle - 3 \langle n_a^2 n_b^2 \rangle + \langle n^4 \rangle),
\end{aligned} \tag{8.19}$$

where we assumed again that correlations do not depend on site indices, and sites with the indices a , b , c , and d are different. In Eq. (8.19), each prefactor containing geometrical coefficients A_i (8.12) determines different angle dependences of a corresponding term.

Thus, varying the geometry of a problem (e.g. angles of two modes, wavelengths of the modes or that of trapping potential determining the lattice period), one has access to different statistical quantities characterizing the quantum state of ultracold atoms.

8.4.4 Phase-sensitive and spectral measurements

In the derivation of Eq. (8.10), we have neglected the term $g_0^2/\Delta_{1a} \sum_{i=1}^K |u_1(\mathbf{r}_i)|^2 \hat{n}_i$ in Eq. (8.9) related to the refractive index of atoms for the scattered light. This term is normally very small at large detunings. However, if the scattered mode is confined in a very good optical resonator, the light experiences a very long effective path within the atoms, and this term shifts the phase of the scattered light. In a steady state approximation it amounts to the dispersion shift of a cavity mode.

Equation (8.9) shows that even in the absence of the pump field ($a_0 = 0$), quantum fluctuations of the atom number enter the phase via operators \hat{n}_i of K illuminated sites, which depend on the atomic quantum state. In the simplest case of a traveling wave, $|u_1(\mathbf{r}_i)| = 1$, and the operator $\sum_{i=1}^K \hat{n}_i = \hat{N}_K$ is the number of atoms at K sites. As will be discussed below, in the Mott insulator state, the expectation value of this quantity $N_K = \langle \hat{N}_K \rangle$ does not fluctuate. In the superfluid state with $K = M$, N_M is equal to the total number of atoms N , and also is fixed. However for $K < M$, N_K fluctuates strongly and, as will be discussed,

for $K \ll M$ corresponds to a coherent state with $\langle \hat{N}_K^2 \rangle = \langle \hat{N}_K \rangle^2 + \langle \hat{N}_K \rangle$. Those statistical properties of the atomic states are reflected in the phase of the light field. In particular, measurements of the dispersion shift of a cavity mode will show a frequency distribution reflecting the distribution of atom numbers.

This also opens an alternative spectral method of determining the quantum state of the atoms in a cavity with two degenerate modes. Let us consider the mode a_0 as a dynamical quantity obeying an equation as Eq. (8.9), which can be obtained from the set of Eq. (8.8a), while the second degenerate mode is called a_1 . The atoms lead to the collective normal-mode splitting of two cavity modes as recently experimentally observed [31]. If the coupling coefficient between two degenerate modes, which is equal to $g_0^2/\Delta_{0a}\hat{D}$ [cf. Eq. (8.9) and the definition of the operator \hat{D} in Eq. (8.12)], exceeds the cavity relaxation rate κ , a spectral doublet instead of single maximum can be observed in the spectrum of the output light.

It is quite expected that the collective strong coupling between the modes and thus the spectral splitting depends on the number of atoms in a lattice. Interestingly, from the equations for a_0 and a_1 , it can be shown, that parameters of the normal-mode splitting (e.g. splitting frequency, linewidths) also depend on the atomic quantum state. So, spectral mode-splitting measurements also can be used to distinguish between atomic quantum phases and allow a nondestructive measurement of a quantum phase transition dynamics. In the following we will, however, restrict our study to single frequency measurements and leave a more detailed analysis of phase- and frequency-sensitive phenomena to other works [32].

8.5 Quantum statistical properties of typical atomic distributions

Let us briefly summarize some key statistical properties of typical states of N atoms at M lattice sites, i.e: the Mott insulator state (MI), superfluid state (SF), and a multisite coherent-state approximation to the SF state.

The MI state represents a simple product of local Fock states at each site with precisely n_i atoms at a site i . As a consequence, atom numbers at each site \hat{n}_i (as well as the number of atoms at K sites \hat{N}_K) do not fluctuate, and there is no quantum correlations between sites:

$$|\Psi_{\text{MI}}\rangle = \prod_{i=1}^M |n_i\rangle_i, \quad (8.20a)$$

$$\langle \hat{n}_i^2 \rangle_{\text{MI}} = n_i^2, \quad (8.20b)$$

$$(\Delta n_i)_{\text{MI}}^2 = 0, \quad (8.20c)$$

$$\langle \hat{N}_K^2 \rangle_{\text{MI}} = N_K^2, \quad (8.20d)$$

$$(\Delta \hat{N}_K)_{\text{MI}}^2 = 0, \quad (8.20e)$$

$$\langle \hat{n}_a \hat{n}_b \rangle_{\text{MI}} = n_a n_b, \quad (8.20f)$$

$$\langle \delta \hat{n}_a \delta \hat{n}_b \rangle_{\text{MI}} = 0, a \neq b. \quad (8.20g)$$

Similarly to Eq. (8.20f), (8.20g), all two-, three-, and four-site quantities in Eq. (8.19) factorize. From the light-scattering point of view, this is the most classical atomic state, which corre-

sponds to periodically ordered pointlike atoms. We will further consider the commensurate filling with $n_i = N/M$ atoms at each site.

The SF state corresponds to a BEC where each atom is in the zero quasi-momentum Bloch-state of the lowest band and is equally delocalized over all sites. Hence, the atom numbers at a given site (and the number of atoms at $K < M$ sites) fluctuate. As a consequence of the total atom number conservation, the numbers of particles at two different sites $a \neq b$ are anticorrelated.

$$|\Psi_{\text{SF}}\rangle = \frac{1}{\sqrt{N!}} \left(\frac{1}{\sqrt{M}} \sum_{i=1}^M b_i^\dagger \right)^N |0\rangle, \quad (8.21a)$$

$$\langle \hat{n}_i \rangle_{\text{SF}} = \frac{N}{M}, \quad (8.21b)$$

$$\langle \hat{n}_i^2 \rangle_{\text{SF}} = \frac{N(N-1)}{M^2} + \frac{N}{M}, \quad (8.21c)$$

$$(\Delta n_i)_{\text{SF}}^2 = \frac{N}{M} \left(1 - \frac{1}{M} \right), \quad (8.21d)$$

$$\langle \hat{N}_K \rangle_{\text{SF}} = K \frac{N}{M}, \quad (8.21e)$$

$$\langle \hat{N}_K^2 \rangle_{\text{SF}} = K^2 \frac{N(N-1)}{M^2} + K \frac{N}{M}, \quad (8.21f)$$

$$(\Delta N_K)_{\text{SF}}^2 = K \frac{N}{M} \left(1 - \frac{K}{M} \right), \quad (8.21g)$$

$$\langle \hat{n}_a \hat{n}_b \rangle_{\text{SF}} = \frac{N^2}{M^2} \left(1 - \frac{1}{N} \right), \quad (8.21h)$$

$$\langle \delta \hat{n}_a \delta \hat{n}_b \rangle_{\text{SF}} = -\frac{N}{M^2}. \quad (8.21i)$$

All two-, three-, and four-site quantities in Eq. (8.19) also do not factorize. The SF state (8.21a) is a superposition of all possible multisite Fock states of N atoms at M sites. The expectation values in the SF state can be calculated using normal ordering and the following relations:

$$b_i |\Psi_{\text{SF}}(N, M)\rangle = \sqrt{\frac{N}{M}} |\Psi_{\text{SF}}(N-1, M)\rangle, \quad (8.22a)$$

$$\langle \Psi_{\text{SF}} | b_i^{\dagger m} b_i^m | \Psi_{\text{SF}} \rangle = \frac{N(N-1)\dots(N-m+1)}{M^m}, \quad (8.22b)$$

where Eq. (8.22a) relates SFs with N and $N-1$ atoms.

We will introduce another, coherent, quantum state, which is often considered as an approximation to the SF state, and represents a product of local coherent states at each site. In this approximate state, the numbers of particles at a given site and at any $K \leq M$ sites fluctuate. Moreover, the total number of particles at M sites is also a fluctuating quantity, which is a disadvantage of this approximation. Similarly to the MI state, correlations between

several different sites are absent.

$$|\Psi_{\text{Coh}}\rangle = e^{-N/2} \prod_{i=1}^M e^{\sqrt{N/M} b_i^\dagger} |0\rangle_i, \quad (8.23a)$$

$$\langle \hat{n}_i \rangle_{\text{Coh}} = \frac{N}{M}, \quad (8.23b)$$

$$\langle \hat{n}_i^2 \rangle_{\text{Coh}} = \frac{N^2}{M^2} + \frac{N}{M}, \quad (8.23c)$$

$$(\Delta n_i)_{\text{Coh}}^2 = \frac{N}{M}, \quad (8.23d)$$

$$\langle \hat{N}_K \rangle_{\text{Coh}} = K \frac{N}{M}, \quad (8.23e)$$

$$\langle \hat{N}_K^2 \rangle_{\text{Coh}} = K^2 \frac{N^2}{M^2} + K \frac{N}{M}, \quad (8.23f)$$

$$(\Delta N_K)_{\text{Coh}}^2 = K \frac{N}{M}, \quad (8.23g)$$

$$\langle \hat{n}_a \hat{n}_b \rangle_{\text{Coh}} = \frac{N^2}{M^2}, \quad (8.23h)$$

$$\langle \delta \hat{n}_a \delta \hat{n}_b \rangle_{\text{Coh}} = 0, \quad (8.23i)$$

and we have

$$b_i |\Psi_{\text{Coh}}(N, M)\rangle = \sqrt{\frac{N}{M}} |\Psi_{\text{Coh}}(N, M)\rangle, \quad (8.24a)$$

$$\langle \Psi_{\text{Coh}} | b_i^{\dagger m} b_i^m | \Psi_{\text{Coh}} \rangle = \frac{N^m}{M^m}. \quad (8.24b)$$

Comparing Eqs. (8.21), (8.22) for the SF state and Eqs. (8.23), (8.24) for the coherent one, we can state that under the approximation $N, M \rightarrow \infty$, but finite N/M , the coherent state is a good approximation for local one-site quantities and correlations between different sites. Moreover, if $K \ll M$, the SF expectation values related to the nonlocal \hat{N}_K operator are also well approximated by corresponding quantities in the coherent state. Nevertheless, if the number of sites K is of the order of M , the coherent-state approximation fails for those quantities.

One can prove even a more general statement for the functions $\langle \hat{D}^* \hat{D} \rangle$ (8.13) and $\langle \hat{D}^{*2} \hat{D}^2 \rangle$ (8.19), which determine the intensity and statistics of light and are the most important quantities in this work. If the number of sites illuminated by light, K , is much smaller than the total number of lattice sites M , the coherent-state is a good approximation for calculating characteristics of scattered light in the limit $N, M \rightarrow \infty$, but finite N/M . If, in opposite, the number of sites interacting with light is of the order of the total number of sites in the lattice, this approximation, in general, gives wrong results. As will be shown, it fails for light scattering in the directions of diffraction maxima. The proof of the statement is based on the consideration of the orders of sums in Eqs. (8.13), (8.19), which contain geometrical coefficients A_i and are proportional to the powers of K , whereas factors containing atom fluctuations have powers of M in denominators.

Thus, light scattering from the region of a SF optical lattice with $K \ll M$ sites is equivalent to the light scattering from the atoms in the coherent state (in absolute values both

K and M can be very large). Moreover, in the directions outside diffraction maxima, the coherent-state approximation works well even in the case where any number of sites is illuminated.

In the following, discussing all states, we will use the notations $n = N/M$ for the atomic “density” (expectation value of the particle number at each site) and $N_K = KN/M = nK$ for the expectation value of the particle number at K sites. These two parameters fully characterize light scattering in the MI and coherent states, while all three parameters N , M , and K are necessary to characterize scattering in the SF phase. For definitiveness, we will discuss a case with large values of N , M , and K where difference between odd and even number of lattice sites vanishes. Nevertheless, note that physical problems including BECs with large atom number loaded into lattices with small site numbers are also of great importance [33, 34]. Results for this case, can be obtained from expressions of this section and Eqs. (8.13) and (8.19).

8.6 Example: 1D optical lattice in a transversally pumped cavity

Before considering a general angular distribution of scattered light, we would like to present the most striking prediction of our model describing the difference between atomic quantum states, observable by light scattering. Let us consider a configuration of Fig. 8.1 where the pump (traveling or standing wave) is orthogonal to the lattice ($\theta_0 = 0$), and the scattered light is collected along the lattice axis ($\theta_1 = \pi/2$) by a standing- or traveling-wave cavity. This geometry coincides with the one considered in the context of cavity cooling [35–37] and lattices in optical cavities [30]. Atoms are assumed to be trapped at each lattice site ($d = \lambda/2$) at field antinodes.

In this case, the operator \hat{D} (8.12) is reduced to $\sum_{k=1}^K (-1)^{k+1} \hat{n}_k$, which, independently on an atomic state, gives zero for the expectation value of the field amplitude proportional to $\langle \hat{D} \rangle$ (here we assume even K). This corresponds to the classical destructive interference between atoms separated by $\lambda/2$. In contrast, the photon number in a cavity $a_1^\dagger a_1$ is proportional to $\langle \hat{D}^* \hat{D} \rangle = (\langle \hat{n}^2 \rangle - \langle \hat{n}_a \hat{n}_b \rangle) K$ [cf. Eq. (8.13c)], which is determined by statistics of a particular state, and is equal to zero for the MI state and to N_K for the SF state.

Thus, atoms in a MI state scatter no photons into a cavity, while a SF scatters number of photons proportional to the atom number:

$$\langle a_1 \rangle_{\text{MI}} = \langle a_1 \rangle_{\text{SF}} = 0, \quad \text{but} \quad \langle a_1^\dagger a_1 \rangle_{\text{MI}} = 0, \quad \langle a_1^\dagger a_1 \rangle_{\text{SF}} = |C|^2 N_K. \quad (8.25)$$

Hence, already the mean photon number provides information about a quantum state of ultracold atoms.

The photon number fluctuations $(\Delta n_{\text{ph}})^2$ (8.18) are also different for various states. In the MI state, the variance $(\Delta |D|^2)^2 = \langle \hat{D}^{*2} \hat{D}^2 \rangle - \langle \hat{D}^* \hat{D} \rangle^2$ is zero, $(\Delta |D|^2)_{\text{MI}}^2 = 0$, whereas in the SF state, Eq. (8.19) gives a very strong noise $(\Delta |D|^2)_{\text{SF}}^2 = 2N_K^2$ (in highest order of N_K).

Nonlinear light-matter dynamics in a cavity can lead to a new self-organized phase [36, 38] where all atoms occupy only each second site leading to doubling of the lattice period, $d = \lambda$.

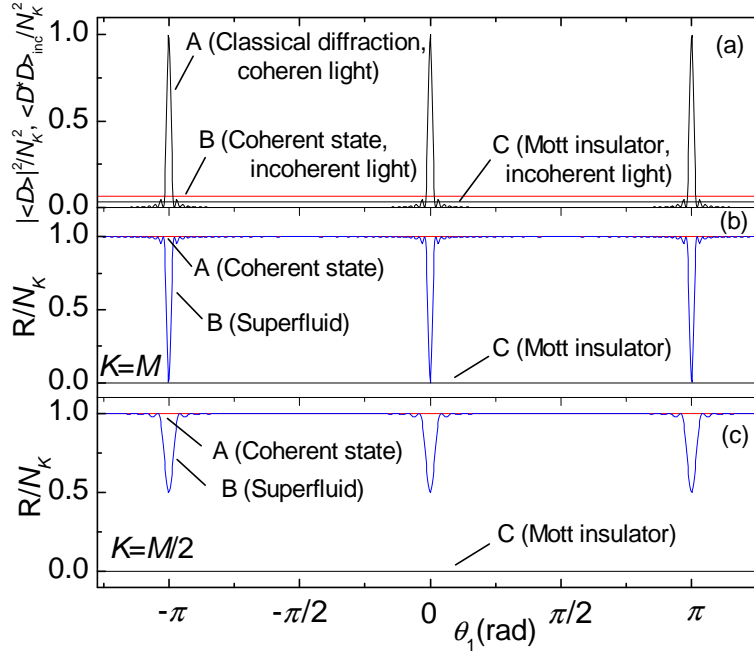


Figure 8.2. Intensity angular distributions for two traveling waves, the pump is transverse to the lattice ($\theta_0 = 0$). (a) Intensity of classical diffraction of coherent light (curve A), isotropic intensity of incoherent light scattering, Eq. (8.14), for coherent atomic state (line B) and MI state (line C); (b) noise quantity, Eq. (8.27), for coherent atomic state (constant value 1, line A), SF with all sites illuminated $K = M$ (curve B), and MI (constant value 0, line C); (c) the same as in (b) but for partially illuminated SF with $K = M/2$. $N = M = 30$.

The operator \hat{D} (8.12) is then reduced to $\sum_{k=1}^K \hat{n}_k = \hat{N}_K$. Thus, if the final self-organized state is a MI with $d = \lambda$, the photon number in a cavity is $\langle a_1^\dagger a_1 \rangle_{\text{Self-org}} = |C|^2 N_K^2$, which is proportional to the atom number squared and has a superradiant character. This result coincides with the theory of self-organization with classical center-of-mass motion [38].

8.7 Results and Discussion

In the following we will compare light scattering from atoms in the following states: MI, SF with all sites illuminated ($K = M$ using the notation SF_M), and partially illuminated SF under the approximation $N, M \rightarrow \infty$, finite $n = N/M$, $K \ll M$, which will be denoted as the “coherent” taking into account the equivalence proved in Sec. V. The results for the SF_K state with any K can be obtained from the general Eqs. (8.13), (8.19), and (8.21).

8.7.1 Two traveling waves and discussion of essential physics

For two traveling waves, which can be free-space modes or fixed by ring cavities, the geometrical coefficients (8.12) are $A_m = \exp(im\alpha_-)$ ($\alpha_- = k_{0x}d \sin \theta_0 - k_{1x}d \sin \theta_1$), and Eq. (8.13e) for the noise quantity is reduced to

$$R = \langle \delta \hat{n}_a \delta \hat{n}_b \rangle \frac{\sin^2(K\alpha_-/2)}{\sin^2(\alpha_-/2)} + (\langle \delta \hat{n}^2 \rangle - \langle \delta \hat{n}_a \delta \hat{n}_b \rangle)K, \quad (8.26)$$

where the first term has the angle dependence of classical diffraction (8.11), and the angle dependence in the second term in Eq. (8.13e) is reduced to a constant (isotropic) one, K . In the MI and coherent states, where pair correlations $\langle \delta \hat{n}_a \delta \hat{n}_b \rangle$ are absent, the first term is zero. In the MI state, on-site density fluctuations $\langle \delta \hat{n}^2 \rangle$ are also zero giving the zero value of the noise quantity (8.26), while in the coherent state, it is the on-site fluctuations $\langle \delta \hat{n}^2 \rangle = n$ that give isotropic contribution to R . Thus, we have

$$R_{\text{MI}} = 0, \quad (8.27a)$$

$$R_{\text{Coh}} = nK = N_K, \quad (8.27b)$$

$$R_{\text{SF}_K} = -\frac{N}{M^2} \frac{\sin^2(K\alpha_-/2)}{\sin^2(\alpha_-/2)} + \frac{N}{M}K. \quad (8.27c)$$

It is important to note, that in the SF state (8.27c), even in a large optical lattice with $N, M \rightarrow \infty$, very small pair correlations $\langle \delta \hat{n}_a \delta \hat{n}_b \rangle = -N/M^2$ can give a significant angle-dependent contribution to the noise quantity, which occurs near a diffraction maximum ($\alpha_- = 2\pi l, l = 0, 1, \dots$), where the geometrical factor is equal to K^2 , and if the number of the illuminated sites K is of the order of M . This demonstrates the importance of nonlocal correlations and invalidity of the coherent-state approximation under those conditions. Outside the diffraction maximum, where the geometrical factor is small, pair correlations do not play any role and the coherent-state approximation works well even for all sites illuminated.

Figure 8.2 shows several angle dependences of the scattered light in the case of two traveling waves. As an example, in all figures, we will consider atoms at each lattice sites providing $d = \lambda_{0,1}/2$. In Fig. 8.2(a), the angular distribution of classical diffraction $|\langle D \rangle|^2$ (curve A) is shown. In the case of $d = \lambda_{0,1}/2$ and the pump being orthogonal to the lattice ($\theta_0 = 0$), only the zero-order diffraction maxima at $\theta_1 = 0, \pi$ are possible in the classical picture. Corresponding noise quantities R for the coherent (constant lines A) and SF_K (curves B) states are displayed in Figs. 8.2(b) and 8.2(c) (in MI, the noise is zero, which is displayed by lines C). According to Eq. (8.27), the intensity fluctuations are isotropic for the coherent atomic state, while there is suppression of intensity noise under scattering from the SF. The suppression occurs in the regions of diffraction maxima. For all sites illuminated, $K = M$ [cf. Fig. 8.2(b)], the suppression is total, while for $K = M/2$ it is only partial [cf. Fig. 8.2(c)]. Outside the maxima, the dependence for SF_K is well approximated by that for the coherent state for any K .

It is important to underline, that in a broad range of angles, the number of scattered photons from the SF (or coherent) state is nonzero, even if the expectation value of the electromagnetic field vanishes, which manifests the appearance of nonclassical entanglement

between the light and manybody atomic system. Moreover, in contrast to MI state, atoms in SF state scatter photons at angles, where the classical diffraction does not exist.

For example, in a simple configuration considered in Sec. VI where the pump is orthogonal to the lattices ($\theta_0 = 0$), and the scattered light is collected by a cavity along the lattice axis ($\theta_1 = \pi/2$), the atoms in the MI state scatter no photons as in classical diffraction minimum. In contrast, atoms in the SF_K state scatter the number of photons $a_1^\dagger a_1 = |C|^2 \langle \hat{D}^* \hat{D} \rangle = |C|^2 N_K$, proportional to the number of the atoms illuminated [cf. Eq. (8.27) and Fig. 8.2(b) at the angle $\theta_1 = \pi/2$].

For two traveling waves, the expression for \hat{D} (8.12), in a diffraction maximum where all atoms radiate in phase with each other and $\alpha_- = 2\pi l$, is reduced to the operator \hat{N}_K . Thus, the quantity $\langle \hat{D} \rangle = N_K = nK$ is the expectation value of the atom number at K sites and proportional to the average atom number at a single site. The intensity of the light scattered into a diffraction maximum is determined by $\langle \hat{D}^* \hat{D} \rangle = \langle N_K^2 \rangle$, while noise $R = (\Delta N_K)^2$ gives the atom number variance at K sites. The latter statement corresponds to Figs. 8.2(b) and 8.2(c) displaying the total noise suppression in SF_M state, where the total atom number at all sites $K = M$ does not fluctuate, while for $K < M$, N_K is a fluctuating quantity and the noise suppression is only partial.

At the angle of a classical diffraction “minimum” (for $K \gg 1$ this is approximately valid for any angle outside narrow regions of maxima), the expectation value of the field amplitude is zero, as well as the first terms in Eqs. (8.13c), (8.13d), (8.13e), and both the intensity $\langle \hat{D}^* \hat{D} \rangle$ and noise R are proportional to the quantity $\langle \hat{n}^2 \rangle - \langle \hat{n}_a \hat{n}_b \rangle$ giving the difference between local and nonlocal fluctuations. For two traveling waves, the coefficient of proportionality is isotropic and equal to K [cf. Eq. (8.26)].

For scattering of incoherent light (8.14), the intensity is proportional to the local quantity $\langle \hat{n}^2 \rangle$ and is shown in Fig. 8.2(a) for MI (curve C) and coherent, almost the same as in SF, (curve B) states. This quantity can be also obtained under coherent scattering of two traveling waves, if one tunes the angles such that the geometrical factor of the first term in Eq. (8.26) is equal to K . Practically, this variant is easy to achieve only for a diffraction pattern with diffraction maxima, which are not too narrow.

Hence, in an optical experiment, both global statistical quantities related to $K \leq M$ sites, local quantities reflecting statistics at a single site, and pair correlations can be obtained. It is important, that local statistics can be determined by global measurements, i.e., an optical access to a single site is not necessary.

Therefore, light scattering gives a possibility to distinguish different quantum states of ultracold atoms. As demonstrated by Eq. (8.27) and Fig. 8.2, MI and SF_M states are distinguishable in diffraction “minima” and in incoherent light, while they are indistinguishable (for traveling waves) in maxima, because the total atom number contributing to the maximum does not fluctuate. The SF_M and coherent states can be distinguished in diffraction maxima only. The MI and coherent states can be distinguished in any angle of the scattering pattern.

Measurements of the noise quantity discussed or, alternatively, related quantities for quadratures (8.16) or photon number variance (8.18), give the values, which are different in orders of the emitter number N_K for different quantum states. Nevertheless, for large N_K ,

there could be practical problems in the subtraction of large values in a diffraction maximum to get the noise contribution. In some papers, a similar problem even led to a conclusion about state indistinguishability by intensity measurements in BEC [14, 19, 20] and, hence, to a necessity to measure photon statistics. A rather involved method to suppress the strong classical part of scattering using a dark-state resonance in BEC was proposed in Ref. [16]. In contrast to homogeneous ensembles, in optical lattices, this problem has a natural solution: measurements outside diffraction maxima are free of the strong classical-like part and thus directly reflect density fluctuations.

The classical analogy of the difference in light scattering from different atomic states consists in different density fluctuations in different states. In particular, classical density fluctuations would also lead to impossibility of obtaining a perfect diffraction minimum, where contributions from all sites should precisely cancel each other.

Scattering at diffraction maxima can be treated as superradiant one, since the intensity of the scattered light is proportional to the number of phase-synchronized emitters squared N_K^2 . In diffraction minima, destructive interference leads to the total (subradiant) suppression of coherent radiation for MI state; whereas for SF_K state, the intensity is nonzero and proportional to the number of emitters N_K , which is analogous to the emission of independent (non-phase-synchronized) atoms.

Nevertheless, the quantum treatment gives a deeper insight into the problem. In the SF state, at the angles of classical diffraction minima, the expectation value of the electromagnetic field is zero, while the photon number takes a nonzero value, which can be explained as follows. Equation (8.21a) shows that the SF state is a superposition of all possible multisite Fock states of N atoms at M sites. Under the light-matter interaction, the Fock states corresponding to different distributions of atoms at lattice sites become entangled to scattered light of different phases and amplitudes. In contrast to the classical case, light fields entangled to various atomic distributions do not interfere with each other, which is due to the orthogonality of the Fock states, providing a sort of which-way information. This leads to a difference from the classical (or MI with the only multisite Fock state) case and nonzero expectation value of the photon number. The absence of interference gives also an insight into the similarity of scattering from the SF state to the scattering from independent (non-phase-synchronized) atoms, where interference is also absent.

8.7.2 Standing waves

If at least one of the modes is a standing wave, the angle dependence of the noise becomes richer. In an experiment, this configuration corresponds to a case where the scattered light is collected by a standing-wave cavity, whose axis can be tuned with respect to the lattice axis [30]. Except for the appearance of new classical diffraction maxima represented by the first terms in Eqs. (8.13c), (8.13d), (8.13e), which depend on the phase parameters $\alpha_{\pm} = k_{0x}d \sin \theta_0 \pm k_{1x}d \sin \theta_1$, the angle dependence of the second term is also not an isotropic one, as it was for two traveling waves. This second, “noise,” term includes a sum of the geometrical coefficients squared, which is equivalent to the effective doubling of the lattice period (or doubling of the light frequency) and leads to the appearance of new spatial harmonics in the light angular distribution. Such period doubling leads to the appearance of the peaks in the noise distribution at the angles, where classical diffraction does not exist.

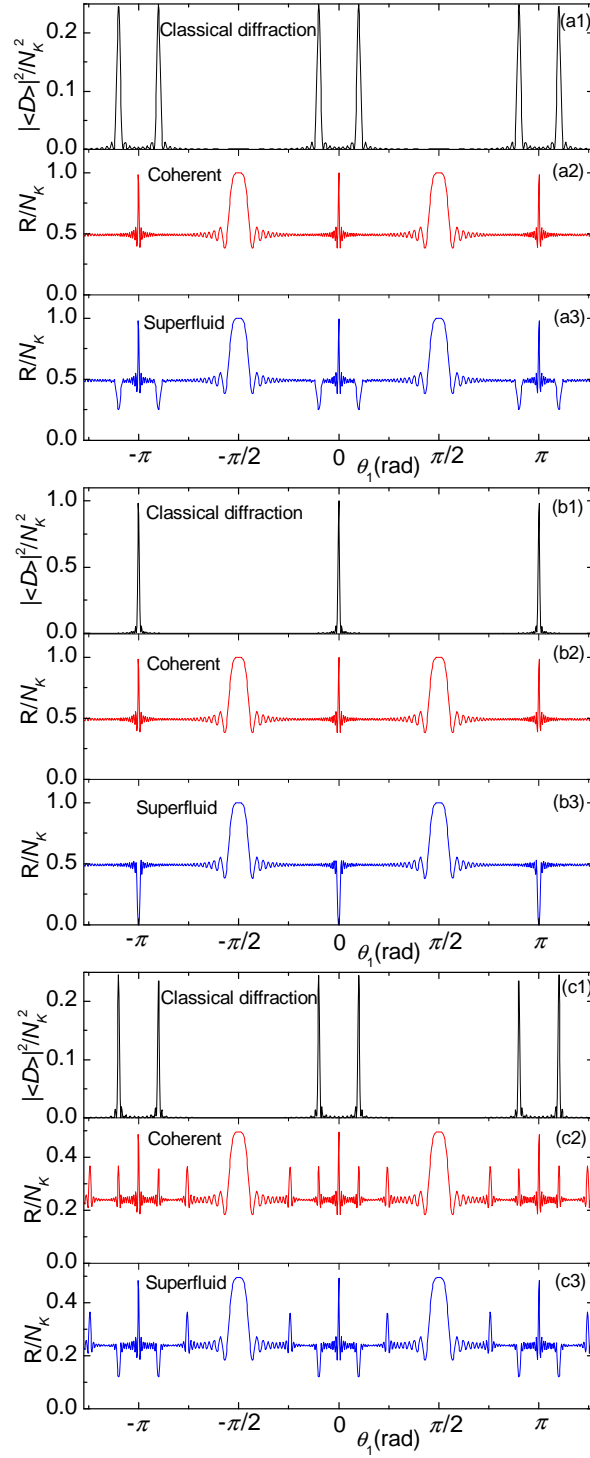


Figure 8.3. Intensity angular distributions for scattering into a standing-wave cavity. (a) Traveling-wave pump at $\theta_0 = 0.1\pi$; (b) traveling or standing-wave pump at $\theta_0 = 0$; (c) standing-wave pump at $\theta_0 = 0.1\pi$. Intensities of classical diffraction are shown in Figs. (a1), (b1), and (c1); noise quantities for coherent state are shown in Figs. (a2), (b2), and (c2) and for SF in Figs. (a3), (b3), and (c3). $N = M = K = 30$.

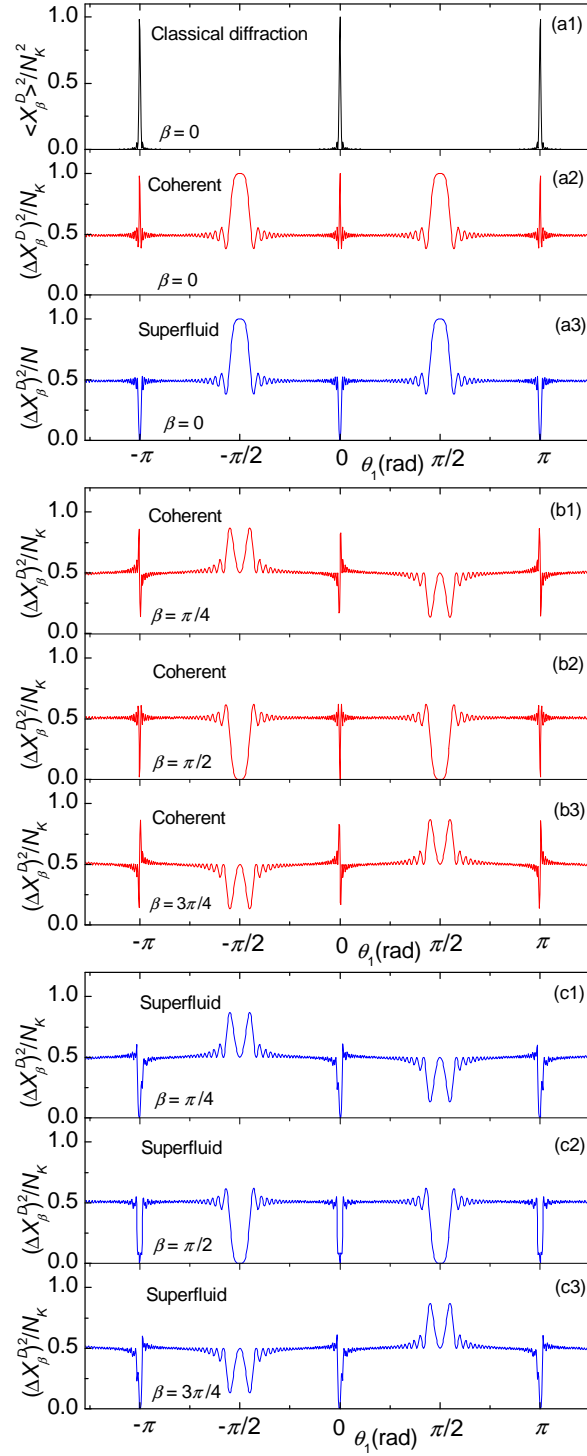


Figure 8.4. Quadrature angular distributions for two traveling waves. (a) Quadrature for classical diffraction (a1), quadrature variance for coherent (a2) and SF (a3) states, pump-homodyne phase difference $\beta = 0$; (b) quadrature variance for coherent state for $\beta = \pi/4$ (b1), $\beta = \pi/2$ (b2), $\beta = 3\pi/4$ (b3); (c) quadrature variance for SF for $\beta = \pi/4$ (c1), $\beta = \pi/2$ (c2), $\beta = 3\pi/4$ (c3). $\theta_0 = 0$, $N = M = K = 30$.

In Fig. 8.3(a), angular distributions of the scattered light are shown for a traveling-wave pump, which is almost orthogonal to a lattice ($\theta_0 = 0.1\pi$), while the probe is a standing wave. Classical diffraction pattern [cf. Fig. 8.3(a1)] is determined by $|A|^2$ through the parameters α_{\pm} and shows zero-order diffraction maxima in transmission ($\theta_1 = \theta_0$ and its counterpart due to the presence of the standing-wave cavity at $\theta_1 = \pi + \theta_0$) and reflection ($\theta_1 = \pi - \theta_0$ and the counterpart at $-\theta_0$). The intensity noise for atoms in the coherent state [cf. Fig. 8.3(a2)] is determined by $\sum_{i=1}^K |A_i|^2$ through another parameter $2\alpha_1 = 2k_{1x}d \sin \theta_1$ and has different characteristic features at $\theta_1 = 0, \pi$, and $\pm\pi/2$. It is the latter feature that corresponds to the effective frequency doubling and appears at an angle, where classical diffraction has a minimum. In the case of SF_M state [cf. Fig. 8.3(a3)], pair correlations in Eqs. (8.13d) and (8.13e) are nonzero, hence, both geometrical factors contribute to the noise distribution, which has the features at angles characteristic to both classical scattering and the light noise of the coherent-state case. Outside the characteristic features, the noise distribution is isotropic and takes a nonzero value similar to the case of two traveling waves [cf. Fig. 8.2]. Figure 8.3(b) shows a simpler situation, where the pump is precisely orthogonal to the lattices ($\theta_0 = 0$).

In Fig. 8.3(c), a situation similar to Fig. 8.3(a) is shown for the case where both the pump and probe are standing waves. While classical diffraction still depends on the parameters α_{\pm} , the factor $\sum_{i=1}^K |A_i|^2$ determining the intensity noise depends on four parameters $2\alpha_{0,1} = 2k_{0,1x}d \sin \theta_{0,1}$ and $2\alpha_{\pm}$. Thus, in the light noise from a lattice in the coherent and SF states, the features are placed at the positions of classical zero-order diffraction maxima and the angles, which would correspond to the classical scattering from a lattice with a doubled period $d = \lambda$, where the appearance of first-order diffraction maxima is possible. Similar to Fig. 8.3(a), features at $\theta_1 = 0, \pi$, and $\pi/2$ also exist. In the case $\theta_0 = 0$, the angular distribution for two standing waves is identical to that of one standing wave shown in Fig. 8.3(b).

In the SF_M state, there are two types of diffraction maxima. In the first one, the noise can be completely suppressed due to the total atom number conservation, similarly to the case of traveling waves. This occurs, if the condition of the maximum is fulfilled for both of two traveling waves forming a single standing wave [cf. Fig. 8.3(b)]. In the second type, even for $K = M$, only partial noise suppression is possible, since only one of the traveling waves is in a maximum, while another one, being in a minimum, produces the noise [cf. Figs. 8.3(a) and 8.3(c)]. In contrast to two traveling modes, in the second type of maxima, one can distinguish between SF_M and MI states, since MI produces no noise in any direction.

8.7.3 Quadratures and photon statistics

An analysis of the angular distribution of the quadrature variance $(\Delta X_{\beta}^D)^2$ (8.16b) shows, that even for two traveling waves, new peaks due to effective period doubling appear [see Fig. 8.4(a)]. Additionally, the amplitude of noise features can be varied by the phase difference between the pump and homodyne beams β , which is shown in Figs. 8.4(b) for the coherent and in Fig. 8.4(c) SF_M states. In the coherent state, all peaks are very sensitive to β . In the SF_M state, the noise suppression at diffraction maxima is insensitive to variations of β , whereas other peaks are β -dependent. The relation of $(\Delta X_{\beta}^D)^2$ to the quadrature variance of the light field is given by Eq. (8.15c).

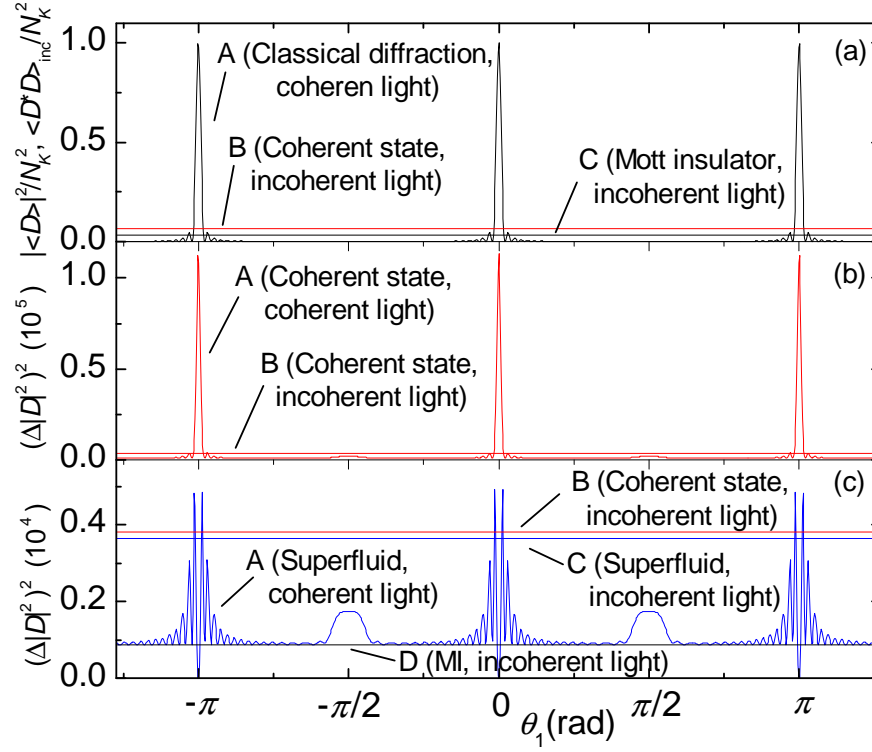


Figure 8.5. Angular distributions of photon-number variances for two traveling waves. (a) Intensity of classical diffraction (curve A), isotropic intensity of incoherent light scattering, Eq. (8.14), for coherent atomic state (line B) and MI state (line C); (b) normal ordered photon-number variance for coherent atomic state under scattering of coherent, Eq. (8.28) (curve A), and incoherent (line B) light; (c) normal ordered photon-number variance for SF state under scattering of coherent, Eq. (8.28) (curve A), and incoherent (line C) light, variance for coherent (line B) and MI (curve D) states under scattering of incoherent light. Normal ordered photon-number variance for MI state under scattering of coherent light is zero for all angles. $\theta_0 = 0$, $N = M = K = 30$.

The angle dependence of the variance $(\Delta|D|^2)^2 = \langle \hat{D}^{*2} \hat{D}^2 \rangle - \langle \hat{D}^* \hat{D} \rangle^2$, which is proportional to the normal ordered photon-number variance and determines the light statistics (8.18), also shows anisotropic features due to frequency doubling even for two traveling waves (Fig. 8.5). In this case, Eq. (8.19) is reduced to

$$\begin{aligned}
\langle \hat{D}^{*2} \hat{D}^2 \rangle &= \left(\frac{\sin(K\alpha_-/2)}{\sin(\alpha_-/2)} \right)^4 \langle n_a n_b n_c n_d \rangle \\
&+ 2 \left(\frac{\sin(K\alpha_-/2)}{\sin(\alpha_-/2)} \right)^3 \frac{\cos(K\alpha_-/2)}{\cos(\alpha_-/2)} (\langle n_a^2 n_b n_c \rangle - \langle n_a n_b n_c n_d \rangle) \\
&- 4 \left(\frac{\sin(K\alpha_-/2)}{\sin(\alpha_-/2)} \right)^2 [(K-2)\langle n_a n_b n_c n_d \rangle - (K-3)\langle n_a^2 n_b n_c \rangle - \langle n_a^3 n_b \rangle] \\
&+ \left(\frac{\sin K\alpha_-}{\sin \alpha_-} \right)^2 (\langle n_a n_b n_c n_d \rangle - 2\langle n_a^2 n_b n_c \rangle + \langle n_a^2 n_b^2 \rangle) \\
&+ 2K^2 (\langle n_a n_b n_c n_d \rangle - 2\langle n_a^2 n_b n_c \rangle + \langle n_a^2 n_b^2 \rangle) \\
&+ K (-6\langle n_a n_b n_c n_d \rangle + 12\langle n_a^2 n_b n_c \rangle - 4\langle n_a^3 n_b \rangle - 3\langle n_a^2 n_b^2 \rangle + \langle n^4 \rangle),
\end{aligned} \tag{8.28}$$

where the first four terms has features at angles typical to classical diffraction, the fourth term is also responsible for the doubled-frequency feature, and the last two terms contribute to the isotropic component.

For the coherent state, the light scattered into a diffraction maximum displays a very strong noise (equal to $4N_K^3 + 6N_K^2 + N_k$ because $\langle \hat{D}^{*2} \hat{D}^2 \rangle = N_K^4 + 6N_K^3 + 7N_K^2 + N_k$ and $\langle \hat{D}^* \hat{D} \rangle = N_K^2 + N_K$), which is much stronger than the isotropic component (N_K^2 in highest order of N_K) and the features at $\theta_1 = \pm\pi/2$ ($2N_K^2$ in highest order of N_K) [Fig. 8.5(b)]. In SF_M state, the noise at maxima can be suppressed, while at other angles, in highest order of N_K , it is equal to that of the coherent state [Fig. 8.5(c)]. In MI state, the variance $(\Delta|D|^2)^2$ is zero for all angles. Conclusions about state distinguishing by measuring light statistics are very similar to those drawn from the intensity and amplitude measurements, which have been discussed in Sec. VIIA, including scattering of incoherent light (see Fig. 8.5 and the discussion of Fig. 8.2).

In experiments, the nontrivial angle dependence of the noise can help in the separation of the light noise reflecting atom statistics from technical imperfections.

8.8 Conclusions

We studied off-resonant collective light scattering from ultracold atoms trapped in an optical lattice. Measuring the light field allows to characterize the quantum state of atoms in a nondestructive way and in particular distinguish between different atomic states. The scattered light differs in intensity, quadrature variances, and photon statistics. A measurement of the intensity angular distribution provides information about atom number fluctuations in a finite lattice region, local quantum statistics at single sites, and pair correlations. Note that even local statistics can be determined by global measurements without an optical access to particular sites. Alternatively to angle-resolved measurements, variations of the mode wavelengths with respect to the wavelength of a trapping beam can be considered.

Light scattering as a diagnostic tool has particular advantages for optical lattices in contrast to scattering from a homogeneous BEC. Here one has a natural way to suppress the strong classical scattering background by looking at the directions of diffraction minima. In these directions the expectation value of the field amplitude vanishes while the intensity (photon number) is nonzero and directly reflects quantum fluctuations. Furthermore, in an optical lattice, the signal is sensitive not only to the periodic density distribution, but also to the periodic density fluctuations, giving an access to even very small nonlocal pair correlations. These can be obtained by measuring light at diffraction maxima.

As the most striking example, we considered light scattering from a 1D lattice in a transversally pumped optical cavity as in a setup involving collective cavity cooling [36, 38–40]. The number of photons scattered into the cavity is zero for the Mott insulator phase but proportional to the atom number in the superfluid phase. Both states have almost the same average density but different quantum uncertainties. So the superfluid state is a quantum superposition of different Fock states corresponding to all possible distributions of N atoms at M sites. Under illumination by a coherent light, various Fock states become entangled to scattered light states with different amplitudes and phases. In contrast to classical scattering, where the atoms are described by c-number center-of-mass positions [41], for a quantum description of the atomic motion the light field amplitudes corresponding to different atomic distributions do not interfere. This is due to the orthogonality of Fock states forming the superfluid providing a sort of which way information.

In the example configuration, the cavity-field amplitude is determined by the atom number operators $\hat{n}_i = b_i^\dagger b_i$. Hence, the expectation value of the field amplitude is sensitive to the average density only. In contrast, the intracavity photon number reflects the second moments of atom number operators (e.g. density-density correlations), while photon statistics reflects the forth moments.

Let's emphasize that other physical systems are possible, where the light amplitude depends on the matter-field amplitudes b_i , while the intensity is sensitive to density operators \hat{n}_i . The latter situation is typical to configurations, where two or more atomic subsystems exist and can interact with each other, in particular, through light fields. The examples are matter-wave superradiance and amplification, where two or more momentum states of cold atoms were observed [11, 12, 42, 43], and interaction between two BECs with different internal [44–47] or motional [48] atomic states. In the framework of our paper, matter-field amplitudes b_i can also contribute to light amplitudes a_l , if the tunneling between lattice sites is important, which we have considered in the general model in Sec. II. In the rest of the paper, the lattice was assumed deep leading to negligible tunneling.

In general, a variety of optical effects can be sensitive to a quantum state of an ultracold matter, if the density operators enter measurable quantities nonlinearly, such that the expectation value of those quantities cannot be simply expressed through expectation values of density operators. For instance, the $\chi^{(3)}$ nonlinearity [49] and refractive index of a gas, where nonlocal field effects are important [50], were shown to depend on atom statistics. In this paper, we focused on such nonlinear quantities as intensity, quadrature variances, and photon statistics of scattered light [51]. Phase-sensitive and spectral characteristics mentioned in Sec. IV.D reflect the dependence of the dispersion of a medium on the quantum state of matter [32, 52]. Moreover, such dispersion effects (e.g. cavity-mode shift) will reflect atom statistics not only in light intensity, but even in light amplitudes $\langle a_l \rangle$.

So far we have neglected the dynamic back action of scattered field on atoms. This can be well justified in a deep lattice where the momentum transfer is by far not enough to change the atomic vibrational state as long as not too many photons are scattered. Even without energy transfer the information one gets from the light will induce measurement back-action. This should have intriguing consequences for multiple consecutive measurements on the light scattered from optical lattices.

Acknowledgments

This work was supported by the Austrian Science Fund FWF (grants P17709 and S1512).

Bibliography

- [1] D. Jaksch, C. Bruder, J. I. Cirac, C. W. Gardiner, and P. Zoller, *Phys. Rev. Lett.* **81**, 3108 (1998).
- [2] M. Greiner, O. Mandel, T. Esslinger, T. Hänsch, and I. Bloch, *Nature* **415**, 39 (2002).
- [3] S. Fölling, F. Gerbier, A. Widera, O. Mandel, T. Gericke, and I. Bloch, *Nature* **434**, 481 (2005).
- [4] E. Altman, E. Demler, and M. D. Lukin, *Phys. Rev. A* **70**, 013603 (2004).
- [5] J. Stenger, S. Inouye, A. P. Chikkatur, D. M. Stamper-Kurn, D. E. Pritchard, and W. Ketterle, *Phys. Rev. Lett.* **82**, 4569 (1999).
- [6] P. B. Blakie, R. J. Ballagh, and C. W. Gardiner, *Phys. Rev. A* **65**, 033602 (2002).
- [7] R. Roth and K. Burnett, *Phys. Rev. A* **68**, 023604 (2003).
- [8] T. Stöferle, H. Moritz, C. Schori, M. Kohl, and T. Esslinger, *Phys. Rev. Lett.* **92**, 130403 (2004).
- [9] C. Menotti, M. Krämer, L. Pitaevskii, and S. Stringari, *Phys. Rev. A* **67**, 053609 (2003).
- [10] A. M. Rey, P. B. Blakie, G. Pupillo, C. J. Williams, and C. W. Clark, *Phys. Rev. A* **72**, 023407 (2005).
- [11] M. G. Moore, O. Zobay, and P. Meystre, *Phys. Rev. A* **60**, 1491 (1999).
- [12] H. Pu, W. Zhang, and P. Meystre, *Phys. Rev. Lett.* **91**, 150407 (2003).
- [13] L. You, M. Lewenstein, and J. Cooper, *Phys. Rev. A* **51**, 4712 (1995).
- [14] Z. Idziaszek, K. Rzazewski, and M. Lewenstein, *Phys. Rev. A* **61**, 053608 (2000).
- [15] Ö. E. Müstecaplıoglu and L. You, *Phys. Rev. A* **62**, 063615 (2000).
- [16] Ö. E. Müstecaplıoglu and L. You, *Phys. Rev. A* **64**, 033612 (2001).

- [17] J. Javanainen, Phys. Rev. Lett. **75**, 1927 (1995).
- [18] J. Javanainen and J. Ruostekoski, Phys. Rev. A **52**, 3033 (1995).
- [19] J. I. Cirac, M. Lewenstein, and P. Zoller, Phys. Rev. Lett. **72**, 2977 (1994).
- [20] J. I. Cirac, M. Lewenstein, and P. Zoller, Phys. Rev. A **50**, 3409 (1994).
- [21] H. Saito and M. Ueda, Phys. Rev. A **60**, 3990 (1999).
- [22] G. A. Pratavia and M. C. de Oliveira, Phys. Rev. A **70**, 011602(R) (2004).
- [23] J. Javanainen and J. Ruostekoski, Phys. Rev. Lett. **91**, 150404 (2003).
- [24] I. B. Mekhov, C. Maschler, and H. Ritsch, quant-ph/0610073, to be published in Phys. Rev. Lett.
- [25] T. Bourdel, T. Donner, S. Ritter, A. Öttl, M. Kohl, and T. Esslinger, Phys. Rev. A **73**, 043602 (2006).
- [26] I. Teper, Y. J. Lin, and V. Vuletic, Phys. Rev. Lett. **97**, 023002 (2006).
- [27] G. Birkel, M. Gatzke, I. H. Deutsch, S. L. Rolston, and W. D. Phillips, Phys. Rev. Lett. **75**, 2823 (1995).
- [28] M. Weidemüller, A. Hemmerich, A. Görlitz, T. Esslinger, and T. W. Hänsch, Phys. Rev. Lett. **75**, 4583 (1995).
- [29] S. Slama, C. von Cube, M. Kohler, C. Zimmermann, and P. W. Courteille, Phys. Rev. A **73**, 023424 (2006).
- [30] C. Maschler and H. Ritsch, Phys. Rev. Lett. **95**, 260401 (2005).
- [31] J. Klinner, M. Lindholdt, B. Nagorny, and A. Hemmerich, Phys. Rev. Lett. **96**, 023002 (2006).
- [32] I. B. Mekhov, C. Maschler, and H. Ritsch, quant-ph/0702125.
- [33] G. Cennini, C. Geckeler, G. Ritt, and M. Weitz, Phys. Rev. A **72**, 051601(R) (2005).
- [34] T. Anker, M. Albiez, B. Eiermann, M. Taglieber, and M. Oberthaler, Opt. Express **12**, 11 (2004).
- [35] P. Domokos, A. Vukics, and H. Ritsch, Phys. Rev. Lett. **92**, 103601 (2004).
- [36] A. Black, J. Thompson, and V. Vuletic, J. Phys. B **38**, S605 (2005).
- [37] J. K. Asbóth, P. Domokos, H. Ritsch, and A. Vukics, Phys. Rev. A **72**, 53417 (2005).
- [38] P. Domokos and H. Ritsch, Phys. Rev. Lett. **89**, 253003 (2002).
- [39] T. Elsässer, B. Nagorny, and A. Hemmerich, Phys. Rev. A **69**, 33403 (2004).

- [40] S. Slama, C. von Cube, B. Deh, A. Ludewig, C. Zimmermann, and P. W. Courteille, Phys. Rev. Lett. **94**, 193901 (2005).
- [41] U. Eichmann, J. C. Bergquist, J. J. Bollinger, J. M. Gilligan, W. M. Itano, D. J. Wineland, and M. G. Raizen, Phys. Rev. Lett. **70**, 2359 (1993).
- [42] S. Inouye, A. P. Chikkatur, D. M. Stamper-Kurn, J. Stenger, D. E. Pritchard, and W. Ketterle, Science **285**, 571 (1999).
- [43] E. D. Trifonov, Opt. Spectrosk. **98**, 497 (2005) [Opt. Spectrosk. **98**, 497 (2005)].
- [44] H. Zeng, W. Zhang, and F. Lin, Phys. Rev. A **52**, 2155 (1995).
- [45] J. Ruostekoski and D. F. Walls, Phys. Rev. A **55**, 3625 (1997).
- [46] C. P. Search and P. R. Berman, Phys. Rev. A **64**, 043602 (2001).
- [47] C. P. Search, Phys. Rev. A **64**, 053606 (2001).
- [48] J. Ruostekoski, M. J. Collett, R. Graham, and D. F. Walls, Phys. Rev. A **57**, 511 (1998).
- [49] T. Hiroshima and Y. Yamamoto, Phys. Rev. A **53**, 1048 (1996).
- [50] O. Morice, Y. Castin, and J. Dalibard, Phys. Rev. A **51**, 3896 (1995).
- [51] After having finished this work, we became aware of a closely related research in the group of P. Meystre. We are grateful to him for sending us the preprint quant-ph/0610029 and stimulating discussions.
- [52] I. B. Mekhov, C. Maschler and H. Ritsch, in *Books of abstracts for the XX International Conference on Atomic Physics, ICAP, Innsbruck, 2006*, edited by C. Roos and H. Häfner (Institute for Quantum Optics and Quantum Information, Innsbruck, 2006), p. 309 and conference web-site.

CHAPTER 9

PUBLICATION

Probing Quantum Phases of Ultracold Atoms in Optical Lattices by Transmission Spectra in Cavity QED[†]

Nature Physics **3**, 319 (2007)

I. B. Mekhov^{1,2}, C. Maschler¹, and H. Ritsch¹

*1) Institut für theoretische Physik, Universität Innsbruck,
A-6020 Innsbruck, Austria*

*2) St. Petersburg State University, V. A. Fock Institute of Physics,
St. Petersburg, Russia*

Studies of ultracold gases in optical lattices provide a means for testing fundamental and application-oriented quantum many-body concepts of condensed-matter physics in well controllable atomic systems [1]; examples include strongly correlated phases and quantum-information processing. Standard methods to observe quantum properties of BoseEinstein condensates are based on matterwave interference between atoms released from traps [2–6], a method that ultimately destroys the system. Here, we propose a new approach on the basis of optical measurements that conserves the number of atoms. We prove that atomic quantum statistics can be mapped on transmission spectra of high- Q cavities, where atoms create a quantum refractive index. This can be useful for studying phase transitions [7] for example, between Mott insulator and superfluid states as various phases show qualitatively distinct light scattering. Joining the paradigms of cavity quantum electrodynamics and ultracold gases could enable conceptually new investigations of both light and matter at ultimate quantum levels. We predict effects accessible in experiments that recently became possible [8].

All-optical methods to characterize atomic quantum statistics were proposed for homogeneous BEC [9–13] and some modified spectral properties induced by BEC's were attributed to collective emission [9, 10], recoil shifts [12] or local field effects [14].

We show a completely different phenomenon directly reflecting atom quantum statistics due to state-dependent dispersion. More precisely, the dispersion shift of a cavity mode depends on the atom number. If the atom number in some lattice region fluctuates from realization to realization, the modes get a fluctuating frequency shift. Thus, in the cavity

[†]The primary contribution of the author of the present thesis performed to this publication was the installation of the model and the calculation of certain generic examples and statistical quantities. He also acted as a discussion partner on all other aspects of the work.

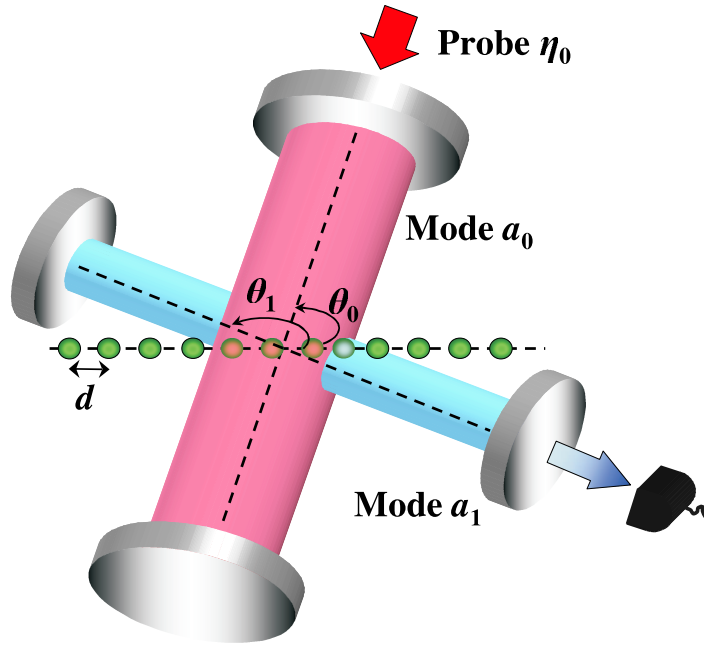


Figure 9.1. Schematic setup. Atoms are periodically trapped in an optical lattice created by laser beams, which are not shown in this figure. Additionally, the atoms are illuminated by two light modes at the angles $\theta_{0,1}$ with respect to the lattice axis.

transmission-spectrum, resonances appear at different frequencies directly reflecting the atom number distribution function. Such a measurement allows then to calculate atomic statistical quantities, e.g., mean value and variance reflected by spectral characteristics such as the central frequency and width.

Different phases of a degenerate gas possess similar mean-field densities but different quantum amplitudes. This leads to a superposition of different transmission spectra, which e.g. for a superfluid state (SF) consist of numerous peaks reflecting the discreteness of the matter-field. Analogous discrete spectra reversing the role of atoms and light, thus reflecting the photon structure of electromagnetic fields, were obtained in cavity QED with Rydberg atoms [15] and solid-state superconducting circuits [16]. A quantum phase transition towards a Mott insulator state (MI) is characterized by a reduction of the number of peaks towards a single resonance, because atom number fluctuations are significantly suppressed [17, 18]. As our detection scheme is based on nonresonant dispersive interaction independent of a particular level structure, it can be also applied to molecules [19, 20].

We consider the quantized motion of N two-level atoms in a deep periodic optical lattice with M sites formed by far off-resonance standing wave laser beams [1]. A region of $K \leq M$ sites is coupled to two quantized light modes whose geometries (i.e. axis directions or wavelengths) can be varied. This is shown in Fig. 9.1 depicting two cavities crossed by a 1D string of atoms in equally separated wells generated by the lattice lasers (not shown). In practice two different modes of the same cavity would do as well.

As shown in the Methods section, the Heisenberg equations for the annihilation operators of two light modes a_l ($l = 0, 1$) with eigenfrequencies ω_l and spatial mode functions $u_l(\mathbf{r})$ are

$$\begin{aligned} \dot{a}_l &= -i \left(\omega_l + \delta_l \hat{D}_{ll} \right) a_l - i \delta_m \hat{D}_{lm} a_m - \kappa a_l + \eta_l(t), \\ \text{with } \hat{D}_{lm} &\equiv \sum_{i=1}^K u_l^*(\mathbf{r}_i) u_m(\mathbf{r}_i) \hat{n}_i, \end{aligned} \quad (9.1)$$

where $l \neq m$, $\delta_l = g^2/\Delta_{la}$, g is the atom-light coupling constant, $\Delta_{la} = \omega_l - \omega_a$ are the large cavity-atom detunings, κ is the cavity relaxation rate, $\eta_l(t) = \eta_l e^{-i\omega_{lp}t}$ gives the external probe and \hat{n}_i are the atom number operators at a site with coordinate \mathbf{r}_i . We also introduce the operator of the atom number at illuminated sites $\hat{N}_K = \sum_{i=1}^K \hat{n}_i$.

In a classical limit, Eq. (9.1) corresponds to Maxwell's equations with the dispersion-induced frequency shifts of cavity modes $\delta_l \hat{D}_{ll}$ and the coupling coefficient between them $\delta_l \hat{D}_{10}$. For a quantum gas those quantities are operators, which will lead to striking results: atom number fluctuations will be directly reflected in such measurable frequency-dependent observables. Thus, cavity transmission-spectra will reflect atomic statistics.

Eq. (9.1) allows to express the light operators a_l as a function $f(\hat{n}_1, \dots, \hat{n}_M)$ of atomic occupation number operators and calculate their expectation values for prescribed atomic states $|\Psi\rangle$. We start with the well known examples of MI and SF states and generalize to any $|\Psi\rangle$ later.

From the viewpoint of light scattering, the MI state behaves almost classically as precisely $\langle \hat{n}_i \rangle_{\text{MI}} = q_i$ atoms are well localized at the i th site with no number fluctuations. For negligible tunneling, it is represented by a product of Fock states, i.e.,

$$|\Psi\rangle_{\text{MI}} = \prod_{i=1}^M |q_i\rangle_i \equiv |q_1, \dots, q_M\rangle, \quad (9.2)$$

with expectation values

$$\langle f(\hat{n}_1, \dots, \hat{n}_M) \rangle_{\text{MI}} = f(q_1, \dots, q_M), \quad (9.3)$$

since $\hat{n}_i |q_1, \dots, q_M\rangle = q_i |q_1, \dots, q_M\rangle$. For simplicity we consider equal average densities $\langle \hat{n}_i \rangle_{\text{MI}} = N/M \equiv n$ ($\langle \hat{N}_K \rangle_{\text{MI}} = nK \equiv N_K$).

In our second example, SF state, each atom is delocalized over all sites leading to local number fluctuations at a lattice region with $K < M$ sites. Mathematically it is a superposition of Fock states corresponding to all possible distributions of N atoms at M sites:

$$|\Psi\rangle_{\text{SF}} = \sqrt{\frac{N!}{M^N}} \sum_{q_1, \dots, q_M} \frac{1}{\sqrt{q_1! \dots q_M!}} |q_1, \dots, q_M\rangle. \quad (9.4)$$

Although its average density $\langle \hat{n}_i \rangle_{\text{SF}} = N/M$ is identical to a MI, it creates different light transmission spectra. Expectation values of light operators can be calculated from

$$\langle f(\hat{n}_1, \dots, \hat{n}_M) \rangle_{\text{SF}} = \frac{1}{M^N} \sum_{q_1, \dots, q_M} \frac{N!}{q_1! \dots q_M!} f(q_1, \dots, q_M), \quad (9.5)$$

representing a sum of all possible “classical” terms. Thus, all these distributions contribute to scattering from a SF, which is obviously different from $\langle f(\hat{n}_1, \dots, \hat{n}_M) \rangle_{\text{MI}}$ (9.3) with only a single contributing term.

In the simple case of only one mode a_0 ($a_1 \equiv 0$), the stationary solution of Eq. (9.1) for the photon number reads

$$a_0^\dagger a_0 = f(\hat{n}_1, \dots, \hat{n}_M) = \frac{|\eta_0|^2}{(\Delta_p - \delta_0 \hat{D}_{00})^2 + \kappa^2}, \quad (9.6)$$

where $\Delta_p = \omega_{0p} - \omega_0$ is the probe-cavity detuning. We present transmission spectra in Fig. 9.2 for the case, where $|u_0(\mathbf{r}_i)|^2 = 1$, and $\hat{D}_{00} = \sum_{i=1}^K \hat{n}_i$ reduces to \hat{N}_K . For a 1D lattice (see Fig. 9.1), this occurs for a traveling wave at any angle, and standing wave transverse ($\theta_0 = \pi/2$) or parallel ($\theta_0 = 0$) to the lattice with atoms trapped at field maxima.

For an MI, the averaging of Eq. (9.6) according to Eq. (9.3) gives the photon number $\langle a_0^\dagger a_0 \rangle_{\text{MI}}$, as a function of the detuning, as a single Lorentzian described by Eq. (9.6) with width κ and frequency shift given by $\delta_0 \langle \hat{D}_{00} \rangle_{\text{MI}}$ (equal to $\delta_0 N_K$ in Fig. 9.2). Thus, for MI, the spectrum reproduces a simple classical result of a Lorentzian shifted due to dispersion.

In contrast, for a SF, the averaging procedure of Eq. (9.5) gives a sum of Lorentzians with different dispersion shifts corresponding to all atomic distributions $|q_1, \dots, q_K\rangle$. So, if each Lorentzian is resolved, one can measure a comb-like structure by scanning the detuning Δ_p . In Figs. 9.2a and 9.2c, different shifts of the Lorentzians correspond to different possible atom numbers at K sites (which due to atom number fluctuations in SF, can take all values $0, 1, 2, \dots, N$). The Lorentzians are separated by δ_0 . Thus, we see that atom number fluctuations lead to the fluctuating mode shift, and hence to multiple resonances in the spectrum. For larger κ the spectrum becomes continuous (Fig. 9.2b), but broader than that for MI.

Scattering of weak fields does not change the atom number distribution. However, as the SF is a superposition of different atom numbers in a region with K sites, a measurement projects the state into a subspace with fixed N_K in this region, and a subsequent measurement on a time scale short to tunneling between sites will yield the same result. One recovers the full spectrum of Fig. 9.2 by repeating the experiment or with sufficient delay to allow for redistribution via tunneling. Such measurements will allow a time dependent study of tunneling and buildup of long-range order. Alternatively, one can continue measurements on the reduced subspace after changing a lattice region or light geometry.

We now consider two modes with $\omega_0 = \omega_1$, the probe injected only into a_0 (Fig. 9.1) and the mentioned geometries where $\hat{D}_{00} = \hat{D}_{11} = \hat{N}_K$ (see Fig. 9.3). From Eq. (9.1), the stationary photon number $a_1^\dagger a_1 = f(\hat{n}_1, \dots, \hat{n}_M)$ is

$$a_1^\dagger a_1 = \frac{\delta_1^2 \hat{D}_{10}^\dagger \hat{D}_{10} |\eta_0|^2}{[\hat{\Delta}_p'^2 - \delta_1^2 \hat{D}_{10}^\dagger \hat{D}_{10} - \kappa^2]^2 + 4\kappa^2 \hat{\Delta}_p'^2}, \quad (9.7)$$

where $\hat{\Delta}_p' = \Delta_p - \delta_1 \hat{D}_{11}$.

In a classical (and MI) case, Eq. (9.3) gives a two-satellite contour (9.7) reflecting normal-mode splitting of two oscillators $\langle a_{0,1} \rangle$ coupled through atoms. This was recently observed [21] for collective strong coupling, i.e., the splitting $\delta_1 \langle \hat{D}_{10} \rangle$ exceeding κ . The splitting depends

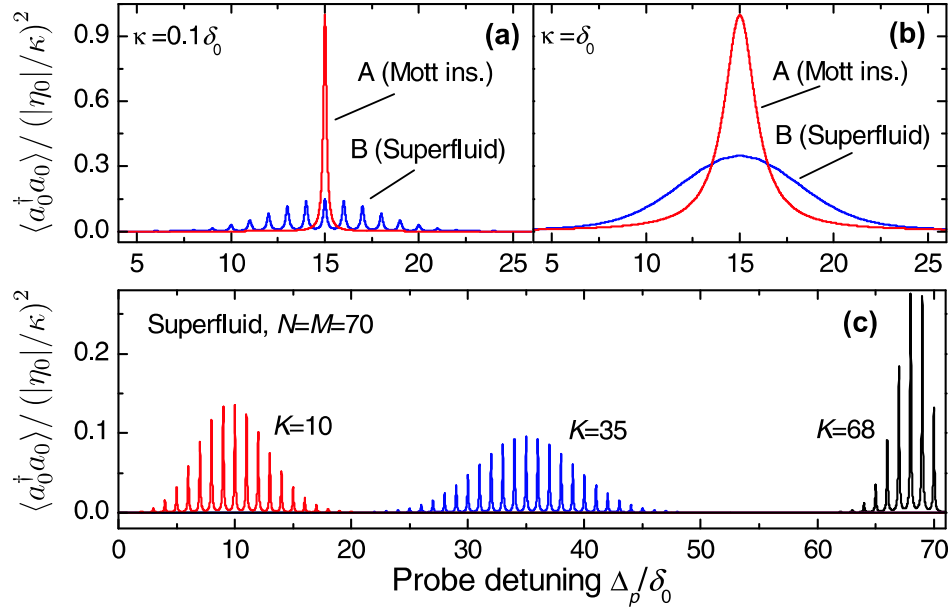


Figure 9.2. Photon number in a single cavity mode. (a) Single Lorentzian for MI (curve A) reflects non-fluctuating atom number. Many Lorentzians for SF (curve B) reflect atom number fluctuations, which are imprinted on the positions of narrow resonances. Here κ is smaller than satellite separation δ_0 ($\kappa = 0.1\delta_0$), $N = M = 30$, $K = 15$. (b) The same as in (a) but $\kappa = \delta_0$ gives smooth broadened contour for SF. (c) Spectra for SF with $N = M = 70$ and different number of sites illuminated $K = 10, 35, 68$. The transmission spectra have different forms, since different atom distribution functions correspond to different K . $\kappa = 0.05\delta_0$.

on the geometry (see Eq. (9.1)) representing diffraction of one mode into another. Thus, our results can be treated as scattering from a “quantum diffraction grating” generalizing Bragg scattering, well-known in different disciplines. In diffraction maxima (i.e. $u_1^*(\mathbf{r}_i)u_0(\mathbf{r}_i) = 1$) one finds $\hat{D}_{10} = \hat{N}_K$ providing the maximal classical splitting. In diffraction minima, one finds $\hat{D}_{10} = \sum_{i=1}^K (-1)^{i+1} \hat{n}_i$ providing both the classical splitting and photon number are almost zero.

In SF, Eq. (9.5) shows that $\langle a_1^\dagger a_1 \rangle_{\text{SF}}$ is given by a sum of all classical terms with all possible normal mode splittings. In a diffraction maximum (Figs. 9.3a,b), the right satellite is split into components corresponding to all possible N_K or extremely broadened. In a minimum (Figs. 9.3c,d), the splittings are determined by all differences between atom numbers at odd and even sites $\sum_{i=1}^K (-1)^{i+1} q_i$. Note that there is no classical description of the spectra in a minimum, since here the classical field (and $\langle a_1^\dagger a_1 \rangle_{\text{MI}}$) are simply zero for any Δ_p . Thus, for two cavities coupled at diffraction minimum, the difference between the SF and MI states is even more striking: one has a structured spectrum instead of zero signal. Moreover, the difference between atom numbers at odd and even sites fluctuates even for the whole lattice illuminated, giving nontrivial spectra even for $K = M$.

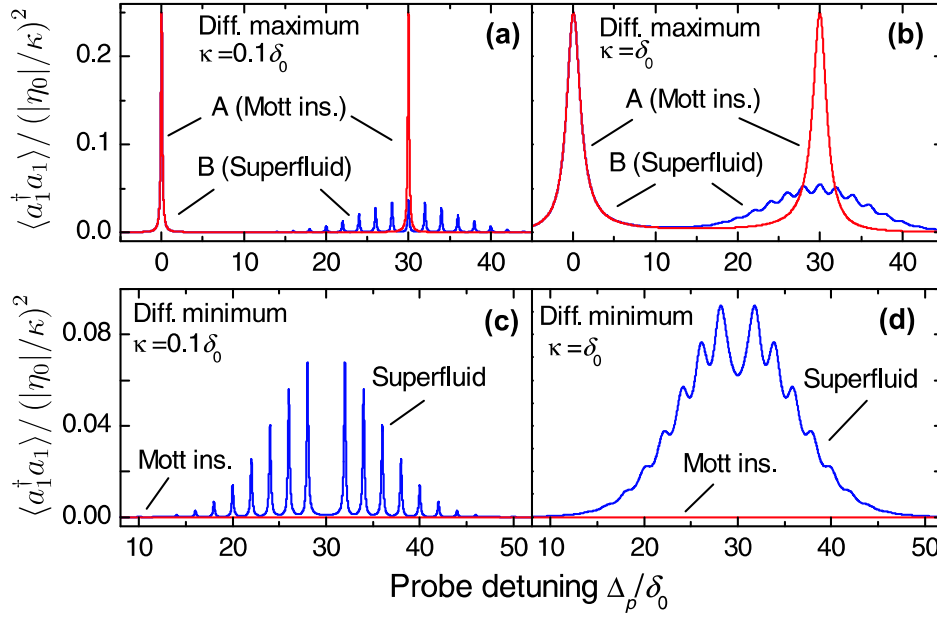


Figure 9.3. Photon number in one of two strongly coupled modes. (a) Diffraction maximum, doublet for MI (curve A) and spectrum with structured right satellite for SF (curve B). Structure in the satellite reflects atom number fluctuations in SF, while narrow spectrum for MI demonstrates vanishing fluctuations. Here κ is smaller than satellite separation $2\delta_0$ ($\kappa = 0.1\delta_0$), $K = 15$. (b) The same as in (a) but $\kappa = \delta_0$ gives broadened satellite for SF. (c) Diffraction minimum, zero field for MI and structured spectrum for SF. Nonzero structured spectrum for SF reflects fluctuating difference between atom numbers at odd and even sites, which exists even for the whole lattice illuminated, $K = M$. Here κ is smaller than satellite separation $2\delta_0$ ($\kappa = 0.1\delta_0$), $K = 30$. (d) The same as in (c) but $\kappa = \delta_0$ gives broadened contour for SF. $N = M = 30$ in all figures.

In each of the examples in Figs. 9.2 and 9.3, the photon number depends only on one statistical quantity, now called q , $f(q_1, \dots, q_M) = f(q)$. For the single mode and two modes in a maximum, q is the atom number at K sites. For two modes in a minimum, q is the atom number at odd (or even) sites. Therefore, expectation values for some state $|\Psi\rangle$ can be reduced to $\langle f \rangle_\Psi = \sum_{q=0}^N f(q) p_\Psi(q)$, where $p_\Psi(q)$ is the distribution function of q in this state.

In high- Q cavities ($\kappa \ll \delta_0 = g^2/\Delta_{0a}$), $f(q)$ is given by a narrow Lorentzian of width κ peaked at some frequency proportional to q ($q = 0, 1, \dots, N$). The Lorentzian height is q -independent. Thus, $\langle f \rangle_\Psi$ as a function of Δ_p represents a comb of Lorentzians with the amplitudes simply proportional to $p_\Psi(q)$.

This is our central result. It states that the transmission spectrum of a high- Q cavity $\langle a^\dagger a(\Delta_p) \rangle_\Psi$ directly maps the distribution function of ultracold atoms $p_\Psi(q)$, e.g., distribution function of atom number at K sites. Various atomic statistical quantities characterizing a particular state can be then calculated: mean value (given by the spectrum center), variance (determined by the spectral width) and higher moments. Furthermore, transitions between

different states will be reflected in spectral changes. Deviations from idealized MI and SF states [22] are also measurable.

For SF, using $p_{\text{SF}}(q)$ (see Methods), we can write the envelopes of the comb of Lorentzians shown in Figs. 9.2a,c and 9.3a,c. As known, the atom number at K sites fluctuates in SF with the variance $(\Delta N_K)^2 = N_K(1 - K/M)$. For example, Fig. 9.2c shows spectra for different lattice regions demonstrating Gaussian and Poissonian distributions with the spectral width $\sigma_\omega = \delta_0 \sqrt{(\Delta N_K)^2}$, directly reflecting the atom distribution functions in SF. For $K \approx M$ the spectrum narrows, and, for the whole lattice illuminated, shrinks to a single Lorentzian as in MI.

The condition $\kappa < \delta_0 = g^2/\Delta_{0a}$ is already met in present experiments. In the recent work [8], where setups of cavity QED and ultracold gases were joined to probe quantum statistics of an atom laser with ^{87}Rb atoms, the parameters are $(g, \Delta_{0a}, \kappa) = 2\pi \times (10.4, 30, 1.4)$ MHz. The setups of cavity cooling [23, 24] are also very promising.

For bad cavities ($\kappa \gg \delta_0 = g^2/\Delta_{0a}$), the sums can be replaced by integrals. The broad spectra in Figs. 9.2b and 9.3b,d are then given by convolutions of $p_\Psi(q)$ and Lorentzians. For example, curve B in Fig. 9.2b represents a Voigt contour, well-known in spectroscopy of hot gases. Here, the “inhomogeneous broadening” is a striking contribution of quantum statistics.

In summary, we exhibited that transmission spectra of cavities around a degenerate gas in an optical lattice are distinct for different quantum phases of even equal densities. Similar information is also contained in the field amplitudes $\langle a_{0,1} \rangle$ contrasting previous suggestions [13] that $\langle a_{0,1} \rangle$ probes only the average density. This reflects (i) the orthogonality of Fock states corresponding to different atom distributions and (ii) the different frequency shifts of light fields entangled to those states. In general also other optical phenomena and quantities depending nonlinearly on atom number operators should similarly reflect the underlying quantum statistics [25–27].

Methods

Derivation of Heisenberg equations

A manybody Hamiltonian for our system presented in Fig. 9.1 is given by

$$H = \sum_{l=0,1} \hbar \omega_l a_l^\dagger a_l + \int d^3 \mathbf{r} \Psi^\dagger(\mathbf{r}) H_{a1} \Psi(\mathbf{r}), \quad (9.8)$$

with

$$H_{a1} = \frac{\mathbf{p}^2}{2m_a} + V_{\text{cl}}(\mathbf{r}) + \hbar g^2 \sum_{l,m=0,1} \frac{u_l^*(\mathbf{r}) u_m(\mathbf{r}) a_l^\dagger a_m}{\Delta_{ma}}, \quad (9.9)$$

where $a_{0,1}$ are the annihilation operators of the modes of frequencies $\omega_{0,1}$, wave vectors $\mathbf{k}_{0,1}$, and mode functions $u_{0,1}(\mathbf{r})$; $\Psi(\mathbf{r})$ is the atom-field operator. In the effective single-atom Hamiltonian H_{a1} , \mathbf{p} and \mathbf{r} are the momentum and position operators of an atom of mass m_a trapped in the classical potential $V_{\text{cl}}(\mathbf{r})$, and g is the atom–light coupling constant. We

consider off-resonant scattering where the detunings between fields and atomic transition $\Delta_{la} = \omega_l - \omega_a$ are larger than the spontaneous emission rate and Rabi frequencies. Thus, in H_{a1} the adiabatic elimination of the upper state, assuming linear dipoles with adiabatically following polarization, was used.

For a one-dimensional lattice with period d and atoms trapped at $x_j = jd$ ($j = 1, 2, \dots, M$) the mode functions are $u_{0,1}(\mathbf{r}_j) = \exp(ijk_{0,1x}d + i\phi)$ for traveling and $u_{0,1}(\mathbf{r}_j) = \cos(jk_{0,1x}d + \phi)$ standing waves with $k_{0,1x} = |\mathbf{k}_{0,1}| \cos \theta_{0,1}$, $\theta_{0,1}$ are angles between the mode and lattice axes, ϕ is some spatial phase shift (cf. Fig. 9.1).

Assuming the modes $a_{0,1}$ much weaker than the trapping beam, we expand $\Psi(\mathbf{r})$ using localized Wannier functions [7] corresponding to the potential $V_{cl}(\mathbf{r})$ and keep only the lowest vibrational state at each site (we consider a quantum degenerate gas): $\Psi(\mathbf{r}) = \sum_{i=1}^M b_i w(\mathbf{r} - \mathbf{r}_i)$, where b_i is the annihilation operator of an atom at site i at a position \mathbf{r}_i . Substituting this expansion in the Hamiltonian H , one can get a generalized Bose-Hubbard model [7] including light scattering. In contrast to “Bragg spectroscopy”, which involves scattering of matter waves [4], and our previous work [28], we neglect lattice excitations here and focus on light scattering from atoms in some prescribed quantum states.

Neglecting atomic tunneling, the Hamiltonian reads:

$$H = \sum_{l=0,1} \hbar \omega_l a_l^\dagger a_l + \hbar g^2 \sum_{l,m=0,1} \frac{a_l^\dagger a_m}{\Delta_{ma}} \left(\sum_{i=1}^K J_{i,i}^{lm} \hat{n}_i \right),$$

where $\hat{n}_i = b_i^\dagger b_i$. For deep lattices the coefficients $J_{i,i}^{lm} = \int d\mathbf{r} w^2(\mathbf{r} - \mathbf{r}_i) u_l^*(\mathbf{r}) u_m(\mathbf{r})$ reduce to $J_{i,i}^{lm} = u_l^*(\mathbf{r}_i) u_m(\mathbf{r}_i)$ neglecting spreading of atoms, which can be characterized even by classical scattering [29]. The Heisenberg equations obtained from this Hamiltonian are given by Eq. (9.1), where we have added a relaxation term. Strictly speaking, a Langevin noise term should be also added to Eq. (9.1). However, for typical conditions its influence on the expectation values of normal ordered field operators is negligible (see e.g. [30]). In this paper, we are interested in the number of photons $\langle a_l^\dagger a_l \rangle$ only, which is a normal ordered quantity. Thus, one can simply omit the noise term in Eq. (9.1).

Simple expressions for spectral line shapes in SF state

We will now derive expressions for the spectra presented in Figs. 9.2 and 9.3 demonstrating relations between atomic quantum statistics and the transmission spectra for the SF state. As has been mentioned in the main text, in all examples presented in Figs. 9.2 and 9.3, the photon number depends only on a single statistical quantity, which we denote as q . Using this fact, the multinomial distribution in Eq. (9.5) reduces to a binomial, which can be directly derived from Eq. (9.5): $\langle f \rangle_{SF} = \sum_{q=0}^N f(q) p_{SF}(q)$ with $p_{SF}(q) = N!/[q!(N-q)!](Q/M)^q(1-Q/M)^{N-q}$ and a single sum instead of M ones. Here Q is the number of specified sites: Q is equal to K for one mode and two modes in a maximum; Q is the number of odd (or even) sites for two modes in a minimum ($Q = M/2$ for even M). This approach can be used for other geometries, e.g., for two modes in a minimum and $K < M$, where Eq. (9.5) can be reduced to a trinomial distribution.

As a next approximation we consider $N, M \gg 1$, but finite N/M , leading to the Gaussian distribution $p_{\text{SF}}(q) = 1/(\sqrt{2\pi}\sigma_q) \exp[-(q - \tilde{q})^2/2\sigma_q^2]$ with central value $\tilde{q} = NQ/M$ and width $\sigma_q = \sqrt{N(Q/M)(1 - Q/M)}$.

In high- Q cavities ($\kappa \ll \delta_0 = g^2/\Delta_{0a}$), $f(q)$ is a narrow Lorentzian of width κ peaked at some q -dependent frequency, now called Δ_p^q . Since the Lorentzian height is q -independent, $\langle f \rangle_{\text{SF}}$ as a function of Δ_p is a comb of Lorentzians with the amplitudes proportional to $p_{\text{SF}}(q)$.

Using the Gaussian distribution $p_{\text{SF}}(q)$, we can write the envelope of such a comb. For a single mode [Fig. 9.2a,c, Eq. (9.6)], we find $\Delta_p^q \approx \delta_0 q$ with the envelope

$$\langle a_0^\dagger a_0(\Delta_p^q) \rangle_{\text{SF}} = \frac{\alpha \delta_0}{\sqrt{2\pi}\sigma_\omega} e^{-(\Delta_p^q - \tilde{\Delta}_p)^2/2\sigma_\omega^2},$$

where the central frequency $\tilde{\Delta}_p = \delta_0 N_K$, spectral width $\sigma_\omega = \delta_0 \sqrt{N_K(1 - K/M)}$, and $\alpha = |\eta_0|^2/\kappa^2$. So, the spectrum envelopes in Fig. 9.2a,c are well described by Gaussians of widths strongly depending on K .

For $K \rightarrow 0$ and $K \rightarrow M$, the binomial distribution $p_{\text{SF}}(q)$ is well approximated by a Poissonian distribution, which is demonstrated in Fig. 9.2c for $K = 10$ and $K = 68$. For $K = M$ the spectrum shrinks to a single Lorentzian, since the total atom number at M sites does not fluctuate.

In other examples (Figs. 9.3a and 9.3c), the above expression is also valid, although with other parameters. For two modes in a diffraction maximum (Fig. 9.3a), the central frequency, separation between Lorentzians and width are doubled: $\tilde{\Delta}_p = 2\delta_0 N_K$, $\Delta_p^q \approx 2\delta_0 q$ and $\sigma_\omega = 2\delta_0 \sqrt{N_K(1 - K/M)}$; $\alpha = |\eta_0|^2/(2\kappa^2)$. The left satellite at $\Delta_p = 0$ has a classical amplitude $|\eta_0|^2/(4\kappa^2)$.

The nonclassical spectrum for two waves in a diffraction minimum (Fig. 9.3c) is centered at $\tilde{\Delta}_p = \delta_0 N$, with components at $\Delta_p^q \approx 2\delta_0 q$, and is very broad, $\sigma_\omega = \delta_0 \sqrt{N}$; $\alpha = |\eta_0|^2/\kappa^2$.

For bad cavities ($\kappa \gg \delta_0$), the sums can be replaced by integrals with the same parameters $\tilde{\Delta}_p$ and σ_ω as for $\kappa < \delta_0$. For a single mode, Fig. 9.2b represents a Voigt contour

$$\langle a_0^\dagger a_0(\Delta_p) \rangle_{\text{SF}} = \frac{|\eta_0|^2}{\sqrt{2\pi}\sigma_\omega} \int_0^\infty \frac{e^{-(\omega - \tilde{\Delta}_p)^2/2\sigma_\omega^2} d\omega}{(\Delta_p - \omega)^2 + \kappa^2}.$$

For two modes in a diffraction minimum the photon number (Fig. 9.3d) is

$$\langle a_1^\dagger a_1 \rangle_{\text{SF}} = \frac{|\eta_0|^2}{\sqrt{2\pi}\sigma_\omega} \int_{-\infty}^\infty \frac{\omega^2 e^{-\omega^2/2\sigma_\omega^2} d\omega}{(\Delta_p'^2 - \omega^2 - \kappa^2)^2 + 4\kappa^2 \Delta_p'^2},$$

where $\Delta_p' = \Delta_p - \tilde{\Delta}_p$, while in a maximum (Fig. 9.3b)

$$\langle a_1^\dagger a_1 \rangle_{\text{SF}} = \frac{|\eta_0|^2}{4\sqrt{2\pi}\sigma_\omega} \int_0^\infty \frac{\omega^2 e^{-(\omega - \tilde{\Delta}_p)^2/2\sigma_\omega^2} d\omega}{[\Delta_p(\Delta_p - \omega) + \kappa^2]^2 + \kappa^2 \omega^2}.$$

Bibliography

- [1] Bloch, I. Ultracold quantum gases in optical lattices. *Nat. Phys.* **1**, 23–30 (2005).
- [2] Fölling, S. *et al.* Spatial quantum noise interferometry in expanding ultracold atom clouds. *Nature* **434**, 481–484 (2005).
- [3] Altman, E., Demler, E., & Lukin, M. D. Probing many-body states of ultracold atoms via noise correlations. *Phys. Rev. A* **70**, 013603 (2004).
- [4] Stöferle, T., Moritz, H., Schori, C., Köhl, M. & Esslinger, T. Transition from a strongly interacting 1D superfluid to a Mott insulator. *Phys. Rev. Lett.* **92**, 130403 (2004).
- [5] Gritsev, V., Altman, E., Demler, E. & Polkovnikov, A. Full quantum distribution of contrast in interference experiments between interacting one-dimensional Bose liquids. *Nat. Phys.* **2**, 705–709 (2006).
- [6] Schellekens, M. *et al.* Hanbury Brown Twiss effect for ultracold quantum gases. *Science* **310**, 648–651 (2005).
- [7] Jaksch, D., Bruder, C., Cirac, J. I., Gardiner, C. W. & Zoller, P. Cold bosonic atoms in optical lattices *Phys. Rev. Lett.* **81**, 3108–3111 (1998).
- [8] Bourdel, T. *et al.* Cavity QED detection of interfering matter waves. *Phys. Rev. A* **73**, 043602 (2006).
- [9] You, L., Lewenstein, M. & Cooper, J. Line shapes for light scattered from Bose-Einstein condensates. *Phys. Rev. A* **50**, R3565–R3568 (1994).
- [10] Javanainen, J. Optical signatures of a tightly confined Bose condensate. *Phys. Rev. Lett.* **72**, 2375–2378 (1994).
- [11] You, L., Lewenstein, M., & Cooper, J. Quantum field theory of atoms interacting with photons. II. Scattering of short laser pulses from trapped bosonic atoms. *Phys. Rev. A* **51**, 4712–4727 (1995).
- [12] Javanainen, J. & Ruostekoski, J. Off-resonance light scattering from low-temperature Bose and Fermi gases. *Phys. Rev. A* **52**, 3033–3046 (1995).
- [13] Parkins, A. S. & Walls, D. F. The physics of trapped dilute-gas Bose-Einstein condensates. *Phys. Rep.* **303**, 1-80 (1998).
- [14] Morice, O., Castin, Y. & Dalibard, J. Refractive index of a dilute Bose gas. *Phys. Rev. A* **51**, 3896–3901 (1995).
- [15] Brune, M., *et al.* Quantum Rabi oscillation: a direct test of field quantization in a cavity. *Phys. Rev. Lett.* **76**, 1800–1803 (1996).
- [16] Gambetta, J. *et al.* Qubit-photon interactions in a cavity: Measurement-induced dephasing and number splitting. *Phys. Rev. A* **74**, 042318 (2006).

- [17] Campbell, G. K. *et al.* Imaging the Mott insulator shells by using atomic clock shifts. *Science* **313**, 649–652 (2006).
- [18] Gerbier, F., Fölling, S., Widera, A., Mandel, O. & Bloch, I. Probing number squeezing of ultracold atoms across the superfluid-Mott insulator transition. *Phys. Rev. Lett.* **96**, 090401 (2006).
- [19] Volz, T. *et al.* Preparation of a quantum state with one molecule at each site of an optical lattice. *Nat. Phys.* **2**, 692–695 (2006).
- [20] Winkler, K. *et al.* Repulsively bound atom pairs in an optical lattice. *Nature* **441**, 853–856 (2006).
- [21] Klinner, J., Lindholdt, M., Nagorny, B. & Hemmerich, A. Normal mode splitting and mechanical effects of an optical lattice in a ring cavity. *Phys. Rev. Lett.* **96**, 023002 (2006).
- [22] Lewenstein, M. *et al.* Ultracold atomic gases in optical lattices: Mimicking condensed matter physics and beyond. cond-mat/0606771.
- [23] Maunz, P. *et al.* Cavity cooling of a single atom. *Nature* **428**, 50–52 (2004).
- [24] Hood, C. J., Lynn, T. W., Doherty, A. C., Parkins, A. S. & Kimble, H. J. The atom-cavity microscope: single atoms bound in orbit by single photons. *Science* **287**, 1447–1453 (2000).
- [25] Mekhov, I. B., Maschler, C. & Ritsch, H. Cavity enhanced light scattering in optical lattices to probe atomic quantum statistics. quant-ph/0610073.
- [26] Mekhov, I. B., Maschler, C. & Ritsch, H., Light scattering from atoms in an optical lattice: optical probe of quantum statisticsin, *Books of abstracts for the XX International Conference on Atomic Physics, ICAP, Innsbruck, 2006*, p. 309 and conference web-site.
- [27] Chen, W., Meiser, D. & Meystre, P. Cavity QED determination of atomic number statistics in optical lattices. quant-ph/0610029.
- [28] Maschler, C. & Ritsch, H. Cold atom dynamics in a quantum optical lattice potential. *Phys. Rev. Lett.* **95**, 260401 (2005).
- [29] Slama, S., von Cube, C., Kohler, M., Zimmermann, C. & Courteille, P. V. Multiple reflections and diffuse scattering in Bragg scattering at optical lattices. *Phys. Rev. A* **73**, 023424 (2006).
- [30] Davidovich, L. Sub-Poissonian processes in quantum optics. *Rev. Mod. Phys.* **68**, 127 (1996).

Acknowledgments

The work was supported by FWF (P17709 and S1512). While preparing this manuscript, we became aware of a closely related research in the group of P. Meystre. We are grateful to him for sending us the preprint [\[27\]](#) and stimulating discussions.

Correspondence and request for materials should be addressed to I.B.M.

Competing financial interests

The authors declare that they have no competing financial interests.

Part III

Self-Organization of Atoms in Optical Lattices

CHAPTER 10

BACKGROUND: SELF-ORGANIZATION OF ATOMS IN A CAVITY

The last part of this thesis is devoted to a microscopic view on the self-organization process of atoms in a cavity field and its onset. In this background chapter we present a qualitative overview of the phenomenon of self-organizing atoms into a regular lattice in a cavity field, first investigated in our group [1]. In our studies here, we consider motion of the atoms along the direction of the pumping laser. This leads to slightly simplified calculations, but essentially contains all the underlying physics. The single-particle Hamiltonian for this situation, was derived in Sec. 3.3. Since this self-organization process, of course, relies on many-body physics, we have to derive a corresponding Bose-Hubbard Hamiltonian, as well. This can be found in the second part of this chapter.

Some of the results in the subsequent chapters have been obtained with Monte-Carlo wave function simulations, performed by Andras Vukics. In order to avoid an overloading of this thesis, we will not present a background chapter on the Monte-Carlo method, and instead refer to [2].

10.1 Collective Cooling and Spatial Self-Organization of Atoms

The strong coupling of a single atom inside a high- Q optical resonator allows for efficient cooling and trapping of this atom [3–7]. The underlying cooling mechanism is fundamentally different to usual laser cooling schemes and relies on the complex nonlinear interaction between cavity field and atom and on the presence of a dissipation channel, independent of spontaneous emission. Essentially, the atom scatters into the cavity mode, which can lose photons and hence energy via the cavity mirrors.

Conventional laser cooling schemes are not altered by the presence of many atoms, since they depend merely on single atom processes. For resonator-induced forces, though, this is drastically different. Here, all atoms interact, mediated by the intracavity field, to which all atoms are simultaneously coupled. Hence, the positions and velocities of the atoms influence each other and modify the scattering properties of each atom and therewith the cooling process. This leads to cooperative effects, providing for perspectives to significantly enhance the cooling efficiency.

This cooperative effect requires direct coherent driving of the atoms instead of exciting the cavity mode. We presented this so-called “atom pumping” setup already in chapters 5 and 6. We consider N two-level atoms, transversally illuminated by a red-detuned pumping laser (see Fig. 10.1). The atoms scatter photons in the cavity mode, with a field amplitude

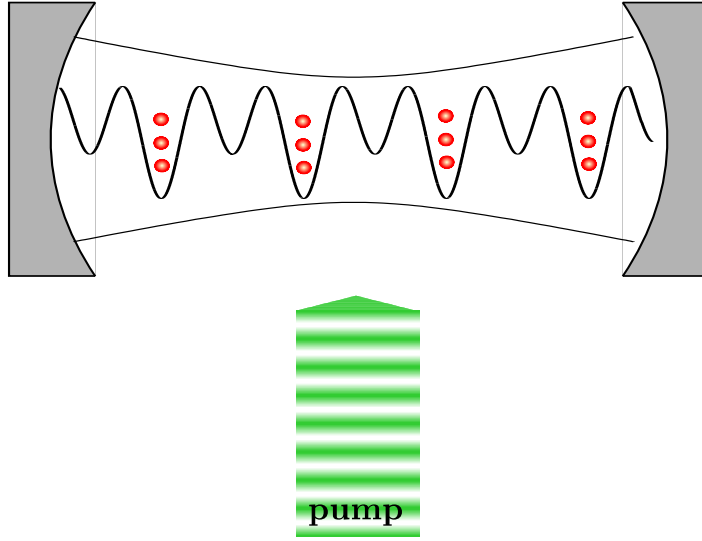


Figure 10.1. Schematic diagram of atoms, coherently excited from a laser, perpendicular to the cavity axis. This modifies the lattice potential (periodicity $\lambda/2$), by altering the depths of neighboring sites, leading to an array with periodicity λ . After a self-organization process the atoms form a density grating corresponding to this potential.

and phase, determined by each atoms' position. The key point is now, that interference between the emitted light fields from the various atoms has a drastic influence on the common scattering rates, as in ordinary Bragg scattering by a periodic pattern of atoms. Hence, the contributions of atoms in adjacent wells of an optical lattice cancel, since they are separated by half a wavelength and scatter fields with a phase difference of π . This would inhibit an intracavity field buildup for a uniform atomic distribution. Nevertheless, density fluctuations allow for a small field with some random corresponding phase. This induces a runaway process via atomic redistribution mediated by the cavity field. Due to the red detuning, the atoms are attracted by the antinodes of the optical lattice. This periodic localization leads to collective emission into the cavity mode direction, inducing deeper potential wells and further localization, which provides for a stabilization of the emerging atomic pattern.

As we mentioned above, the periodic pattern must be a grating with periodicity $\lambda/2$, which would only lead to destructive interference. Instead, the uniform gas spontaneously breaks the translational symmetry, and organizes itself in one of two possible patterns. Either all atoms accumulate at all “even” numbered or all “odd” numbered sites of the optical lattice with periodicity $\lambda/2$, generated by a standing wave with wavelength λ . The reason for this, lies in an additional force term proportional to $\cos(kx)$ [see Eq. (5.3)], instead of the quadratic dependence $\propto \cos^2(kx)$ of the dipole force of the optical lattice. This force, originating from the recoil accompanying the scattering corresponding to the atomic pumping, has opposite signs for neighboring wells. Hence, whilst one lattice well is deepened by this force, the depth of the subsequent neighboring well is reduced (see Fig. 10.1). Density fluctuations lead to a momentary unbalance of the populations in neighboring wells, inducing a runaway process, until all atoms are in the same class of well. The field intensity corresponding to this final

state depends quadratically on the atom number N , an obvious sign of the cooperativity in this process. For a suitable choice of parameters, this process leads to efficient cooling and trapping of the atoms, by means of the cavity loss, which dissipates the increased kinetic energy of the atoms, when they fall into the lattice wells. Heating processes limit the cooling temperature to some finite value.

In seminal experiments by Vuletić and coworkers [8–10], strongly enhanced emission (by orders of magnitude) was observed, as soon as the pumping laser intensity exceeded a certain threshold. This led to efficient cooling of large ensembles. Since a phase difference of π between the two possible regular gratings exist, a heterodyne measurement of the time phase allows to observe the symmetry breaking between the two patterns, induced by density fluctuations.

Moreover, this self-organization effect persists also in a two-dimensional situation, if the pumping field is a standing wave field, generated by counterpropagating laser beams. Here, the atoms organize in one of two equivalent rectangular arrays in form of a checkerboard. In Fig. 10.2, we schematically depict the two patterns and their spatial offset, leading to the phase difference in the scattered light.

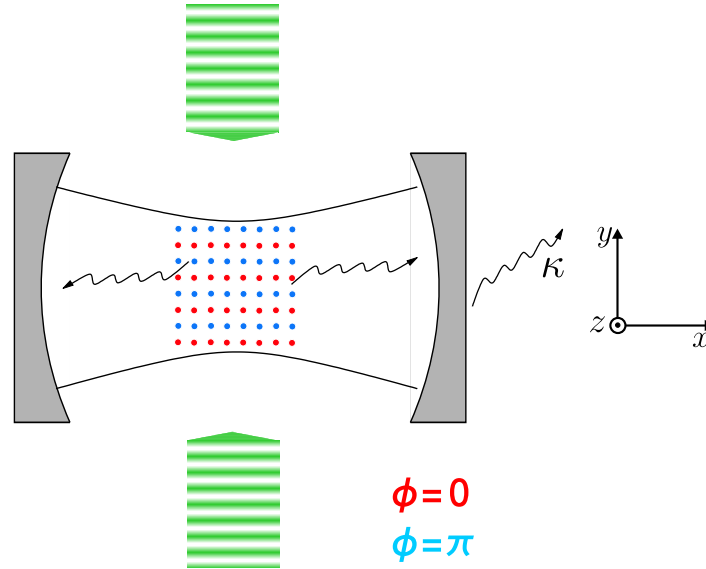


Figure 10.2. In two dimensions the atoms self-organize in a checkerboard pattern. The two different but equivalent density gratings, depicted by blue and red balls, emit light into the cavity mode with a phase difference of π .

An additional point has to be added to the above discussion. Zippilli et al. [11, 12] argued that, if the pumping field is close to resonance, Bragg scattering cannot explain the dramatic suppression of atomic fluorescence, which allows the cavity loss to be the dominant dissipation channel. In fact, for atom numbers below a certain threshold value, i.e. $N \ll N_0$, the intensity of the cavity field depends quadratically on the atom number, and the number of excited atoms is close to the free-space excitation population. The resulting enhancement of the scattering rate into the cavity can be well described by Bragg scattering. However, for

$N \gg N_0$, the total power of dissipation via spontaneous emission loses ground, since it scales as $1/N$. In this regime, leaking of cavity photons is the main dissipation channel and the intracavity intensity is approximately constant and independent of N . A closer look reveals, that for $\Delta_c \approx 0$ and $\kappa < \Gamma$, the cavity field and the pumping laser field have opposite phases and mutually cancel at atomic positions. Hence, the atoms localize at positions, where atomic excitations and fluorescence are strongly suppressed. Therefore, the ratio of scattering in the cavity mode to free-space scattering increases with N , even in the saturation regime, where the intensity of the cavity field is constant.

Note, that this collective effect is different to other, recently demonstrated, collective phenomena. For the collective atomic recoil laser in a ring cavity (CARL) [13–17], a magneto-optical trap is required, in order to stabilize the atoms, since their center of mass is continuously accelerated by the CARL process.

10.2 The Bose-Hubbard Hamiltonian for Transverse Motion

In Sec. 3.3 we described the setup for our studies concerning the onset of the self-organization process, to which this chapter is devoted. We considered motion of particles, in the optical lattice, generated by the pumping laser field. The coupling of the particles to the cavity mode, though, is responsible for collective effects, including the self-ordering of particles in one of two stable patterns.

In this section we have to correctly address a single particle Hamiltonian, which we implement in a second-quantized Hamiltonian, allowing for a many-body description. Starting from (3.51), we adiabatically eliminate the excited states simply by replacing the Pauli matrices σ_{\pm} by their steady state values

$$\sigma_- = -\frac{\zeta \cos(k_p \hat{y}) + g_0 \cos(k \hat{x}) a}{\gamma - i \Delta_a} \quad \text{and} \quad \sigma_+ = -\frac{\zeta \cos(k_p \hat{y}) + g_0 \cos(k \hat{x}) a^\dagger}{\gamma + i \Delta_a}. \quad (10.1)$$

Here k_p denotes the wavenumber of the pumping field lattice, whereas k is the wavenumber of the cavity lattice. To the contrary of (3.52), we incorporated the position in the cavity field via $\cos(k \hat{x})$, which in fact is necessary in the second-quantized formalism. Nevertheless, since we neglect motion along the cavity axis, we can omit the momentum operator \hat{p}_x and replace \hat{x} by a c-number x_0 . Then, the replacement of the expressions for the excitation operators yield

$$H_{\text{eff}} = \frac{\hat{p}_y^2}{2m} - \hbar [\Delta_c - U_0 \cos^2(k x_0)] a^\dagger a + V_0 \cos^2(k_p \hat{y}) + \text{sgn}(U_0) \sqrt{\hbar U_0 V_0} \cos(k_p \hat{y}) \cos(k x_0) (a + a^\dagger), \quad (10.2)$$

where the potential depth of the lattice corresponding to the pumping laser field and the cavity field (per photon), respectively, are given by $V_0 = \hbar \zeta^2 \Delta_a / (\gamma^2 + \Delta_a^2)$ and $U_0 = g_0^2 \Delta_a / (\gamma^2 + \Delta_a^2)$. The particle motion is now only one-dimensional, and we can apply the general second-quantized Hamiltonian (2.20). Here, we have to implement all terms, corresponding to particle motion. Since $\cos^2(k x_0) a^\dagger a$ originally depended on particle motion, we will include also

this term. Furthermore, without loss of generality, we can set $x_0 = 0$. Hence, we get:

$$H = \int_{\mathbb{R}} dy \Psi^\dagger(y) \left[\frac{\hat{p}_y^2}{2m} + V_0 \cos^2(k_p \hat{y}) + \text{sgn}(U_0) \sqrt{\hbar U_0 V_0} \cos(k_p \hat{y}) (a + a^\dagger) + \hbar U_0 a^\dagger a \right] \Psi(y) \\ - \hbar \Delta_c a^\dagger a + \frac{1}{2} \int_{\mathbb{R}} \int_{\mathbb{R}} dx dy \Psi^\dagger(x) \Psi^\dagger(y) U(x, y) \Psi(x) \Psi(y). \quad (10.3)$$

Here $\Psi(y)$ denotes the field operator for the bosonic particles. Now, proceeding along the lines of Sec. 2.3.1, we consider one-dimensional on-site interactions $U(x, y) = g_{1D} \delta(x - y)$ and expand the field operator in the Wannier basis, where we only take the lowest energy band into account, i.e.

$$\Psi(x) = \sum_{i=1}^M w(x - x_i) b_i. \quad (10.4)$$

Here $w(x)$ is the Wannier function, corresponding to the lowest band, and b_i is the bosonic annihilation operator for a particle at site i . Moreover, the same arguments concerning the relevance of the various tunneling contributions as in Sec. 2.3.1 are valid. Hence, we only have to consider next-neighbor hopping and only one term for the on-site interactions. Here, due to the existence of $\cos(k_p y)$, a new term appears, which allows the system to break the translational symmetry of the lattice. The associated matrix elements

$$\tilde{J}_{kl} = \text{sgn}(U_0) \sqrt{\hbar U_0 V_0} \int_{\mathbb{R}} dy w(y - y_k) \cos(k_p y) w(y - y_l) \quad (10.5)$$

have vanishing values for tunneling, i.e. $\tilde{J}_{n,n\pm 1} = 0$ for all n , if we neglect tunneling to other than adjacent sites:

$$\begin{aligned} \frac{\tilde{J}_{n,n\pm 1}}{\text{sgn}(U_0) \sqrt{\hbar U_0 V_0}} &= \int_{\mathbb{R}} dy w(y - y_{n\pm 1}) \cos(k_p y) w(y - y_n) \\ &= (-1)^n \int_{\mathbb{R}} dy w(y \pm a) \cos(k_p y) w(y) \\ &= \pm (-1)^n \int_{\mathbb{R}} dy w\left(y + \frac{a}{2}\right) \sin(k_p y) w\left(y - \frac{a}{2}\right) = 0, \end{aligned}$$

since $w(y + a/2)w(y - a/2)$ is even ($a = \pi/k$). A similar argument shows, that the on-site elements have alternating signs, i.e. $\tilde{J}_{n,n} = -\tilde{J}_{n\pm 1,n\pm 1}$. As a last step, the assumption of a constant atom number, allows to neglect constant terms in the second quantized Hamiltonian:

$$H = J \sum_{\langle k,l \rangle} b_k^\dagger b_l + \tilde{J} \sum_k (-1)^k \hat{n}_k (a + a^\dagger) - (\Delta_c - N U_0) a^\dagger a + \frac{U}{2} \sum_k \hat{n}_k (\hat{n}_k - 1). \quad (10.6)$$

Note, that to the contrary of chapter 2, here J is the matrix element, corresponding to the total energy $J = \int_{\mathbb{R}} dy w(y - a) \left(-\frac{\hbar^2}{2m} \frac{d^2}{dy^2} + V_0 \cos^2(ky) \right) w(y)$. The operator for the particle number at site k is denoted by $\hat{n}_k = b_k^\dagger b_k$ and $\tilde{J} = \tilde{J}_{00}$. This is the modified Bose-Hubbard Hamiltonian, providing for the many-body plus cavity field dynamics, which we use in the remaining two chapters of this thesis.¹

¹In chapter 12, the lattice definition is slightly different. There, the lattice potential is proportional to $\sin^2(k_p y)$, leading to lattice sites at $y_n = \pi/2 + na$ for $n \in \mathbb{Z}$. Nevertheless, this amounts just to a global phase shift, having no influence on matrix elements or any other properties of the dynamics.

Bibliography

- [1] P. Domokos and H. Ritsch, *Collective Cooling and Self-Organization of Atoms in a Cavity*, Phys. Rev. Lett. **89**, 253003 (2002).
- [2] A. Vukics and H. Ritsch, *C++QED: An Object-Oriented Framework for Wave-Function Simulations of Cavity QED Systems*, Eur. J. Phys. D **44**, 585 (2007).
- [3] P. Horak, G. Hechenblaikner, K. M. Gheri, H. Stecher, and H. Ritsch, *Cavity-Induced Atom Cooling in the Strong Coupling Regime*, Phys. Rev. Lett. **79**, 4974 (1997).
- [4] G. Hechenblaikner, M. Gangl, P. Horak, and H. Ritsch, *Cooling an Atom in a Weakly Driven High-Q Cavity*, Phys. Rev. A **58**, 3030 (1998).
- [5] C. J. Hood, T. W. Lynn, A. C. Doherty, A. S. Parkins, and H. J. Kimble, *The Atom-Cavity Microscope: Single Atoms Bound in Orbit by Single Photons*, Science **287**, 1447 (2000).
- [6] P. W. H. Pinkse, T. Fischer, P. Maunz, and G. Rempe, *Trapping an Atom with Single Photons*, Nature (London) **404**, 365 (2000).
- [7] P. Maunz, T. Puppe, I. Schuster, N. Syassen, P. W. H. Pinkse, and G. Rempe, *Cavity Cooling of a Single Atom*, Nature (London) **428**, 50 (2004).
- [8] H. W. Chan, A. T. Black, and V. Vuletić, *Observation of Collective-Emission-Induced Cooling of Atoms in an Optical Cavity*, Phys. Rev. Lett. **90**, 063003 (2003).
- [9] A. T. Black, H. W. Chan, and V. Vuletić, *Observation of Collective Friction Forces Due to Spatial Self-Organization of Atoms: From Rayleigh to Bragg Scattering*, Phys. Rev. Lett. **91**, 203001 (2003).
- [10] A. T. Black, J. K. Thompson, and V. Vuletić, *Collective Light Forces on Atoms in Resonators*, J. Phys. B: At. Mol. Opt. Phys. **38**, 605 (2005).
- [11] S. Zippilli, G. Morigi, and H. Ritsch, *Suppression of Bragg Scattering by Collective Interference of Spatially Ordered Atoms with a High-Q Cavity Mode*, Phys. Rev. Lett. **93**, 123002 (2004).
- [12] S. Zippilli, G. Morigi, and H. Ritsch, *Collective Effects in the Dynamics of Driven Atoms in a High-Q Cavity*, Eur. Phys. J. D **31**, 507 (2004).
- [13] D. Kruse, C. von Cube, C. Zimmermann, and Ph. W. Courteille, *Observation of Lasing Mediated by Collective Atomic Recoil*, Phys. Rev. Lett. **91**, 183601 (2003).
- [14] B. Nagorny, Th. Elsässer, and A. Hemmerich, *Collective Atomic Motion in an Optical Lattice Formed Inside a High-Finesse Cavity*, Phys. Rev. Lett. **91**, 153003 (2003).
- [15] Th. Elsässer, B. Nagorny, and A. Hemmerich, *Optical Bistability and Collective Behavior of Atoms Trapped in a High-Q Ring Cavity*, Phys. Rev. A **69**, 033403 (2004).

-
- [16] C. von Cube, S. Slama, D. Kruse, C. Zimmermann, Ph. W. Courteille, G. R. M. Robb, N. Piovella, and R. Bonifacio, *Self-Synchronization and Dissipation-Induced Threshold in Collective Atomic Recoil Lasing*, Phys. Rev. Lett. **93**, 083601 (2004).
- [17] S. Slama, C. von Cube, B. Deh, A. Ludewig, C. Zimmermann, Ph. W. Courteille, *Phase-Sensitive Detection of Bragg Scattering at 1D Optical Lattices*, Phys. Rev. Lett. **94**, 193901 (2005).

CHAPTER 11

PUBLICATION

Entanglement Assisted Fast Reordering of Atoms in an Optical Lattice within a Cavity at $T = 0$ [†]

Optics Communications **273**, 446 (2007)

C. Maschler¹, H. Ritsch¹, A. Vukics², and P. Domokos²

1) *Institut für theoretische Physik, Universität Innsbruck,
A-6020 Innsbruck, Austria*

2) *Research Institute of Solid State Physics and Optics, Hungarian Academy of Sciences,
H-1525 Budapest P.O. Box 49, Hungary*

Laser-illuminated atoms in an optical resonator exhibit a phase transition between the homogenous distribution and two possible ordered configurations in the optical lattice formed by the cavity and pump fields. At zero temperature, atom-field entanglement plays a crucial role in the spatial reordering of the atoms from a homogeneous towards the two ordered states, where all atoms occupy either only even or only odd lattice sites. Concurrent with the buildup of atom-field entanglement, the homogeneous atomic cloud evolves immediately into the superposition of the two stable patterns entangled with opposite cavity field amplitudes. This possibility is absent in a factorized (classical) treatment of atoms and field and should be generic for spontaneous symmetry breaking in quantum phase transitions in optical potentials.

Laser light with spatially modulated intensity, far red detuned from an atomic resonance creates a designable optical potential to trap and manipulate ultra-cold atoms [1]. Constructing a periodic lattice potential enables tailored implementations of the Bose-Hubbard Hamiltonian [2] to study quantum phase transitions [3] or ideas of quantum information processing [4]. Whilst the effect of a free-space laser field can be well approximated by an external potential via factorizing field and atomic dynamics, a field enclosed in a cavity is influenced by the atoms and takes part in the coupled atom-field dynamics [5, 10]. Nowadays in optical cavity QED using cold atoms in high finesse Fabry-Perot resonators the regime of strong light-matter interaction is experimentally accessible [6–8]. Here even a single cavity photon exerts significant forces and the quantum properties of the optical forces can no longer be ignored [9, 11].

[†]The primary contribution of the author of the present thesis to this publication were the calculations concerning the Bose-Hubbard model, while the Monte Carlo calculations were performed by A. V. The toy model was described by H. R. The author of the present thesis also acted as a discussion partner for all the aspects of this work.

In this paper we discuss some fundamental consequences of the back-action of a particle's motion on the potential it moves in. In particular, we concentrate on the physics of such an intrinsic feedback mechanism at the quantum level. Here the potential and thus the force the particles feel can be in a superposition state entangled with their position. As an experimentally accessible example we consider a laser-illuminated degenerate gas moving in the optical potential generated by a high-Q cavity field. As theoretically predicted [12] and subsequently demonstrated in experiment [13] this system exhibits a phase transition in the classical, thermal gas limit [14].

This phenomenon is briefly summarized as follows. For red detuning (high field seeking atoms), above a threshold pump intensity the atoms spontaneously break the continuous translational symmetry along the cavity axis (see the geometry in Fig. 11.1(b), although in this paper the motion will be restricted only along the pump field) and form one of two regular patterns that maximize light scattering from the pump into the cavity. Here the atoms arrange along Bragg planes optimally coupling the pump and the cavity fields. The two possible patterns (their configuration is similar to the black and white fields of a checkerboard) lead to superradiant light scattering proportional to the square of the particle number, however, with opposite phases of the cavity field amplitude. For a thermal cloud, the onset of self-organization can be understood as originating from an amplification of the atomic density fluctuations by feedback through the cavity field. For a random distribution of atoms on different lattice sites the scattering into the cavity mode enlarges the potential depth of those lattice sites, where more atoms sit. This subsequently leads to trapping of more atoms at these sites in a runaway process towards the ordered pattern.

In this paper we will concentrate on the regime of quantized atomic motion at $T = 0$, where the onset of atomic order and symmetry breaking is more intricate. Using an atomic BEC as an initial state the atoms have a kinetic energy much less than the recoil energy so that their wave function is flat on the wavelength scale [8]. Since the atoms form a linear refractive medium in the large atom-field detuning limit and coherent high-intensity pumping is employed, it is tempting to use a “classical” (mean-field) description of the scattered light field and calculate the back-action using a mean-field approximation of the condensate. This approximate mean-field model predicts that no light is scattered into the cavity from the initially homogeneous atomic distribution as the field amplitudes scattered into the cavity from different parts of the atomic wave function separated by half a wavelength interfere destructively. Thus one expects no light scattering at start and self-organization would occur on a very slow time scale only due to an eventual asymmetry of the initial wavefunction. As we will show later in this work, this conclusion is only valid for a “classical” (or factorized) description of the cavity field amplitude as it is widely applied for off resonant light scattering [15].

The cavity field in fact realizes a *quantum feedback* [16] for the atomic motion in which atom-field entanglement is a crucial element. In this case scattered field amplitudes with opposite phases do not necessarily cancel, but entangle to different atomic wave functions [17]. If these are orthogonal, “which way information” prevents the interference of the corresponding field amplitudes. Although the quantum average of the field amplitude is zero, the photon number in the cavity can grow fast. This is clearly incompatible with a classical field approximation or a factorization of the atom and field dynamics. The important point now is that the two opposite phase components of the cavity field superposition create opposite

forces pulling the corresponding parts of the atomic wave functions towards the respective self-organized configuration. Hence self-organization starts immediately even at $T = 0$ in the full quantum description of the ultracold atom and cavity system.

Note that this dynamics conserves symmetry and exhibits accelerated evolution towards a macroscopic superposition state of the atoms entangled with the field. Decoherence via cavity photon loss will induce spontaneous symmetry breaking later, which amounts to measurement induced relative atomic localization [18].

The remaining part of this paper is organized as follows. Before starting a detailed analysis of the coupled atom-field dynamics underlying the self-organization process, we will first briefly discuss some key aspects in a simplified mechanical system. Then we present the Hamiltonian of the optical system. We apply the Bose-Hubbard-type model introduced in [9] to numerically investigate the transient dynamics of initially homogeneous many-atom matter waves. The validity of the approximations (i.e. using the lowest lying levels in the Wannier basis) is then checked by the Monte-Carlo wave function method, developed for the specific system in [11].

The toy model with only two degrees of freedom describes the motion of a particle on a seesaw. The potential the atom experiences is determined by the tilt angle of the seesaw φ which is a dynamical variable coupled to the atom's position x as depicted in Fig. 11.1(a). Adding weak linear restoring forces both to the particle excursion and to the angular motion of the seesaw, the corresponding potential energy can be written as

$$\begin{aligned} V(x, \varphi) &= \omega_x^2 x^2 + \omega_\varphi^2 \varphi^2 - 2J \sin(\varphi)x \\ &\approx \omega_x^2 x^2 + \omega_\varphi^2 \varphi^2 - 2J\varphi x \\ &= (\omega_x x - \omega_\varphi \varphi)^2 - 2\varphi x(J - \omega_x \omega_\varphi) . \end{aligned} \quad (11.1)$$

In classical mechanics $x = \varphi = 0$ is a stationary point, which is unstable for $J > \omega_x \omega_\varphi$. A small perturbation from $x = 0$ triggers to tilt the seesaw slowly in one of the directions and the particle runs off with increasing acceleration. Obviously the closer the particle is to the origin initially, the longer it will stay near $x = 0$.

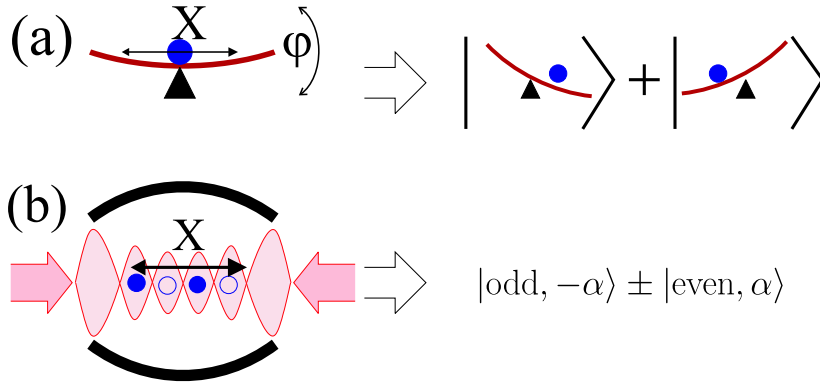


Figure 11.1. Scheme of the quantum seesaw (a) and the corresponding atom-cavity system (b).

However, the situation is different if x and φ are quantum variables. In this case we have two quantum oscillators $(\hat{x}, \hat{\varphi})$ with nonlinear coupling $J\hat{\varphi}\hat{x}$. Even for a perfectly balanced initial wavepacket with $\langle\hat{\varphi}\rangle = \langle\hat{x}\rangle = 0$ we find fast decay. Since the seesaw can evolve into a superposition of right and left tilt, the right part of the wave packet will push it to the right and start accelerating to the right with amplitude $\varphi(t)$, while the second half moves left with opposite tilt $-\varphi(t)$. Hence a quantum seesaw immediately leaves its unstable equilibrium and escapes towards right and left simultaneously, forming an entangled superposition of both possibilities. Although the expectation values of \hat{x} and $\hat{\varphi}$ remain zero (or grow slowly for a small initial asymmetry), their variances rapidly grow in time. Note that any factorization assumption for the two quantum degrees of freedom eliminates this decay possibility, which thus is essentially tied to the possibility of entanglement.

After this excursion to basic mechanics, which makes things look simple, let us now return to the more complex dynamics of ultracold atoms trapped in a 1D optical lattice perpendicular to a cavity (Fig. 11.1(b)). Here the cavity field takes the role of the seesaw potential. It is modified by the atoms through photon scattering between the mode and the lattice laser which is assumed far red detuned from the atoms but close to resonance with the cavity mode. Through interference between cavity and lattice field the particles influence the potential they move in.

In the limit of large atom-laser detuning (small atomic saturation) a corresponding single-atom Hamiltonian reads [5]:

$$H = \frac{p^2}{2m} + V_0 \sin^2(kx) - \hbar(\Delta_c - U_0) a^\dagger a + \sqrt{\hbar V_0 U_0} \sin(kx) (a + a^\dagger), \quad (11.2)$$

where a and a^\dagger are the cavity photon annihilation and creation operators. The optical lattice depth is given by V_0 , Δ_c denotes the detuning between the lattice field and the cavity resonance, and U_0 describes the shift of the cavity resonance frequency per atom ($V_0, U_0 < 0$). This enables us to construct an N-atom Hamiltonian in second quantized form. On expanding the atomic operators in a localized Wannier basis of the lattice potential and keeping only the lowest vibrational state, the following Bose-Hubbard type Hamiltonian [9] is obtained:

$$H = \sum_{m,n} J_{m,n} b_m^\dagger b_n - \hbar \left(\Delta_c - U_0 \sum_n b_n^\dagger b_n \right) a^\dagger a + (a + a^\dagger) \sum_{m,n} \hbar \tilde{J}_{m,n} b_m^\dagger b_n. \quad (11.3)$$

The operator b_n annihilates an atom at the site $kx = (n - 1/2)\pi$. The coupling matrix elements for the kinetic and potential energy $p^2/2m + V_0 \sin^2(kx)$ between sites m and n are denoted by $J_{m,n}$, whereas $\tilde{J}_{m,n}$ gives the matrix elements of $\sqrt{U_0 V_0 / \hbar} \sin(kx)$. Onsite interaction between atoms is neglected. The model holds as long as the scattering induced potential change is much smaller than the depth of the lattice potential, $|U_0| \ll |V_0|$.

Due to the periodicity of the system, it is enough to consider only two sites, left and right, centered on $kx = \pm\pi/2$. The matrix elements $J_{l,r} = J$, $\tilde{J}_{l,l} = -\tilde{J}_{r,r} = \tilde{J}$ are important, the others either vanish or amount to additive constants. The effective Hamiltonian reads

$$H = J (b_l^\dagger b_r + b_r^\dagger b_l) + \hbar(\Delta_c - U_0 N) a^\dagger a + \hbar \tilde{J} (b_l^\dagger b_l - b_r^\dagger b_r) (a + a^\dagger), \quad (11.4)$$

where $N = b_l^\dagger b_l + b_r^\dagger b_r$ is the total number of atoms.

We first attempt to apply a “classical” (mean-field) approximation to the cavity mode and replace the operators a and a^\dagger by their expectation values $\alpha(t)$ and $\alpha^*(t)$. As we are dealing with off resonant scattering from a coherent laser field with high photon number, this assumption looks reasonable. It is essentially equivalent to assuming a factorized atom-field state with this latter being in a coherent state. The atomic motion is governed by

$$H = J \left(b_l^\dagger b_r + b_r^\dagger b_l \right) + \hbar \tilde{J} \left(b_l^\dagger b_l - b_r^\dagger b_r \right) 2\text{Re} \{ \alpha(t) \}, \quad (11.5)$$

where $\alpha(t)$ fulfills a c-number equation [9] containing expectation values of atomic operators and a damping term with decay rate κ :

$$\dot{\alpha}(t) = [i(\Delta_c - U_0 N) - \kappa] \alpha(t) - i \tilde{J} \langle b_l^\dagger b_l - b_r^\dagger b_r \rangle. \quad (11.6)$$

By construction, entanglement is absent in this model and a perfectly symmetric atomic distribution with no average field implies $\dot{\alpha}(t) = \alpha(t) = 0$ and is stationary. The system can escape from this stationary solution only by spontaneous symmetry breaking. As shown in Fig. 11.2, starting with a tiny initial population asymmetry reveals the bistability of the system and will dynamically confine the atoms to one of the two wells correlated with a nonzero field amplitude. The characteristic time required for this is determined by the size of the (thermal) fluctuations.

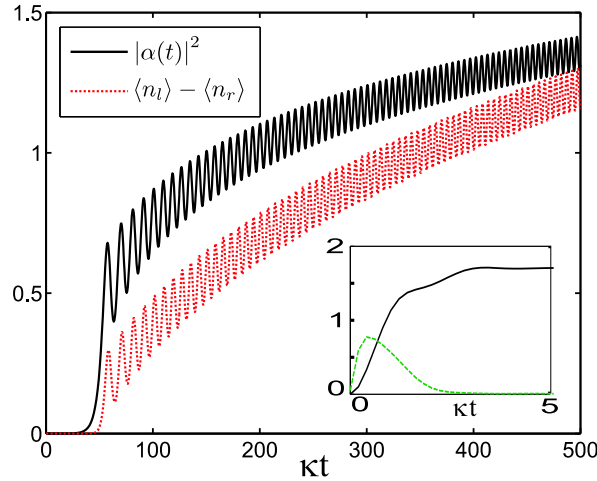


Figure 11.2. (a) Time evolution of the field intensity (dashed line) and site-occupation difference (solid line) for mean-field approximation (c.f. Eq. (11.6)) and taking four atoms. The initial distribution deviates slightly from a symmetric one, $U_0 = -0.25\kappa$, $\Delta_c = -2/3\kappa$, $V_0 = -4\hbar\kappa$ and $\kappa = 1\frac{\hbar k^2}{m}$. The insert shows the much faster growth of the field intensity (solid line) and entanglement of the corresponding quantum model (note the different time range).

However, the numerical solution of the full quantum dynamics reveals that this mean field approach is a very poor approximation. In sharp contrast to the mean-field approximation the quantum solution of Eq. (11.4) exhibits an instant increase of the photon number and fast self-organization as shown by the solid line in the inset of Fig. 11.2. Essentially the buildup

of a nonclassical field with atom-field entanglement in the quantum solution generates this fast dynamics.

As a better approximation to the full quantum solution of Eq. (11.4) we formally solve the operator Heisenberg equation for a in the bad cavity limit, where the field adiabatically follows the atomic dynamics. The genuine quantum properties of the cavity field a are then represented in terms of the atomic population difference operator:

$$a = -i \frac{\tilde{J}}{\kappa - i(\Delta_c - U_0 N)} \left(b_l^\dagger b_l - b_r^\dagger b_r \right). \quad (11.7)$$

As the atom number $\hat{N} = N$ is a constant of motion, the dynamics takes place in irreducible subspaces. It is instructive to consider first the single atom subspace where the entanglement-assisted decay, analogous to the quantum seesaw mechanism, can already be seized. For a single atom, $b_i^\dagger b_i$ acts as a projector on the i -th well. Hence, depending on the atom's position the field $\langle a \rangle$ changes sign and vanishes for a symmetric atomic state. However, the photon number operator $a^\dagger a \propto (b_l^\dagger b_l - b_r^\dagger b_r)^2$ is proportional to the unit operator in the single atom subspace, so that the photon number is nonzero independent of the atomic state and in particular also for a symmetric state. This implies that, in contrast to the mean-field description, even a perfect symmetric initial population triggers the growth of the photon number although the mean field vanishes, $\langle a \rangle = 0$.

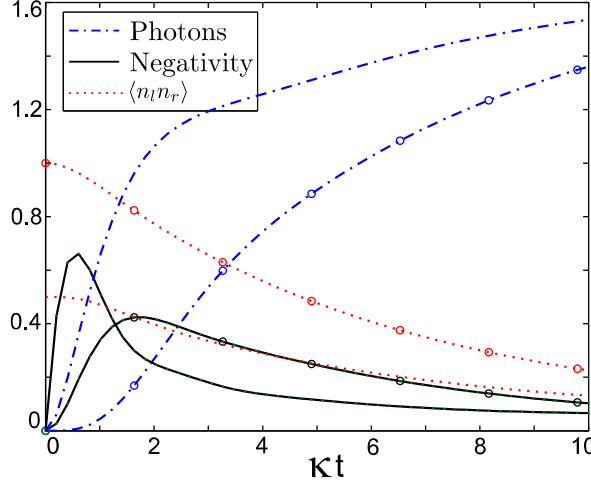


Figure 11.3. Entanglement (solid lines), photon number (dot-dashed lines), and the two-site atom-atom correlation function (dotted lines) for two atoms in two wells. Lines with extra circles show the case of exactly one atom in each well at start (Mott state), while the others correspond to a symmetric superposition state for each atom (superfluid state). The parameters are $U_0 = -2\kappa$, $\Delta_c = -6\kappa$, $J = 0.01\kappa$ and $\tilde{J} = 1.6\kappa$

The dynamics is qualitatively quite similar for two atoms as shown in Fig. 11.3. One can monitor the self-organization process by looking at the probability for the two atoms sitting in different wells ($\langle n_l n_r \rangle$), which decays during the self-organization process. Note that the

entanglement decays on a longer time scale, due to environmental effects, than the formation of the self-organized state. Interestingly there is a marked dependence on the specific quantum state producing an initially symmetric population distribution. The *superfluid* state, when both atoms are in a symmetric superposition of the two wells, $(1/2 (b_l^\dagger + b_r^\dagger)^2 |0\rangle)$, self-organizes faster than the *Mott insulator* state $(b_l^\dagger b_r^\dagger |0\rangle)$, indicated by the lines with circles in the figure). The Mott state is a perfectly balanced initial state with exactly one atom in each well without any quantum density fluctuations. The corresponding steady-state field, given in Eq. (11.7), is an eigenstate with zero eigenvalue. Nevertheless, tunneling induces coherence between the left and right sites and subsequently the entanglement drives the decay towards the self-organized state.

Let us now go one step further towards realistic modeling and check the lattice model by the Monte Carlo Wave Function (MCWF) method [11]. This method allows to solve the coupled atom-field dynamics given by Eq. (11.2) including cavity decay and atomic spontaneous emission. The atomic motion is limited to one wavelength with periodic boundary conditions, however, it is not restricted to the lowest-energy Wannier-basis states. The energy and photon number dependent tunneling is automatically included in the wave function trajectories.

The full atom-cavity density operator can be approximated by an ensemble average. For a deep enough potential $V_0 < -10E_r$, where $E_r = (\hbar k)^2/2m$ is the recoil energy, and small U_0 , an excellent agreement with the lattice model is obtained. As an instructive example the evolution of the mean photon number and the negativity characterizing the atom-field entanglement is plotted in Fig. 11.4. Here we have chosen some detuning between the cavity mode and the pump light to get photon number oscillations, which highlights the connection between photon number and entanglement at the self- organizations onset.

Light scattering creates photons immediately in the cavity in a superposition state of two phases entangled to an atomic state. The photon number oscillates in parallel with the atom-field entanglement. Note the very good agreement with the quantum lattice model, which predicts more entanglement since less atomic states are available (just the lowest Wannier basis states).

Looking at individual trajectories reveals that the system evolves into the “stochastic” state

$$|\psi_{\pm}\rangle = 1/\sqrt{2} (|\text{left}\rangle |\alpha\rangle \pm |\text{right}\rangle |-\alpha\rangle), \quad (11.8)$$

where $|\text{left}\rangle |\alpha\rangle$ ($|\text{right}\rangle |-\alpha\rangle$) means an atomic wave packet centered on the left (right) with coherent field states of amplitude α ($-\alpha$). It is checked by inspecting the numerical wavefunction that the field state components $|\pm\alpha\rangle$ are indeed very close to a coherent state, i.e., to the class of states that is usually considered classical. However, even a linear medium scattering classical light can generate a nonclassical field if the scatterer position is in a quantum superposition state. The state of Eq. (11.8) stochastic in the sense that each photon loss event flips the relative sign of the two contributions. Although no phase information is extracted from the counted photons, the density matrix evolves into a left-right mixed state if one does not keep exactly track of the counts. Hence entanglement decays on the time scale of cavity loss.

The sensitivity of the self-organized state to quantum fluctuations can be studied by launching the system from the ordered initial state $|r\rangle |-\alpha\rangle$. As we see in Fig. 11.5 tunneling

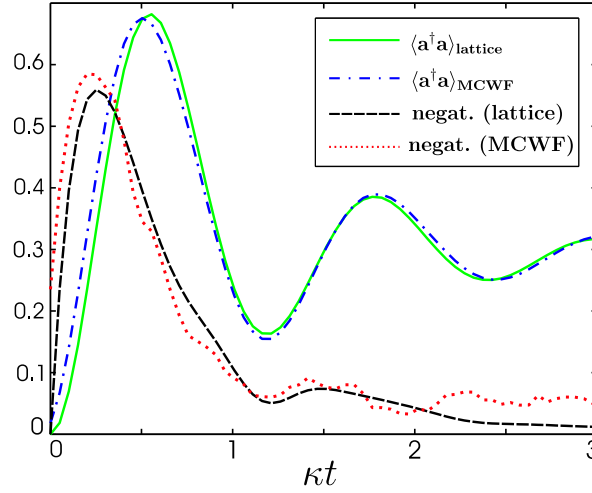


Figure 11.4. Fast correlated growth of entanglement (i.e. logarithmic negativity) and photon number for a single atom starting in a symmetric state and a vacuum field. Parameters: $U_0 = -4\kappa$, $\Delta_c = -9\kappa$, $V_0 = -2\kappa$, $\kappa \approx 40 \frac{\hbar k^2}{m}$. The results of the MCWF simulations (dotted and dashed-dotted line) agree very well with the lattice model (dashed and solid line).

is suppressed as the effective potential is deeper than V_0 and this state is remarkably stable. Nevertheless the atom can escape owing to some large quantum fluctuation and the field amplitude collapses. Again we end up in the state of Eq. (11.8), where $\langle x \rangle = \langle a \rangle = 0$, while the photon number is nonzero: $\langle a^\dagger a \rangle \approx |\alpha|^2$. Hence in terms of the quantum seesaw we see that even if it is tilted to one direction, fluctuations eventually enable the system to escape from this state to a symmetric final state again.

In summary, at the example of self-organization of ultracold atoms in an optical lattice we found that a full quantum description of the field and the possibility of entanglement is an essential ingredient for correctly describing dynamical decay of a quantum system from an unstable equilibrium point. The classical (factorized atom-field state) description of the optical potential predicts a stationary homogeneous distribution, while a quantum description implies immediate atomic ordering via atom-field entanglement formation. The entanglement involves states that cannot be described as small quantum fluctuations around a large mean-field, even if starting the system from coherent states with large photon and atom number. Entanglement enabled decay can be a generic feature in the dynamics of quantum phase transitions induced by a classical control parameter, whenever the quantum system acts even minimally back on its control. Recent progress in cavity QED should allow to study such models in the laboratory with current technology.

We acknowledge funding from the Austrian Science Foundation (P17709), the National Scientific Fund of Hungary (T043079, T049234, NF68736).

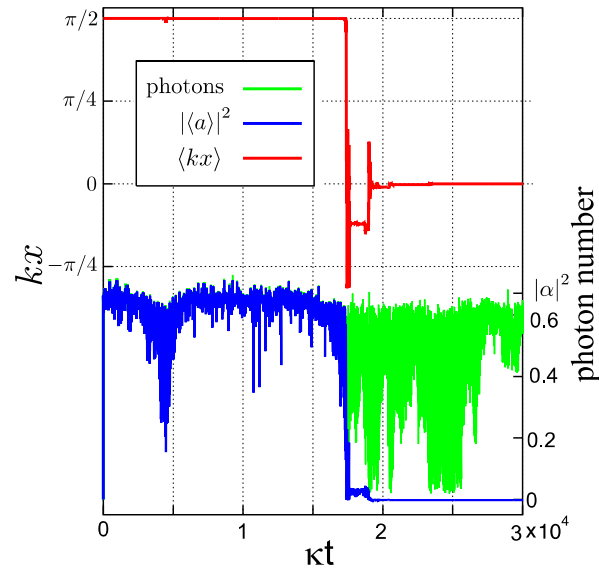


Figure 11.5. Dynamic formation of a symmetrically self-organized state. The atom is initially well localized in the right well ($\langle x \rangle = -\frac{\pi}{2}$) and generates approximately a coherent field of intensity $\langle a^\dagger a \rangle \approx |\langle a \rangle|^2 \approx |\alpha|^2$. Due to fluctuations it eventually escapes and evolves into the state of Eq. (11.8), having no mean field but non-vanishing photon number: $\langle a \rangle = 0$, $\langle a^\dagger a \rangle \approx |\alpha|^2$. Parameters: $U_0 = -\kappa/2$, $\Delta_c = -1.2\kappa$, $V_0 = -2\hbar\kappa$, $\kappa \approx 200 \frac{\hbar k^2}{m}$.

Bibliography

- [1] M. A. Kasevich, *Science* **298**, 1363 (2002).
- [2] D. Jaksch, C. Bruder, J. I. Cirac, C. W. Gardiner, and P. Zoller, *Phys. Rev. Lett.* **81**, 3108 (1998); D. Jaksch and P. Zoller, *Ann. Phys.* **315**, 52 (2005).
- [3] M. Greiner, O. Mandel, T. Esslinger, T. W. Hänsch, and I. Bloch, *Nature* **415**, 39 (2002).
- [4] P. Zoller, *et. al.*, *Eur. Phys. J. D* **36**, 203 (2005).
- [5] P. Domokos and H. Ritsch, *J. Opt. Soc. Am. B* **20**, 1098 (2003).
- [6] P. Maunz, T. Puppe, I. Schuster, N. Syassen, P. W. H. Pinkse, and G. Rempe, *Nature* **428**, 50 (2004).
- [7] A. Boca, R. Miller, K. M. Birnbaum, A. D. Boozer, J. McKeever, and H. J. Kimble, *Phys. Rev. Lett.* **93**, 233603 (2004).
- [8] A. Öttl, S. Ritter, M. Köhl, and T. Esslinger, *Phys. Rev. Lett.* **95**, 090404 (2005); T. Bourdel, T. Donner, S. Ritter, A. Öttl, M. Köhl, and T. Esslinger, *Phys. Rev. A* **73**, 43602 (2006).

- [9] C. Maschler and H. Ritsch, Phys. Rev. Lett. **95**, 260401 (2005); C. Maschler and H. Ritsch, Opt. Comm. **243**, 145 (2004).
- [10] S. Zippilli and G. Morigi, Phys. Rev. Lett. **95**, 143001 (2005); *ibid.*, Phys. Rev. A **72**, 053408 (2005).
- [11] A. Vukics, J. Janszky, and P. Domokos, J. Phys. B. **38**, 1453 (2005).
- [12] P. Domokos and H. Ritsch, Phys. Rev. Lett. **89**, 253003 (2002).
- [13] A. T. Black, H. W. Chan, and V. Vuletic, Phys. Rev. Lett. **91**, 203001 (2003).
- [14] J. K. Asbóth, P. Domokos, H. Ritsch, and A. Vukics, Phys. Rev. A **72**, 053417 (2005).
- [15] S. Inouye, A. P. Chikkatur, D. M. Stamper-Kurn, J. Stenger, D. E. Pritchard, and W. Ketterle, Science **285**, 571 (1999), and references therein.
- [16] S. Lloyd, Phys. Rev. A **62**, 022108 (2000).
- [17] C. Cohen Tannoudji, Atoms in electromagnetic fields, World Scientific Singapore, 1994.
- [18] A. V. Rau, J. A. Dunningham, and K. Burnett, Science **301**, 1081 (2003).
- [19] G. Vidal and R. F. Werner, Phys. Rev. A **65**, 032314 (2002).

CHAPTER 12

PUBLICATION

Microscopic Physics of Quantum Self-Organisation of Optical Lattices in Cavities[†]

New Journal of Physics **9**, 255 (2007)

A. Vukics, C. Maschler, and H. Ritsch

*Institut für theoretische Physik, Universität Innsbruck,
A-6020 Innsbruck, Austria*

We study quantum particles at zero temperature in an optical lattice coupled to a resonant cavity mode. The cavity field substantially modifies the particle dynamics in the lattice, and for strong particle-field coupling leads to self-organisation of the particles, a configuration with only every second site occupied. We study the growth of this order out of a homogeneous initial distribution for few particles. Simulations reveal that the growth dynamics crucially depends on the initial quantum many-body state of the particles and can be monitored via the cavity fluorescence. Studying the relaxation time of the ordering reveals inhibited tunneling due to the interaction with the cavity field. However, the relaxation becomes very quick for strong coupling.

12.1 Introduction

Ultracold atoms in an optical lattice formed by a far detuned laser field constitute an ideal system to study quantum phase transitions, i.e., phase transitions at zero temperature [1]. In the most prominent example first predicted theoretically [2] and confirmed experimentally [3] it was found that the particle ground state changes from a superfluid state where all atoms are delocalised to a perfectly ordered Mott insulator state for increasing lattice depth. More complex phases as supersolids, etc. were predicted if long range interactions or mixed species setups [4, 5] are used, but these are harder to realize and measure experimentally. While the final states are well understood, these phase transitions require the buildup or decay of long range correlations, the mechanism and time scale of which is not fully understood.

In a parallel development a dynamical transition to a self-organised phase in optical lattices was found for classical particles, when the lattice is placed inside an optical resonator.

[†]The primary contribution of the author of the present thesis to this publication were all the calculations concerning the Bose-Hubbard model. He also acted as a discussion partner for all the aspects of this work.

It originates from interference of the resonantly enhanced light field scattered by the atoms into the cavity mode with the lattice light itself and leads to a preferred occupation of every second site [6]. For a finite temperature cloud thermal density fluctuations are amplified and lead to a runaway self-organisation by feedback from the cavity field. However, for a BEC ($T \approx 0$) the initial density is perfectly homogeneous and only quantum fluctuations which go beyond a mean field description of the cold gas can start the self-organising process when the cavity interaction is switched on. Tunnelling results in a dynamical change of the atomic phase at $T = 0$ which gets irreversible only if cavity decay is included. In this work we study this *quantum* dynamics on the microscopic level and show how it depends on the precise quantum properties of the initial atomic state beyond any mean field density.

The paper is also intended to show the limitations of the effective Bose-Hubbard type model developed earlier [7] for atom-cavity systems. We demonstrate that in the regime of moderate coupling the low-dimensional Bose-Hubbard approach reproduces very well the results of a full Monte Carlo wave-function simulation, while it breaks down in the regime of stronger coupling. Even in this regime, however, it predicts the steady state surprisingly well, whereas the relaxation time to this state is predicted wrong. We show that the relaxation time of the system exhibits a highly non-trivial behaviour. In the regime of moderate atom-cavity coupling the relaxation time is composed of the timescale of photon counts and that of tunnelling. The combination of these two time scales leads to a minimum behaviour in the relaxation time, while for stronger coupling the relaxation becomes very quick, a behaviour observed in the full simulations but not reproducible with the Bose-Hubbard approach.

We first describe our system, the model, and solution methods applied. Afterwards, we go on investigating the dynamics of a single atom in the system. Although self-organisation cannot be defined in this case, we demonstrate that already here the relaxation time exhibits the same behaviour we find later for two atoms, and here it is easier to give a qualitative picture of this behaviour. We finally turn to the case of two atoms and show how the increasing coupling results in a transition from a $T = 0$ homogeneous initial condition into a self-organised configuration in steady state.

12.2 System, Models

The proposed setup is depicted in Figure 12.1. It consists of a one dimensional optical lattice within a cavity sustaining a single mode with its axis aligned orthogonally to the lattice axis — such systems have been studied in diverse theoretical contexts before [8–11], and are available experimentally [12, 13]. We assume that the cavity mode function is constant along the lattice direction, still, as we will see below, it modifies significantly the dynamics of atoms in the lattice.

A standard quantum optical model for the system with a single atom moving in one dimension along the lattice axis is obtained by adiabatic elimination of the atomic excited state(s). This is justified in the regime where the driving — in our case, the laser generating the lattice (pump) — is far detuned from the atomic transition frequency [14, 15]. The Hamiltonian for a single atom and the cavity then reads ($\hbar = 1$):

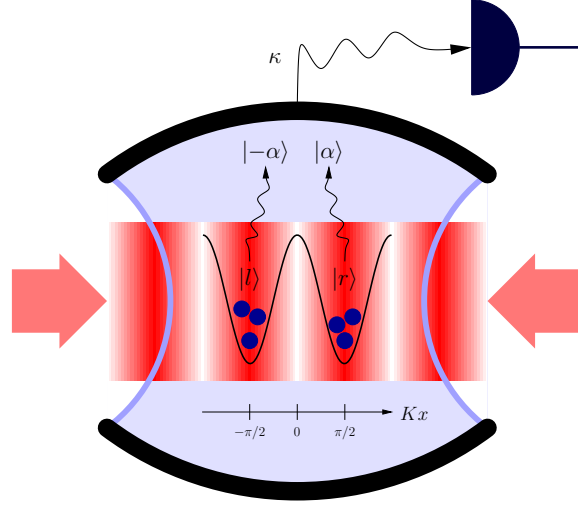


Figure 12.1. Scheme of the system consisting of a one dimensional optical lattice with lattice axis x and a cavity sustaining a single EM mode aligned orthogonally.

$$H = \frac{p^2}{2\mu} + V_0 \sin^2(Kx) - (\Delta_C - U_0) a^\dagger a + \text{sign}(U_0) \sqrt{U_0 V_0} \sin(Kx) (a^\dagger + a). \quad (12.1)$$

Here x , p , and μ are the atomic position and momentum operators and the mass, respectively; a is the cavity field operator, $\Delta_C = \omega - \omega_C$ is the cavity detuning — ω is the laser, ω_C is the cavity frequency —, and K is the lattice field wave number. The first two terms describe the atomic motion in the lattice, which appears as a classical potential after the elimination of the atomic internal dynamics. The potential depth for a two-level atom $V_0 = \eta^2/\Delta_A$ where η is the pump Rabi frequency and $\Delta_A = \omega - \omega_A$, ω_A is the atomic transition frequency. The third term is the free Hamiltonian of the cavity mode with the detuning shifted by $U_0 = g^2/\Delta_A$ where g is the atom-cavity interaction coupling constant. The last term describes the atom-mode interaction which stems from stimulated absorption from the pump followed by stimulated emission into the cavity mode and the reverse process. Atomic spontaneous emission is strongly suppressed due to the large atom-pump detuning and therefore neglected. The cavity mode is, however, coupled to the surrounding EM modes, resulting in the decay of cavity photons (escape through the mirrors). The process is described by the Liouvillean dynamics [16]

$$\mathcal{L}\rho = \kappa \left(2a\rho a^\dagger - [a^\dagger a, \rho]_+ \right). \quad (12.2)$$

Note that model (12.1)-(12.2) is not specific to a two-level atom but generally applicable to linearly polarisable particles, atoms and molecules alike. In this case the parameter U_0 is proportional to the susceptibility of the particles [15]. In the following we shall hence speak about *particles* without any further specification.

As described theoretically [6, 17] and observed experimentally [18] the model (12.1)-(12.2) features a phase transition termed self-organisation for a finite temperature classical

gas. As this occurs for red-detuned driving, i.e., high field seeking particles with $U_0, \Delta_C < 0$ we will restrict ourselves to this case. Self-organisation can be qualitatively understood as follows: The system has three steady-state configurations in a mean field description: (i) an “unorganised” configuration where the particles are equally distributed through all lattice sites and scatter no light into the cavity due to destructive interference and (ii) two “organised” configurations in which the particles occupy either only the even or only the odd sites of the lattice and scatter superradiantly into the cavity. In the latter case the last term in the Hamiltonian (12.1) deepens the lattice potential *at the positions of the particles*, so that they are *self-trapped* or “self-organised”.

Configurations (ii) have lower energy and entropy (lower symmetry) than configuration (i). At a given temperature the system chooses between configuration (i) and one of configurations (ii) so as to minimise the free energy. Lowering the temperature results in a phase transition when the symmetry of configuration (i) is spontaneously broken into the lower symmetry of one of configurations (ii).¹

The above qualitative picture is modified by the fact that the system never reaches thermal equilibrium with some external heat bath as energy is continuously flowing through the system from the pump via scattering on the particles into the cavity field and then out via the cavity loss channel. Self-organisation is therefore a dynamical phase transition for which the above mentioned configurations are steady-state patterns. In steady state the particles have a momentum distribution determined by the cavity field fluctuations, which, in most cases of physical interest, resembles very much a thermal distribution [19]. In this sense it is justified to speak about an effective temperature of the particles and use the picture of an equilibrium phase transition as we did above.

Let us now turn to the case of zero temperature and envisage a fixed number of classical point particles at each lattice site. In contrast to above, no matter whether we are above or below the threshold, no dynamics will arise because a homogeneous gas scatters no field into the cavity due to destructive interference. If no photons are present initially, such a classical gas cannot break the symmetry and is unable to escape the initial homogeneous configuration (i).

In the following we show that this is quite different for quantum particles at $T = 0$, a situation which can be prepared by loading a BEC or particles coupled out from a BEC into the cavity [20, 21]. Interestingly, in this case both for a Mott insulator and superfluid state (BEC) as initial condition, quantum fluctuations and the possibility of tunnelling between lattice sites immediately start self-organisation and the superradiant build-up of the cavity photon number. This is combined with an intricate measurement-induced dynamics related to the information gained via the dissipation channel of the photon-loss.

Let us emphasise that there are two main differences as compared to the above-described classical self-organisation: the initial temperature of the particles is zero and the particles in the lattice are confined strongly enough so that hopping between the lattice sites is due solely to tunnelling. Redistribution thus is a coherent quantum process and requires no direct inter-particle interaction.

¹Note that self-organisation is a phase transition without any direct particle-particle interaction: only an effective interaction exists generated by the single cavity mode with which all particles interact.

We are using two approaches to the problem. The first one is the direct simulation of the system (12.1)-(12.2) by the Monte Carlo wave-function (MCWF) method, which unravels the corresponding Master equation in terms of individual quantum trajectories. This approach takes into account the full particle and cavity dynamics, with the cavity decay accounted for by quantum jumps. We are using a new simulation framework presented in Reference [22]. The second approach analogous to standard Bose Hubbard models is based on a second-quantised form of the Hamiltonian (12.1): $\int dx \Psi^\dagger(x) H \Psi(x)$ where the field operator $\Psi(x)$ is restricted to the lowest vibrational band of the lattice.

To obtain the smallest possible system useful for studying self-organisation, we restrict the dynamics to only one lattice wavelength, that is, two lattice sites (cf. Figure 12.1) with periodic boundary condition. This is the smallest system which can seize the difference between the configurations described above and contains all the essential physics.

With two lattice sites the lowest vibrational band constitutes a two-dimensional Hilbert space, for which the localised Wannier basis with state $|l\rangle$ localised at the left and $|r\rangle$ at the right lattice site can be used. Hence $\Psi(x) = \langle x|l\rangle b_l + \langle x|r\rangle b_r$, where b_l and b_r are the corresponding bosonic annihilation operators. Putting the restricted field operator back into the second-quantised Hamiltonian we obtain the Bose-Hubbard type Hamiltonian:

$$H_{\text{BH}} = J \left(b_l^\dagger b_r + b_r^\dagger b_l \right) - (\Delta_C - NU_0) a^\dagger a + \tilde{J} \left(b_l^\dagger b_l - b_r^\dagger b_r \right) \left(a^\dagger + a \right), \quad (12.3)$$

where $J \equiv \langle l| (p^2/(2\mu) + V_0 \sin^2(Kx)) |r\rangle$ and $\tilde{J}/(\text{sign}(U_0)\sqrt{U_0 V_0}) \equiv \langle l| \sin(Kx) |l\rangle = -\langle r| \sin(Kx) |r\rangle$.

The dynamics of particles in cavities as described by such Hamiltonians in system configurations different from the one investigated here has been discussed in Refs. [7, 23, 24]. A very attractive feature of Hamiltonian (12.3) is that it is simple enough so that together with the Liouvillean (12.2) the full time-dependent Master equation can be solved even for several particles. For discussions below we will imagine this Master equation as unravelled in quantum trajectories.

12.3 Discussion

Self-organisation of an initially thermal gas of classical point-like particles in the system with classical cavity field (coherent state) has been described above to set the scene for the two-particle quantum results presented in Section 12.5, and to raise two questions concerning quantum particles in a quantum-mechanically described cavity field:

1. whether in the steady state of the quantum Master equation (12.1)-(12.2) there is some transition, a quantum analogue for the above-described self-organisation, which is a classical dynamical phase transition [17].
2. if there is such a transition then whether there is a mechanism via which an ultracold homogeneous gas can escape the unorganised configuration and evolve into the organised one(s), which is not possible with a classical mean-field description of either the atoms or the cavity field [25].

In Section 12.5 both questions will be answered to the positive for the case of two particles in the system restricted to two lattice sites, which is the smallest system for which the two questions make sense. For two particles we certainly cannot expect a “quantum phase transition”. Nonetheless, we do observe a very smooth transition in the structure of the quantum steady state, which is analogous to self-organisation as it happens in the second order density correlation.

From the discussion in Section 12.2 we also see that unlike in the classical case, where the model could be solved even for several thousand particles [6, 14, 17], full quantum mechanical solution for several particles is difficult. Indeed, to account for the dynamical nature of the lattice, i.e., the fact that the field scattered by the particles from the pump into the cavity modifies the potential felt by the particles (cf. last term in the Hamiltonian (12.1)), several single-particle states has to be incorporated in the simulation: In the MCWFS we typically use 30 momentum eigenstates (for details see Reference [22]). For N particles this gives a 30^N dimensional Hilbert space, which is further multiplied by the cavity-field Hilbert space. With nowadays computational resources this approach can be practically pursued up to two particles. In the Bose-Hubbard approach, on the other hand, there are only two single-particle states, but these are defined by the lattice potential solely. Hence it remains to be demonstrated that this approach can be applied at all to describe self-organisation, a phenomenon *based on* the dynamical nature of the lattice. This problem is also addressed in Section 12.5 where we compare our two-particle MCWFS and Bose-Hubbard results.

12.4 Single-particle dynamics

We first consider the dynamics of a single particle initially prepared in one of the localised states (say, $|r\rangle$). Without coupling to the cavity ($U_0 = 0$) the particle moves unperturbed in the lattice via tunnelling, which, in the case of two sites corresponds to an oscillation between states $|r\rangle$ and $|l\rangle$. This can be monitored via the expectation value $\langle Kx \rangle$, which, as displayed in Figure 12.2 (a) (red line), oscillates accordingly between $\pm\pi/2$ (cf. also Figure 12.1).

This simple behaviour is significantly modified in the presence of even a weakly coupled cavity, $U_0 \neq 0$. Now the particle scatters photons from the lattice field into the cavity mode, depending on its state. Photons can decay according to the Liouvillean (12.2) and allow to monitor the particle motion. The decay of a cavity photon can be modelled by a quantum jump, which is mathematically described by the application of the cavity field operator a on the state vector of the system. This, in turn, changes the whole particle-field wave function and thus gives feedback on the particle localisation.

When the coupling is weak enough, the field in the cavity will be small, and the contribution of the last term of Hamiltonian (12.1) to the potential felt by the particle (second term in the same Hamiltonian) is negligible, so that it still makes sense to define the localised particle states solely from the lattice potential.

We assume that these states are *well* localised. When a point-like particle is placed into the lattice at position x in steady state it radiates a coherent field $|\alpha(x)\rangle$ into the cavity where the amplitude is determined by the Liouvillean dynamics (12.1)-(12.2) and reads

$$\alpha(x) = \frac{\sqrt{U_0 V_0}}{U_0 - \Delta_C - i\kappa} \sin(Kx) = \frac{\sqrt{U_0 V_0}}{\kappa} \frac{1}{1 - i} \sin(Kx), \quad (12.4)$$

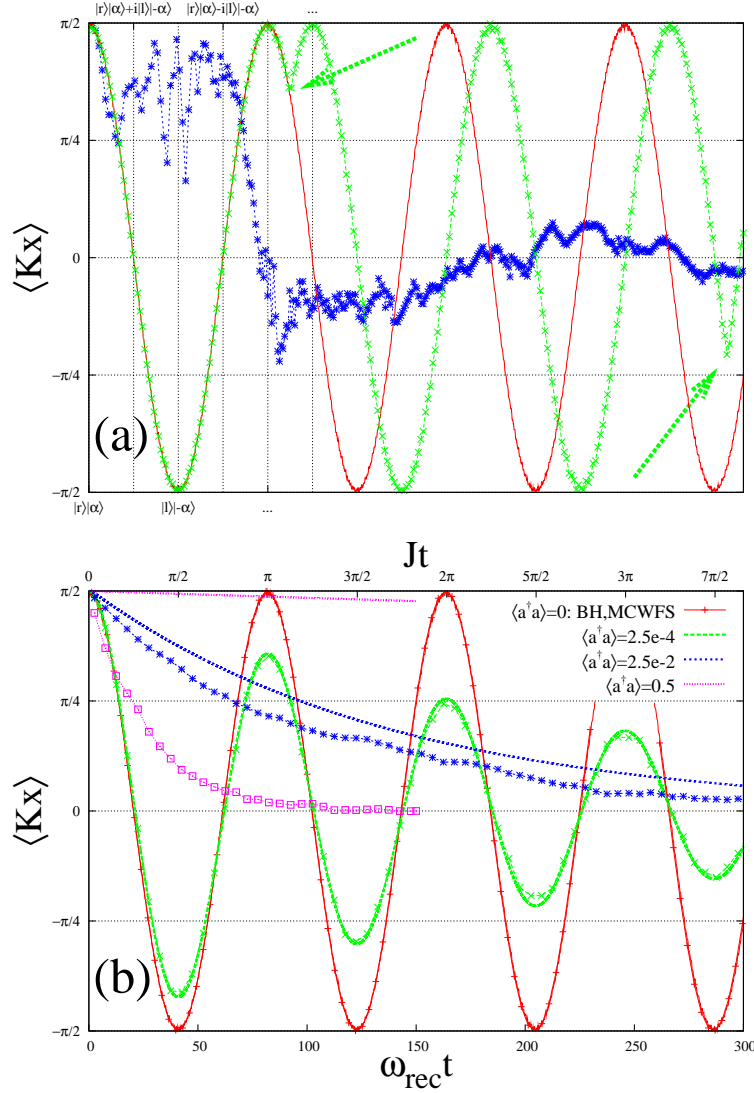


Figure 12.2. Simulated data for a single particle in the lattice-cavity system. Parameters: $V_0 = -10\omega_{\text{rec}}$, $\kappa = 10\omega_{\text{rec}}$, $\Delta_C - U_0 = -\kappa$, with the recoil frequency $\omega_{\text{rec}} \equiv \hbar K^2/(2\mu)$. The colour code: red corresponds to $U_0 = 0$, green to $U_0 = -0.005\omega_{\text{rec}}$, blue to $U_0 = -0.5\omega_{\text{rec}}$, and magenta to $U_0 = -10\omega_{\text{rec}}$; with maximal cavity photon numbers amounting to 0, $2.5 \cdot 10^{-4}$, $2.5 \cdot 10^{-2}$, and 0.5, respectively. (a) Example single MCWF trajectories. On the green trajectory green arrows mark the instants of cavity decays (photon escapes): the resulting jump in the tunnelling oscillation's phase is visible. (b) Ensemble average data — Lines without points: solution of the time-dependent Master equation based on the Bose-Hubbard Hamiltonian (12.3). Lines with points: ensemble average of several MCWF trajectories.

where the second equality holds under the resonance condition $\Delta_C - NU_0 = -\kappa$ (N is the particle number), to which we restrict ourselves in the following. This makes that the cavity field increases monotonically with increasing coupling.

Accordingly, in state $|r\rangle$ the particle will radiate an approximately coherent state $|\alpha\rangle$, while in state $|l\rangle$ a coherent state with opposite phase $|- \alpha\rangle$, where $\alpha = \alpha(x = \pi/(2K))$. It can also be expressed from the Bose-Hubbard model as $\alpha = \tilde{J}/(\kappa(1-i))$.

If we assume that tunnelling is much slower than cavity field evolution, then the latter will follow adiabatically the former. Without cavity jumps the system evolves coherently and since the back action of the cavity field on the particle motion is negligible by our assumption, this evolution amounts to an oscillation between states $|r, \alpha\rangle$ and $|l, -\alpha\rangle$, hence at a given time instant t the overall state of the particle-cavity system reads approximately

$$|\Psi(t)\rangle = \cos(Jt)|r, \alpha\rangle + i \sin(Jt)|l, -\alpha\rangle. \quad (12.5)$$

Now imagine that at time t a jump happens: Immediately after the jump the state of the system reads

$$|\Psi'(t)\rangle \propto a|\Psi(t)\rangle \propto \cos(Jt)|r, \alpha\rangle - i \sin(Jt)|l, -\alpha\rangle, \quad (12.6)$$

that is, the cavity jump is reflected back onto the particle motion and results in a jump of the phase of the tunnelling oscillation.

This behaviour is verified by the simulations, an example trajectory is displayed in Figure 12.2 (a) (green line). Here the parameters were chosen such that the maximal expectation value of the cavity photon number is only $2.5 \cdot 10^{-4}$ — this maximum is achieved when the particle is prepared perfectly localised at a lattice site.

The jump is a stochastic event and in ensemble average the jumps of the phases on individual trajectories result in a dephasing and hence damping of the oscillation. This behaviour, as displayed in Figure 12.2 (b) (green lines) is verified by both the MCWFS and the simulation of the time-dependent Master equation based on the Bose-Hubbard Hamiltonian (12.3). In this regime of very low cavity photon number, the correspondence between the two models is very good. Increasing the photon number results in several jumps happening in one tunnelling cycle: in ensemble average this corresponds to the over-damped regime of the tunnelling oscillation (cf. Figure 12.2 (a-b) blue line).

The above picture of the dynamics on one Monte Carlo trajectory is not valid in the regime of stronger coupling where the photon number is higher. Here the cavity field modifies significantly the potential felt by the particle and hence the states $|r\rangle$ and $|l\rangle$ defined solely by the lattice potential lose their significance because many other particle spatial states enter the dynamics. Cavity decays are much more frequent, and the stronger field fluctuations are reflected back onto the potential. Accordingly, as we observe in Figure 12.2 (magenta line), the Bose-Hubbard approach being based on those two states breaks down in this regime.

The steady state of the dynamics is, quite independently of the coupling, the mixed state $\rho_{ss} \approx (|r, \alpha\rangle\langle r, \alpha| + |l, -\alpha\rangle\langle l, -\alpha|)/2$. As displayed in Figure 12.3, the relaxation time to this state, that is, the time scale of the damping of the tunnelling oscillation exhibits a non-trivial behaviour. For moderate coupling, according to the discussion above, this is composed of two time scales: the time scale of cavity photon decay, and that of tunnelling. The former being inversely proportional to the photon number gets faster with increasing coupling.

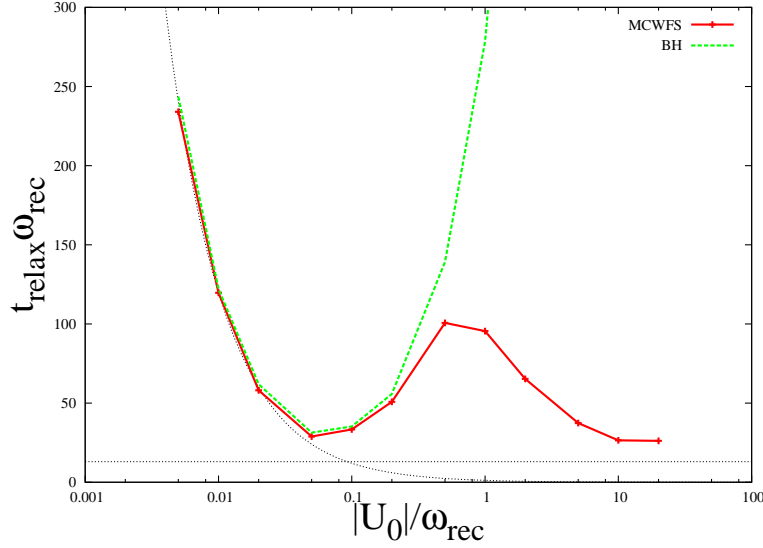


Figure 12.3. Relaxation time of the damping of the tunnelling oscillation simulated with the MCWF and Bose-Hubbard approach. Same parameters as above. The dotted hyperbole has been fit on the weak-coupling part of the data and is proportional to the cavity photon count rate. The dotted horizontal line is the time scale of tunnelling with no coupling.

On the other hand the latter *gets slower*, a behaviour verified by both the MCWF and the Bose-Hubbard approach. In the following we give an interpretation in the framework of the Bose-Hubbard approach. Here, when initially in the state $|r, \alpha\rangle$, the system first evolves into $|l, \alpha\rangle$ via tunnelling (first term of Hamiltonian (12.3)), and this state is then transformed into $|l, -\alpha\rangle$ by the dissipative cavity evolution on a timescale of κ^{-1} , since in steady state the particle in state $|l\rangle$ radiates the approximately coherent field $|\alpha\rangle$. States $|r, \alpha\rangle$ and $|l, \alpha\rangle$, however, have different energies because of the last term in Hamiltonian (12.3), so that the tunnelling becomes non-resonant and hence slows down as compared to the free (no-cavity) case. Using the α value calculated above from the Bose-Hubbard approach the energy difference reads $\Delta = 2\tilde{J}^2/\kappa \propto |U_0|$. With increasing U_0 the energy difference increases, so that tunnelling gets slower. The above discussion is summarised in Figure 12.4.

The combination of one accelerating and one slowing time scale results in the minimum behaviour of the relaxation time in Figure 12.3 around $U_0 = -0.05\omega_{\text{rec}}$. Ultimately, with high enough coupling the cavity-generated potential starts to dominate the lattice potential, in which regime strong fluctuations and self-trapping lead to fast relaxation as observed in the MCWFS (red line $|U_0| \gtrsim \omega_{\text{rec}}$). Obviously, the Bose-Hubbard approach is unable to reproduce the behaviour in this regime.

12.5 Two-particle dynamics

Having understood the dissipative quantum dynamics of a single particle in our lattice-cavity system, we now turn to the case of two particles. Two particles on two lattice sites with

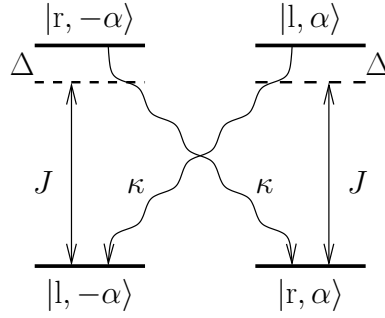


Figure 12.4. Effective level scheme for one particle in the Bose-Hubbard approach. Tunnelling acts as an off-resonant driving while the dissipative cavity field dynamics as damping of the higher-lying states.

periodic boundary conditions is the minimal system that can exhibit the difference between the configurations described above for self-organisation. In the Bose-Hubbard approach where there is only one state at each lattice site the Hilbert space for the particles is spanned by only three states: $|1, 1\rangle \equiv |0\rangle$ — the Mott insulator (MI) state, which corresponds to the homogeneous distribution or unorganised configuration —, and $|2, 0\rangle \equiv |-\rangle$ and $|0, 2\rangle \equiv |+\rangle$ corresponding to the two organised configurations. $|0\rangle$ scatters no field (and no photons) into the cavity due to destructive interference between the fields scattered by the two particles, while $|-\rangle$ and $|+\rangle$ scatter $|-2\alpha\rangle$ and $|2\alpha\rangle$, respectively, the factor 2 being due to constructive interference. The difference between the two configurations can be monitored via the density correlation $\langle n_l n_r \rangle$, which is 1 for the MI state and 0 in the subspace spanned by $|\pm\rangle$.

When the particles are initially in the MI state, then for $U_0 = 0$ at time t the particle state is

$$|\Psi(t)\rangle = \cos(2Jt)|0\rangle + \frac{i}{\sqrt{2}} \sin(2Jt) (|-\rangle + |+\rangle). \quad (12.7)$$

With $U_0 \neq 0$ under the simplifying conditions we discussed above for the single particle case we have for the joint system

$$|\Psi(t)\rangle = \cos(2Jt)|0, 0\rangle + \frac{i}{\sqrt{2}} \sin(2Jt) (|-, -2\alpha\rangle + |+, 2\alpha\rangle). \quad (12.8)$$

If a jump happens in this state (application of a), then the state immediately after the jump reads

$$|\Psi'(t)\rangle \propto a|\Psi(t)\rangle \propto |-, -2\alpha\rangle - |+, 2\alpha\rangle. \quad (12.9)$$

There are two points worth noting here: Firstly, the quantum jump in the photon number erases all information about the phase of the tunnelling oscillation in the particle Hilbert space. Secondly, after the escape of one single photon from the cavity tunnelling stops immediately. Indeed, in the state (12.9) both $|-, -2\alpha\rangle$ and $|+, 2\alpha\rangle$ tunnels to $|0, 0\rangle$ (note that we assume again the cavity field following adiabatically the tunnelling), but their phases are opposite, and hence the two paths interfere destructively. A second jump at $t' > t$, however, makes the phases match again, and puts the state $|\Psi''(t')\rangle \propto a|\Psi'(t)\rangle \propto |-, -2\alpha\rangle + |+, 2\alpha\rangle$ back into the tunnelling cycle (12.8). An example MCWF trajectory exhibiting this behaviour

is plotted in Figure 12.5(a) (green line). We observe that a quantum jump brings the system into the state (12.9), signalled by $\langle n_1 n_r \rangle = 0$, and it remains there until the next jump, when it starts to oscillate anew.

In ensemble average these stochastic “dark” periods of the tunnelling oscillation lead to damping just as in the single-particle case. The final steady state is always a mixture

$$\rho_{ss} = w|0, 0\rangle\langle 0, 0| + \frac{1-w}{2}(|-, -2\alpha\rangle\langle -, -2\alpha| + |+, 2\alpha\rangle\langle +, 2\alpha|). \quad (12.10)$$

At this point it becomes clear that any mean-field description of this system is bound to fail: a mean cavity field description would prohibit the possibility of a coherent superposition of different particle configurations radiating different fields as in (12.8), which is essential for the onset of the dynamics from a homogeneous zero-temperature initial condition (see also [25]). On the other hand, a particle mean field cannot seize the difference between states (12.10) with different w , because this appears only in the density *correlation*.

As displayed in Figure 12.5 (b), our two approaches for simulating the damping agree well in the regime of moderate coupling. However, just as in the single-particle case, strong coupling — in the regime where the cavity-generated potential dominates the lattice one — results in extremely quick damping, which cannot be reproduced by the Bose-Hubbard approach. Here the relaxation time exhibits the same behaviour as we have seen in the single-particle case (cf. Figure 12.6 (a)): with increasing coupling it has a minimum, after which the Bose-Hubbard approach gives a monotonic increase of the relaxation time, while the MCWFS gives a peak, and for even stronger coupling very quick relaxation. For the interpretation of this behaviour the same discussion applies as above for the single-particle case.

Increasing coupling results in a decrease of the weight w of the MI component in steady state, cf. Figure 12.6 (b), and with strong enough coupling ($|U_0| \gtrsim 10\omega_{\text{rec}}$ in our case) the steady state is confined solely into the self-organised subspace. This proves our initial assertion that even when the system is started from a $T = 0$ homogeneous state (here the MI state) self-organisation can occur. On the same Figure we also see that this is confirmed by both approaches, only the relaxation time of the process is predicted wrongly by the Bose-Hubbard approach for strong coupling.

It is easy to see that starting the system from the superfluid (SF) state

$$|\text{SF}\rangle \propto |0\rangle + \frac{1}{\sqrt{2}}(|-\rangle + |+\rangle) \quad (12.11)$$

instead of the MI as above does not change the steady state since already the first quantum jump erases the information about the initial condition completely. The process of relaxation will, however, be different. This process can be monitored by a time resolved analysis of the intensity escaping the cavity, which is proportional to the cavity photon number: an example is displayed in Figure 12.7. Here, we are in the over-damped regime of the tunnelling oscillation. When prepared in the MI state, the particles do not scatter initially, and the buildup of the cavity field occurs on the time scale of the self-organisation process. With the SF initial state, on the other hand, some field is built up almost instantly (on the time scale of κ^{-1}), because in the SF the states $|\pm\rangle$ have finite weight; while the rest of the field is built up on the longer time scale.

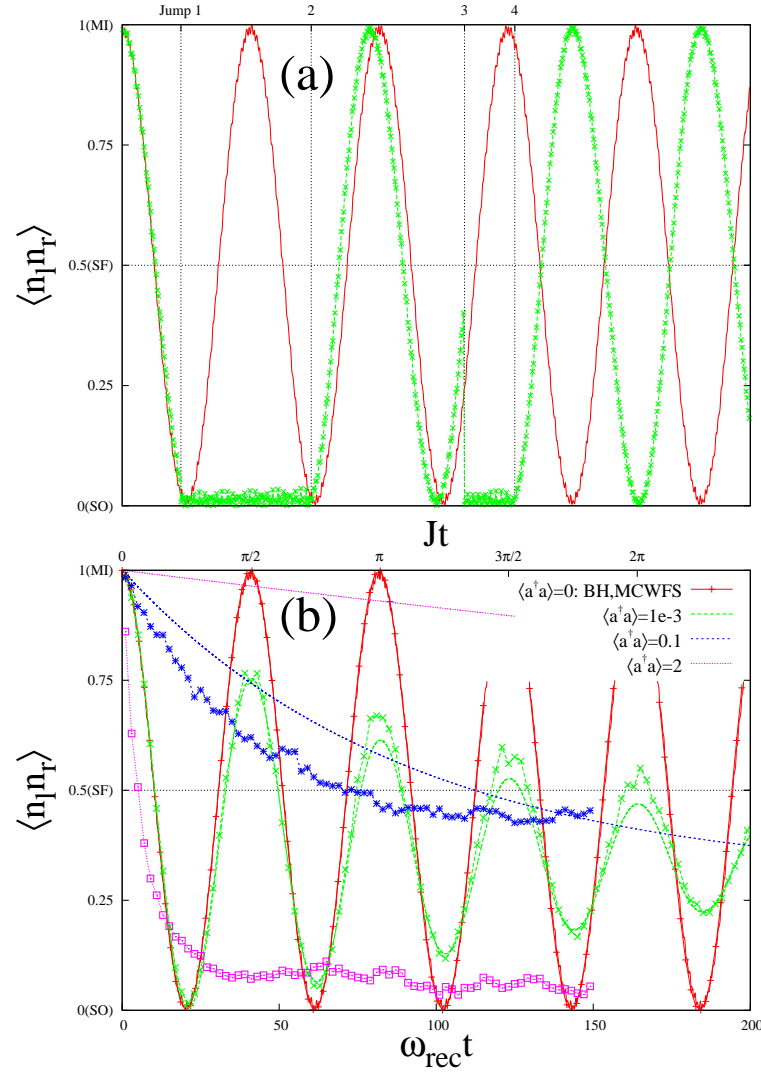


Figure 12.5. Simulated data for two particles in the lattice-cavity system with same parameters as above. The colours correspond to the same values of U_0 , here with maximal cavity photon numbers amounting to 0, 10^{-3} , 0.1, and 2. (a) Example single MCWF trajectories — the vertical dotted lines mark the time instants of cavity decays on the trajectory plotted in green. (b) Ensemble average data — lines without points: data stemming from the Bose-Hubbard approach; lines with points: MCWF approach.

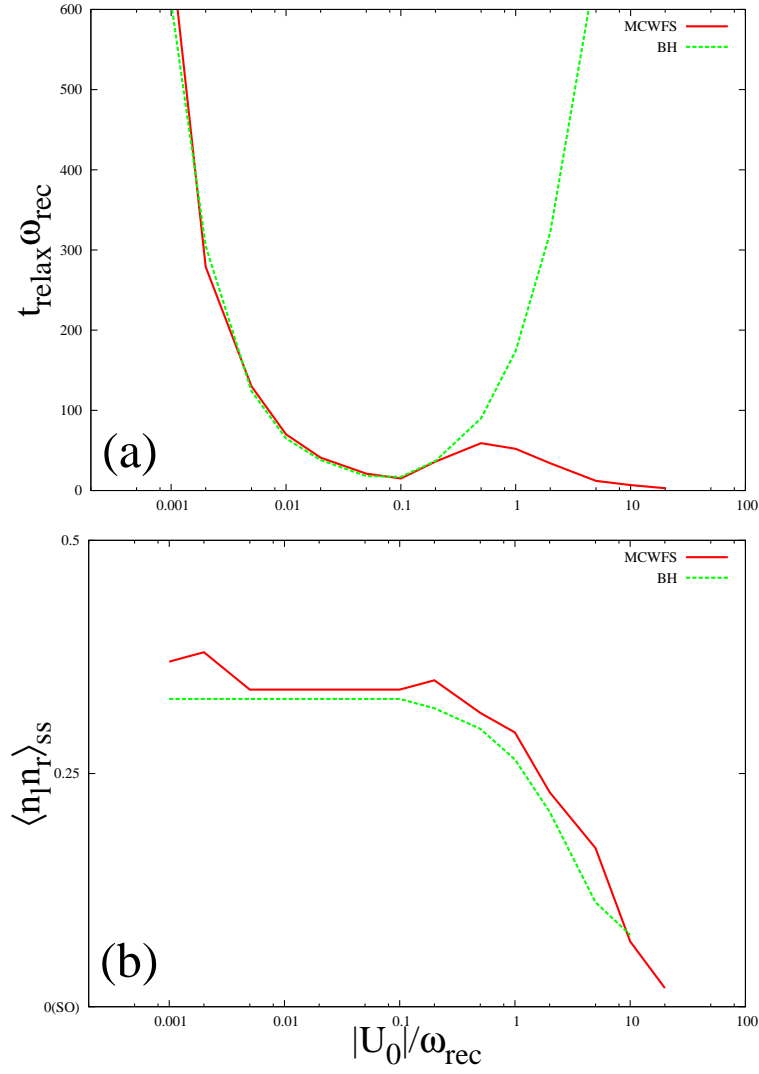


Figure 12.6. (a) Relaxation time for two particles and (b) weight of the MI component in the steady-state mixture (12.10) — $\langle n_l n_r \rangle_{\text{ss}} = w$ — as functions of the coupling. Same parameters as above.

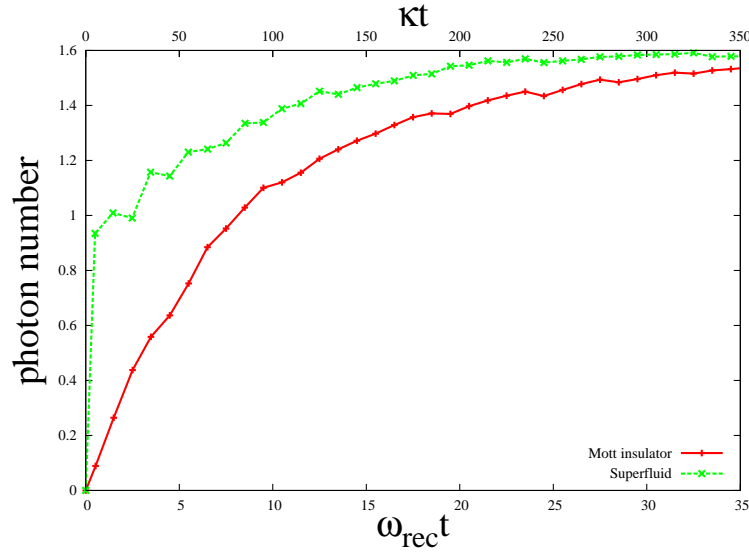


Figure 12.7. Initial build-up of the cavity photon number with the particles prepared initially in the Mott insulator or superfluid state. $U_0 = -10\omega_{\text{rec}}$, other parameters are the same as above.

12.6 Conclusions

In summary, we have seen that coupling two particles in an optical lattice to a cavity induces an irreversible reorganisation of the particles, a process which can be monitored directly in an experiment by the time-resolved analysis of the intensity escaping the cavity. We have shown that no classical or mean-field description of either the particles or the cavity field can account for the phenomenon. For strong enough coupling the process leads to a fast self-organisation of the particles, a configuration in which they occupy every second site in the lattice, and scatter superradiantly into the cavity. An important conclusion of the work is that while an effective low-dimensional Bose-Hubbard type model cannot reproduce the time evolution in the strong-coupling regime as observed in more detailed simulations, it can still predict the steady state remarkably well. This model can therefore be used in the future for a high number of particles to study possible quantum phase transitions occurring in the steady state of this dissipative system.

Bibliography

- [1] S. Sachdev, *Quantum Phase Transitions*, (Cambridge University Press, 1999).
- [2] D. Jaksch, C. Bruder, J. I. Cirac, C. W. Gardiner, and P. Zoller, Phys. Rev. Lett. **81** 3108 (1998).
- [3] M. Greiner, O. Mandel, T. Esslinger, T. W. Hänsch, and I. Bloch, Nature **415**, 39 (2002).
- [4] H. P. Büchler and G. Blatter, Phys. Rev. Lett. **91**, 130404 (2003).
- [5] V. W. Scarola, E. Demler, and S. Das Sarma, Phys. Rev. A **73**, 051601(R) (2006).

- [6] P. Domokos and H. Ritsch, Phys. Rev. Lett. **89**, 253003 (2002).
- [7] C. Maschler and H. Ritsch, Phys. Rev. Lett. **95**, 260401 (2005).
- [8] P. Domokos, A. Vukics, and H. Ritsch, Phys. Rev. Lett. **92**, 103601 (2004).
- [9] S. Zippilli and G. Morigi, Phys. Rev. Lett. **95**, 143001 (2005).
- [10] J. Metz, M. Trupke, and A. Beige, Phys. Rev. Lett. **97**, 040503 (2006).
- [11] K. Murr, Phys. Rev. Lett. **96**, 253001 (2006).
- [12] B. Nagorny, T. Elsässer, and A. Hemmerich, Phys. Rev. Lett. **91**, 153003 (2003).
- [13] S. Nussmann *et al.*, Nat. Phys. **1**, 122 (2005).
- [14] P. Domokos and H. Ritsch, J. Opt. Soc. Am. B **20**, 1098 (2003).
- [15] A. Vukics and P. Domokos, Phys. Rev. A **72**, 031401 (2005).
- [16] C. W. Gardiner and P. Zoller, *Quantum Noise*, 2nd Ed., (Springer, Berlin, 2000).
- [17] J. K. Asbóth, P. Domokos, H. Ritsch, and A. Vukics, Phys. Rev. A **72**, 053417 (2005).
- [18] A. T. Black, H. W. Chan, and V. Vuletić, Phys. Rev. Lett. **91**, 203001 (2003).
- [19] A. Vukics, J. Janszky, and P. Domokos, J. Phys. B **38**, 1453 (2005).
- [20] A. Öttl, S. Ritter, M. Köhl, and T. Esslinger, Phys. Rev. Lett. **95**, 090404 (2005).
- [21] A. Öttl, S. Ritter, M. Köhl, and T. Esslinger, Rev. Sci. Instrum. **77**, 063118 (2006).
- [22] A. Vukics and H. Ritsch, Eur. Phys. J. D (to be published). [accepted for publication]
- [23] C. Maschler and H. Ritsch, Opt. Commun. **243**, 145 (2004).
- [24] J. Larson, B. Damski, G. Morigi, and M. Lewenstein, cond-mat/0608335.
- [25] C. Maschler, H. Ritsch, A. Vukics, and P. Domokos, Opt. Commun. **273**, 446 (2007).

CURRICULUM VITAE

Christoph Maschler,
October 2007

General

Current Address: Institute for Theoretical Physics, University of Innsbruck,
Technikerstraße 25, A-6020 Innsbruck, Austria.
Date of Birth: 7th July, 1975.
Place of Birth: A-6511 Zams, Austria.
Citizenship: Austrian
Languages Spoken: German (Native), English (Fluent), French (Basic knowledge)

Elementary Education

1981 - 1985 Elementary School, Zams, Austria.
1985 - 1993 High School, Landeck, Austria.

Academic Education

Oct 1993 - Jul 1995	Study of Mechanical Engineering, Technical University Vienna, Austria.
Oct 1995	Start of studies: Physics, Mathematics and High School Teaching Certification, University of Innsbruck, Austria.
Jun 2001 - May 2002	Diploma thesis, <i>Two Atoms in a Highly Elongated, Cigar-Shaped Trap with Separable Interaction</i> , supervised by o.Univ.-Prof. Dr. Peter Zoller, Institute for Theoretical Physics, University of Innsbruck.
May, 28, 2002	MSc Degree in Physics with distinction, Institute for Theoretical Physics, University of Innsbruck.
Feb 2003 - Feb 2004	Diploma thesis, <i>Mathematische Grundlagen der Quantenmechanik</i> , supervised by Prof. Wolfgang Förg-Rob, Institute for Mathematics, University of Innsbruck.
Dec, 4, 2002	Finished High School Teaching Certification in Physics.
Feb, 19, 2002	MSc Degree in Mathematics with distinction, Institute for Mathematics, University of Innsbruck.
Mar, 16, 2002	Finished High School Teaching Certification in Mathematics.
Jun 2003 - present	PhD student in Prof. Dr. Helmut Ritsch's group, Institute for Theoretical Physics, University of Innsbruck.

Research Experience

Jun 2001 - May 2002	MSc Thesis research at the Institute for Theoretical Physics, University of Innsbruck, supervised by Prof. Peter Zoller, working on topics in quantum mechanical scattering theory.
Aug 2002 - Jan 2003	Temporary Research Assistant at the Institute for Mathematics, University of Vienna, with Prof. Peter Markowich, working on topics in mathematical physics.
Feb 2003 - May 2004	Research at the Department of Anesthesiology and Critical Care Medicine, Medical University of Innsbruck, with Dr. Anton Amann, working in data analysis.
Feb 2003 - Feb 2004	MSc Thesis research at the Institute for Mathematics, University of Innsbruck, supervised by Prof. Wolfgang Förg-Rob, working on topics in mathematical foundation of quantum mechanics.
Jun 2003 - Present	PhD Thesis research at the Institute for Theoretical Physics, University of Innsbruck, supervised by Prof. Helmut Ritsch.

Teaching Experience

Oct 1997 - Jan 1998	Tutor, Institute for Mathematics, University of Innsbruck. Tutor for “Analysis 1”.
Mar 1998 - Jul 1998	Tutor, Institute for Mathematics, University of Innsbruck. Tutor for “Analysis 2”.
Oct 1998 - Jan 1999	Tutor, Institute for Mathematics, University of Innsbruck. Tutor for “Mathematics for Physicists”.
Mar 1999 - Jul 1999	Tutor, Institute for Mathematics, University of Innsbruck. Tutor for “Mathematics for Physicists 2”.
Oct 1999 - Jan 2000	Tutor, Institute for Theoretical Physics, University of Innsbruck. Tutor for “Electrodynamics”.
Mar 2000 - Jul 2000	Tutor, Institute for Theoretical Physics, University of Innsbruck. Tutor for “Theoretical Mechanics”.
Oct 2000 - Jan 2001	Tutor, Institute for Theoretical Physics, University of Innsbruck. Tutor for “Thermodynamics”.
Oct 2004 - Jan 2005	Tutor, Institute for Theoretical Physics, University of Innsbruck. Tutor for “Quantum Mechanics 2”.
Mar 2005 - Jul 2005	Tutor, Institute for Theoretical Physics, University of Innsbruck. Tutor for “Theoretical Physics 3”.
Oct 2005 - Jan 2006	Tutor, Institute for Theoretical Physics, University of Innsbruck. Tutor for “Introduction to Theoretical Physics”.
Sep 2006 - Jul 2007	High School Teacher, HTL Anichstraße, Innsbruck. Teacher for “Electrical Engineering” and “Applied Mathematics”.

Preprints

1. C. Maschler, I. B. Mekhov, and H. Ritsch, *Ultracold Atoms in Optical Lattices Generated by Quantized Light Fields*, arXiv: quant-ph/0710.4220.

Publications - Articles

1. C. Maschler and H. Ritsch, *Quantum Motion of Laser-Driven Atoms in a Cavity Field*, Opt. Comm. **243**, 145 - 155 (2004).
2. C. Maschler and H. Ritsch, *Cold Atom Dynamics in a Quantum Optical Lattice Potential*, Phys. Rev. Lett. **95**, 260401 (2005).
3. C. Maschler, H. Ritsch, A. Vukics, and P. Domokos, *Entanglement Assisted Fast Re-ordering of Atoms in an Optical Lattice within a Cavity at $T = 0$* , Opt. Comm. **273**, 446 - 450 (2007).
4. I. B. Mekhov, C. Maschler, and H. Ritsch, *Cavity Enhanced Light Scattering in Optical Lattices to Probe Atomic Quantum Statistics*, Phys. Rev. Lett. **98**, 100402 (2007).

5. I. B. Mekhov, C. Maschler, and H. Ritsch, *Probing Quantum Phases of Ultracold Atoms in Optical Lattices by Transmission Spectra in Cavity QED*, Nature Physics **3**, 319 - 323 (2007).
6. A. Vukics, C. Maschler, and H. Ritsch, *Microscopic Physics of Quantum Self-Organisation of Optical Lattices in Cavities*, New J. Phys. **9**, 255 (2007).
7. I. B. Mekhov, C. Maschler, and H. Ritsch, *Light Scattering from Ultracold Atoms in Optical Lattices as an Optical Probe of Quantum Statistics*, Phys. Rev. A (in press).

Publications - MSc Thesis

1. C. Maschler, *Two Atoms in a Highly Elongated, Cigar-Shaped Trap with Separable Interaction*, MSc Thesis for Physics, University of Innsbruck, May 2002.
2. C. Maschler, *Mathematische Grundlagen der Quantenmechanik*, MSc Thesis for Mathematics, University of Innsbruck, February 2004.

Conference Contributions

- *Meeting of the Spezialforschungsbereich (SFB) for Control and Measurement of Coherent Quantum Systems*,
Innsbruck, Austria, February 2002.
- 54th *Annual Meeting of the Austrian Society of Physics (ÖPG)*,
Linz, Austria, September 2004.
- 11th *Young Atom Opticians (YAO) Conference*,
Hannover, Germany, February 2005.
- *Obergurgl Quantum Optics Meeting 2005*,
Obergurgl, Austria, March 2005.
- 55th *Annual Meeting of the Austrian Society of Physics (ÖPG)*,
Vienna, Austria, September 2005.
- 3rd *International Workshop on the Theory of Quantum Gases and Quantum Coherence*,
Cortona, Italy, November 2005.
- 2nd *Term-Review of the Spezialforschungsbereich (SFB) for Control and Measurement of Coherent Quantum Systems*,
Innsbruck, Austria, January 2006.
- 20th *International Conference on Atomic Physics (ICAP 2006)*,
Innsbruck, Austria, July 2006.

- *QUROPE Winter School on Quantum Information: Ensemble-based Quantum Information Processing*,
Obergurgl, Austria, February 2007.
- *AMOP Spring Conference of the German Physical Society (DPG)*,
Düsseldorf, Germany, March 2007.
- *Workshop on Quantum Engineering with Neutral Atoms and Light*,
Herrsching am Ammersee, Germany, June 2007.
- *d-fine's Science in Finance Workshop*,
Schlosshotel Kronberg, Germany, October 2007.

